University of Nevada, Reno

Calibration of the AASHTO MEPDG for Flexible Pavements to Fit Nevada's Conditions

A thesis submitted in partial fulfillment of the
requirements for the degree of Master of Science in
Civil and Environmental Engineering

by

Peter Nabhan

Dr. Elie Y. Hajj / Thesis Advisor

August, 2015

THE GRADUATE SCHOOL

We recommend that the thesis
prepared under our supervision by

PETER ANTOINE NABHAN

Entitled

Calibration of the AASHTO MEPDG for Flexible Pavements to Fit Nevada's Conditions

be accepted in partial fulfillment of the
requirements for the degree of

MASTER OF SCIENCE

Elie Y. Hajj, Ph.D., Advisor

Peter E. Sebaaly, Ph.D., Committee Member

Mariah Evans, Ph.D., Graduate School Representative

David W Zeh, Ph.D., Graduate Dean, Graduate School

August, 2015

ABSTRACT

The Mechanistic-Empirical Pavement Design Guide (MEPDG) consists of transferring pavement mechanical responses such as stresses and strains into predicted distresses. The nationally calibrated models for rutting, bottom-Up fatigue cracking, top-down fatigue cracking, International roughness Index (IRI), thermal cracking and reflective cracking need to be recalibrated to properly fit Nevada's local conditions for materials, traffic, and climate.

This study focuses on the local calibration of the fatigue bottom-up cracking and the rutting models. For this purpose, data was collected from the Nevada Department of Transportation (NDOT) Pavement Management Systems (PMS) database and converted to match the MEPDG models requirements. Additionally, field-produced mixtures were sampled from 45 paving projects to develop a materials database. These mixtures were collected from all three districts and tested for dynamic modulus, binder properties, rutting, and fatigue. This was completed to characterize the polymer-modified asphalt binder mixtures technologies in Nevada which was one of the main factors that mandated a local Pavement-ME calibration as the nationally calibrated models used unmodified binders.

The calibration was performed by optimizing the local calibration factors to reduce the sum of error squared between predicted and measured distresses data. The calibration for rutting was conducted for new and rehabilitated sections from the three districts. On the other hand, the fatigue calibration separated new and rehabilitated sections but combined between district II and III as most mixes from these districts use the PG64-28NV binder as opposed to District I where PG 76-22NV binder is predominantly used. The final calibration sets for rutting and fatigue cracking were 6 and 4 respectively.

This thesis recommends additional performance monitoring of the polymer-modified paved sections as the calibration was validated using only 10 years of performance data. Future recalibration could be undertaken to increase the accuracy of the models.

ACKNOWLEDGEMENTS

The author would like to thank Dr. Elie Hajj for his valuable guidance and assistance throughout the course of the research, Dr. Peter Sebaaly for his constant encouragement and counseling, Dr. Mena Souliman for his important suggestions and all his colleagues, friends and family who assisted both morally and physically for the completion of this project.

TABLE OF CONTENTS

LIST OF TABLES

LIST OF FIGURES

CHAPTER 1 : INRODUCTION

1.1. Background

The American Association of State Highway and Transportation Officials (AASHTO) Mechanistic-Empirical Pavement Design Guide (MEPDG) developed under National Cooperative Highway Research Program (NCHRP) Project 1-37A has been introduced as a new design procedure to replace the AASHTO 1993 Guide for Design of Pavement Structures. Unlike its empirical based predecessor, the MEPDG uses a mechanistic-empirical procedure that analyzes the pavement's responses such as stresses, strains, and deflections to predict future pavement conditions.

The pavement condition is evaluated using a set of transfer functions that estimate distress levels for a particular pavement section subjected to a certain climate and traffic loading. These transfer functions or performance models were calibrated using performance data from the Long Term Pavement Performance (LTPP) database that incorporates data from all around the United States; consequently, the local calibration of these models becomes necessary to take into account state-specific material properties, traffic, climatic conditions, and construction practices.

The calibration's main objective is to use the AASHTOWare Pavement-ME software outputs for a certain pavement section and try to relate them to field performance measurements. This is done by optimizing the calibration coefficients to minimize the sum of square errors between field measured and software predicted distresses. The local calibration guide NCHRP 1-40B project provides guidelines for local calibration and validation.

1.2. Problem Statement

The Nevada Department of Transportation (NDOT) in an effort to implement the AASHTO MEPDG has partnered with the University of Nevada, Reno (UNR) researchers to develop a material database representative of the state's HMA mixtures. This database covers dynamic modulus testing, asphalt binder testing, and asphalt mixture rutting and fatigue performance relationships. The content of this database is a major material input into the Pavement-ME calibration. Pavement performance of NDOT's monitored and managed roads (State routes, Interstate routes, US routes etc.) was used to correlate the MEPDG's prediction models to actual field distresses. It was found that the Pavement-ME software was over predicting major distresses such as rutting and roughness and under predicting other distresses such as bottom-up fatigue cracking. To verify this assumption, a section from the US 395 Highway was modeled in the Pavement-ME software using the national models and the results were compared to field measurements. Figures 1.1 to 1.3 below illustrate the major distresses evolution with time.

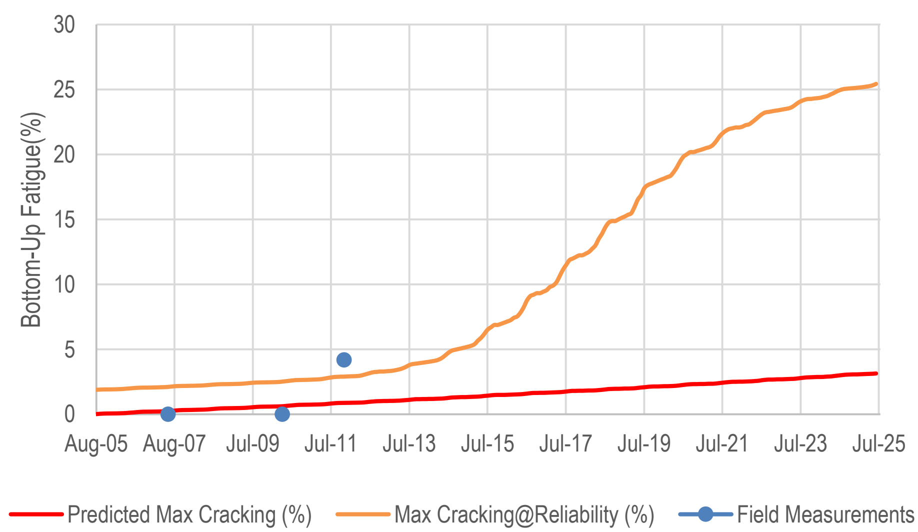

Figure 1.1-Predicted Bottom-Up Fatigue Evolution with Time.

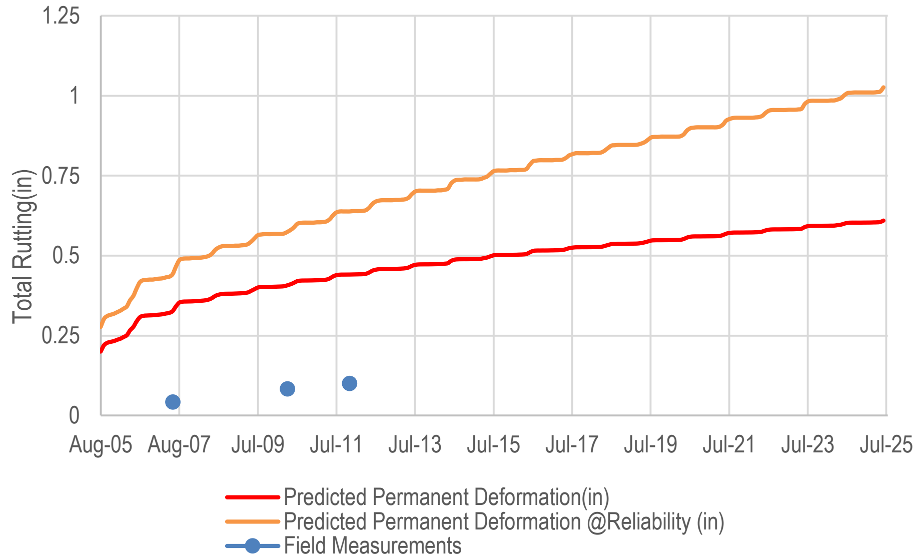

Figure 1.2-Total Predicted Rutting Evolution with Time.

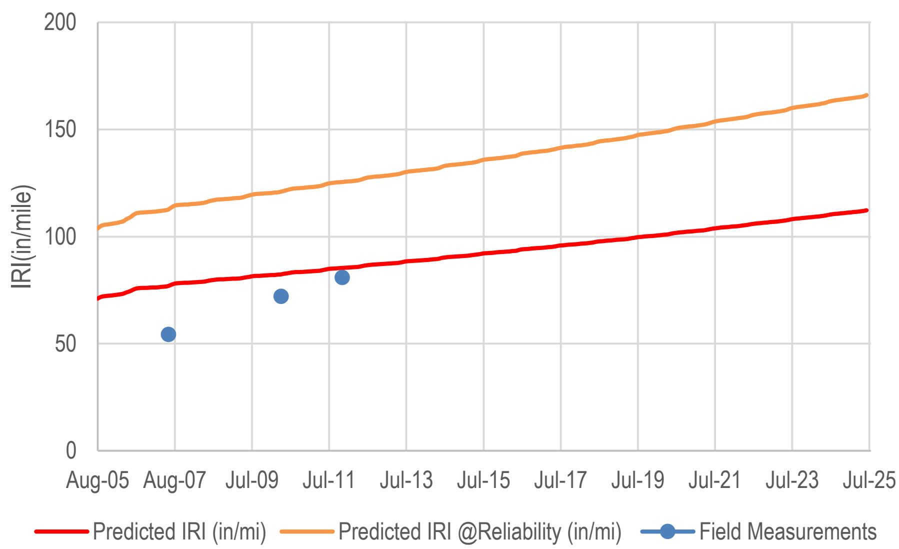

Figure 1.3-Predicted Roughness Evolution with Time.

The figures above clearly show that the field measured bottom-up fatigue cracking is higher than the predicted values. On the other hand, the predicted rutting and roughness distresses are noticeably larger than the field measurements which in most cases can lead to an overly designed pavement. This discrepancy is majorly due to the fact that the nationally calibrated models were based on data collected from sections with conventional dense graded hot asphalt mixtures with unmodified asphalt binders. Considering that the state of Nevada transitioned to using polymer modified binders since 2002 (PG64-28NV and PG76-22NV), the local calibration of these models becomes necessary. The MEPDG models that require calibration for NDOT's flexible pavements are rutting and fatigue bottom-up cracking. The top-down fatigue cracking is being reassessed and re-implemented under the NCHRP 1-52 project, hence it will not be considered in this calibration. Additionally, the asphalt overlay reflective cracking model developed under the NCHRP project 1-41 was not implemented in the Pavement-ME software used in this calibration. The newest version ME Design software version 2.2 released on August 12^{th} 2015 successfully integrated this model in rehabilitation designs. Accordingly, the roughness model which takes into account the top-down fatigue cracking and reflective cracking among other distresses was excluded from this calibration.

1.3. Objective

This study was conducted to provide NDOT with performance models calibrated to Nevada's conditions for new and rehabilitated flexible pavements. For this purpose, the major tasks carried out in this research were:

- Develop a database consisting of Pavement-ME software inputs proper to Nevada such as materials, traffic loads, and climatic data.
- Collect NDOT's Pavement Management System Data relevant to the projects used in the calibration and validation process.
- Conduct the calibration of the MEPDG performance models for rutting and bottom-up fatigue cracking.
- Validate the local calibration factors and recommendations.
- Conduct a sensitivity analysis of the calibrated models to selected input parameters.

CHAPTER 2 LITERATURE REVIEW

2.1. Overview of the AASHTO MEPDG Design Method

The American Association of State Highways Officials (AASHO) funded the construction of the AASHO road test in Ottawa, Illinois. The purpose of this project was the study of the asphalt concrete (AC) and Portland cement concrete (PCC) performance under truck loading. This road test was the foundation of the empirical equations used to establish the AASHTO 1993 design guide. However, the AASHO road test was conducted in a single climatic area with limited material types and a single subgrade layer type. These drawbacks coupled with the empirical properties of the 1993 AASHTO design guide accentuated the need for an improved design procedure. The AASHTO Joint Task Force on Pavements (JTFP) undertook the responsibility of developing a new design guide under the NCHRP 1-37A, this guide eventually became the MEPDG.

The MEPDG combines mechanistic approaches used to characterize in-service pavement responses with empirical relationships used to relate pavement damage to distresses. The MEPDG covers the design of flexible and rigid pavements for new and rehabilitated sections taking into consideration material properties, traffic data, and climatic data. Rather than obtaining a structural thickness output the MEPDG allows the designer the freedom in selecting which distress level is more prominent as well as the respective failure reliability. Trial pavement designs are analyzed and the results are compared to distress reliability limits; if the design's distresses fail the performance criteria the design is rejected and the layer thicknesses are changed. Furthermore, the MEPDG is distinct from the AASHTO 1993 guide by the fact that it accommodates the user with three hierarchical levels of data input. The data inputs can be of high accuracy (laboratory/field measured) or less accurate (based on historical databases or regression equations). The three levels of data inputs defined in the MEPDG are as follows:

- Level 1: In this level the most accurate data is used. It is usually site specific and requires extensive field/laboratory testing such as dynamic modulus testing or nondestructive deflection testing (NDT).
- Level 2: The data used in this level is less accurate than level 1, historical regional databases or regression equations are commonly used.
- Level 3: For this level, software default values are used due to the lack of specific project data.

2.1.1. MEPDG Methodologies & Concepts

The MEPDG introduced new concepts when defining project specific design inputs such as traffic, climate, and materials. These concepts are discussed briefly below:

Materials

One of the main breakthroughs in the MEPDG is the introduction of the visco-elastic properties of the asphalt materials. This allows the software to take into consideration the time-temperature dependency of the asphalt materials. Instead of assigning a single modulus for the asphalt concrete, the dynamic modulus and the binder viscosity properties are introduced, resulting in a more adequate structural response under different temperatures and traffic loadings. Another input that makes the MEPDG a state-of-art design method is the addition of the base and subgrade gradation properties and soil water characteristic curve (SWCC) parameters, those help predict the change in moisture and temperature profiles along the pavement section.

Climate

The MEPDG introduced the Enhanced Integrated Climatic Model (EICM) that uses temperature and heat flow to predict the change in pavement and unbound materials behavior. The EICM uses historical data from nearby weather stations to predict the temperature profile in the pavement layers, the moisture content and the freeze/thaw depth that can greatly affect the pavement's load bearing capacity.

Traffic

MEDPG shifted from Equivalent Single Axle Load (ESAL) used in the AASHTO 1993 to a more accurate representation of the truck loading that requires axle load distribution/spectra for different vehicle classes. This traffic analysis requires the collection of Weigh in Motion (WIM) data for each specific project. NDOT's Traffic Monitoring Systems (TMS) efforts to collect WIM, Automatic Vehicle Classification (AVC), and traffic counts data have been very successful in defining the truck traffic vehicle loads and distribution, which is a very essential input in the MEPDG design.

2.1.2. MEPDG Software

The latest version of the AASHTOWare Pavement-ME software (MEDesign Version 2.1.22) used in this calibration is the result of eight years of development and monitoring by AASHTO and NCHRP agencies. This version includes multiple corrections and enhancements from the previous versions. The major enhancement made to this software is the capability to analyze backcalculation data and utilize it in the thickness optimization for each station. The backcalulation report contains specific distresses for each station along with the required design layer thicknesses for the different stations. This is very important for overlay designs since the inclusion of Non-Destructive testing (NDT) data in the analysis generates more accurate results.

Another major enhancement made to the software is the introduction of the subgrade modulus in the sensitivity analysis. This is very important because in some cases the subgrade modulus varies along the project. The effects of the modulus change on the pavement performance can be captured by the sensitivity analysis. Additionally, the new version of the ME-Design software offers the option of automatic update.

The main issue still to be resolved in future versions is the effect of the depth of water table on pavements' performance. The NCHRP study 1-47 proved that for a depth of water table exceeding 12 feet the effect on the pavement distresses is very minimal. Nevertheless, the software fails to show any influence of the water table on predicted distresses even for values smaller than 12 feet.

2.2. Calibration Methodologies

Calibration is typically any mathematical process used to eliminate bias and increase precision between two sets of data. Bias is defined as the difference between the mean of a set of data and a reference value. Precision, on the other hand, is a measure of variability in the data, lower precision is observed when the data is more scattered. Figure 2.1 below outlines the difference between bias and precision. In pavement applications, biased models usually result in under or over-designed pavements sections. In order to eliminate the bias and improve the precision of the MEPDG models the residual error between measured and software predicted distresses is minimized resulting in a more adequate model prediction that represents actual field conditions.

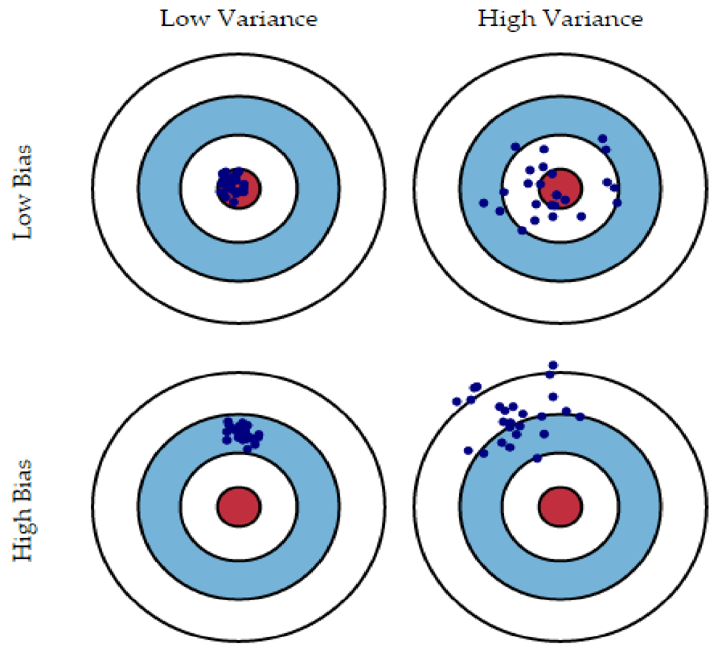

Figure 2.1- Example of Bias and Precision (Scott Fortmann-Roe, 2012)

Calibration is a two-phased process consisting first of running a simulation section representing a constructed field section using actual layer thicknesses, material properties, climate, traffic loads using the nationally calibrated model to predicted distresses. Then comparing the field measured distresses to software predicted distresses. In this step, numerical optimization is used to change the prediction models factors in order to eliminate the error between the sets of data and to obtain a good fit.

2.2.1. Statistical Method for MEPDG Calibration

The statistical approach consists of comparing software predicted distresses for specific road segments to actual field measurements. The first step in assessing the local bias and variability is comparing the mean predictions from the national calibration models to actual field measurements. This requires plotting the predicted versus measured distresses. Figure 2.2 below shows an example of predicted versus measured total rutting.

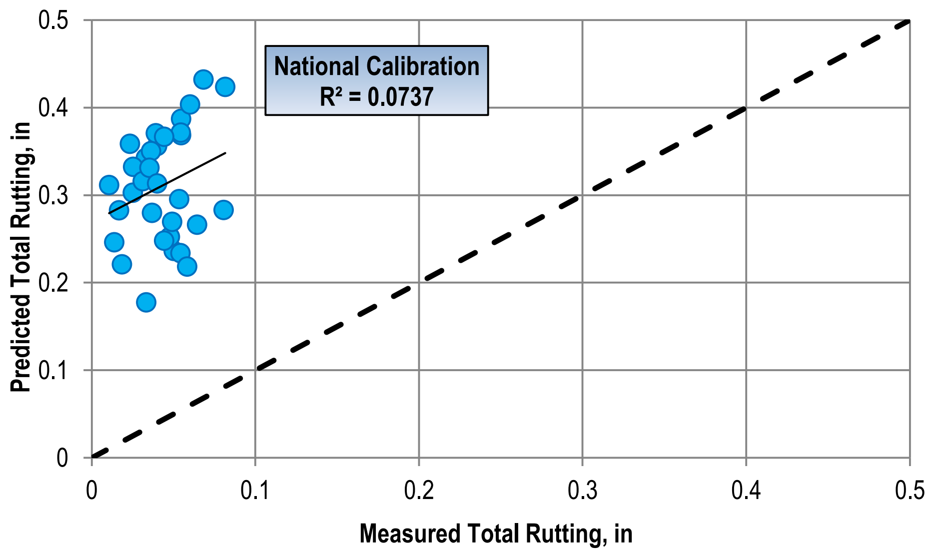

Figure 2.2-Predicted vs measured Rutting using the National Calibration Models.

Figure 2.2 outlines the difference between the software predicted values and the equality line which represents the null hypothesis. This hypothesis states that there is no bias or variability between measured and predicted values. The null hypothesis is described as follows:

$$H_0 = \sum(y_{predicted} - x_{measured}) \tag{2.1}$$

where:

$y_{predicted}$ =Predicted value using the model, and

$x_{measured}$ =Actual Measured Value.

The model's regression parameters are then calculated (intercept, slope, and R-square), and the decision of accepting or rejecting the hypothesis is made. If the hypothesis is rejected a recalibration of the model becomes necessary. For the purpose of the calibration the following equations were used:

$$\text{Error}_i = predicted_i - measured_i \tag{2.2}$$

$$Sum\ of\ errors = \sum Error_i \tag{2.3}$$

$$SSE = \sum (Error_i)^2 \tag{2.4}$$

$$SE = \sqrt{\frac{SSE}{N-1}} \tag{2.5}$$

$$R^2 = 1 - \left[\left(\frac{N-v}{N-1}\right) * \left(\frac{S_e}{S_y}\right)^2\right] \tag{2.6}$$

where:

i = Data observation,

N = Total number of data points,

R^2 = Coefficient of correlation,

v = Number of regression coefficients, and

Sy = Standard deviation of the measured data.

To minimize the variability in the data the sum of squared errors (SSE) should be reduced. This number represents the absolute value of the errors, thus reducing SSE would lead to a lower bias in the data. The optimization was conducted using the Microsoft Excel Solver by changing beta factors in the performance model in order to obtain the best fit. The solver option used in Microsoft Excel is the Generalized Reduced Gradient (GRG2) algorithm used for smooth nonlinear problems developed by Lasdon (1978). The Microsoft Excel solver uses the trial "plugging in" method which consists of iteration runs and observing the results calculated by the optimum and constraint cells. This method is more time efficient than the typical "trial and error" method because it adjusts trial values depending on the output variation to save a lot of optimization time.

To present the optimization process the rutting calibration is discussed below. In the case of rutting the Equation 2.7 is used to calculate the total accumulated deformation in the AC layer. The Equation 2.8 below represents the MEPDG rutting model for unbound materials, it is used for the granular base and the subgrade separately.

$$\frac{\varepsilon_p}{\varepsilon_r} = k_z * \beta_{r1} * 10^{k1} * T^{k1\beta r1} * N^{k3\beta r3} \tag{2.7}$$

where:

εp = Accumulated plastic strain in the AC layer (in./in.),

εr = Resilient or elastic strain at the mid-depth of each AC sublayer (in./in.),

k_z = Factor for depth confinement correction,

T = Pavement temperature (°F),

N = Number of axle-load repetitions,

k_1, k_2, k_3 = Field calibration parameters, district dependent for Nevada's mixtures, and

$\beta_{r1}, \beta_{r2}, \beta_{r3}$ = Local field calibration parameters set at 1.0 in the NCHRP national calibration.

The permanent AC deformation is calculated by multiplying the accumulated plastic strain by the total Hot Mix Asphalt (HMA) layer thickness.

$$\delta_a(N) = \beta_{s1} k_1 * \varepsilon_v * h \left(\frac{\varepsilon_0}{\varepsilon_y}\right) e^{-\left(\frac{\rho}{N}\right)^{\beta}} \tag{2.8}$$

Where:

δ_a = Permanent deformation for the layer/sub-layer (in.),

N = Number of axle-loads repetitions,

ε_v = Average vertical resilient strain in the layer/sub-layer calculated from the structural response model,

h = Thickness of the unbound layer (in),

ε_r = Resilient strain imposed in laboratory test to obtain material properties ε_o, β and ρ, (in./in.),

ε_o, β, and ρ = Material properties obtained from imposed resilient strain in the laboratory,

β_{s1}= Local calibration coefficient use for the unbound base layer (β_b) or subgrade layer (β_{sg}),

k_1 = National calibration coefficient, equal to 2.03 for granular materials and 1.35 for fine-grained materials,

The total predicted rut depth is obtained by adding the AC rutting, granular base rutting and the subgrade rutting. The calibration was conducted following these steps. First, the AC rutting factors β_{r2} and β_{r3} were changed in the software. In this calibration, 16 factor combinations were run in the Pavement-ME software as β_{r2} and β_{r3} were assigned the values of 0.7, 0.8, 0.9 and 1.0. The results obtained for every combination of β_{r2} and β_{r3} were compared to actual field measurements. The AC rutting was first optimized by minimizing the sum of square errors between measured and predicted AC rutting. This was done by multiplying the predicted AC rutting value by β_{r1}. Table 2.1 below shows an example of optimization results, in this case β_{r1} is changed from 1.0 to 0.1405. Figure 2.3 illustrates an example of the AC layer rutting calibration.

Table 2.1-Sum of Square Errors Optimization Example for Asphalt Rutting.

	Before Optimization	After Optimization
Sum Error Asphalt	1.2509	0.00344
Sum Error Square Asphalt	0.1035	0.0004

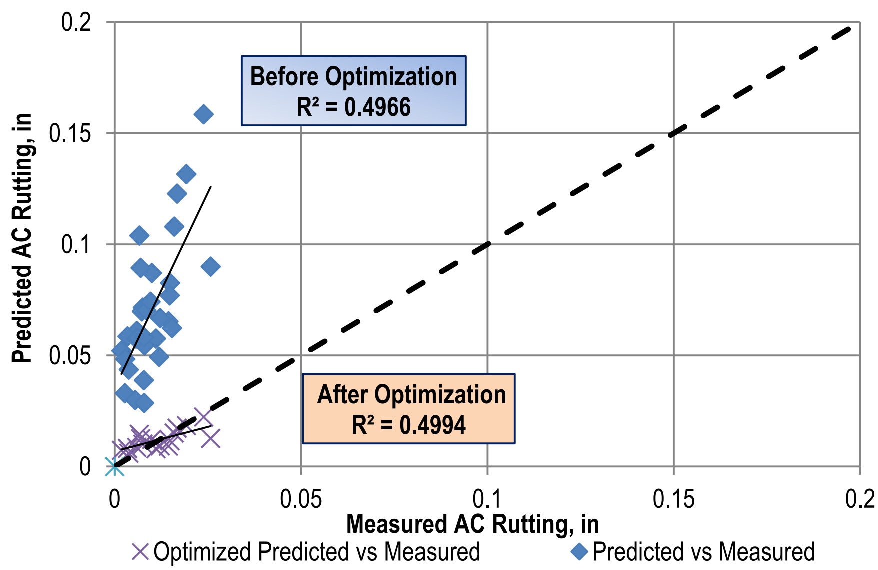

Figure 2.3- Predicted vs Measured AC Rutting Calibration Example.

The following step is the optimization of the base and subgrade factors β_{base} and $\beta_{subgrade}$. These factors are linear multipliers similar to the β_{r1} factor for the AC. The total rutting is calculated using the following Equation 2.9 below.

$$Total\ Rutting = \beta_{r1} * ACRut + \beta_b * BaseRut + \beta_{sg} * SGRut \quad (2.9)$$

The sum of square errors for the total rutting is minimized using β_{r1} from the AC rutting optimization and changing the calibration factors for base and subgrade. In this example

β_{base} is changed from 1.0 to 0.199 and $\beta_{subgrade}$ from 1.0 to 0.0506. Table 2.2 and Figure 2.4 below present the optimization results for the total rutting calibration.

Table 2.2-Sum of Square Errors Optimization Example for Total Rutting.

	Before Optimization	After Optimization
Sum Error Total Rutting	-3.5358	0.0046
Sum Error Square Total Rutting	0.7741	0.0043

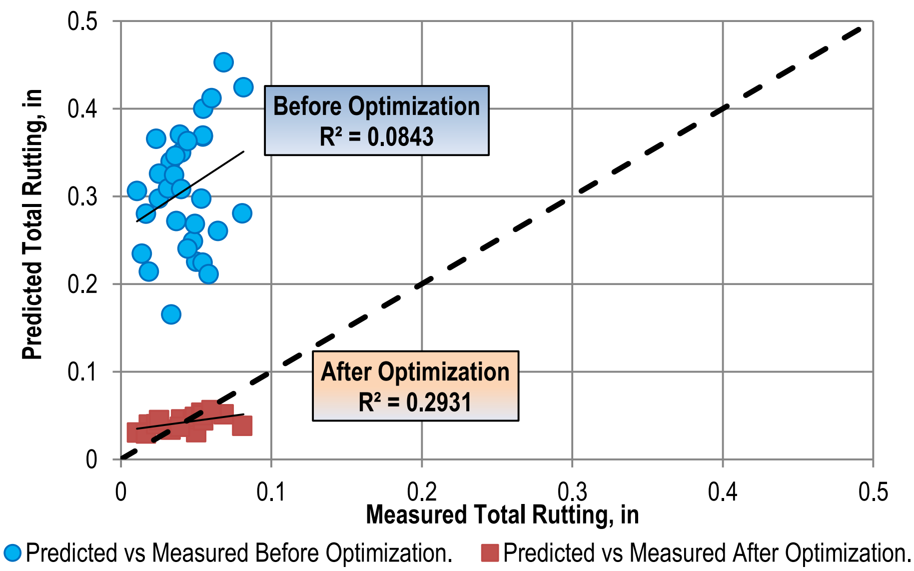

Figure 2.4-Predicted versus Measured Total Rutting Calibration Example.

2.3. Calibration Experiences

The MEPDG national calibration was performed using the LTPP database that contains data from all across the United States. This data does not specifically represent the climate, materials, and traffic conditions found in the state of Nevada. The recalibration or local calibration of these distress prediction models is necessary in order to obtain accurate results that can be related to actual pavement field performance. This section contains a brief discussion of the calibration and implementation methodologies on both the national and local level.

2.3.1. National Calibration

The national calibration was conducted under the NCHRP project 1-37A. This project produced a mechanistic-empirical design guide along with software and training materials. The design guide covered new and rehabilitated sections for both flexible and rigid pavements. This section illustrates the national calibration process for rutting and fatigue cracking in flexible pavements.

2.3.1.1. Rutting Calibration

Rutting is a major distress in flexible pavements that is caused by the accumulation of permanent strains in the pavement layers. The initial rutting equation related permanent deformation to temperature and load repetition. Equation 2.10 below shows the asphalt rutting model prior to the national calibration.

$$\frac{\varepsilon_p}{\varepsilon_r} = 10^{k1} * T^{k2} * N^{k3} \tag{2.10}$$

where:

εp = Accumulated plastic strain in the AC layer (in./in.),

εr = Resilient or elastic strain at the mid-depth of each AC sublayer (in./in.),

T = Pavement temperature (°F),

N = Number of axle-load repetitions,

K_1, K_2, K_3 = Regression coefficients where K_1 = -3.1552, K_2 = 1.734, and K_3 = 0.39937.

The national calibration conducted by El-Baysouni et al. (2002) introduced a factor K_z to take into consideration the thickness of the asphalt layer and modified the regression coefficients K_1, K_2, K_3 by adding a coefficient multiplier. Equation 2.11 below shows the calibration of the asphalt rutting model.

$$\frac{\varepsilon_p}{\varepsilon_r} = k_z * \beta_{r1,National} * 10^{k1} T^{k2*\beta_{r2,national}} N^{k3*\beta_{r3,National}} \quad (2.11)$$

The calibration was performed on a large number of sections from the LTPP project. The purpose of this calibration was to increase the precision of the predictions. Simulation runs were initially conducted using $\beta_{r2,\ National}$ *and* $\beta_{r3,\ National}$ for values of 0.8, 1.0, and 1.2. Additional runs were required in order to capture the best factor combination. It was found that the combination of $\beta_{r2,\ National}$ *and* $\beta_{r3,\ National}$ equal to 0.9 and 1.2 was producing the best results. The optimization was run using these values to minimize the sum of errors between measured and predicted rutting. The final set of calibration factors were $\beta_{r1,\ National}$ =0.509, $\beta_{base,\ National}$=1.674, and $\beta_{subgrade,\ National}$=1.35. Equation 2.12 below shows the final nationally calibrated asphalt rutting model.

$$\frac{\varepsilon_p}{\varepsilon_r} = k_z 10^{-3.35412} T^{1.5606} N^{0.479244} \quad (2.12)$$

2.3.1.2. Fatigue Calibration

Fatigue cracking is a pavement distress related to structural inadequacy. The fatigue cracking model is based on Miner's law of cumulative damage. The damage being the ratio between the cumulative predicted load repetitions to the allowable number of load repetition as shown in Equation 2.13. The calibration of the fatigue cracking model was conducted by El-Basyouny and Witczak (2002).

$$Damage = \sum_{i=1}^{T} \frac{n_i}{N_i} \quad (2.13)$$

where:

T= total load interval,

n= actual load repetitions for period i,

N=allowable load repetitions to failure for period i.

The allowable load repetitions is expressed as a function of the tensile strain at a given depth and the asphalt layer modulus. The MEPDG fatigue cracking model was given by the Equation 2.14 below.

$$N_f \;= K_1 * \;\beta_{f1,National} * \left(\frac{1}{\varepsilon_t}\right)^{\beta_{f2,National} * \;K_2} * \left(\frac{1}{E}\right)^{\beta_{f3,National} * \;K_3} \tag{2.14}$$

where:

N_f = Allowable number of load repetitions to fatigue cracking

ε_i = Tensile strain at the critical location, in/in

E = Dynamic modulus of the asphalt material (psi)

$\beta_{f1,National}, \beta_{f2,National}, \beta_{f3,National}$= National calibration factors.

K_1, K_2, K_3 = Material constants from laboratory testing

$K_1 = 0.00432 * C$, $C = 10^M$, $M = 4.84(\frac{V_b}{V_a + V_b} - 0.69)$, $K_2 = 3.291$, $K_3 = 0.854$.

The national calibration focused on eliminating the bias between the model predictions and field measurements. Therefore, multiple combinations of the strain and dynamic modulus calibration factors were used in simulation runs. These factors are shown in Table 2.3 below.

Table 2.3- National Calibration Factors for Fatigue Simulations.

Combination Number	βf2	βf3
1	0.8	0.8
2		1.5
3		2.5
4	1.0	0.8
5		1.5
6		2.5
7	1.2	0.8
8		1.5
9		2.5

The combination number 9 (1.2, 2.5) from the Table 2.3 above resulted in the lowest error. The final nationally calibrated fatigue cracking model is shown in the Equation 2.15.

$$N_f = 0.00432 * C * 0.007566 * \left(\frac{1}{\varepsilon_t}\right)^{3.9492} * \left(\frac{1}{E}\right)^{1.281} \quad (2.15)$$

Bottom-up fatigue transfer function

Bottom-up fatigue or alligator cracking is usually more prone in thin asphalt pavements. The cracking initiates at the bottom of the asphalt layer where the tensile stress is the highest and propagates to the surface. In the MEPDG, bottom-up fatigue cracking is estimated using a sigmoidal function. This function is given in the Equation 2.16 below.

$$FC = \left(\frac{6000}{1+e^{C1-C2Log(D)}}\right) * \frac{1}{60} \quad (2.16)$$

where:

FC=Fatigue cracking as a percentage of the total lane area (%),

D= Damage (%), and

C_1, C_2 = Regression coefficients.

This equation was based on two assumptions (El-Baysouni et al., 2002):

- The fatigue cracking is best expressed as a function of damage using a sigmoidal mathematical function. This relationship is limited by 0 ft^2 cracking as a minimum and 6000 ft^2 cracking as a maximum (total section area 12ft*500ft).
- For a damage of 100% the alligator cracking is at 50%.

The national calibration used the damage predictions from Miner's law to estimate the damage for the different sections in the database. The damage was then introduced in the sigmoidal function and the results were compared to actual field observations. The regression coefficients were optimized to reduce the sum of errors between the measured and predicted values. This resulted in the following Equation 2.17 below. Figure 2.5 represents the fatigue cracking as a function of the damage.

$$FC = \left(\frac{6000}{1+e^{C_1 * C'_1 + C_2 * C'_2 Log(Damage)}}\right) * \frac{1}{60} \tag{2.17}$$

where:

$C_1 = C_2$= Local calibration coefficient= 1.0 for the national calibration,

$C'_2 = -2.40874 - 39.748 * (1 + h_{ac})^{-2.856}$, and

$C'_1 = -2 * C'_2$.

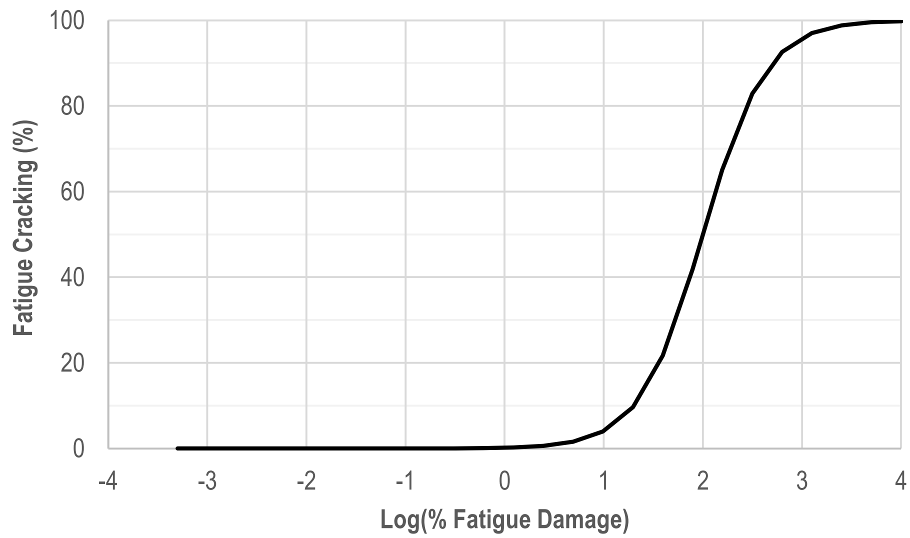

Figure 2.5-Nationally Calibrated Bottom-Up Fatigue Cracking Transfer Function.

Top-Down cracking transfer function

The top-down fatigue cracking is a characteristic of thick pavement sections. It is caused by a combination of high surface tensile stresses and binder hardening. Top-down fatigue cracking is also estimated from the calculated damage by a sigmoidal function shown in Equation 2.18 as follows. The national calibration focused on reducing the sum of errors to improve the fit of the data and reduce bias. The final regression coefficients were 7 and 3.5 for C_1 and C_2, respectively. Figure 2.6 illustrates the longitudinal cracking as a function of the damage.

$$FC = \left(\frac{1000}{1+e^{C1-C2Log(D)}}\right) * 10.56 \qquad (2.18)$$

where:

$F.C.$ = Longitudinal cracking (ft/mile)

D = Damage in percentage

C_1, C_2 = Regression coefficients

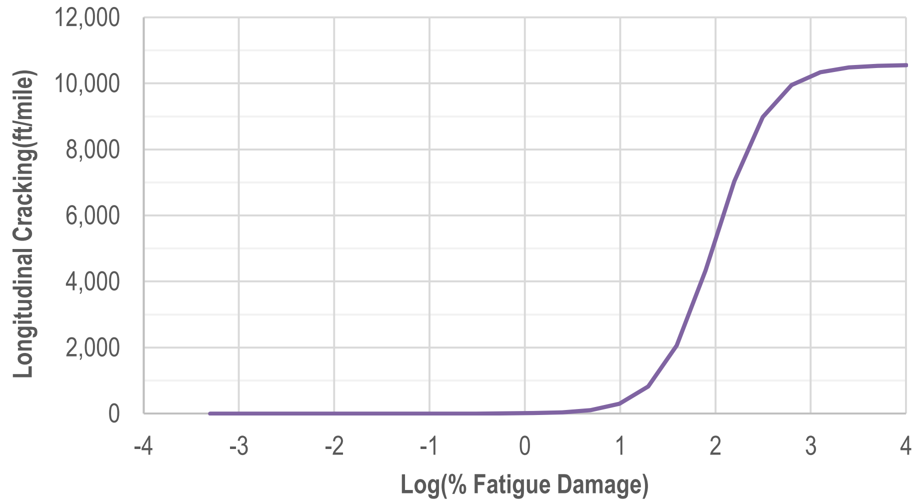

Figure 2.6-Nationally Calibrated Top-Down Fatigue Cracking Transfer Function.

2.3.1. Local Calibration

The MEPDG calibration was completed in several states across the country while others are still in the process of transitioning from previously used design methods. This section summarizes some of the work completed by different states.

Utah

Darter et al. (2009) performed the MEPDG calibration of flexible and rigid pavements for the Utah Department of Transportation (UDOT). The calibration was conducted using the goodness of fit method as outputs from MEPDG prediction models were compared to Utah's measured distress data. Linear regression was used to calculate the bias in the distress predictions. The regression was then compared to the null intercept hypothesis using a significance level of 5 percent. This test determines whether the linear analysis has an intercept equal or significantly different than zero. The second hypothesis verified whether the regression had a slope of 1.0 at the same 5 percent reliability level. It should be noted that a linear regression with an intercept of zero and a slope of 1.0 gives the lowest bias between measured and predicted data.

In this study, the roughness model was tested using the paired t-test to determine whether the data belonged to the same population. The calibrated models passed all the tests which validated the calibration process. The study concluded that the calibrated rutting models improved the predictions whereas the calibrated alligator cracking model was only valid at low cracking levels. The study also recommended a continuation of level 1 data inputs collection for further recalibration; this complements UDOT's efforts to completely remove Marshall mix designs mixtures from the calibration database and replace them by HMA Superpave mixes.

Arizona

Souliman et al. (2009) from Arizona State University (ASU) developed a local calibration for the state of Arizona. HMA rutting, fatigue and roughness models were calibrated. The calibration used data from 37 LTPP sections to correlate between software predictions and field measured distresses. The findings confirmed that the nationally calibrated model was under estimating alligator cracking and AC rutting while over estimating the longitudinal cracking and the subgrade rutting. The research recommended more material testing to improve the data accuracy (level 1 inputs) and continuous monitoring of new pavement sections in order to conduct future recalibrations to increase the precision of the models.

North Carolina

The North Carolina calibration was conducted by Kim et al. (2011) using a total of 46 sections. The prediction models calibration was performed using 22 LTPP sections as theses sections contained complete distresses and materials information. The remaining 24 non-LTPP sections were used to validate the calibrated models. The calibration in this study used two optimization approaches, the first one was run using the generalized reduced gradient, and the second approach used the genetic algorithm (GA) technique. The genetic algorithm differs from the GRG method by the fact that it is a non-smooth optimization process. Another characteristic of the GA is the selectiveness freedom within the database. The algorithm can eliminate sets of data if they are found to be a bad fit within the constraints of the problem which helps to avoid getting stuck at certain optimum values. The local calibration successfully reduced the bias and standard deviation in the flexible pavement rutting and fatigue cracking. However, it was recommended that an extensive project specific data collection effort should be conducted in order to increase the validity of the calibration as some LTPP sections demonstrated irregularities in distresses: some sections had decreasing rutting with time when no maintenance works were performed. The study also focused on characterizing 12 sampled asphalt mixtures and stressed on the importance of using local k factors to reduce the variability of the predictions. The research suggested including additional mixtures that represent new asphalt technologies such as reclaimed asphalt pavement (RAP) in order to have a representative database for all paving mixtures.

Oregon

Oregon's researchers (Williams et al., 2013) looked into the MEPDG nationally calibrated models and found that for Asphalt Concrete sections the software was over predicting the rutting notably in the subgrade layers. The alligator and thermal cracking predictions were found to be under-predicting distresses compared to the actual field measurements. The calibration was conducted using the sum of square error optimization for rutting, fatigue, and thermal cracking. Twelve combinations of β_{r2} *and* β_{r3} were used in the software for rutting as shown in the Table 2.4 below.

Table 2.4- Different β_{r2} and β_{r3} Values used in the Rutting Calibration.

Combination Number	βf2	βf3
1	0.8	0.8
2		0.9
3		1
4		1.2
5	1	0.8
6		0.9
7		1
8		1.2
9	1.2	0.8
10		0.9
11		1
12		1.2

The rutting and alligator fatigue cracking calibration helped eliminate the bias and improve the accuracy of the results. The longitudinal cracking calibration, although providing reasonable results, was still showing a high degree of variability. This raised questions concerning the practicality of the current longitudinal cracking model. The study also recommended the addition of more projects towards a more developed database along with supplementary level 1 input data to increase the precision of future recalibrations.

Iowa

The researchers (Ceylan et al., 2013) at the Institute for Transportation at Iowa State University used advanced sensitivity analysis of the MEPDG inputs to come to a better understanding of the prediction models' calibration process. The calibration used a total of 35 Jointed Plain Concrete Pavement (JPCP), 35 HMA sections, and 60 composite pavement sections. It was found that locally calibrated models for JPCP faulting, transverse cracking and IRI improved the accuracy of the predictions and reduced the scatter. For asphalt pavements, it was established that the national rutting model overestimated granular base and subgrade deformation while underestimating the HMA rutting; the local model improved the predictions. Top-down cracking models were optimized to reduce the error. However, a good correlation was found between the national model predictions and Iowa's pavement performance for bottom-up fatigue cracking and roughness.

Colorado

The investigation performed by researchers at Colorado looked into the MEPDG model calibration for flexible and rigid pavements (Mallela et al., 2013). The calibration/validation database covered one hundred twenty-six new HMA, new JPCP, HMA over JPCP, and JPCP over JPCP pavements. Optimization was run to increase the goodness of fit between measured and predicted data. The calibrated models improved all the predictions for major distresses. The Colorado calibration focused a lot on model verification; as a result, simulation design runs were conducted using MEPDG and compared to designs obtained using older methods and practices. Additionally, Colorado Department of Transportation (CDOT) looked into calibrating the standard deviation models in order to more properly represent the field observations in Colorado. Table 2.5 below shows a comparison between the nationally calibrated and the CDOT standard deviation functions. Higher rutting is observed in the Colorado models for AC, base, and subgrade as illustrated in Figures 2.7 to 2.9 below. Figure 2.10 presents a comparison between the Colorado fatigue standard deviation model and the nationally calibrated model. The Colorado models predicts higher fatigue deviation.

Table 2.5-Standard Deviation Equations Comparison.

Standard Deviation Model	Nationally Calibrated	Colorado Models
AC Rutting	$0.24 * ACRut^{0.8026} + 0.001$	$0.2052 * ACRut^{0.4} + 0.001$
Base Rutting	$0.1477 * BASERut^{0.67} + 0.001$	$0.2472 * BASERut^{0.67} + 0.001$
Subgrade Rutting	$0.1235 * SUBRut^{0.5} + 0.001$	$0.1822 * SUBRut^{0.5} + 0.001$
Alligator Cracking	$1.13 + \frac{13}{e^{7.57-15.5\log(damage+0.0001)}}$	$1 + \frac{15}{e^{-1.6673-2.4656\log(damage)}}$
Transverse Cracking	$0.1468 * TRANS + 65.027$	$0.1468 * TRANS + 65.027$
Longitudinal Cracking	$200 + \frac{2300}{1 + e^{1.072-2.1654\log(damage+0.0001)}}$	

where:

ACRut = Predicted rutting in the asphalt layers (in.),

BaseRut = Predicted rutting in the base layers (in.),

SubRut = Predicted rutting in the subgrade layers (in.),

Damage = Predicted bottom-up or top-down damage respectively (%), and

Trans = Predicted transverse cracking (feet/mile).

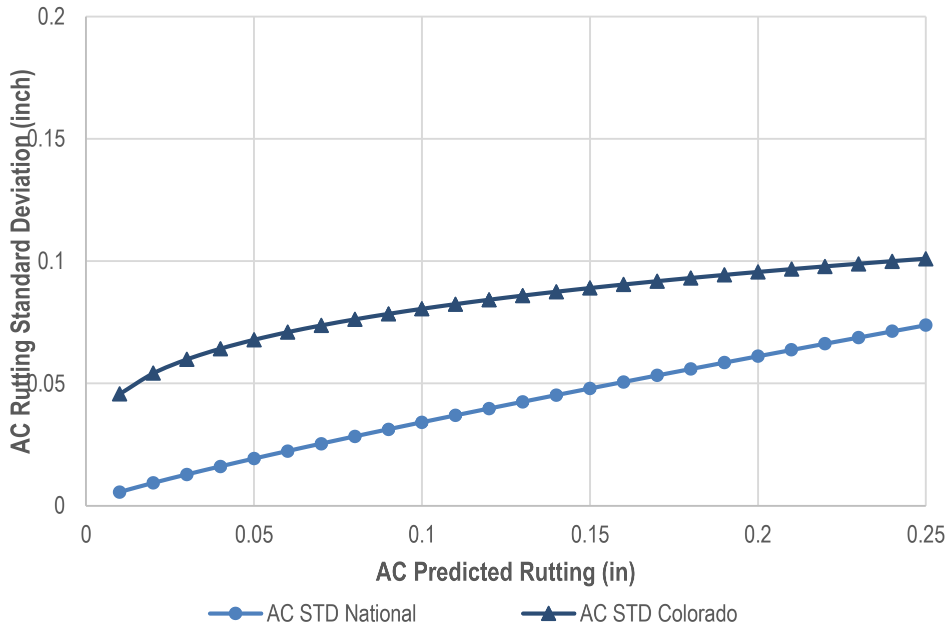

Figure 2.7-Colorado AC Rutting Standard Deviation Model.

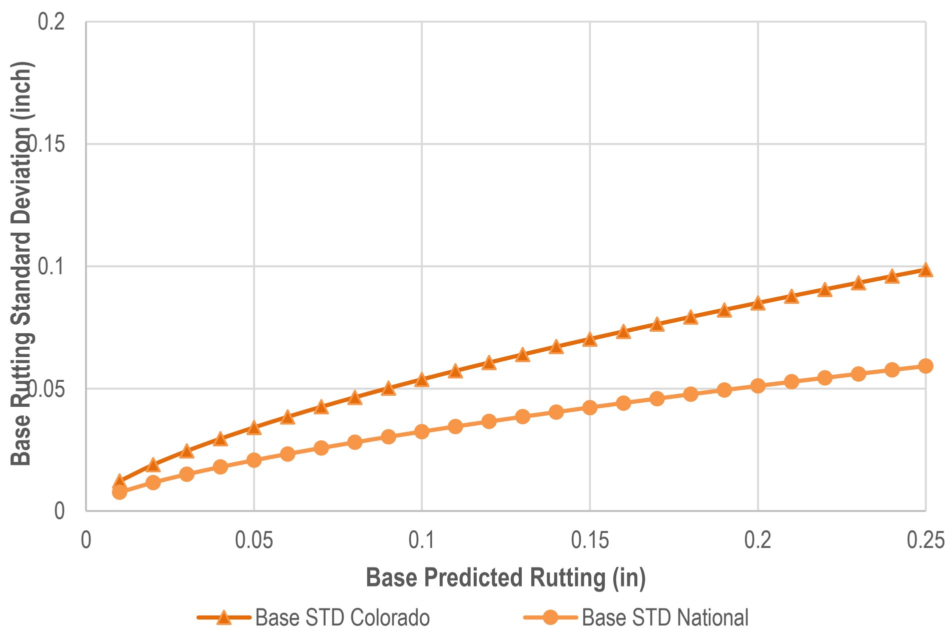

Figure 2.8-Colorado Base Rutting Standard Deviation Model.

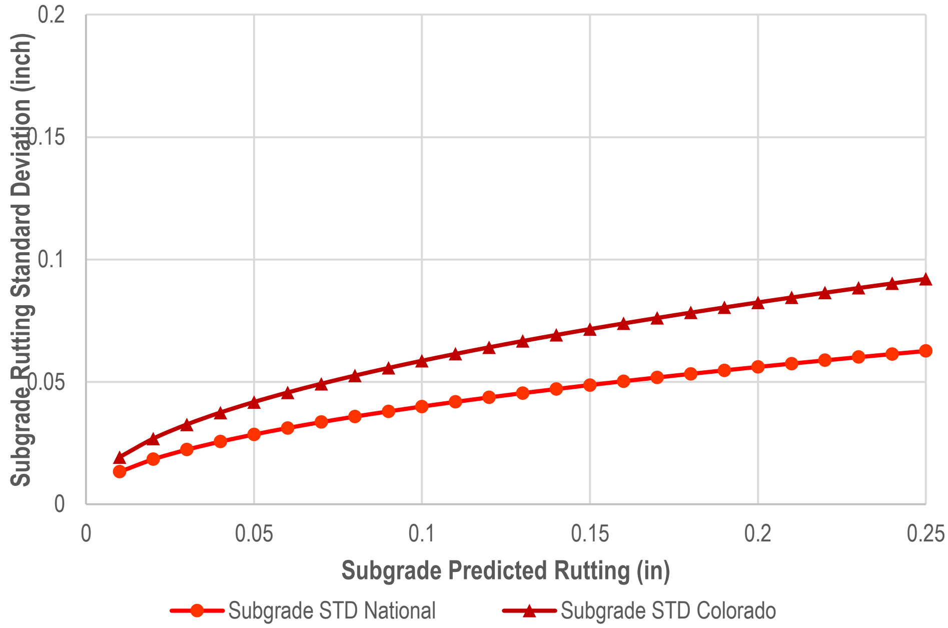

Figure 2.9-Colorado Subgrade Rutting Standard Deviation Model.

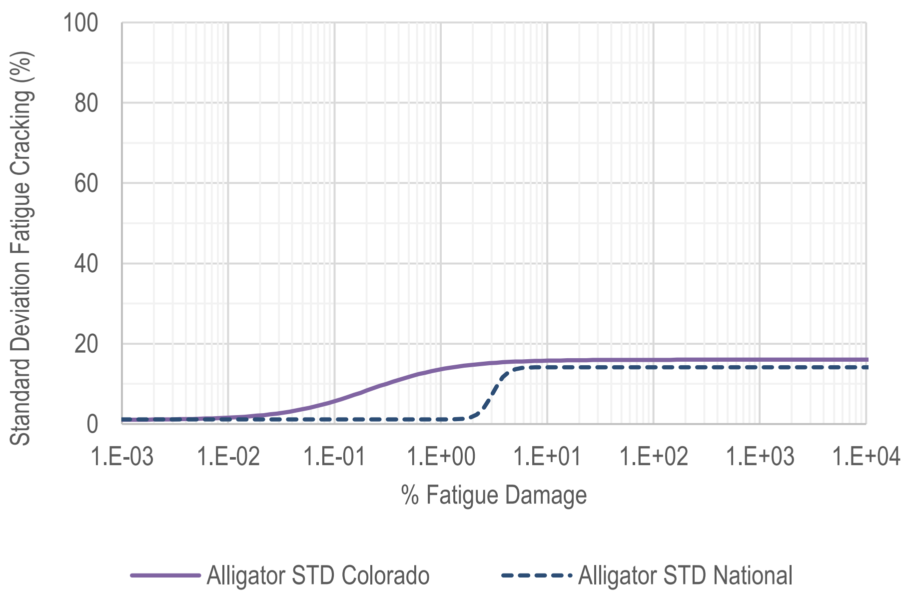

Figure 2.10-Colorado Fatigue Cracking Standard Deviation Model.

Summary

This section summarizes the local calibration models from the various studies examined above. Table 2.6 presents the different sets of local calibration factors for rutting, fatigue, and roughness. Figure 2.11 illustrates the longitudinal cracking transfer function and Figure 2.12 shows the alligator cracking transfer function for the different models.

Table 2.6- Calibration Factors Summary from Different States

Distress	Calibration Factors	National Model	Utah	Arizona	North Carolina	Oregon	Iowa	Colorado
AC Rutting	β_{r1}	1	0.56	0.69	0.9475	1.48	1	1.34
	β_{r2}	1	1	1	0.8622	1	1.15	1
	β_{r3}	1	1	1	1.3539	0.9	1	1
Base Rutting	β_b	1	0.604	0.37	0.5377	0	0	0.4
Subgrade Rutting	β_{sg}	1	0.4	0.14	1.5	0	0	0.84
Fatigue Cracking	β_{f1}	1	1	249.009	3.5	1	1	130.367
	β_{f2}	1	1	1	0.7236	1	1	1
	β_{f3}	1	1	1.233	0.6	1	1	1.218
Bottom-Up Cracking	C_1	1	1	1	0.2438	0.56	1	0.07
	C_2	1	1	4.5	0.2438	0.225	1	2.35
	C_3	0	0	0	0	0	0	0
	C_4	6,000	6,000	6,000	6,000	6,000	6,000	6,000
Longitudinal Cracking	C_1	7	7	7	7	1.453	0.82	7
	C_2	3.5	3.5	3.5	3.5	0.097	1.18	3.5
	C_3	0	0	0	0	0	0	0
	C_4	1,000	1,000	1,000	1,000	1,000	1,000	1,000
IRI	C_1	40	40	1.228	40	40	40	35
	C_2	0.4	0.4	0.118	0.4	0.4	0.4	0.3
	C_3	0.008	0.008	0.008	0.008	0.008	0.008	0.02
	C_4	0.015	0.015	0.028	0.015	0.015	0.015	0.019

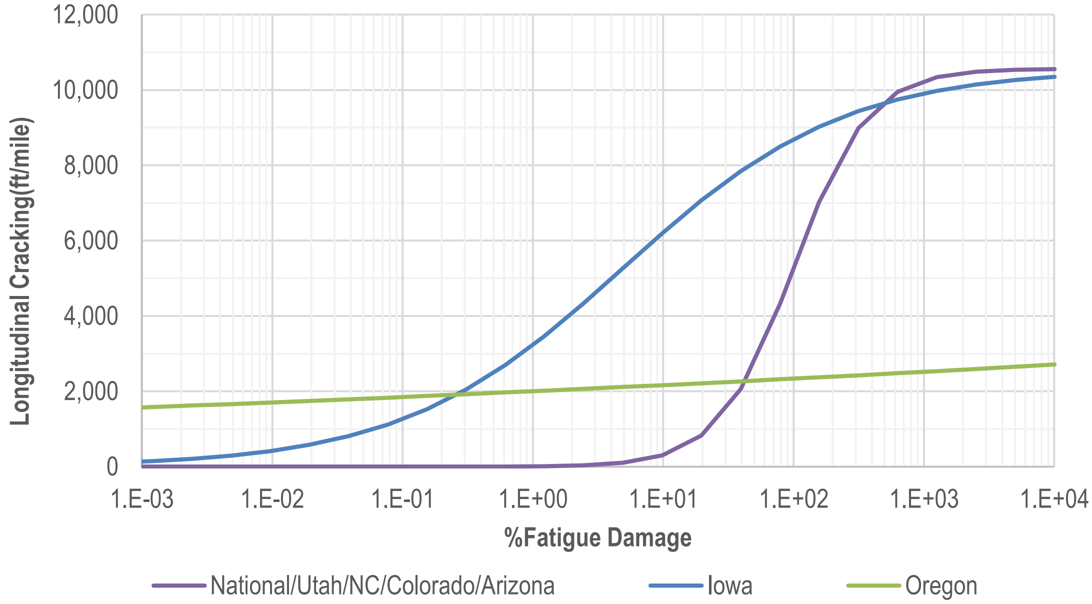

Figure 2.11-Longitudinal Cracking Transfer Function from Different States' MEPDG Calibration.

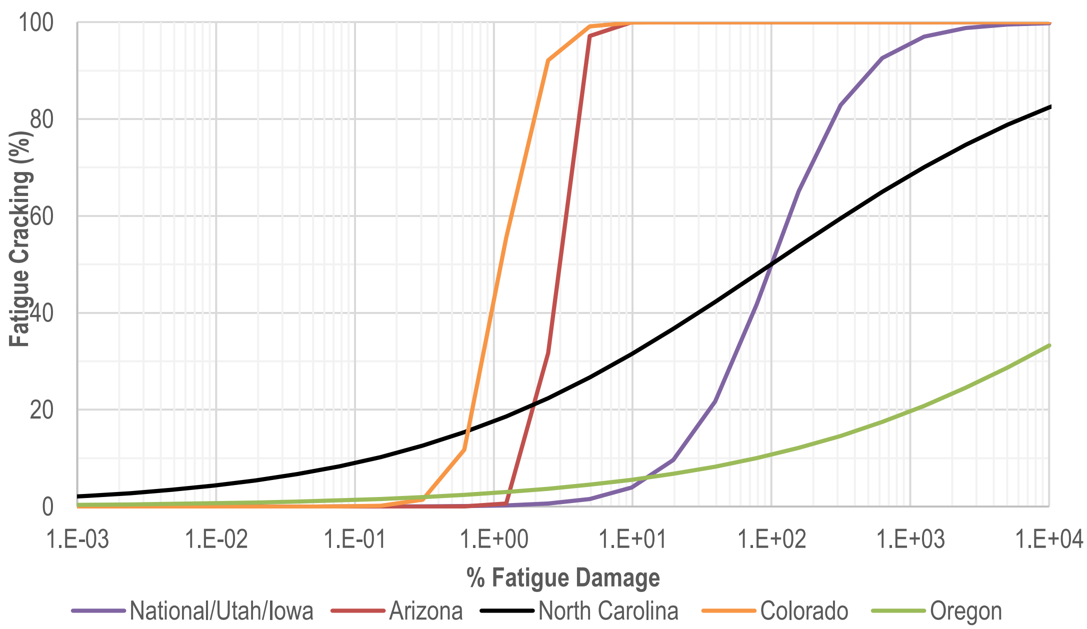

Figure 2.12-Alligator Cracking Transfer Function from Different States' MEPDG Calibration.

Figure 2.11 clearly shows that in the case of Oregon calibration the transfer function does not have the full sigmoidal shape within the standard damage range. The model from Iowa predicts high longitudinal cracking for low damage values as opposed to the national prediction models. From Figure 2.12 the Oregon model is highly different than the national model and seems to predict lower fatigue cracking values (30%) for high damage. The Colorado and Arizona transfer functions predict high fatigue cracking for low fatigue damage: the cracking is at 100% for a damage of 5% in Colorado compared to 10000% damage in the national model. This is mainly due to the fact that the initial assumptions for the fatigue cracking transfer function (50% cracking for a 100% damage) were not respected. This assumption is only verified when C_1=C_2. This was not the case for Oregon (C_1=0.56; C_2=0.225), Arizona (C_1=4.5; C_2=1.0), and Colorado (C_1=0.07; C_2=2.35).

CHAPTER 3 DATA COLLECTION

The MEPDG local calibration is very sensitive to data collection. Accurate level 1 data increase the possibility of achieving a good calibration; whereas the results obtained using level 2 or 3 inputs might not be as representative of the local conditions and properties. Researchers at NDOT and UNR spent significant efforts in establishing an MEPDG database that represents the state's specific conditions. Feaster et al. (2012) worked on characterizing 26 field-produced asphalt mixtures to create a level 2 asphalt material database from level 1 laboratory testing. Pavement distresses from the NDOT pavement management system (PMS) database were converted to MEPDG distress units and compared to software outputs. Traffic data were collected using NDOT's traffic reports and web-based software. The detailed data collection procedure is explained in this section.

3.1. Asphalt Binders and Mixtures Characterization

The MEPDG implementation for the state of Nevada began in 2005 when the Western Research Superpave Center (WRSC) at UNR started the mixtures' evaluation project. Multiple asphalt mixtures were collected from the state's three districts (I, II, and III) and evaluated using laboratory performance testing for dynamic modulus, asphalt binder viscosity, Repeated Load Triaxial (RLT), and Flexural Beam Fatigue. The main purpose of this project was to create a level 2 regional material database from level 1 laboratory testing that takes into consideration the polymer-modified asphalt binders used in Nevada. This study looked into creating sub-groups based on asphalt binder or aggregate sources/types within the different districts. For every grouping an average value, standard deviation, and coefficient of variation were computed. Table 3.1 presents the list of sampled and characterized contracts used in the calibration. It is worth mentioning that 18 additional mixtures were collected and are currently being tested at the WRSC.

Table 3.1- List of Contracts Sampled for NDOT MEPDG Calibration.

Contract	District	Binder Grade	Sampling Year	County	Binder Source	Aggregate Source	Mix Type
3214	1	PG76-22NV	2005	Clark	KPA	Sloan	2C
3239	2	PG64-28NV	2005	Lyon	Paramount	Hunewill	2
3248	3	PG64-28NV	2005	Humboldt	KPA	HU 82-01	2C
3257	1	PG76-22NV	2005	Clark	Ergon	Blue Diamond	2
3247	1	PG76-22NV	2006	Clark	Ergon	Blue Diamond	2C
3260	1	PG76-22NV	2006	Clark	Ergon	Blue Diamond	2C
3274	1	PG76-22NV	2006	Clark	Ergon	Spring Mountain	2C
3312	1	PG 76-22NV	2007	Clark	SEM	Tecopa Pit	2
3325	1	PG76-22NV	2007	Clark	SEM	Blue Diamond	2C
3331	1	PG76-22NV	2007	Clark	SEM	Sloan	2C
3323	2	PG64-28NV	2007	Churchill	Paramount	CH 10-03	2
3330	3	PG64-28NV	2007	Humboldt	Idaho	Hunewill	2C
3329	3	PG64-28NV	2008	Elko	Idaho	EL 84-15 & EL 14-01	2C
3338	2	PG64-28NV	2008	Douglas & Carson	Paramount	Bertagnolli	2
3348	2	PG64-28NV(TR)	2008	Pershing	Paramount	PE 83-02	2C
3358	2	PG64-28NV	2008	Washoe	Paramount	Lockwood	2C
3348	2	PG64-28PM	2008	Pershing	Valero	PE 83-02	2C
3350	3	PG64-28PM	2008	Lander & Eureka	Valero	HU 83-08	2C
3368	2	PG76-22NV	2009	Lyon	Paramount	Bertagnolli	2
3372	3	PG64-28NV	2009	Humboldt	Valero	Imlay Pit	2C
3373	2	PG64-28NV	2009	Pershing	Paramount	PE 81-11	2C
3383	1	PG76-22NV	2010	Clark	Ergon	Lone Mountain	2C
3378	2	PG64-28NV	2010	Washoe	Paramount	Marietta	2C
3382	1	PG64-28NV	2010	Lincoln & Nye	Mountain States	LN 16-02	2
3399	2	PG64-28NV	2010	Washoe	Paramount	Lockwood	2C
3399	2	PG64-28 RAP	2010	Washoe	Paramount	Lockwood	2C

3.1.1. Asphalt Binder Viscosity

The asphalt binder viscosity was assessed using the Dynamic Shear Rheometer (DSR) test in accordance with AASHTO T315. This test measures the binder's complex shear modulus (G*) and phase angle (δ). G* is the binder's resistance to deformation under repeated shear deformation while (δ) is the time lag between the applied shear and the resulting strain which is an indication of the visco-elastic properties of the asphalt binder. The detailed results for 17 contract binders are summarized in Table 3.2 below. For the purpose of the MEPDG implementation the asphalt binder data were grouped into NDOT's three districts as presented in Table 3.3.

Table 3.2-Asphalt Binder Laboratory Measured Data.

Contract	Temp (°C)	G* (Pa)	Phase Angle δ (°)
3325	70	4,915	63.2
	76	2,905	65.5
	82	1,740	67.6
3331	64	7,355	58.9
	70	4,385	59.3
	76	2,680	60.3
3323	58	5,495	62.0
	64	3,115	63.1
	70	1,815	64.7
3330	58	5,030	70.2
	64	2,650	71.6
	70	1,435	73.5
3329	58	4,250	69.5
	64	2,290	71.0
	70	1,270	72.8

Table 3.2 -Asphalt Binder Laboratory Measured Data (cont.).

Contract	Temp (°C)	G* (Pa)	Phase Angle δ (°)
3338	58	6,200	63.0
	64	3,490	64.8
	70	2,010	67.1
3348_TR	58	6,795	65.5
	64	3,770	66.4
	70	2,160	67.9
3358	58	6,845	63.6
	64	3,720	65.2
	70	2,070	67.6
3348_PM	58	6,910	63.5
	64	3,795	65.9
	70	2,110	69.1
3350	58	8,640	60.6
	64	4,845	61.5
	70	2,805	62.8
3372	58	4,955	63.4
	64	2,795	64.2
	70	1,620	65.2
3373	58	5,690	61.0
	64	3,235	62.8
	70	1,880	65.2
3383	70	4,615	52.8
	76	3,035	54.3
	82	2,000	56.7
3378	58	4,885	61.6
	64	2,815	61.7
	70	1,680	62.1
3382	64	4,980	60.3
	70	2,980	62.0
	76	1,795	64.2
3399_NR	58	5,295	61.0
	64	3,040	61.7
	70	1,805	62.9
3399_RAP	58	5,450	62.1
	64	3,090	62.7
	70	1,810	63.6

Table 3.3-Asphalt Binder Statistical Grouping for Nevada's Districts.

District-Binder	Temp (°C)	Average		
		G* (Pa)	Standard Deviation G*(Pa)	Phase Angle δ (°)
PG76-22NV-District I	64	7,355	241.7	58.9
	70	4,638	159.0	58.4
	76	2,873	135.1	60
	82	1,870	102.5	62.1
PG64-28NV-District II	58	5,832	666.5	62.5
	64	3,284	319.5	63.5
	70	1,904	150.7	65.1
PG64-28NV-District III	58	5,719	1713.8	65.9
	64	3,145	998.6	67.1
	70	1,783	603.2	68.6

3.1.2. Dynamic Modulus

The dynamic modulus (|E*|) is a measure of the viscoelasticity of asphalt materials; it is calculated as the ratio of stress to strain under sinusoidal loading. The 26 field sampled mixtures were evaluated for |E*| using multiple combinations of loading frequencies and temperatures. The frequencies used in the testing were: 0.1,0.5,1,5,5,10,25 Hz and at temperatures of : 40,70,100,130°F. This data was used to compute the |E*| master curve at a reference temperature of 70°F. The Pavement-ME software uses the master curve to identify the structural response of the asphalt pavement under any temperature and traffic speed combination. The dynamic modulus data obtained served as a level 1 input in the Pavement-ME as opposed to level 3 inputs that use the Witczak model predictions. The dynamic modulus statistical grouping based on NDOTs districts and the appropriate standard deviation are shown in Tables 3.4 to 3.9.

Table 3.4. Mean Dynamic Modulus in psi for Bituminous Plantmix– District I, PG76-22NV Mixture.

	Frequency (Hz) →					
Temperature (deg F)	0.1	0.5	1	5	10	25
40	1,142,867	1,566,757	1,786,152	2,208,295	2,398,327	2,819,783
70	231,733	371,867	459,860	700,905	841,850	1,041,907
100	49,451	79,212	99,621	174,052	225,042	335,073
130	22,928	29,081	38,053	65,800	77,131	107,196

Table 3.5. Standard Deviation of the Dynamic Modulus in psi for Bituminous Plantmix– District I, PG76-22NV Mixture.

	Frequency (Hz) →					
Temperature (deg F)	0.1	0.5	1	5	10	25
40	597,177	769,331	885,742	929,822	950,574	1,202,589
70	128,503	180,266	221,815	275,916	323,141	351,001
100	20,539	35,060	47,540	72,752	93,385	133,289
130	4,625	5,628	11,958	24,227	14,988	28,530

Table 3.6. Dynamic Modulus in psi for Bituminous Plantmix– District II, PG64-28NV Mixture.

	Frequency (Hz) →					
Temperature (deg F)	0.1	0.5	1	5	10	25
40	628,946	885,602	1,008,706	1,324,511	1,472,121	1,685,424
70	122,675	212,544	264,370	436,082	526,218	678,018
100	25,282	41,756	52,208	97,192	126,317	183,386
130	12,340	17,689	23,032	34,827	44,416	71,565

Table 3.7. Standard Deviation of the Dynamic Modulus in psi for Bituminous Plantmix– District II, PG64-28NV Mixture.

	Frequency (Hz) →					
Temperature (deg F)	0.1	0.5	1	5	10	25
40	242,141	308,846	331,602	379,025	408,063	476,517
70	51,149	77,968	94,613	136,398	154,217	213,285
100	6,606	11,168	13,900	25,578	32,393	43,449
130	3,108	5,367	12,895	10,616	12,842	40,220

Table 3.8. Mean Dynamic Modulus in psi for Bituminous Plantmix– District III, PG64-28NV Mixture.

	Frequency (Hz) →					
Temperature (deg F)	0.1	0.5	1	5	10	25
40	661,937	934,530	1,066,170	1,385,400	1,528,233	1,751,700
70	124,687	213,457	266,323	442,423	538,683	706,700
100	34,902	54,718	67,373	118,600	151,013	222,847
130	14,977	20,178	23,423	39,520	50,332	74,025

Table 3.9. Standard Deviation of the Dynamic Modulus in psi for Bituminous Plantmix– District III, PG64-28NV Mixture.

	Frequency (Hz) →					
Temperature (deg F)	0.1	0.5	1	5	10	25
40	182,543	242,103	268,850	298,001	295,474	355,716
70	35,668	52,741	63,106	91,920	110,134	172,209
100	15,863	20,280	23,721	32,310	37,894	67,125
130	3,806	4,710	5,378	8,631	10,416	18,304

3.1.3. Repeated Load Triaxial

The repeated load triaxial (RLT) is used to evaluate an asphalt mixture deformations under repeated loading. In this test, the cylindrical sample is placed in a triaxial confinement chamber and subjected to a repeated axial stress of fixed magnitude and duration. The NDOT's mixtures were tested under a harvesine deviator stress of 45 psi with a 0.1 second loading time and 0.6 second rest period. A confinement pressure of 30 psi is also applied to the sample. The test was conducted at three temperatures of 40, 46, and 58°C and the samples deformation measured. The resulting cumulative permanent strain was plotted versus the number of loading cycles to characterize the permanent deformation of the asphalt mixtures following the Equation 3.1 below.

$$\frac{\varepsilon_p}{\varepsilon_r} = 10^{k_{r1}} T^{k_{r2}} N^{k_{r3}} \qquad (3.1)$$

where:

ε_p =Permanent axial strain (in/in),

ε_r = Resilient axial strain (in/in),

N= Number of loading repetitions,

T = Temperature of the HMA layer (°F), and

kr_1, kr_2, *and* kr_3 are experimentally determined regression coefficients.

The results were grouped under the three NDOT districts as shown in Table 3.10 below. Figure 3.1 illustrates the rutting models for NDOT at a temperature of 104°F.

Table 3.10-Rutting Regression Factors for NDOT's Asphalt Mixtures.

District	Coefficient	Average	Standard Deviation	COV (%)
District I	kr_1	-2.9708	1.0	34.4
	kr_2	1.7435	0.6	33.4
	kr_3	0.3547	0.0	13.7
District II	kr_1	-3.2605	1.2	35.9
	kr_2	2.0054	0.7	33.8
	kr_3	0.3161	0.0	15.3
District III	kr_1	-3.4717	1.1	32.7
	kr_2	2.0258	0.6	30.5
	kr_3	0.3946	0.1	27.5

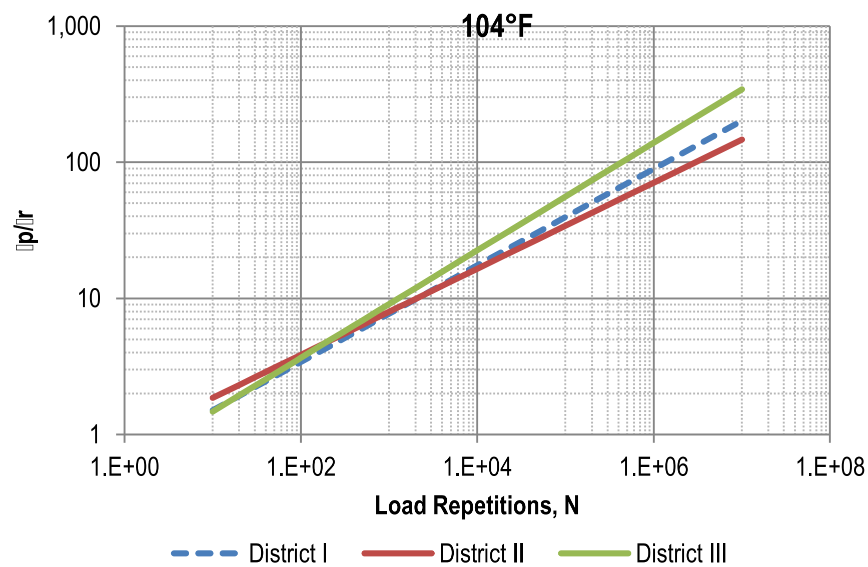

Figure 3.1- Rutting Models for NDOT's Mixtures at 104°F.

3.1.4. Flexural Beam Fatigue

The flexural beam fatigue test consists of placing a 2.5"x2.0"x15" beam specimen in a four point clamp system with free rotation and horizontal translation. The beam is then subjected to a sinusoidal load applied to the two inner clamps. This setup, frequently used in concrete testing, provides pure bending in-between the inner clamps. The NDOT sampled mixtures were tested using the constant strain method at a loading frequency of 10 Hz and at three temperatures of 55, 70, and 85°F. The fatigue failure is defined as the number of loading cycles required to achieve a 50% reduction in the initial flexural stiffness measured at the 50th load cycle. The fatigue regression model used to characterize the fatigue behavior of the eight tested asphalt mixtures is presented in Equation 3.2 below.

$$N_f = k_{f1}\left(\frac{1}{\varepsilon_t}\right)^{k_{f2}}\left(\frac{1}{E}\right)^{k_{f3}} \tag{3.2}$$

where:

N_f = Number of load repetitions to fatigue damage,

ε_t = Applied tensile strain at the bottom of the beam (in/in),

E = Dynamic modulus (psi),

T = Temperature of the HMA layer (°F), and

kf_1, kf_2, and kf_3 are experimentally determined regression coefficients.

The results were grouped according to the asphalt binder types as shown in Table 3.11 below.

Table 3.11-Beam Fatigue Regression Factors for NDOT's Mixtures.

Grouping	Coefficient	Average	Standard Deviation	COV (%)
PG76-22NV	kf_1	214.1758	331.8417	154.9389
	kf_2	5.0284	1.1205	22.2825
	kf_3	2.3072	0.8860	38.4010
PG64-28NV	kf_1	30.0794	46.5733	154.8348
	kf_2	5.0537	1.8018	35.6528
	kf_3	2.8904	1.5173	52.4945

3.1.5. General Asphalt Layer Properties

This section discusses some of the Pavement-ME software inputs required to characterize asphalt materials. The inputs are listed as follows:

- ***Mixture's unit weight***: weight of the asphalt mixture material measured in pounds per cubic foot (pcf). A value of 150 pcf was used in this study.
- ***Effective binder content***: defined as the percentage of effective asphalt content by volume in the asphalt mixture. In the case of sampled mixtures, effective binder content was calculated from lab measured data. For all other sections a value of 8.5% was used.
- ***Air voids***: The percentage of air voids by volume in the constructed asphalt layer after compaction. A typical value of 7% was used for Nevada's pavement sections.
- ***Poisson's ratio***: the ratio of transverse displacement to vertical movement. For asphalt mixtures a common value of 0.35 was used.
- ***Thermal conductivity***: the amount of heat that flows normally across a unitary surface area per unit of time of temperature gradient normal to the surface. The default value 0.67 BTU/hr-ft-° F was used.
- ***Heat capacity:*** the amount of heat required to raise the temperature of a unit mass of material by a unit temperature. The software's default value of 0.23 BTU/lb-°F was used.

3.2. Pavement Management System Data

The MEPDG analysis revolutionized design methods by switching from a single thickness design to multiple designs based on the specified distress limits. This increased the significance of PMS data as it became the failure criteria while also being a software input in rehabilitation designs. This section briefly describes the procedures used in the collection of NDOT PMS data as well as the modifications required to fit the Pavement-ME units.

3.2.1. Data Collection Procedure

Pavement management is defined as the set of procedures used by a state to manage its roadways keeping them at a specified performance level while minimizing costs. NDOT uses the PMS as a tool to monitor the pavement conditions throughout the state. The PMS provides an inventory covering routes mileposts, distresses, serviceability rating, traffic information, paving contracts, and future maintenance and repair strategies. This information is very important as it helps identify the pavement's conditions and distresses evolution with time which will eventually help judge whether the repair strategy was successful or not. The paving contract dates found in the PMS are also significant as they contribute in defining the existing pavement structure. In this study, NDOT PMS data was collected from 1995 to 2011; considering that PMS data is collected every other year, 9 set of data were inspected. The databases were combined and redundant data was eliminated. Design sections were then selected on the basis of district, county, route, and last paving contract guaranteeing that the most recent asphalt layer had the same properties in every section. After further reviewing the historical construction and traffic data some sections were broken down into sub-sections. The distresses were then calculated for every section. NDOT's PMS rutting and IRI units were measured in inch and in/mile respectively, matching the distress definition and the respective units used in the Pavement-ME software. However, alligator fatigue cracking, longitudinal cracking, and transverse cracking data required conversion to conform to the MEPDG units of percent cracking for alligator fatigue and feet/mile for transverse and longitudinal cracking. The collected distresses and respective conversion methods are briefly discussed below:

Rutting

Rutting is defined as a surface deformation under the wheel path that is often accompanied by a pavement uplift along the sides of the rut. The asphalt layer usually exhibits rutting under traffic loading caused by field compaction, poor structural design, or improper mix design (i.e., high asphalt binder content, flat particles). The subgrade can also show rutting problems if the structural design is not adequate to withstand the applied traffic loads. In the PMS data, multiple distress observations are evaluated for every test section and the average value is computed.

Roughness

Roughness is identified as a measure of the pavement surface irregularities that affects the smoothness and comfort of the ride. The roughness is quantified using the International Roughness Index (IRI). The roughness in NDOT's PMS data is measured using the IRI standard in in/mile using a road profilometer.

Alligator Fatigue Cracking

Fatigue cracking is a series of interconnected cracks in the wheel path caused by HMA fatigue failure under repeated traffic loading. The NDOT PMS defines two types of fatigue cracking: Type A representing hair like cracking and Type B representing typical interconnected chicken wire fatigue cracking. Type A fatigue is measured in linear feet whereas Type B fatigue is measured in square feet. The surveying sample unit is 1000 square feet (total length = 100' x total width = 10'). The type A fatigue data is converted using Equation 3.3 below. The Type B conversion is shown in Equation 3.4.

$$\text{Percentage of cracking} = \frac{Fatigue\ extent}{Total\ length} \times 100\% \qquad (3.3)$$

where:

Fatigue extent = length of crack measured in the PMS database (ft), and

Total length = 200 ft = 2 × length of wheel path (100 ft).

$$\text{Percentage of cracking} = \frac{Fatigue\ extent}{Total\ area\ of\ section} \times 100\% \qquad (3.4)$$

where:

Fatigue extent = cracked surface measured in the PMS database (ft^2), and

Total area of section= 1000 ft^2.

Longitudinal and Transverse Cracking

Longitudinal cracking is characterized as cracks occurring outside the wheel path in the direction of the traffic flow. Longitudinal cracking is usually caused by improper compaction or crack reflection from underlying layers. Transverse cracking are fractures perpendicular to the direction of traffic usually caused by HMA shrinkage or binder hardening and reflective cracking. The longitudinal and transverse cracking measurements in the PMS data are expressed in "extent of cracking" which is the length of the crack in linear feet. The unit conversion was completed using the Equation 3.5. The distresses collected for the calibration/validation sections are presented in Appendix A.

$$\text{Longitudinal/Transverse Crack in feet/mile} = \frac{extent\ of\ crack}{0.0189394} \quad (3.5)$$

where:

Extent of crack = length of crack measured in the PMS database (ft), and

0.0189394 is the total length of the survey section (100 ft) converted to miles resulting in a final distress unit of ft/mile matching the MEPDG standard unit.

3.3. MEPDG General Information Data

The AASHTOWare Pavement-ME software require general information inputs, these inputs are described as follows:

- ***Design type***: new pavement design, overlay, and restoration. In this study the pavement sections were either new pavement constructions or overlay pavements.
- ***Pavement type***: flexible or rigid for new construction or asphalt over asphalt, asphalt over concrete etc. for overlay designs. For the purpose of the Nevada MEPDG implementation only new HMA or AC over AC pavements were analyzed.
- ***Design life***: the expected service life of the pavement, a value of 20 years is typically used.
- ***Base construction***: completion date of the construction of the base and subgrade layers.
- ***Pavement construction***: construction date of the bituminous plantmix layer, this date defines the starting point for the binder aging and the thermal cracking models.
- ***Traffic opening***: the expected date in which the pavement is opened for public use. The pavement performance predictions begin at this point.

The general information data for the modeled pavement sections is presented in Tables 3.12 to 3.14 below.

Table 3.12-General Information Data for Calibration/Validation Sections (District I).

Section ID	County	Project Type	Existing Construction	Construction Date	Traffic Opening Date
IR 15-100	Clark	Rehabilitation	6/2/1994	12/8/2004	12/10/2004
IR 15-101	Clark	Rehabilitation	11/17/1995	12/8/2004	12/8/2004
IR 15-103	Clark	Rehabilitation	6/30/2000	11/29/2007	11/29/2007
IR 15-95	Clark	Rehabilitation	11/17/1999	7/20/2006	7/20/2006
IR 15-99A	Clark	Rehabilitation	2/24/1995	9/23/2003	9/23/2003
IR 15-99B	Clark	Rehabilitation	2/24/1995	9/23/2003	9/23/2003
SR 160-12A	Clark	Rehabilitation	8/10/1995	8/25/2005	8/27/2005
SR 160-12B	Clark	Rehabilitation	8/10/1995	8/25/2005	8/27/2005
SR 582-35	Clark	Rehabilitation	8/20/1999	7/25/2003	7/26/2003
IR 15-102	Clark	New	5/1/2002	1/1/2010	1/1/2010
SR 159-6	Clark	New	7/31/1990	10/30/2006	11/12/2006
SR 160-11	Clark	New	9/3/1999	5/18/2007	5/19/2007
SR 160-13	Nye	New	8/15/1996	8/3/2007	8/4/2007
SR 160-8	Clark	New	7/12/1995	8/9/2006	8/10/2006
SR 160-9	Clark	New	10/13/1992	7/12/2009	7/12/2009
SR 318-143	Lincoln	New	6/14/2010	6/14/2010	6/16/2010
SR 318-145	Nye	New	6/14/2010	6/14/2010	6/16/2010
US 93-40	Clark	New	8/1/1995	8/1/2005	8/1/2005
US 95-39	Clark	New	9/15/2007	9/15/2007	9/21/2007

Table 3.13-General Information Data for Calibration/Validation Sections (District II).

Section ID	County	Project Type	Existing Construction	Construction Date	Traffic Opening Date
IR 080-111	Churchill	Rehabilitation	11/6/2001	9/30/2009	9/30/2009
IR 080-116	Pershing	Rehabilitation	9/27/2001	8/26/2008	8/28/2008
IR 080-118	Pershing	Rehabilitation	10/10/2001	11/10/2009	11/10/2009
IR 80-138	Pershing	Rehabilitation	10/27/2001	8/19/2009	8/23/2009
SR 208-22	Lyon	Rehabilitation	10/18/1994	7/13/2006	7/16/2006
US 395-74A	Douglas	Rehabilitation	12/5/1995	7/13/2006	7/20/2006
US 395-74B	Douglas	Rehabilitation	12/5/1995	7/13/2006	7/20/2006
US 395-76	Douglas	Rehabilitation	8/18/1993	7/30/2004	7/30/2004
US 395-80	Washoe	Rehabilitation	10/2/1995	8/25/2006	8/25/2006
US 395-86	Washoe	Rehabilitation	7/23/1991	8/29/2005	8/29/2005
US 395-89	Washoe	Rehabilitation	8/1/1999	12/4/2009	12/8/2009
US 50-136	Douglas	Rehabilitation	5/25/2000	7/22/2008	7/26/2008
US 50-137	Carson City	Rehabilitation	8/6/1990	10/13/2008	10/20/2008
US 50-66	Lyon	Rehabilitation	6/3/1997	5/15/2009	5/18/2009

Table 3.13 -General Information Data for Calibration/Validation Sections (District II) (cont.).

Section ID	County	Project Type	Existing Construction	Construction Date	Traffic Opening Date
IR 080-107	Lyon	New	7/23/1999	9/13/2006	9/27/2006
IR 080-109	Carson City	New	7/23/1999	9/13/2006	9/27/2006
SR 117-1	Churchill	New	11/2/1992	6/22/2006	6/22/2006
SR 208-23	Lyon	New	10/18/1994	7/13/2006	7/13/2006
US 050A-72	Churchill	New	10/15/1999	9/19/2007	9/25/2007
US 395-83	Washoe	New	11/1/1995	11/30/2009	11/30/2009
US 395-90	Washoe	New	8/1/1999	12/4/2009	12/4/2009
US 395-91	Washoe	New	10/18/1995	10/3/2005	10/3/2005
US 50-56	Douglas	New	5/25/2000	10/13/2008	10/13/2008
US 50-58	Douglas	New	5/25/2000	10/13/2008	10/13/2008
US 50-59	Carson City	New	6/21/1997	11/15/2005	11/15/2005

Table 3.14-General Information Data for Calibration/Validation Sections (District III).

Section ID	County	Project Type	Existing Construction	Construction Date	Traffic Opening Date
IR 080-122	Humboldt	Rehabilitation	6/27/1997	11/22/2005	11/29/2005
IR 080-124	Humboldt	Rehabilitation	11/15/2001	5/23/2009	5/23/2009
IR 080-128	Lander	Rehabilitation	11/15/2001	7/20/2009	7/20/2009
IR 080-139	Humboldt	Rehabilitation	10/10/2001	11/30/2009	11/30/2009
IR 080-140	Lander	Rehabilitation	11/1/2001	7/20/2009	7/25/2009
IR 080-141	Eureka	Rehabilitation	8/1/2000	7/20/2009	7/25/2009
IR 080-142	Humboldt	Rehabilitation	12/17/1999	9/7/2007	9/7/2007
IR 80-120	Humboldt	Rehabilitation	12/17/1999	9/7/2007	9/13/2007
IR 80-121	Humboldt	Rehabilitation	10/10/2001	11/30/2009	11/30/2009
IR 080-123	Humboldt	New	6/19/1997	11/1/2005	11/15/2005
IR 080-129	Eureka	New	11/15/2001	7/20/2009	7/20/2009
IR 080-132	Lander	New	6/1/1995	9/18/2006	9/18/2006
IR 80-134	Elko	New	10/27/2001	8/14/2009	8/16/2009
SR 225-26	Elko	New	9/17/1994	10/24/2002	10/31/2002

3.4. Traffic Data

The traffic inputs required to conduct a Mechanistic-Empirical design are more detailed than the previously used AASHTO 1993 ESALs approach. These inputs include the average annual daily truck traffic (AADTT), vehicle classification (VC), monthly adjustment factors (MAF), and axle load distribution factors. The NDOT web-based Traffic Records Information Access (TRINA) software was used to obtain the average annual daily traffic (AADT) for the calibration/validation sections. Additionally, NDOT's yearly traffic reports were utilized to find the appropriate VC and truck percentages for every road type. This section presents the data collection procedure for the required traffic inputs.

Average Annual Daily Truck Traffic

The AADT for every section was collected using the TRINA software http://apps.nevadadot.com/trina/. This software is a web-based geographic information system (GIS) enabled interface that presents the user with maps and traffic reports. The data is measured using a combination of permanent and temporary count stations in order to cover the entire roadway network. The application requires the user to specify the location of the road segment either by inputting the street and city or the latitude and longitude of the segment. The software then adjusts the location to the nearest count station available and the data is populated. The results provide the AADT estimate from 2000 to the latest date available. This AADT data is adjusted to take into consideration hourly and monthly variations, thus no additional monthly adjustments are required. The results also include the station number, route, location, functional classification, longitude, and latitude of the segment.

Average Annual Daily Truck Traffic and Vehicle Class Distribution

The AADTT is the daily truck traffic and is calculated by multiplying the AADT by the percent of trucks in the road segment. The MEPDG requires the input of the AADTT. The vehicle classes are defined by the FHWA and characterized using axle types (single, tandem, tridem, or quad) and axle loads. Light vehicles, mainly passenger cars, are considered to be in classes 1 to 3; these vehicles do not have a significant impact on the pavement's performance. Heavy vehicles (trucks and buses) are considered to be in classes 4 to 13. The classification is conducted using weigh in motion (WIM) data. Annual Traffic Reports from the NDOT website were used to find the truck percentage and the vehicle classification for the road segments using the specified functional classification.

Traffic Growth

The traffic growth is an estimation of the traffic's progression. Traffic growth is calculated using historical databases and advanced analytical methods. The Pavement-ME offers two types of traffic growth: linear and compounded growth methods. Linear growth increases the traffic based on the initial traffic whereas compounded growth calculates the increase based on the added results from the previous years. In this calibration, the Pavement-ME defaults inputs were used (linear growth of 3 percent).

Table 3.15 to 3.17 present the results of the AADT, truck percent, and traffic growth. The vehicle classification distribution for the selected sections is exposed in Tables 3.18 to 3.20.

Table 3.15-Truck Traffic Data for Nevada's MEPDG Calibration/Validation Sections (District I).

Section ID	County	District	AADT	Truck Percentage (%)	AADTT	Traffic Growth Rate (%)
SR 159-6	Clark	I	38,000	4.18%	1,588	3
US 095-39	Clark	I	9,300	19.60%	1,823	3
SR 318-143	Lincoln	I	1,100	19.60%	216	3
SR 318-145	Nye	I	1,100	19.60%	216	3
SR 160-13	Nye	I	14,478	4.41%	638	3
SR 160-8	Clark	I	13,868	4.41%	612	3
SR 160-11	Clark	I	15,700	4.41%	692	3
US 093-40	Clark	I	2,900	19.60%	568	3
SR 160-9	Clark	I	12,038	4.41%	531	3
IR 015-102	Clark	I	15,813	4.41%	697	3
SR 582-35	Clark	I	26,385	4.18%	1,103	3
IR 015-103	Clark	I	15,700	32.88%	5,162	3
SR 160-12A	Clark	I	24,000	4.41%	1,058	3
SR 160-12B	Clark	I	24,000	4.41%	1,058	3
IR 015-100	Clark	I	17,435	32.88%	5,733	3
IR 015-95	Clark	I	32,000	9.90%	3,168	3
IR 015-99A	Clark	I	23,000	32.88%	7,562	3
IR 015-99B	Clark	I	23,000	32.88%	7,562	3
IR 015-101	Clark	I	17,540	4.41%	774	3

Table 3.16-Truck Traffic Data for Nevada's MEPDG Calibration/Validation Sections (District II).

Section ID	County	District	AADT	Truck Percentage (%)	AADTT	Traffic Growth Rate (%)
US 050A-72	Churchill	II	8,100	19.60%	1,588	3
SR 117-1	Churchill	II	1,697	12.94%	1,823	3
US 050-56	Douglas	II	12,700	19.60%	216	3
US 050-58	Douglas	II	11,250	19.60%	216	3
US 050-59	Carson City	II	10,500	19.60%	638	3
SR 208-23	Lyon	II	560	12.94%	612	3
US 395-90	Washoe	II	15,000	19.60%	692	3
US 395-91	Washoe	II	8,080	19.60%	568	3
US 395-83	Washoe	II	30,800	19.60%	531	3
IR 080-107	Lyon	II	7,550	32.88%	697	3
IR 080-109	Carson City	II	7,550	32.88%	1,103	3
IR 080-116	Pershing	II	7,200	32.88%	5,162	3
US 395-74A	Douglas	II	5,600	19.60%	1,058	3
US 395-74B	Douglas	II	5,600	19.60%	1,058	3

Table 3.16 -Truck Traffic Data for Nevada's MEPDG Calibration/Validation Sections (District II) (cont.).

Section ID	County	District	AADT	Truck Percentage (%)	AADTT	Traffic Growth Rate (%)
US 050-136	Douglas	II	11,250	19.60%	5,733	3
US 395-89	Washoe	II	20,000	19.60%	3,168	3
US 050-66	Lyon	II	4,706	19.60%	7,562	3
IR 080-138	Pershing	II	7,700	32.88%	7,562	3
US 395-86	Washoe	II	18,750	19.60%	774	3
US 395-76	Douglas	II	11,800	20.88%	1,588	3
US 395-80	Washoe	II	29,075	4.18%	220	3
IR 080-111	Churchill	II	7,100	32.88%	2,489	3
IR 080-118	Pershing	II	8,100	32.88%	2,205	3
SR 208-22	Lyon	II	1,500	12.90%	2,058	3
US 050-137	Carson City	II	11,250	19.60%	72	3

Table 3.17-Truck Traffic Data for Nevada's MEPDG Calibration/Validation Sections (District III).

Section ID	County	District	AADT	Truck Percentage (%)	AADTT	Traffic Growth Rate (%)
SR 225-26	Elko	III	375	17.34%	65	3
IR 080-134	Elko	III	4900	32.88%	1,611	3
IR 080-123	Humboldt	III	6900	32.88%	2,269	3
IR 080-129	Eureka	III	6800	32.88%	2,236	3
IR 080-132	Lander	III	8900	32.88%	2,926	3
IR 080-120	Humboldt	III	5700	32.88%	1,874	3
IR 080-128	Lander	III	7200	32.88%	2,367	3
IR 080-121	Humboldt	III	7400	32.88%	2,433	3
IR 080-124	Humboldt	III	6700	32.88%	2,203	3
IR 080-128	Lander	III	6900	32.88%	2,269	3
IR 080-139	Humboldt	III	7700	32.88%	2,532	3
IR 080-140	Eureka	III	6900	32.88%	2,269	3
IR 080-141	Eureka	III	6900	32.88%	2,269	3
IR 080-142	Humboldt	III	7200	32.88%	2,367	3
IR 080-122	Humboldt	III	6900	32.88%	2,269	3

Table 3.18-Vehicle Classification using NDOT's Traffic Reports (District I).

	Vehicle Class Percentages									
Section ID	**4**	**5**	**6**	**7**	**8**	**9**	**10**	**11**	**12**	**13**
SR 159-6	9.81	39.95	10.77	0.00	8.37	19.38	1.20	2.63	1.20	6.70
US 095-39	2.87	20.52	3.17	0.00	5.35	55.20	1.83	3.37	1.14	6.54
SR 318-143	2.87	20.52	3.17	0.00	5.35	55.20	1.83	3.37	1.14	6.54
SR 318-145	2.87	20.52	3.17	0.00	5.35	55.20	1.83	3.37	1.14	6.54
SR 160-13	2.72	31.52	7.48	0.00	2.95	22.68	3.63	1.59	0.68	26.76
SR 160-8	2.72	31.52	7.48	0.00	2.95	22.68	3.63	1.59	0.68	26.76
SR 160-11	2.72	31.52	7.48	0.00	2.95	22.68	3.63	1.59	0.68	26.76
US 093-40	2.87	20.52	3.17	0.00	5.35	55.20	1.83	3.37	1.14	6.54
SR 160-9	2.72	31.52	7.48	0.00	2.95	22.68	3.63	1.59	0.68	26.76
IR 015-102	2.72	31.52	7.48	0.00	2.95	22.68	3.63	1.59	0.68	26.76
SR 582-35	2.01	10.31	1.37	0.00	3.71	70.92	1.00	2.65	1.22	6.81
IR 015-103	2.01	10.31	1.37	0.00	3.71	70.92	1.00	2.65	1.22	6.81
SR 160-12A	2.72	31.52	7.48	0.00	2.95	22.68	3.63	1.59	0.68	26.76
SR 160-12B	2.72	31.52	7.48	0.00	2.95	22.68	3.63	1.59	0.68	26.76
IR 015-100	2.01	10.31	1.37	0.00	3.71	70.92	1.00	2.65	1.22	6.81
IR 015-95	4.65	19.09	5.96	0.00	3.94	55.76	1.31	3.84	0.91	4.55
IR 015-99A	2.01	10.31	1.37	0.00	3.71	70.92	1.00	2.65	1.22	6.81
IR 015-99B	2.01	10.31	1.37	0.00	3.71	70.92	1.00	2.65	1.22	6.81
IR 015-101	2.72	31.52	7.48	0.00	2.95	22.68	3.63	1.59	0.68	26.76

Table 3.19-Vehicle Classification using NDOT's Traffic Reports (District II).

	Vehicle Class Percentages									
Section ID	**4**	**5**	**6**	**7**	**8**	**9**	**10**	**11**	**12**	**13**
US 050A-72	2.87	20.52	3.17	0.00	5.35	55.20	1.83	3.37	1.14	6.54
SR 117-1	2.29	27.35	5.16	0.00	5.32	42.34	2.13	3.85	1.06	10.48
US 050-56	2.87	20.52	3.17	0.00	5.35	55.20	1.83	3.37	1.14	6.54
US 050-58	2.87	20.52	3.17	0.00	5.35	55.20	1.83	3.37	1.14	6.54
US 050-59	2.87	20.52	3.17	0.00	5.35	55.20	1.83	3.37	1.14	6.54
SR 208-23	2.29	27.35	5.16	0.00	5.32	42.34	2.13	3.85	1.06	10.48
US 395-90	2.87	20.52	3.17	0.00	5.35	55.20	1.83	3.37	1.14	6.54
US 395-91	2.87	20.52	3.17	0.00	5.35	55.20	1.83	3.37	1.14	6.54
US 395-83	2.87	20.52	3.17	0.00	5.35	55.20	1.83	3.37	1.14	6.54
IR 080-107	2.01	10.31	1.37	0.00	3.71	70.92	1.00	2.65	1.22	6.81
IR 080-109	2.01	10.31	1.37	0.00	3.71	70.92	1.00	2.65	1.22	6.81
IR 080-116	2.01	10.31	1.37	0.00	3.71	70.92	1.00	2.65	1.22	6.81
US 395-74A	2.63	21.12	2.35	0.00	5.41	55.12	1.87	2.87	1.01	7.61
US 395-74B	2.63	21.12	2.35	0.00	5.41	55.12	1.87	2.87	1.01	7.61
US 050-136	2.87	20.52	3.17	0.00	5.35	55.20	1.83	3.37	1.14	6.54
US 395-89	2.87	20.52	3.17	0.00	5.35	55.20	1.83	3.37	1.14	6.54
US 050-66	2.87	20.52	3.17	0.00	5.35	55.20	1.83	3.37	1.14	6.54
IR 080-138	2.01	10.31	1.37	0.00	3.71	70.92	1.00	2.65	1.22	6.81
US 395-86	2.87	20.52	3.17	0.00	5.35	55.20	1.83	3.37	1.14	6.54
US 395-76	2.63	21.12	2.35	0.00	5.41	55.12	1.87	2.87	1.01	7.61
US 395-80	9.81	39.95	10.77	0.00	8.37	19.38	1.20	2.63	1.20	6.70
IR 080-111	2.01	10.31	1.37	0.00	3.71	70.92	1.00	2.65	1.22	6.81
IR 080-118	2.01	10.31	1.37	0.00	3.71	70.92	1.00	2.65	1.22	6.81
SR 208-22	2.29	27.35	5.16	0.00	5.32	42.34	2.13	3.85	1.06	10.48

Table 3.20-Vehicle Classification using NDOT's Traffic Reports (District III).

	Vehicle Class Percentages									
Section ID	**4**	**5**	**6**	**7**	**8**	**9**	**10**	**11**	**12**	**13**
SR 225-26	3.07	22.39	4.37	0.00	5.19	51.51	1.54	3.78	0.83	7.33
IR 080-134	2.01	10.31	1.37	0.00	3.71	70.92	1.00	2.65	1.22	6.81
IR 080-123	2.01	10.31	1.37	0.00	3.71	70.92	1.00	2.65	1.22	6.81
IR 080-129	2.01	10.31	1.37	0.00	3.71	70.92	1.00	2.65	1.22	6.81
IR 080-132	2.01	10.31	1.37	0.00	3.71	70.92	1.00	2.65	1.22	6.81
IR 080-120	2.01	10.31	1.37	0.00	3.71	70.92	1.00	2.65	1.22	6.81
IR 080-128	2.01	10.31	1.37	0.00	3.71	70.92	1.00	2.65	1.22	6.81
IR 080-121	2.01	10.31	1.37	0.00	3.71	70.92	1.00	2.65	1.22	6.81
IR 080-124	2.01	10.31	1.37	0.00	3.71	70.92	1.00	2.65	1.22	6.81
IR 080-128	2.01	10.31	1.37	0.00	3.71	70.92	1.00	2.65	1.22	6.81
IR 080-139	2.01	10.31	1.37	0.00	3.71	70.92	1.00	2.65	1.22	6.81
IR 080-140	2.01	10.31	1.37	0.00	3.71	70.92	1.00	2.65	1.22	6.81
IR 080-141	2.01	10.31	1.37	0.00	3.71	70.92	1.00	2.65	1.22	6.81
IR 080-142	2.01	10.31	1.37	0.00	3.71	70.92	1.00	2.65	1.22	6.81
IR 080-122	2.01	10.31	1.37	0.00	3.71	70.92	1.00	2.65	1.22	6.81

Percent of trucks in the design direction and design lane

The percent of trucks in the design direction is the fraction of the trucks expected to travel in that direction. The AADT is typically a measurement of the two-way truck count. The Pavement-ME default value of 50% was used in this study.

The percent of trucks in the design lane is the portion of the truck traveling in the design lane in the design direction. Typical Pavement-ME values were used depending on the number of lanes per direction. The MEPDG recommends a value of 100% if the road is a one lane per direction, 90% for a road with two lanes per direction, and 70% for a three lane per direction roadway.

Operational Speed

The operational speed is the expected traffic speed in miles per hour (mph). The speed limit was used as operational speed in the MEPDG implementation.

Axle configuration

Axle configuration helps the user define a personal configuration using typical axles and tires. This configuration depends on several inputs such as load level, wheel location, and wheel spacing within the axle. These inputs are described as follows:

- ***Average axle width***: the distance between the two outside edges of an axle.
- ***Dual tire spacing***: transverse distance in inches between the centers of a dual tire. It is calculated from the WIM data measured over time by averaging the distance measured between the dual tires of a tandem, tridem, or quad axle for each truck class.
- ***Tire pressure:*** It is accepted that the hot inflation pressure is equal to the contact pressure and is 10% above the cold inflation pressure.

- ***Axle spacing:*** the center-to-center longitudinal spacing between consecutive axles. It is calculated using the WIM data by averaging the distance measured between the axles of a tandem, tridem, or quad axle for each truck class. The spacing has to be specified for every axle type.

In this study, default Pavement-ME software inputs were used as detailed data was not available for all the projects. These inputs are presented in Table 3.21 below.

Table 3.21-Default Axle Configuration Design Inputs.

Parameter	Design Input
Average axle width (ft)	8.5
Dual tire spacing (in.)	12
Tire pressure (psi)	120
Tandem axle spacing (in.)	51.6
Tridem axle spacing (in.)	49.2
Quad axle spacing (in.)	49.2

Lateral Traffic Wander

The lateral wander is a measurement of the traffic distribution over the pavement section. It takes into consideration the effect of vehicles travelling outside the wheel path which can generate additional stresses on the pavement and affect the distresses predictions. The inputs that feed into lateral wander are described as follows:

- ***Mean wheel location***: the distance from the outer edge of the wheel to the pavement marking.
- ***Traffic wander Standard Deviation***: the deviation from the average of the lateral traffic wander.

- ***Design lane width***: Distance between the lane markings or travel lane width.

The default parameters were used in this study. The lateral wander input are shown in Table 3.22.

Table 3.22-Pavement-ME Default Later Wander Inputs.

Parameter	Design Input
Mean wheel location (in.)	18
Traffic wander standard deviation (in.)	10
Design lane width (ft)	12

3.5. Climatic Data Collection

The MEPDG uses the Enhanced Integrated Climatic Model (EICM) to predict the effect of the environmental conditions on the behavior and characteristics of the pavement layers during the service life. The EICM computes moisture profiles across the pavement layers using a suction model based on the soil-water characteristic curve (SWCC) and the water table depth. Zapata et al. (2010) developed a new empirical suction model based on the Thornthwaite Moisture Index (TMI). This model eliminated the use of the depth of the water table as a basis for prediction by balancing between water infiltration and evaporation. The Pavement-ME software gives the user the option of either inputting a personal climatic file (*.icm-file) specific of the project's location, or generating a virtual station based on the climatic stations available in the software. In this study, due of the lack of project specific climatic data the second option was used. The weather stations identified in the Pavement-ME that were relevant to Nevada's projects are shown in Table 3.23 below. Figure 3.2 presents a map of the weather stations used in this study. The weather stations in Nevada were represented by a blue marker whereas the station from California (South Lake Tahoe) was situated using a red marker.

Table 3.23-Pavement-ME Weather Stations Relevant to NDOTs Pavements.

City	State	Latitude[1]	Longitude[1]	Elevation (ft)	Description
Elko	Nevada	40.825	-115.79	5,050	Elko Regional Airport
Ely	Nevada	39.295	-114.85	6,248	Ely Airport
Las Vegas	Nevada	36.079	-115.16	2,127	McCarran International Airport
Las Vegas	Nevada	36.212	-115.20	2,186	North Las Vegas Airport
Lovelock	Nevada	40.066	-118.57	3,902	Derby Field Airport
Mercury	Nevada	36.621	-116.03	3,230	Desert Rock Airport
Reno	Nevada	39.484	-119.77	4,410	Reno Tahoe International Airport
Tonopah	Nevada	38.060	-117.09	5,395	Tonopah Airport
Winnemucca	Nevada	40.902	-117.81	4,296	Winnemucca Municipal Airport
South Lake Tahoe	California	38.894	-120.00	6,260	Lake Tahoe Airport

[1] Latitude and longitude expressed in decimal degrees.

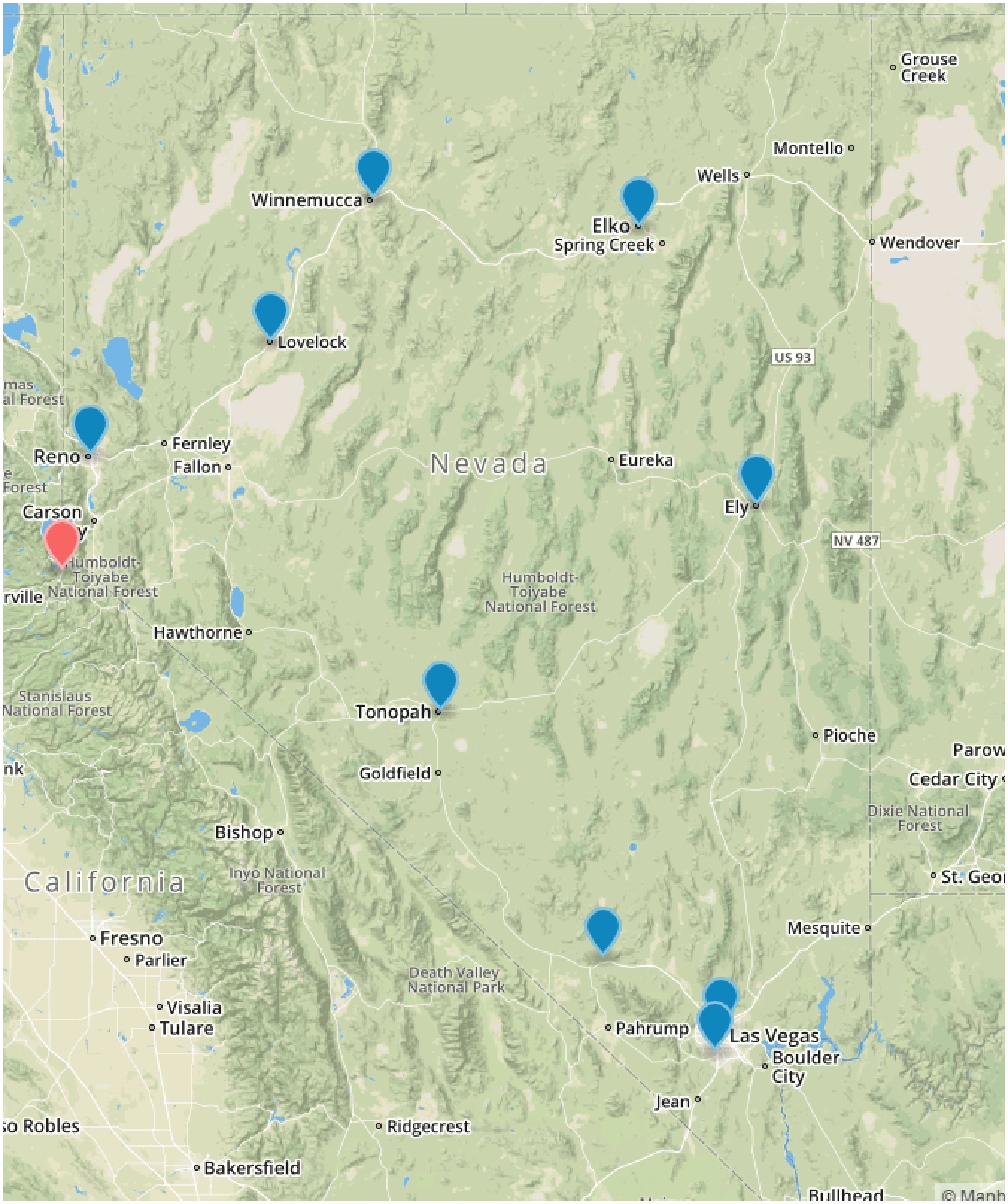

Figure 3.2- Map of Weather Stations Relevant to NDOT's Pavements (*Source:* http://mapbox.com)

In order to utilize the software's weather stations the following inputs are required:

- ***Latitude & Longitude*:** Latitude is the angular distance north or south measured along the meridian. Longitude is the angular distance from the prime meridian at Greenwich, England. Latitude and longitude are determined using the MapQuest web application http://developer.mapquest.com/web/tools/lat-long-finder .
- ***Elevation*:** Elevation is the height of a location to the sea level, expressed in feet. Google maps altitude finder was used to collect this information http://www.daftlogic.com/sandbox-google-maps-find-altitude.htm .
- ***Depth of Water Table*:** This depth is defined as the depth from the top surface of the subgrade to the ground water table. This data is collected using http://pubs.usgs.gov/sir/2006/5100/pdf/Plate01.pdf .

Tables 3.24 to 3.26 illustrate the climatic data collected. The data were inputted into the software and the appropriate weather stations were selected. The selection is based on proximity; typically, stations at a distance less than 100 miles from the project's location were included in the analysis. The other selection criteria is elevation, in this case the difference in elevation between weather station and project was limited to 500 feet.

Table 3.24-Climatic Data Collected for NDOTs Sections (District I).

Section ID	Latitude (°)	Longitude (°)	Elevation(ft)	Water Table (ft)
IR 015-100	36.381	-114.892	2,194	144
IR 015-101	36.448	-114.849	2,120	70
IR 015-103	36.795	-114.125	1,622	72
IR 015-95	35.881	-115.232	3,087	87
IR 015-99A	36.282	-115.033	1,854	43
IR 015-99B	36.282	-115.033	1,854	43
SR 160-12A	36.452	-116.082	3,484	56
SR 160-12B	36.452	-116.082	3,484	56
SR 582-35	36.125	-115.078	1,781	81
IR 015-102	36.652	-114.586	2,293	193
SR 159-6	36.161	-115.316	2,929	32
SR 160-11	36.452	-116.082	3,484	84
SR 160-13	36.452	-116.082	3,484	84
SR 160-8	36.293	-115.999	2,687	87
SR 160-9	36.293	-115.999	2,687	87
SR 318-143	38.706	-115.048	5,603	103
SR 318-145	38.600	-115.080	5,879	79
US 093-40	39.671	-119.999	5,135	85
US 095-39	35.220	-114.860	2,545	120

Table 3.25-Climatic Data Collected for NDOTs Sections (District II).

Section ID	Latitude (°)	Longitude (°)	Elevation(ft)	Water Table (ft)
IR 080-111	39.819	-118.994	4,191	91
IR 080-116	40.455	-118.286	4,274	74
IR 080-118	40.779	-118.005	4,334	84
IR 080-138	40.158	-118.491	3,976	76
SR 208-22	38.814	-119.283	4,843	43
US 395-74A	38.701	-119.551	5,128	78
US 395-74B	38.701	-119.551	5,128	78
US 395-76	38.891	-119.697	4,911	61
US 395-80	39.169	-119.767	4,686	86
US 395-86	39.602	-119.839	5,136	36
US 395-89	39.649	-119.938	5,108	58
US 050-136	39.096	-119.911	6,972	72
US 050-137	39.105	-119.889	7,078	78
US 050-66	39.318	-119.489	4,375	50
IR 080-107	39.619	-119.205	4,163	63
IR 080-109	39.818	-118.994	4,191	91
SR 117-1	39.461	-118.855	3,986	36
SR 208-23	38.733	-119.497	5,109	59
US 050A-72	39.515	-118.945	4,020	70
US 395-83	39.459	-119.781	4,471	71
US 395-90	39.652	-119.989	5,041	41
US 395-91	39.671	-119.999	5,127	77
US 050-56	38.992	-119.949	6,295	65
US 050-58	39.096	-119.911	6,972	72
US 050-59	39.185	-119.711	4,622	52

Table 3.26-Climatic Data Collected for NDOTs Sections (District III).

Section ID	Latitude (°)	Longitude (°)	Elevation(ft)	Water Table (ft)
IR 080-122	40.942	-117.474	4,470	130
IR 080-124	40.816	-117.159	4,479	79
IR 080-128	40.620	-116.907	4,523	43
IR 080-139	40.992	-117.551	4,392	42
IR 080-140	40.620	-116.907	4,524	74
IR 080-141	40.698	-116.548	4,694	64
IR 080-142	41.014	-117.623	4,391	71
IR 080-120	40.968	-117.746	4,479	79
IR 080-121	40.992	-117.551	4,391	91
IR 080-123	40.870	-117.243	4,413	101
IR 080-129	40.694	-116.564	4,610	60
IR 080-132	40.824	-115.807	5,067	67
IR 080-134	41.023	-114.479	5,831	51
SR 225-26	41.237	-115.805	5,920	70

3.6. Unbound Material Data Collection

The base and subgrade layers are considered unbound materials. The base layers include cement treated base (CTB), Roadbed modification (RBM), and aggregate bases. One of the challenges faced was the little guidance offered by the Pavement-ME software for Roadbed modification materials. This issue is being currently fixed under the active NCHRP project 09-51 until then the RBM are considered as a non-stabilized base layer. As a result, when a new bituminous plantmix surface is placed directly on top of an RBM layer the pavement is modeled as a newly constructed pavement. In the MEPDG, non-stabilized materials are defined particularly by the resilient modulus, gradation properties, SWCC parameters, moisture content, and Attenberg limits. The NDOT Standard Specification for Road and Bridge Construction provides data related to the aggregates used in base layers and RBM. Referring to section 704 of the construction manual gradation properties' limits are defined. This same section specifies a minimum R-value for every aggregate base type. Table 3.27 displays the calculated resilient modulus values for the different aggregate layer bases. Table 3.28 presents different gradation properties for the base layer aggregates.

Table 3.27. Resilient Modulus for Base Aggregates.

Aggregate Base[1]	Design Resilient Modulus (psi)
Type 1 Class A	26000
Type 1 Class B	26000
Type 2 Class A	34000
Type 2 Class B	26000

[1] Section 704 of the *2014 Standard Specifications for Road and Bridge Construction*.

Table 3.28. NDOT's Gradation Limits for Base Aggregates.

Sieve Size	Percent Passing by Mass			
	Aggregate Base			
	Type 1 Class A	Type 1 Class B	Type 2 Class A	Type 2 Class B
75 µm (No. 200)	7	7	6	6
1.18 mm (No. 16)	27.5	27.5	27.5	27.5
4.75 mm (No. 4)	47.5	47.5	50	50
19 mm (3/4 in.)			95	95
25 mm (1 in.)	90	90	100	100
37.5 mm (1 1/2 in.)	100	100		

The subgrade layers properties were collected using the web application created using the national catalog of the subgrade soil-water characteristic curve (SWCC) database developed by Zapata et al. (2010) under the NCHRP project 9-23A. This software is a GIS enabled database that requires the geographical coordinates of the projects to generate the respective soil report. Additionally, mileposts coordinates for major routes (i.e., US, Interstate, and State routes) can be found in the application. Once the geographical coordinates are inputted, the location is shown on the map and a soil map character becomes visible. This character is required to generate the corresponding soil report. The data output includes the soil AASHTO classification, top and bottom depth, layer thickness, resilient modulus, gradation properties, plastic limits, and SWCC parameters. An example for the soil unit ‘mn1’ is presented in Table 3.29.

Table 3.29. ASU Soil Output Example for Soil Unit ‘mn1’ (Section IR 080-140).

	Section	**IR 080-140**	
	Layer	**Top Layer**	**Layer 2**
Road Classification and Thicknesses	AASHTO Classification	A-4	A-4
	AASHTO Group Index	0	0
	Top Depth (in)	0	6
	Bottom Depth (in)	6	60
	Thickness (in)	6	54
	% Component	13	13
	Water Table Depth(ft.)	N/A	N/A
	Depth to Bedrock (ft.)	N/A	N/A
Strength Properties	CBR from Index Properties	37	37
	Resilient Modulus (psi)	25,980	25,980
Index Properties	Passing #4 (%)	90	97.5
	Passing #10 (%)	82.5	95
	Passing #40 (%)	75	85
	Passing #200 (%)	55	55
	Passing 0.002 mm (%)	12.5	12.5
	Liquid Limit (%)	28	28
	Plasticity Index (%)	3	3
	Saturated Volumetric Water Content (%)	37	41
	Saturated Hydraulic Conductivity(ft/hr)	1.08E-01	1.08E-01
SWCC Parameters	Parameter af (psi)	2.4042	2.3463
	Parameter bf	1.0201	1.0195
	Parameter cf	0.7619	0.8151
	Parameter hr (psi)	2998.65	3000.02

The resilient modulus values for subgrade were corrected for every layer using the seasonal variations of the unbound materials developed by Sebaaly et al. (2000). This research studied the impact of the environmental changes on the base and subgrade layers moduli values using the summer modulus as a baseline. Table 3.30 presents the seasonal multipliers for subgrade layers from the three districts.

Table 3.30. Seasonal Multipliers for NDOT's MEPDG Implementation.

District	Spring	Summer	Fall	Winter
I	0.79	1.00	0.85	0.77
II	0.70	1.00	1.02	0.81
III	0.70	1.00	1.02	0.81

3.7. Pavement Structure

The pavement structure was determined using historical paving contracts' information and the segment mileposts. The majority of the data was extracted from the NDOT Roadbed structure history reports. These reports present the paving contracts' award and completion date, the segments description, mileposts, and a summary of the paving jobs along with the appropriate layer thicknesses for every route/county combination. In some cases, the crystal reports had no or missing data for the more recent paving jobs requiring additional investigations into the NDOT database. The research team at UNR utilized the As-Constructed CAD drawings in order to compensate for the missing information. The resulting pavement structure was then compared with the sampled cores data and a good correlation was found between the historical database and the actual field construction. An example of the pavement structure record is shown in Table 3.31.

Table 3.31. Pavement Structure for US 50-59.

	Year	**1931**	**1940**	**1967**	**1997**	**2005**
US 050-59	**Structure**			1.5" 120-150 PEN	2" AC-20P	2" PG64-28NV
			5" Plantmix Surface	5" Plantmix Surface	4.5" Plantmix Surface[1]	3" Plantmix Surface[1]
			9" Aggregate Base	9" Aggregate Base	9" Aggregate Base	9" Aggregate Base
		4" Plantmix Surface	4" Plantmix Surface	4" Plantmix Surface	4" Plantmix Surface	4" Plantmix Surface
		3" Aggregate Base	3" Aggregate Base	3" Aggregate Base	3" Aggregate Base	3" Aggregate Base

[1] *Note that cold milling is taken into consideration.*

Once the pavement structure is determined the sections were defined into new or rehabilitated construction. Sections with the most recent bituminous layer placed directly on top of a non-stabilized base layer were modeled as new. Also sections where the new AC layer is placed on top of an old asphalt layer (older than 20 years) were considered as new. In the overlay construction, existing asphalt layers were modeled as visco-elastic layers if they were constructed within 20 years to the time of the rehabilitation and have not been overlaid by an aggregate base. In all other cases, they were modeled as linear elastic base layer with a factor of 0.25. Table 3.32 presents the layer coefficient for different material types found in the historical databases using the AASHTO 1993 layer coefficients.

Table 3.32. Layer Coefficients for NDOT Materials.

Layer Type	Factor a_i
Roadbed Modification	0.15
Asphalt Concrete	0.25
Aggregate Base	0.10
Rubblized PCC	0.20
Cement Treated Base	0.15
Cold in Place Recycling	0.30

In order to calculate the resulting aggregate base modulus, the layer coefficients a_i were multiplied by the respective layer thickness h_i. The sum of the product of $h_i * a_i$ was then divided by the total layer thickness as shown in the Equation 3.6 below.

$$a_{Base} = \frac{\sum(a_i * h_i)}{\sum h_i} \tag{3.6}$$

The resulting base modulus is then calculated using the AASHTO 1993 design guide layer coefficient equation for granular base (Equation 3.7).

$$a_{Base} = 0.249(log_{10}(E_{base}) - 0.977) \tag{3.7}$$

where:

a_{Base}= the resulting layer structural coefficient, and

E_{base}= the resulting resilient modulus (psi).

The calculation steps are illustrated in the Table 3.33. The pavement structures for the various database sections are provided in Appendix B.

Table 3.33. Aggregate Base Resilient Modulus Calculation.

<table>
<tr><td rowspan="6">US 050-59</td><td>Final Structure</td><td>Layer Behavior</td><td>Thicknes s(in)</td><td>Layer Coefficient</td><td>h*ai</td><td>Section Modeled</td><td>Modulus E (psi)</td></tr>
<tr><td>2" PG64-28NV</td><td>Visco-Elastic</td><td>2</td><td>Database</td><td>Databa se</td><td>2"PG 64-28NV</td><td>Database</td></tr>
<tr><td>3" Plantmix Surface</td><td>Elastic</td><td>3</td><td>0.25</td><td>0.75</td><td>19" Aggregat e Base</td><td rowspan="2">35257</td></tr>
<tr><td>9" Aggregate Base</td><td>Elastic</td><td>9</td><td>0.1</td><td>0.9</td><td>0.155[1]</td></tr>
<tr><td>4" Plantmix Surface</td><td>Elastic</td><td>4</td><td>0.25</td><td>1</td><td rowspan="2">Subgrade</td><td rowspan="2">Database NCHRP</td></tr>
<tr><td>3" Aggregate Base</td><td>Elastic</td><td>3</td><td>0.1</td><td>0.3</td></tr>
</table>

[1]*The resulting aggregate base structural coefficient.*

CHAPTER 4 RUTTING CALIBRATION

4.1. Overview

Rutting is defined as the pavement deformation in the wheelpath. It usually occurs in all pavement layers (HMA, Base, or subgrade) and is a good indication of structural inadequacy or mixture's issues. Rutting is considered a safety hazard as ruts tend to fill up with water and can cause vehicle hydroplaning. NDOT's transition to using polymer-modified asphalt mixtures has been very successful in eliminating major HMA rutting. Nonetheless, the rutting models for the three districts require further calibration to relate software predictions to actual field performance. Following the recommendations of the AASHTO manual of practice for local calibration the jack-knifing process was used in the rutting calibration. This procedure suggests combining between the traditional split-sample and jack-knifing approaches to improve the goodness-of-fit of a particular calibration. In this case, the sections obtained above were separated into two groups: one for calibration and another for validation. In this study, 24 out of 26 sampled contracts were used in the calibration as some contracts had missing information. Additional 12 sections were added to the calibration to improve the accuracy of the predictions, which resulted in a total of 36 calibration sections. The calibration was first conducted for each district separately as the k factors differed from one district to the other (Table 3.10). The combination of new and rehabilitated sections predictions resulted in poor correlations for all districts. However, when considering either new or overlay sections separately, the predictions showed less bias. Therefore, the calibration was conducted for each district separately and for new and rehabilitated sections within the respective district totaling in 6 different calibration sets. Figure 4.1 below shows the distribution of the sections considered in the calibration.

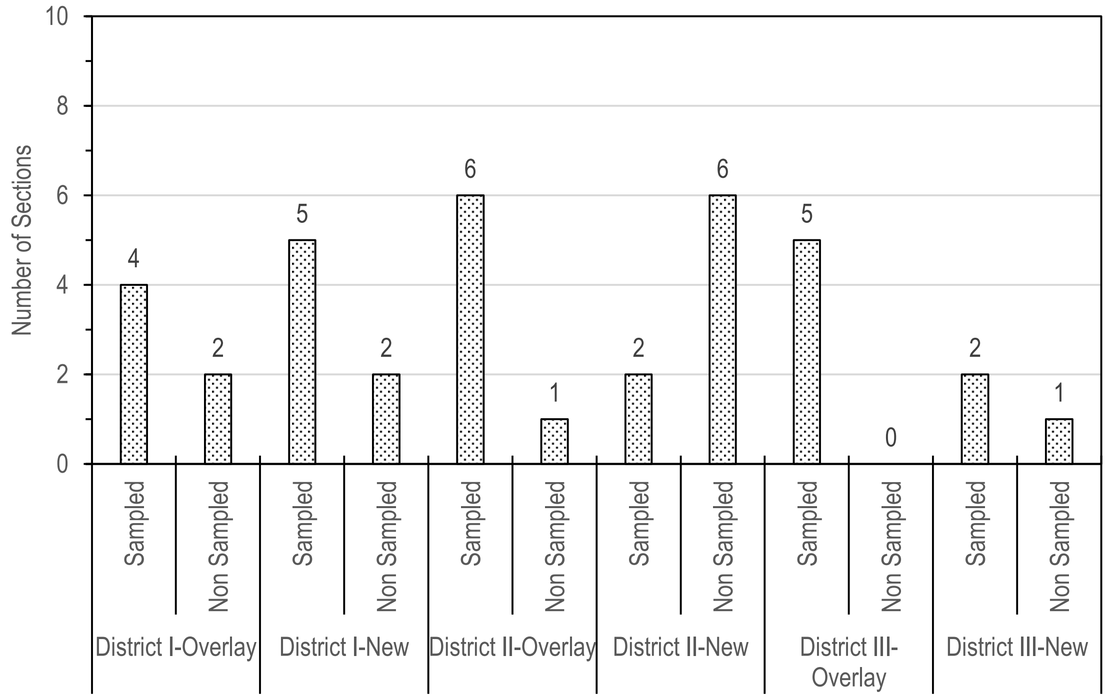

Figure 4.1- Calibration Sections Count as a Function of District & Construction Type.

4.2. Optimization Method

The MEPDG estimates the rutting for each pavement layer separately. The rutting models relate the vertical strain at the mid-depth of each sub-layer to the pavement temperature and the traffic applications. HMA rutting is calculated using an incremental time and thickness approach. Witczak et al. (2002) introduced a depth factor to take into consideration the effect of the confinement of the upper asphalt layers while calculating the incremental rutting throughout the HMA layer. The asphalt and unbound materials rutting was completed using laboratory regression analysis. As discussed in Section 2.2.1

above the HMA rutting model is illustrated in Equation 4.2. Equation 4.3 shows the unbound layer materials rutting model.

$$\frac{\varepsilon_p}{\varepsilon_r} = k_z * \beta_{r1} * 10^{k1} T^{k2*\beta_{r2}} N^{k3*\beta_{r3}} \quad (4.2)$$

Where k_1, k_2, k_3 are the district specific calibration factors developed for NDOT's mixtures (Refer to Table 3.10) and β_{r1}, β_{r2}, β_{r3} as the local calibration factors.

$$\delta_a(N) = \beta_{s1} k_1 * \varepsilon_v * h \left(\frac{\varepsilon_0}{\varepsilon_y}\right) e^{-\left(\frac{\rho}{N}\right)^{\beta}} \quad (4.3)$$

Where β_{s1} is the local calibration factor for base or subgrade layers.

The total rutting is calculated as the sum of asphalt, base, and subgrade layers rutting. The optimization was run to eliminate bias and reduce the scatter of the prediction. The HMA rutting calibration factors β_{r2} and β_{r3} are power coefficient. Therefore, they have to be integrated in the Pavement-ME software runs. On the other hand, β_{r1}, β_{base}, and $\beta_{subgrade}$ are linear coefficients and can be optimized using the excel solver to reduce the sum of square errors. The detailed steps are discussed in the following sections.

4.2.1. Asphalt Rutting Optimization

The pavement sections were run in the Pavement-ME software using 16 different combinations of β_{r2} and β_{r3}. The trial values for each calibration coefficient are 0.7, 0.8, 0.9, and 1.0. The remaining calibration factors were all set to 1.0. The software outputs included the AC rutting, base rutting, and subgrade rutting. Considering that the majority of the rutting comes from the asphalt layer (Li et al., 2009) the predicted AC rutting was optimized at first. The NDOT PMS data does not specify the portion of the AC rut; as a result, it was estimated using the predicted rutting values as shown in Equation 4.4 below.

This equation can also be used to estimate the field measured base and subgrade rutting by substituting the predicted AC rutting by the base or subgrade prediction.

$$Measured\ AC\ Rutting = \frac{Predicted\ AC\ rutting}{Total\ \ predicted\ rutting} * Total\ measured\ Rutting \qquad (4.4)$$

The predicted AC rutting was then multiplied by β_{r1} and the error was calculated by deducting the measured AC rutting from the adjusted predicted rutting. As explained in Section 2.2.1, the Microsoft office solver was used to minimize the sum of square errors. Figure 4.2 illustrates an example of the AC rutting optimization for Overlay construction District I.

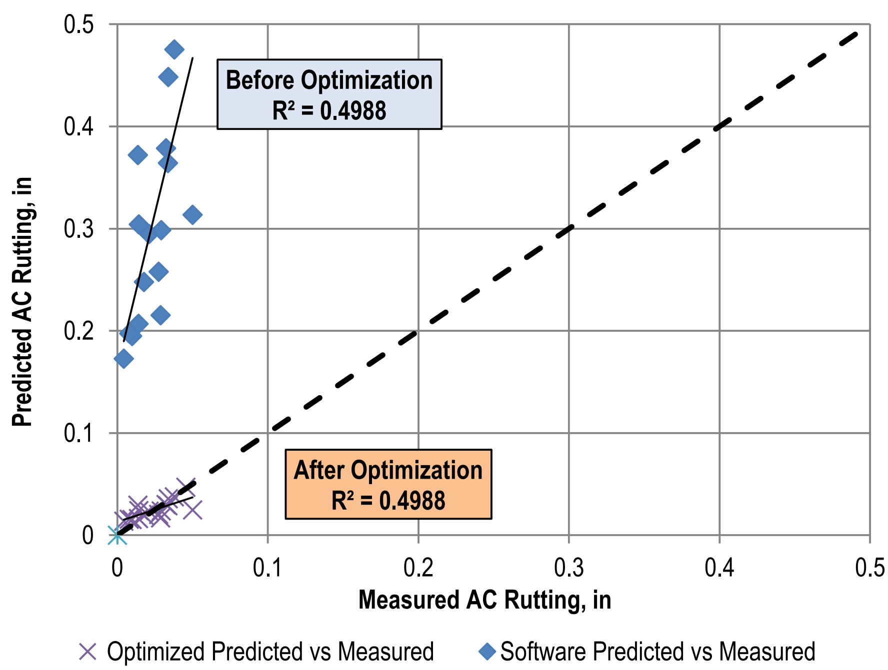

Figure 4.2-AC Rutting Optimization District I (β_{r1} =0.0794, β_{r2}=β_{r3}=1.0).

4.2.2. Total Rutting Optimization

The AC rutting optimization was followed by the total rutting optimization. The predicted base and subgrade layers rutting values were multiplied by β_{base} and $\beta_{subgrade}$, respectively. The predicted total rutting was calculated by adding the adjusted AC, base, and subgrade values. The error between predicted and measured total rutting was then computed. The error was squared and summed for all the pavement sections. The Microsoft excel solver was run to reduce the sum of squared errors by optimizing β_{base}, and $\beta_{subgrade}$ simultaneously. Several iterations were conducted in order to reach the local optimum. The total rutting calibration for district I overlay is shown in Figure 4.3 below.

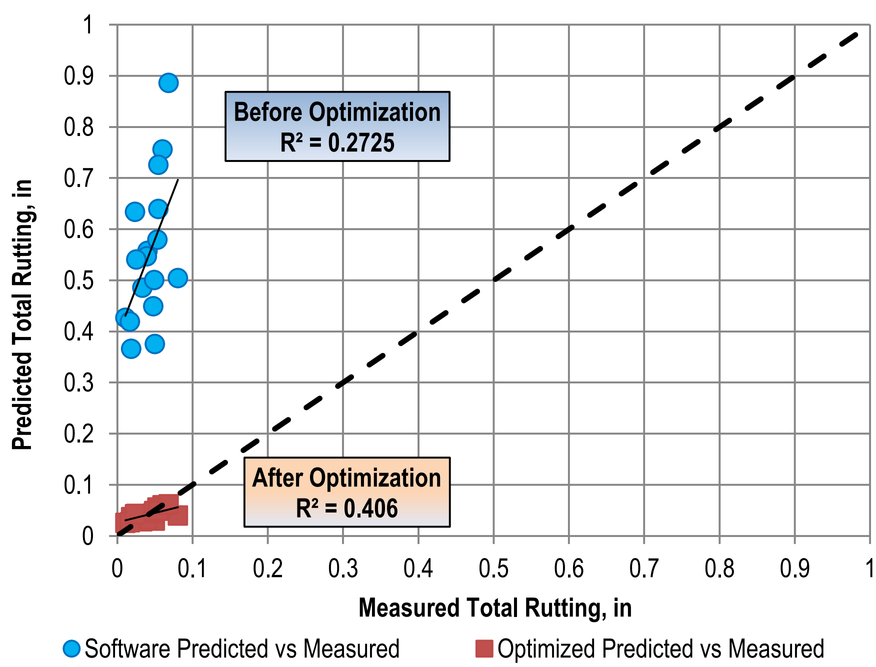

Figure 4.3-Total Rutting Optimization District I-Overlay (β_b =0.1274, β_{sg}=0.0141).

From Figure 4.3 it is clear that applying the local calibration factors for HMA, base and subgrade improved the rutting prediction and increased the R-squared value from 0.273 to 0.406. The models exhibiting the best goodness-of-fit for AC rutting and total rutting were selected from each district. The goodness of fit was determined using the R-squared values. Higher R-squared values usually indicate better model fits. Additional parameters, such as the proportion of asphalt rutting, affected the selection of calibration factors. Table

4.1 below presents the optimization results for district I overlay. The optimization results from the different districts and the respective total rutting and AC rutting plots are exposed in Appendix C.

Table 4.1-Optimization Results for District I-Overlay.

	βr2	βr3	βr1	βbase	βsg	R-squared Total Rutting	R-square Asphalt Rutting
District I-Overlay	0.7	0.7	0.1873	0.2482	0.0922	0.1028	0.4635
	0.7	0.8	0.1865	0.2459	0.0891	0.1151	0.5038
	0.7	0.9	0.2021	0.2063	0.1125	0.0685	0.6639
	0.7	1.0	0.1750	0.2372	0.0772	0.1739	0.5744
	0.8	0.7	0.1721	0.2424	0.0854	0.1252	0.4718
	0.8	0.8	0.1760	0.2373	0.0790	0.1553	0.4960
	0.8	0.9	0.1638	0.2298	0.0710	0.2006	0.5234
	0.8	1.0	0.1540	0.2167	0.0594	0.2555	0.5433
	0.9	0.7	0.1674	0.2286	0.0722	0.1803	0.4496
	0.9	0.8	0.1531	0.2175	0.0631	0.2304	0.4752
	0.9	0.9	0.1405	0.1994	0.0506	0.2901	0.4994
	0.9	1.0	0.1188	0.1783	0.0375	0.3467	0.5176
	1.0	0.7	0.1383	0.1979	0.0548	0.2657	0.4455
	1.0	0.8	0.1208	0.1765	0.0431	0.3237	0.4773
	1.0	0.9	0.1003	0.1522	0.0295	0.3729	0.4964
	1.0	1.0	0.0794	0.1274	0.0141	0.4053	0.4988

Note that the highlighted combination was selected for validation.

4.3. Rutting Validation

The calibrated rutting models were tested using 18 additional pavement sections as shown in Figure 4.4. The rutting registered in the PMS database was compared to the predicted rutting using the Pavement-ME software. It was observed that the calibrated models significantly improved the prediction accuracy. Figure 4.5 presents the validation results of the rehabilitation projects for total rutting and asphalt rutting.

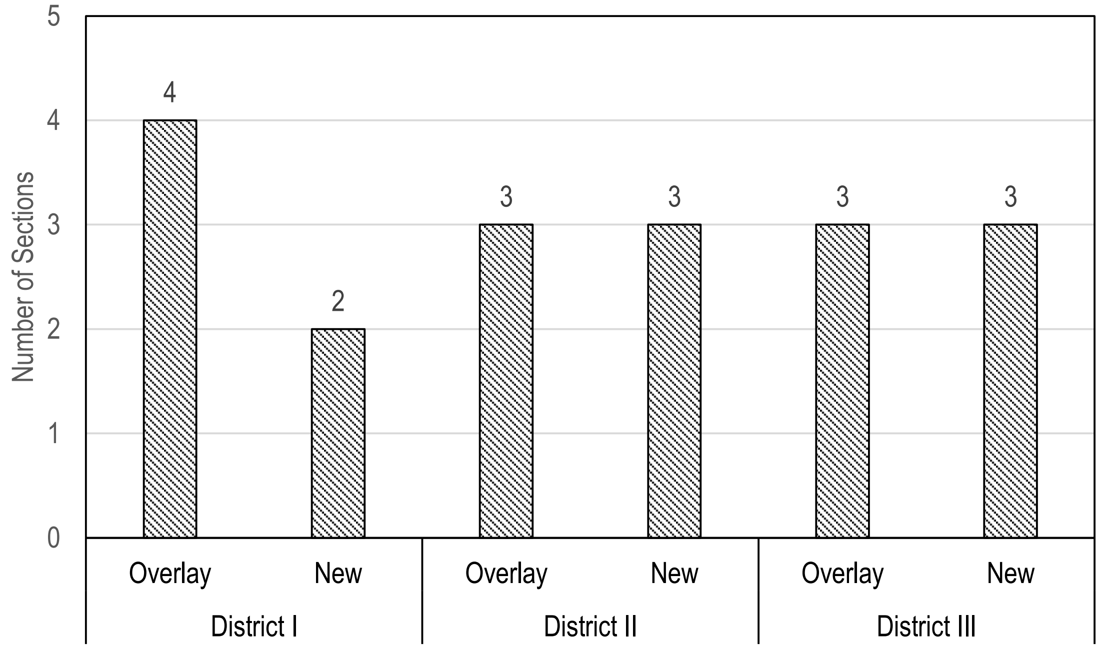

Figure 4.4-Rutting Validation Sections Distribution.

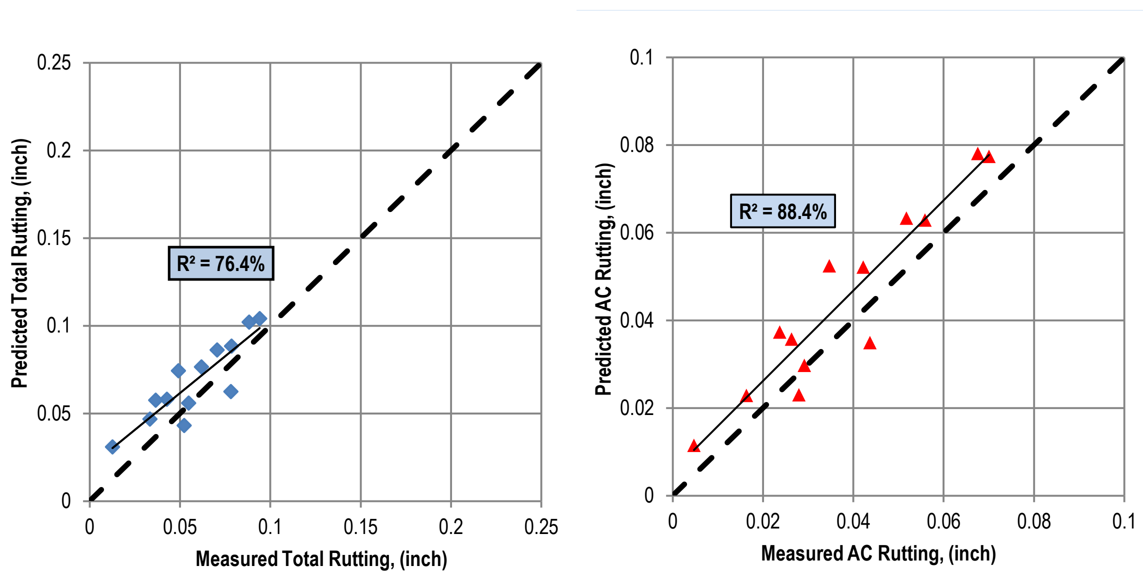

Figure 4.5-Rutting Validation District I -Overlay.

Figure 4.5 clearly illustrates the accuracy of the results as high correlation between predicted and measured rutting is observed. Additional runs were made as a part of the verification process. In this process calibration and validation sections were taken into consideration. The predicted total, AC, base, and subgrade rutting was plotted versus the measured total rutting. Figure 4.6 represents the verification plots for district I rehabilitated sections. The remaining validation/verification plots are presented in appendix D.

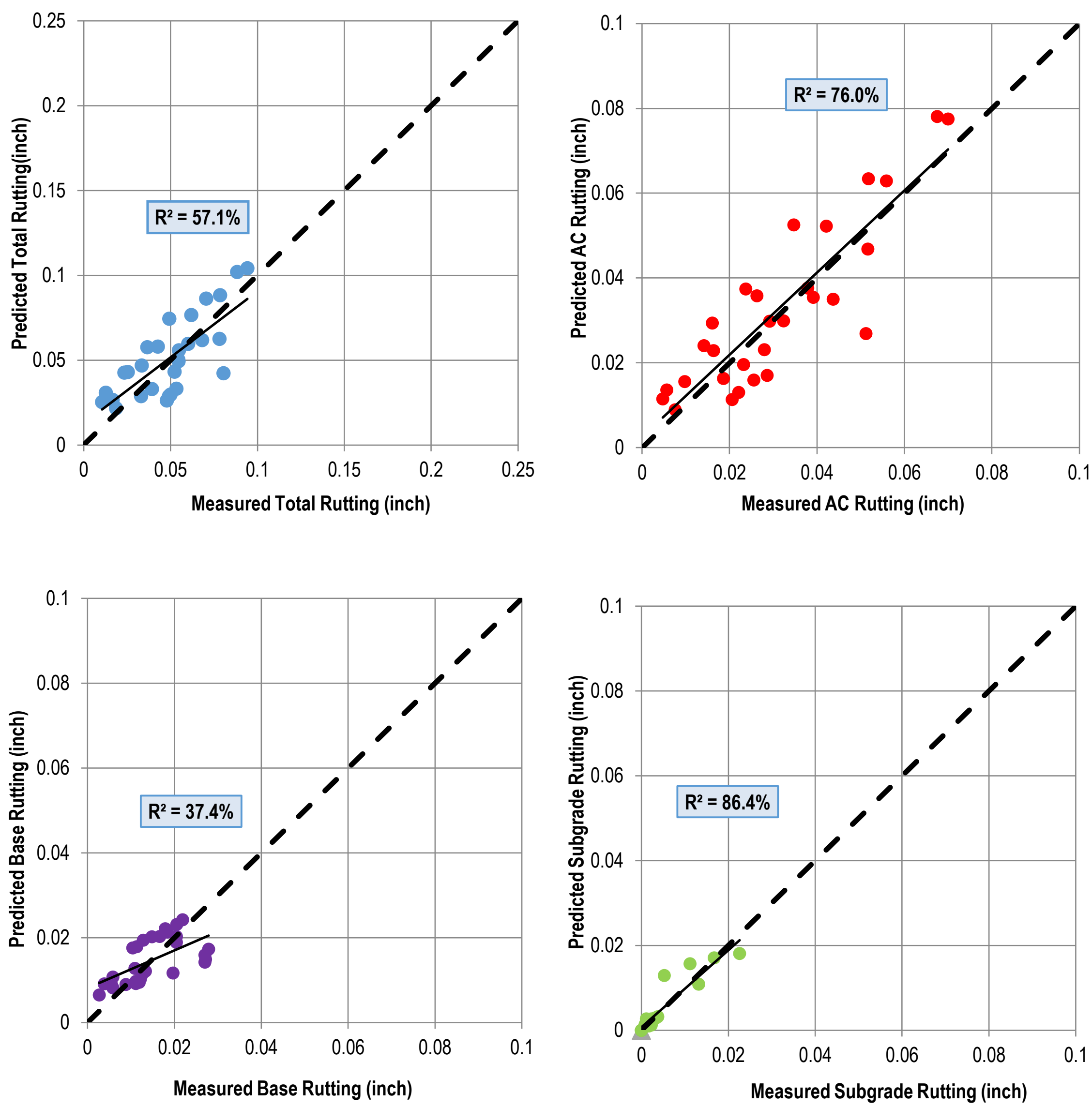

Figure 4.6-Rutting Verification Plots District I -Overlay.

4.4. AC Standard Deviation Calibration

The Pavement-ME software includes formulas that calculate the standard deviation of each predicted distress. These formula are used to estimate the pavement design reliability at any design level. Using the NDOT PMS data and considering that 60% of the total rutting occurs in the HMA layer, the standard deviation for each section used in the calibration/validation was calculated. All the sections were run using the appropriate local calibration factors for rutting to determine the value of the predicted AC rutting. The MEPDG default standard deviation model is shown in Equation 4.5.

$$STD\ (ACRUT)\ = a * ACRut^{b} + 0.001 \quad (4.5)$$

where:

$ACRUT$= predicted mean asphalt rutting from the Pavement-ME software (in.), and

a,b = model parameters = 0.24 and 0.8026 in the nationally calibrated model.

The sum of square errors reduction method was used to reduce the error between measured and predicted standard deviation values. Table 4.2 shows the calibration factors specific to Nevada's pavements. The plots for the different standard deviations are presented in Figure 4.7. Figures 4.8 to 4.13 show the plots for AC rutting standard deviation calibration.

Table 4.2-Standard Deviation Factors for NDOT's Pavements.

District	Section Type	a	b
I	Overlay	0.022859	0.245656
	New	2.000000	1.454605
II	Overlay	0.455358	1.098488
	New	1.687380	1.574905
III	Overlay	0.225536	1.135269
	New	0.428158	1.101886

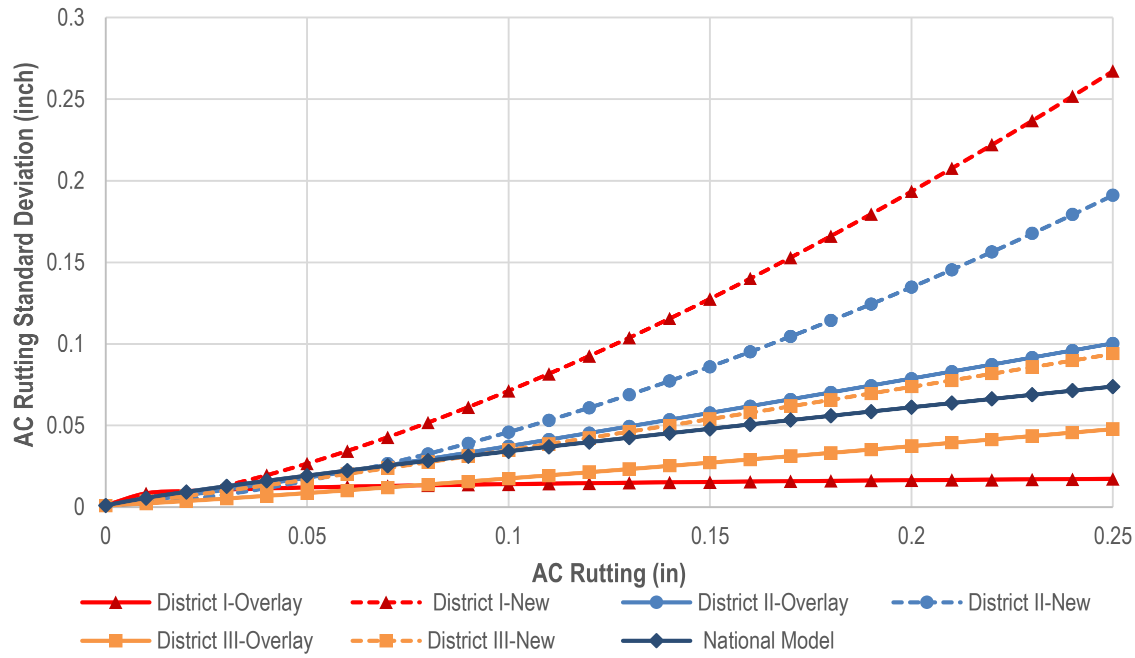

Figure 4.7-Standard Deviation Models as a Function of Predicted AC Rutting.

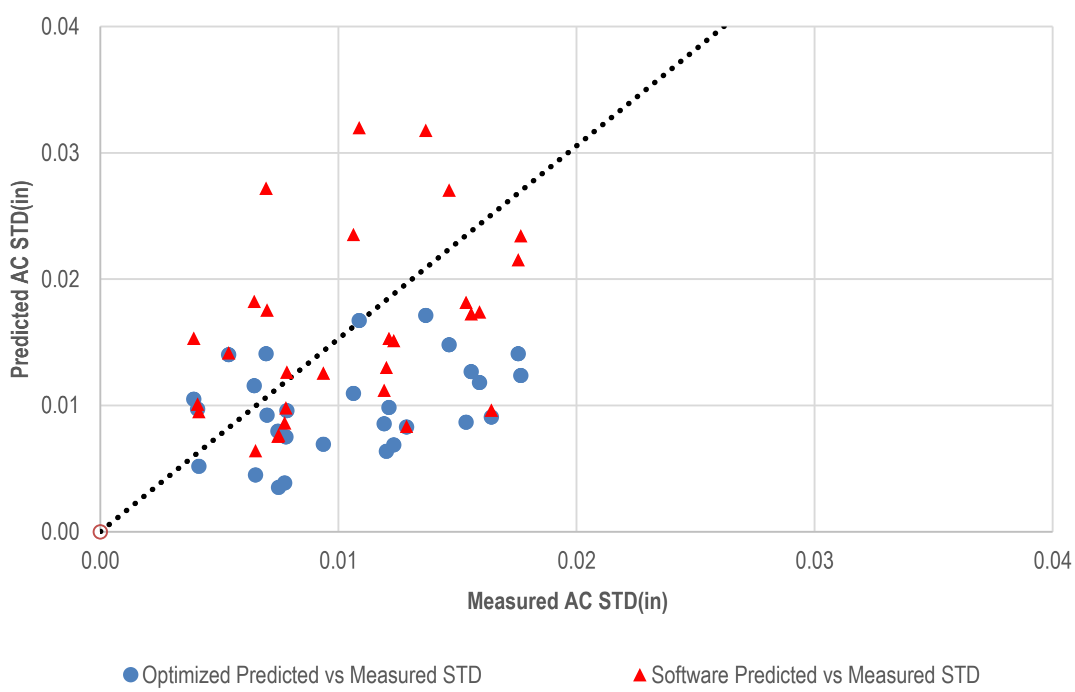

Figure 4.8-AC Standard Deviation Software Predicted vs Measured District I-Overlay.

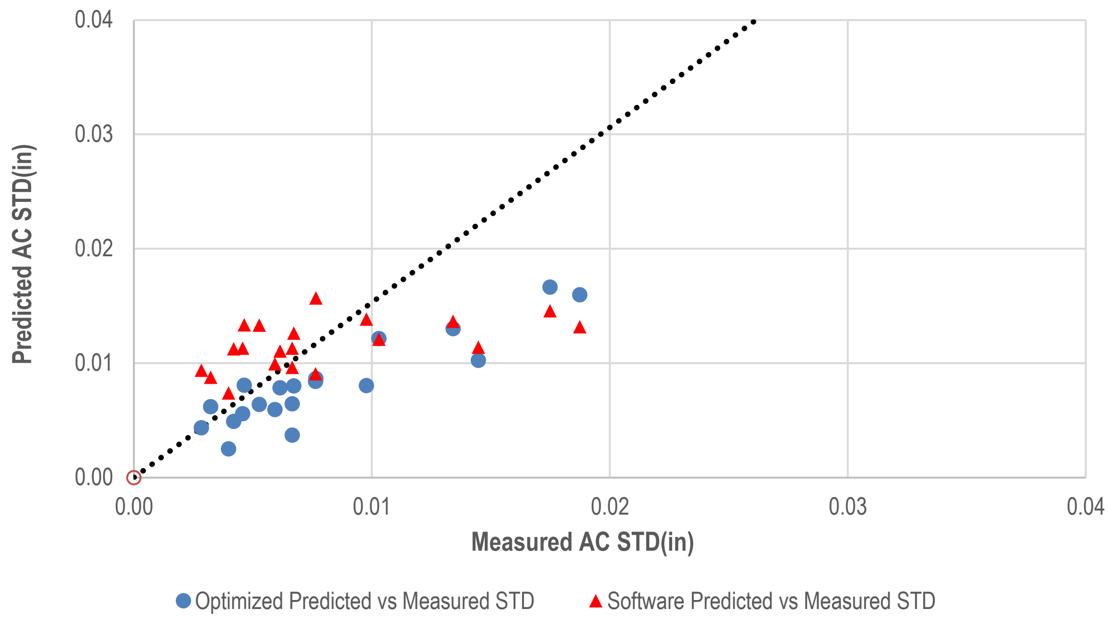

Figure 4.9-AC Standard Deviation Software Predicted vs Measured District I-New.

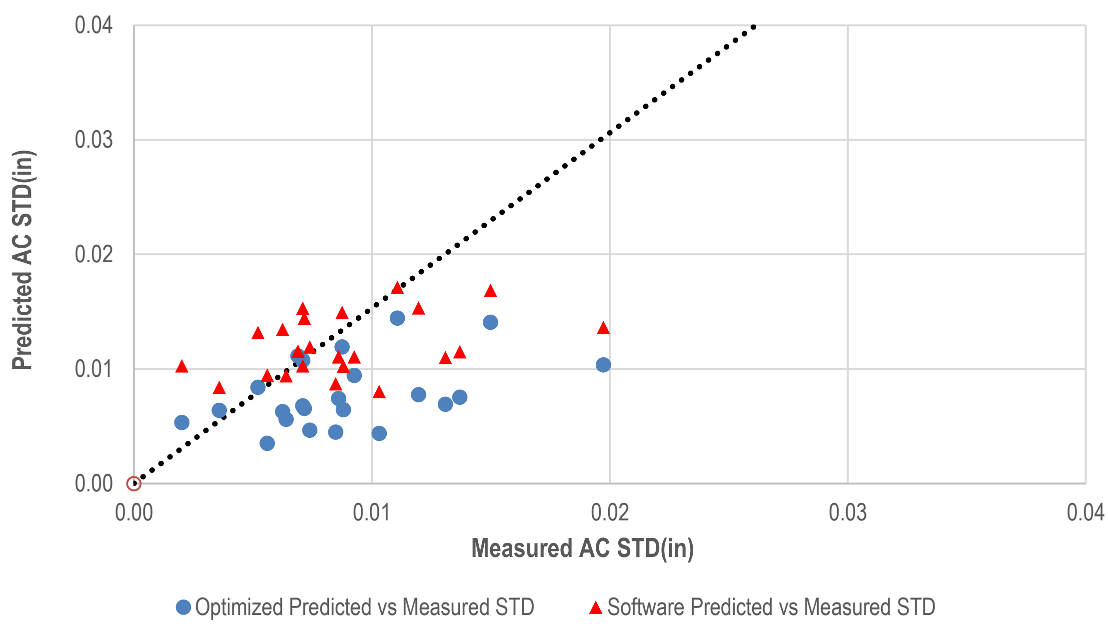

Figure 4.10-AC Standard Deviation Software Predicted vs Measured District II-Overlay.

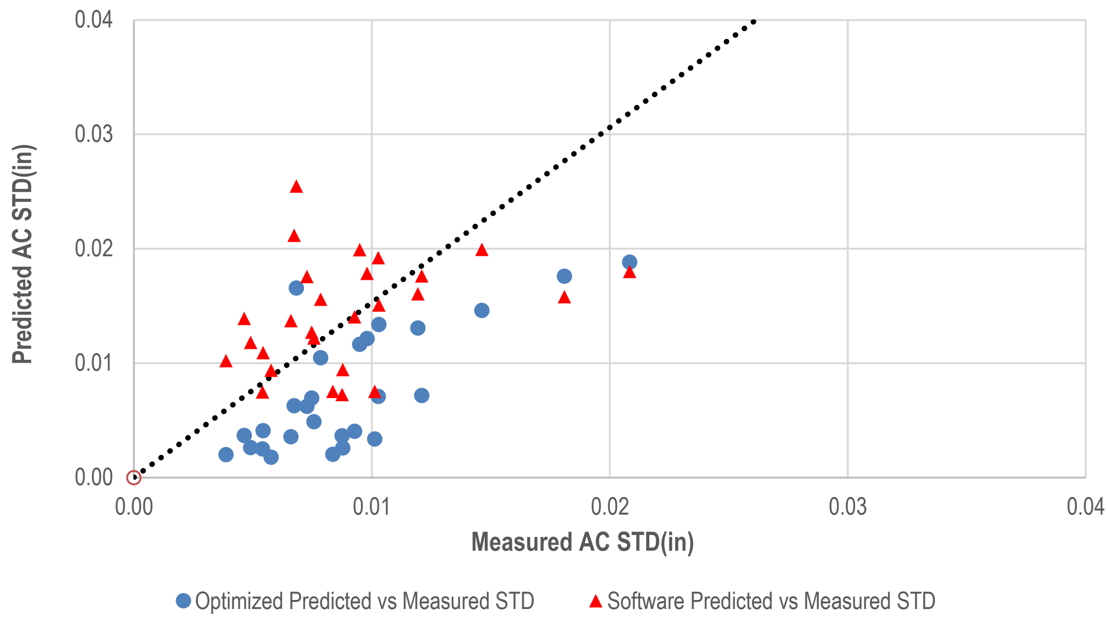

Figure 4.11-AC Standard Deviation Software Predicted vs Measured District II-New.

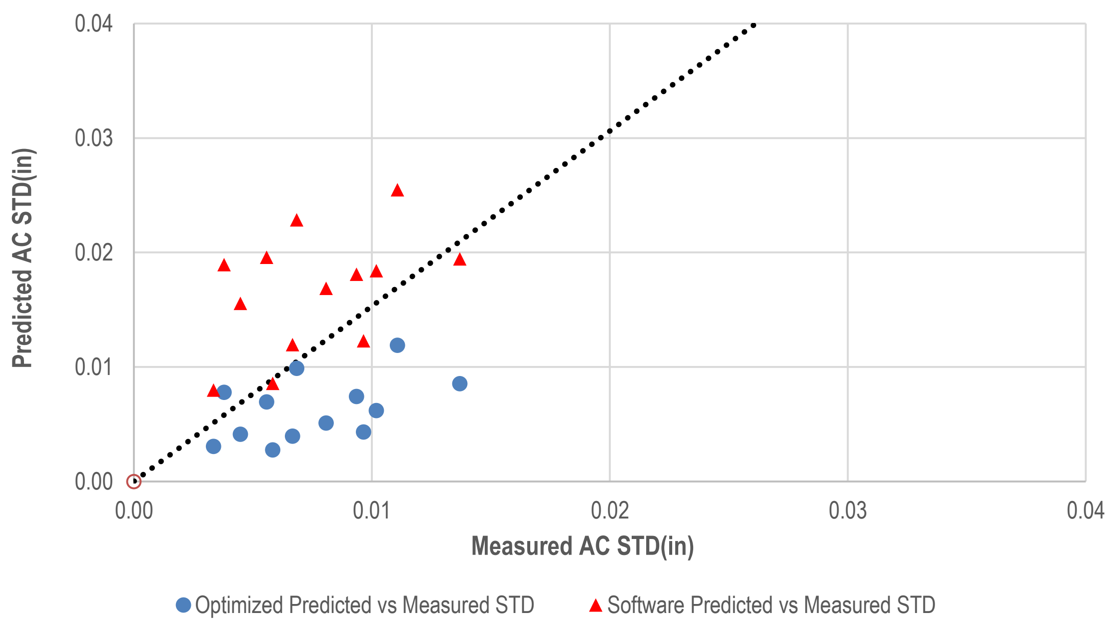

Figure 4.12-AC Standard Deviation Software Predicted vs Measured District III-Overlay.

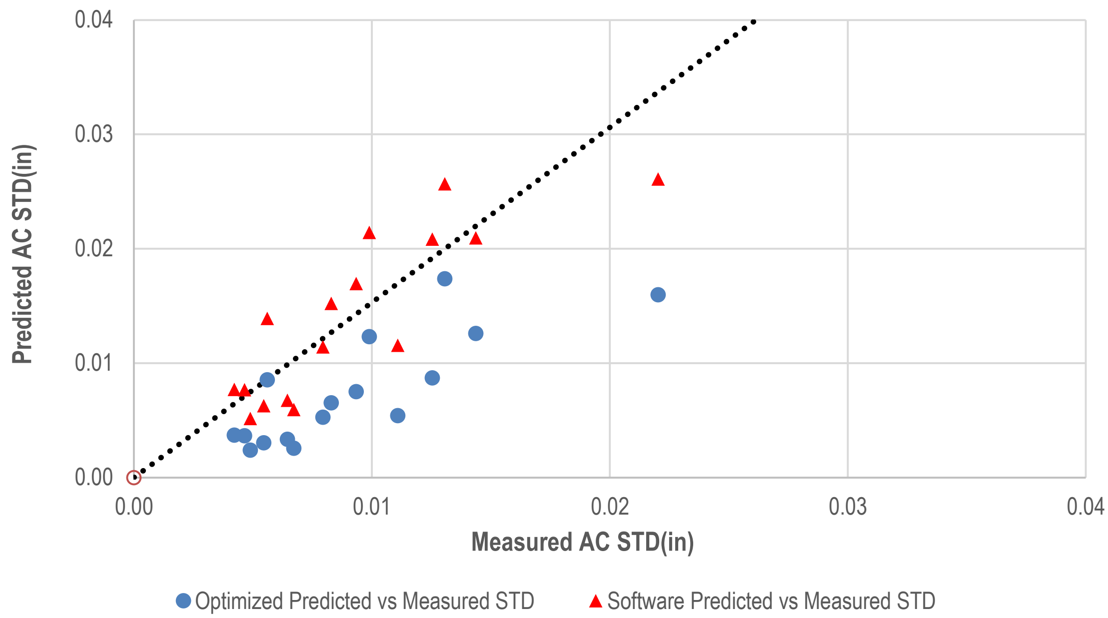

Figure 4.13-AC Standard Deviation Software Predicted vs Measured District III-New.

CHAPTER 5 FATIGUE CALIBRATION

5.1. Overview

Fatigue cracking is one of the major distresses observed in flexible pavements. The MEPDG defines two types of fatigue cracking: alligator cracking expressed as percent of cracking of total lane area, and longitudinal cracking estimated as feet of cracking per mile. Alligator cracking or bottom-up fatigue cracking is initiated at the bottom of the HMA layers under repeated traffic loading. This is primarily due to the tensile stresses and strains developed under asphalt beam bending. Higher values of alligator cracking are typically an indication of structural inadequacy or mixtures issues. Longitudinal cracking or top-down cracking is developed at the surface of the pavement; asphalt aging and stiffening is one of the elements that contribute in the initiation of longitudinal cracking as the HMA layer becomes more susceptible to thermal gradients. Additionally, the combination of tire contact pressure shearing and loading surface tension contributes to the creation of longitudinal cracking.

The nationally calibrated MEPDG models are discussed in this chapter. The fatigue cracking model is calibrated and validated to fit Nevada's conditions. However, the longitudinal cracking model which is being reevaluated under the active NCHRP project 01-52 will not be calibrated. This ongoing study suggests that the current method that uses fatigue damage mechanisms cannot adequately model top down cracking. Furthermore, the NCHRP project 01-42A recommended using asphalt fracture mechanics-based surface cracks propagation models for top-down cracking predictions.

The PMS pavement sections examined showed little or no fatigue. This was expected as the sections considered in this study were recently built (2003) polymer-modified asphalt pavements. The fatigue cracking percentage distribution is exposed in Figure 5.1. About 80% of the data points had less than 10% alligator cracking and no sections had fatigue measurements of more than 20%. This is primarily due to the fact that NDOT does not allow the pavements to reach significant levels of cracking before applying some type of repair strategy. Due to the lack of substantial amounts of data, the sections were grouped as follows: new and rehabilitated sections from district I formed the first group, the second group was a combination of all the sections from district II and III. The first group's sections information is shown in Table 5.1 below. Table 5.2 illustrates the properties of the second group of fatigue calibration sections. Eighteen sections of the total 58 were considered in the fatigue calibration because they exhibited some fatigue distresses.

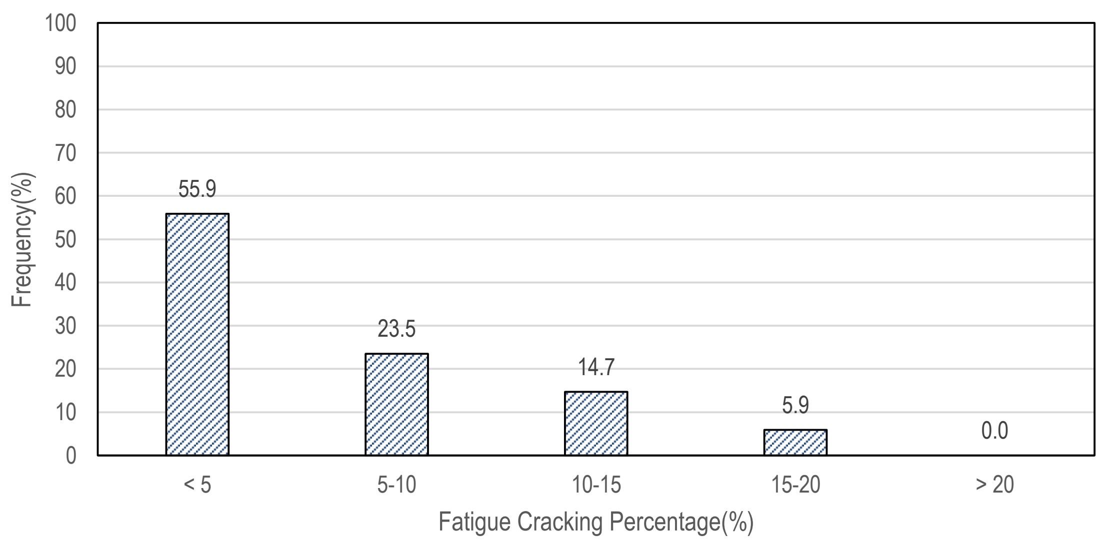

Figure 5.1-Fatigue Cracking Percentage Distribution for NDOT's MEPDG Calibration/Validation Sections.

Table 5.1-District I Fatigue Cracking Calibration Sections.

Section ID	Sampled	New/ Overlay	PMS Collection Date	Bottom-Up Fatigue PMS (%)	Pavement Age (years)	AC Thickness (inch)
IR 015-103	Yes	Overlay	12/28/11	12.27	3.0	3.0
SR 160-11	Yes	Overlay	06/04/09	0.34	4.0	3.0
SR 160-11	Yes	Overlay	01/04/12	1.03	7.0	3.0
IR 015-95	Yes	Overlay	05/05/09	3.81	3.0	2.0
IR 015-95	Yes	Overlay	01/04/12	7.00	5.0	2.0
IR 015-99A	No	Overlay	05/18/09	5.88	6.0	2.0
IR 015-99A	No	Overlay	01/19/12	9.94	9.0	2.0
IR 015-99B	No	Overlay	05/18/09	1.36	6.0	2.0
IR 015-99B	No	Overlay	12/28/11	9.77	8.0	2.0
IR 015-101	No	Overlay	06/20/07	1.29	3.0	2.0
IR 015-101	No	Overlay	05/18/09	2.51	5.0	2.0
IR 015-101	No	Overlay	12/12/11	5.87	7.0	2.0
SR 582-35	No	Overlay	06/13/07	6.57	4.0	2.0
SR 582-35	No	Overlay	04/21/09	11.12	6.0	2.0
SR 582-35	No	Overlay	01/03/12	11.77	9.0	2.0
IR 015-100	No	Overlay	05/28/09	2.50	5.0	2.0
IR 015-100	No	Overlay	12/28/11	5.00	7.0	2.0
SR 160-12B	Yes	New	06/04/09	14.50	2.0	5.0
SR 160-12B	Yes	New	01/05/12	18.67	5.0	5.0
US 093-40	No	New	06/19/07	9.09	2.0	2.0
US 093-40	No	New	04/20/09	11.11	4.0	2.0
US 093-40	No	New	01/05/12	15.63	7.0	2.0
SR 160-13	No	New	07/19/07	1.35	0.5	5.0
SR 160-13	No	New	05/27/09	2.08	2.0	5.0
SR 160-13	No	New	01/09/12	2.40	5.0	5.0

Table 5.2-District II-III Fatigue Cracking Calibration Sections.

Section ID	Sampled	New/Overlay	PMS Collection Date	Bottom-Up Fatigue PMS (%)	Pavement Age (years)	AC Thickness (inch)
US 395-80	No	Overlay	12/20/11	4.37	5.0	1.0
US 395-74A	Yes	Overlay	12/12/11	3.64	6.0	3.0
IR 080-142	Yes	Overlay	01/05/12	0.42	4.5	2.0
IR 080-140	Yes	Overlay	04/30/09	0.14	0.5	2.5
IR 080-140	Yes	Overlay	12/25/11	0.25	3.0	2.5
US 050-59	No	New	12/30/11	1.25	6.0	2.0
US 050A-72	Yes	New	02/17/12	6.25	5.0	3.0
IR 080-123	No	New	06/26/07	0.71	2.0	4.0
IR 080-123	No	New	04/30/09	0.86	4.0	4.0
IR 080-123	No	New	12/14/11	1.58	6.0	4.0

5.2. Fatigue Cracking Model Calibration

The revised MS-1 fatigue cracking model from the NCHRP project 01-37A is shown in Equation 5.1.

$$N_f = 0.00432 * \beta_{f1} * K_1 * C * \left(\frac{1}{\varepsilon_t}\right)^{\beta_{f2} * K_2} * \left(\frac{1}{E}\right)^{\beta_f * K_3} \tag{5.1}$$

where:

kf_1, kf_2, *and* kf_3 are experimentally determined regression coefficients found in Table 3.11 for the NDOT mixtures, and

β_{f1} ,β_{f2}, and β_{f3} are the local calibration coefficients.

$\beta_{f1} = \beta'_{f1} * k'_1$

β'_{f1} = the calibration factor and

k'_1 = the sigmoidal correction factors.

The correction of the β_{f1} was necessary because the initial MS-1 model was developed using the constant stress theory only applicable to sections with HMA layers thicker than 4 inches. This theory is invalid for sections with HMA layers thinner than 4 inches as those can only be analyzed using the constant strain theory. A sigmoidal function was created in order to resolve the issue of thick vs thin AC sections. Equation 5.2 and Figure 5.2 illustrate the sigmoidal correction function.

$$K'_1 = (0.000398 + \frac{0.003602}{1+e^{11.02-3.49*h_{ac}}}) * \left(\frac{1}{0.004}\right) \quad (5.2)$$

where:

H_{ac}= thickness of asphalt layer.

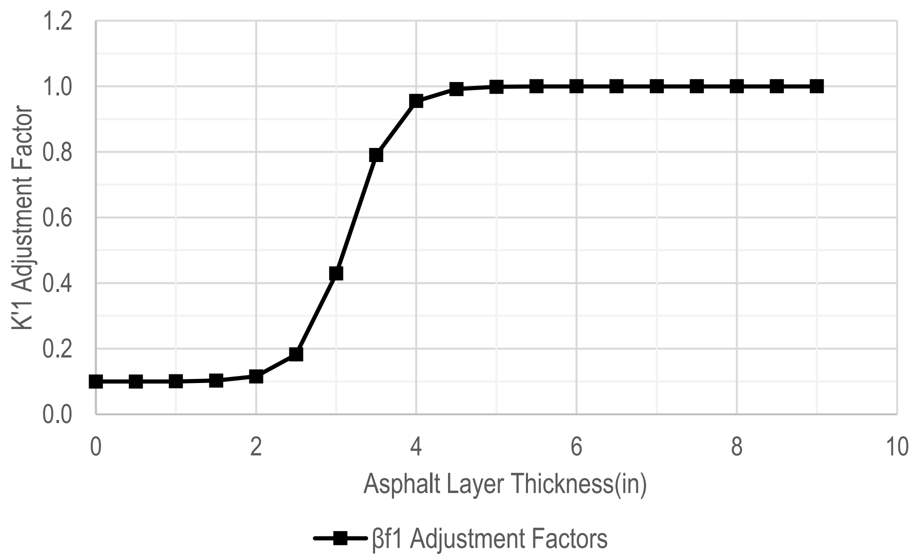

Figure 5.2-Sigmoidal Function for Thin AC Layer βf1 Adjustment.

Figure 5.2 clearly illustrates that for an asphalt layer thickness of 4 inches the adjustment factor approaches a value of 1.0.The calibration of the model called for the optimization of the power coefficients β_{f2}, and β_{f3} using the MEPDG software. The direct multiplier β_{f1} was optimized using the Microsoft excel solver. The calibration sections were run in Pavement-

ME software using the appropriate NDOT fatigue regression coefficients and β_{f2} and β_{f3} trial values of 0.8, 1.0, and 1.2. The 9 combinations and the respective errors generated are shown in Table 5.3 below.

Table 5.3- β_{f2} and β_{f3} Combinations for Fatigue Cracking Calibration and the Respective Sum of Square Errors.

β_{f2}, β_{f3}	SSE-District I-Overlay	SSE-District I-New	SSE-District II-III-Overlay	SSE-District II-III-New
0.8, 0.8	825.0	1,020.1	5,107.5	40,292.7
0.8, 1.0	822.7	134.3	9,320.6	38,163.0
0.8, 1.2	66,133.1	59,484.1	48,135.3	38,163.3
1.0, 0.8	825.0	1,020.9	32.5	44.2
1.0, 1.0	825.0	1,020.8	1,138.4	31,637.1
1.0, 1.2	825.0	943.1	19.3	47,912.4
1.2, 0.8	825.0	1,020.9	32.5	44.4
1.2, 1.0	825.0	1,020.8	32.5	44.3
1.2, 1.2	825.0	1,020.9	88.3	22,756.4

Table 5.3 clearly shows that some combinations resulted in a lower sum of square errors. In general a poor correlation was found between the software predicted values and the field measured values. Some combinations overestimated the distresses predictions (0.8, 1.2) while others estimated very low distresses. For example, in the case of district I-Overlay sections 7 out of 9 combinations had similar almost null predictions which explains why the models showed identical SSE values.

5.2.1. Alligator Cracking Transfer Function

The alligator cracking transfer function relates the damage calculated from Miner's equations to fatigue cracking as explained in section 2.3.1 above. The transfer function is shown in Equation. 5.3.

$$FC = \left(\frac{6000}{1+e^{C1*C'1+C2*C'2Log(Damage)}}\right)*\frac{1}{60} \quad (5.3)$$

where:

FC = fatigue cracking expressed in percentage of lane area,

D= Damage in percentage,

C_1= C_2= regression coefficients used for calibration (C_1= C_2=1.0 in the national model),

The 6000 is the total lane area in square feet (width of 12 feet * length of 500 feet). This value is divided by 60 to obtain the fatigue as a percentage. The C'_2 is a factor that takes into consideration the thickness of the AC layer, and C'_1 is equal to -2*C'_2 .

In order to minimize the error in the fatigue cracking predictions the C_1 and C_2 factors were optimized using an excel solver. It was found that a value of C_1 and C_2 equal to 0.8 reduced the sum of square errors and improved predictions. Figure 5.3 presents the locally calibrated fatigue transfer function along with different combinations of C_1 and C_2 to observe the variations in the transfer function.

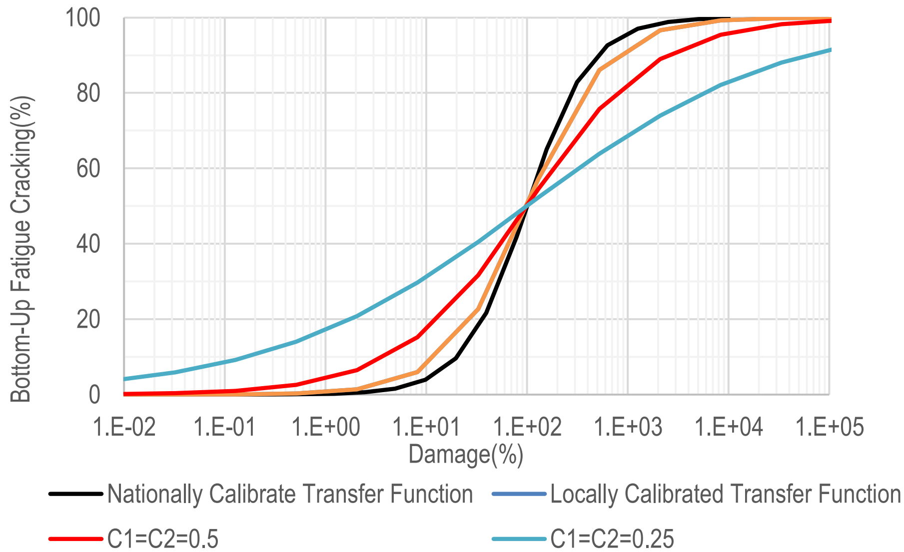

Figure 5.3-Fatigue Cracking Transfer Function for Different C_1 & C_2 Combinations.

The final step of the calibration focused on determining the β_{f1} factor. The Microsoft excel solver was run to reduce the sum of square errors. The results of the optimization are presented in the Tables 5.4 and 5.5 as follows. Figures 5.4 and 5.5 illustrate an example of the fatigue cracking calibration results for district I and district II-III, respectively.

Table 5.4-Optimization Results for District I (C_1=C_2=0.8)

β_{f2}, β_{f3}	β_{f1} Overlay	SSE-Overlay-After Calibration	β_{f1} New	SSE-New- After Calibration
0.8, 0.8	1.0E-04	825.0	1.0E-02	705.4
0.8, 1.0	8.3E-02	671.7	1.3E+00	89.9
0.8, 1.2	7.0E+01	688.6	1.2E+03	147.7
1.0, 0.8	1.0E-04	825.0	1.0E-02	1,020.8
1.0, 1.0	3.1E-06	707.2	1.0E-04	621.4
1.0, 1.2	2.3E-03	716.8	1.5E-01	163.2
1.2, 0.8	1.0E-04	825.0	1.0E-04	1,020.8
1.2, 1.0	1.0E-03	825.0	1.0E-04	1,014.9
1.2, 1.2	1.0E-03	825.0	2.0E-05	172.1

Table 5.5-Optimization Results for District II-III (C_1=C_2=0.8)

β_{f2}, β_{f3}	β_{f1} Overlay	SSE-Overlay-After Calibration	β_{f1} New	SSE-New- After Calibration
0.8, 0.8	4.4E+01	19.3	3.7E+02	28.2
0.8, 1.0	2.6E+05	19.3	1.8E+06	30.3
0.8, 1.2	1.7E+09	19.3	8.9E+09	30.8
1.0, 0.8	2.8E-03	19.3	4.0E-02	25.5
1.0, 1.0	1.3E+01	19.3	1.8E+02	25.5
1.0, 1.2	8.6E-01	19.3	8.5E+05	25.8
1.2, 0.8	1.0E-04	32.5	1.0E-02	44.4
1.2, 1.0	8.0E-04	19.3	3.1E-02	28.5
1.2, 1.2	4.6E+00	19.3	1.5E+02	29.2

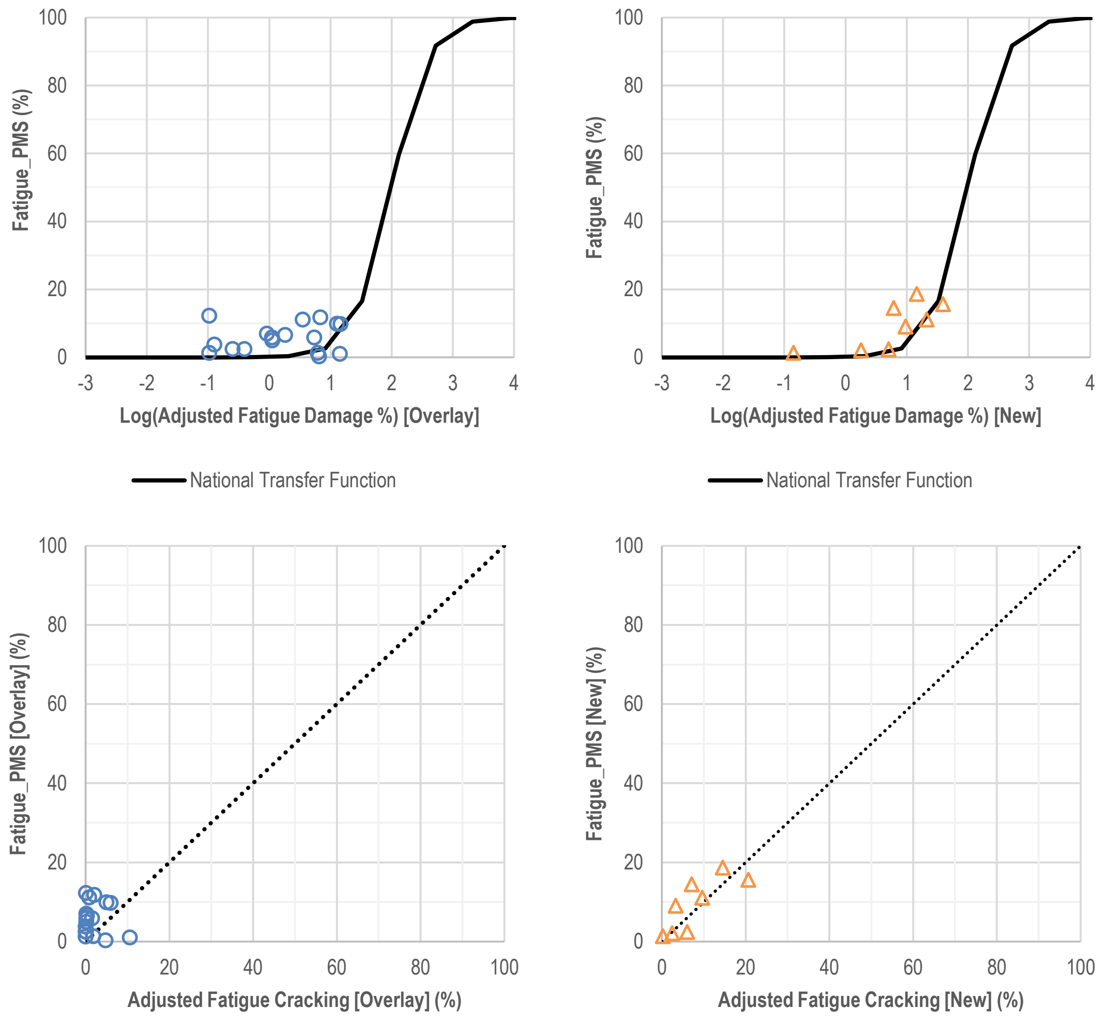

Figure 5.4-Example of Measured PMS Fatigue vs Software Predicted from District I Calibration (β_{f2}=0.8, β_{f3}=1.2).

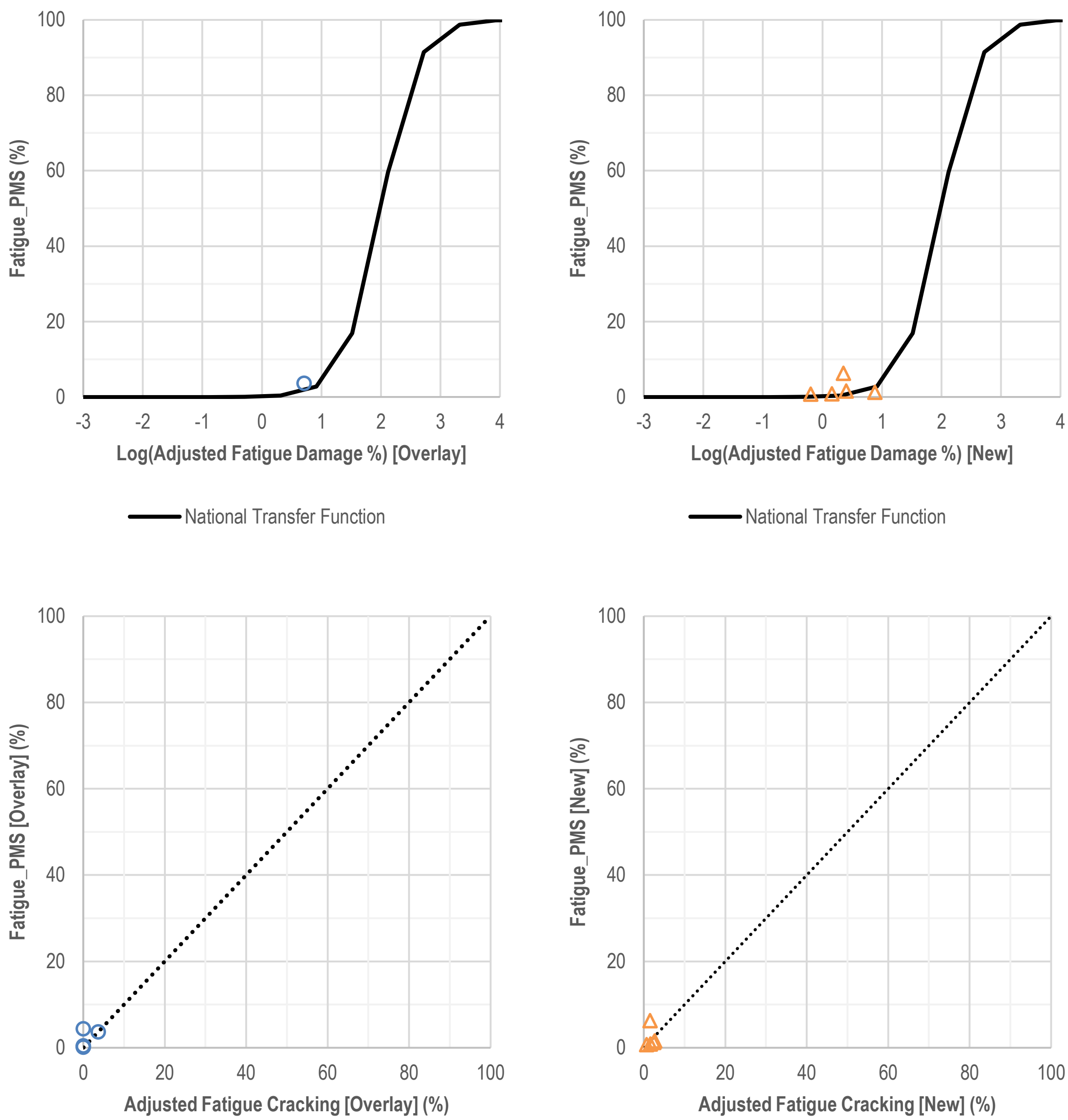

Figure 5.5-Example of Measured PMS Fatigue vs Software Predicted from District II-III Calibration (β_{f2}=1.0, β_{f3}=1.0).

5.2.2. Alligator Cracking Validation

The calibration factors computed from the excel optimization were tested in the AASHTOWare Pavement-ME software as part of a validation process. The final set of calibration factors included the β_{f1} correction for all the software runs. Several verification runs were conducted as a part of an iteration process used to reach optimal values for the calibration factors. The final calibration factors for bottom-up cracking are given in Table 5.6. The alligator fatigue validation plots are presented in Figure 5.6 and Figure 5.7. Figure 5.6 illustrates the verification results from district I by plotting measured fatigue cracking versus software predicted fatigue cracking and damage after calibration. Figure 5.7 represents the measured versus predicted fatigue cracking values from district II-III validation.

Table 5.6-Final Fatigue Cracking Calibration Factors for NDOTs Pavements.

Calibration Factors	District I-Overlay	District I-New	District II-III-Overlay	District II-III-New
AC Fatigue β'_{f1}[1]	0.200	0.005	0.015	50.000
AC Fatigue β_{f2}	0.800	1.000	1.000	1.000
AC Fatigue β_{f3}	1.000	1.000	1.000	1.000
C_1	0.800	0.800	0.800	0.800
C_2	0.800	0.800	0.800	0.800

[1]*Note that the correction factor k'_1 for asphalt layer thickness should be applied.*

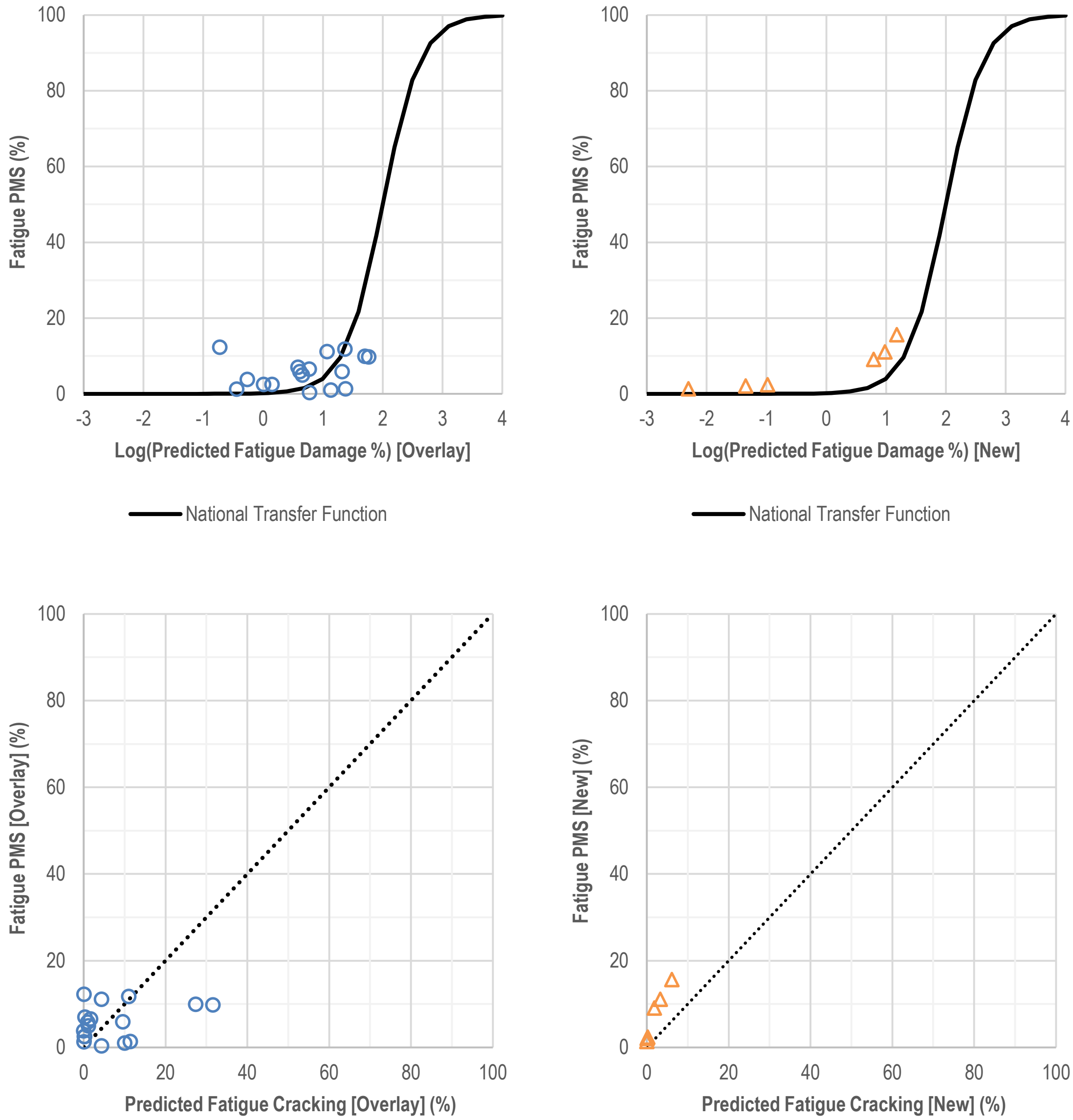

Figure 5.6- Measured PMS Fatigue vs Software Predicted Cracking and Log of Damage from District I Verification.

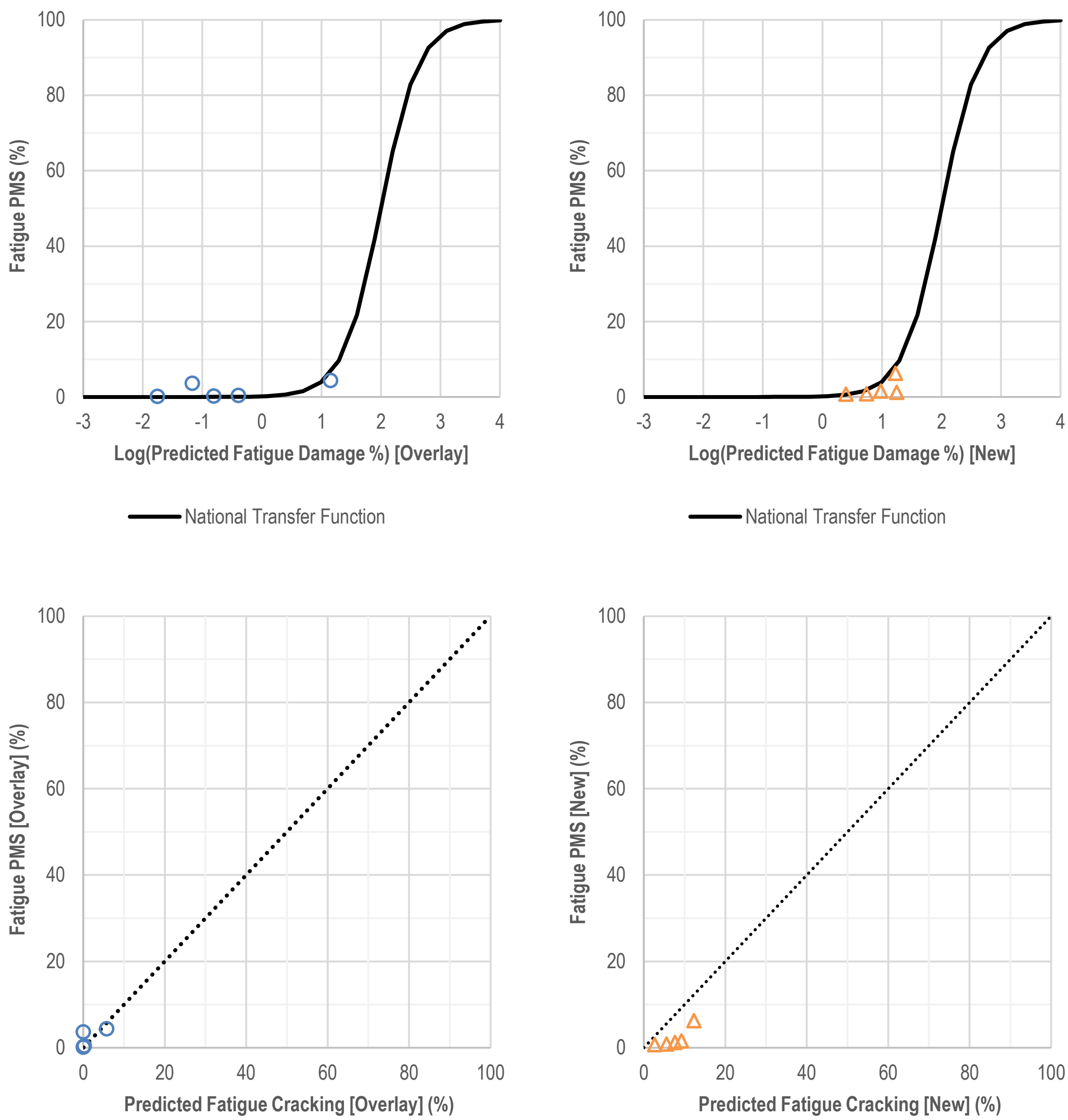

Figure 5.7- Measured PMS Fatigue vs Software Predicted Cracking and Log of Damage from District II-III Verification.

5.2.3. Longitudinal Cracking Transfer Function

The longitudinal fatigue cracking is modeled using a sigmoidal function similar to the bottom-up fatigue cracking. This sigmoidal function transfers calculated damage to longitudinal fatigue cracking in feet/mile. The same fatigue model is used to compute the longitudinal cracking values. Equation 5.4 represents the transfer function used in the longitudinal cracking predictions.

$$FC = \left(\frac{1000}{1+e^{C1-C2Log(D)}}\right) * 10.56 \quad (5.4)$$

where:

F.C. = Longitudinal cracking (ft/mile),

D = Damage in percentage,

C_1, C_2 = Regression coefficients = 7 and 3.5 respectively.

In order to verify the sigmoidal function assumptions (50% cracking occurs at 100% damage), the ratio $C_1=2*C_2$ should be maintained in any local calibration. Figure 5.8 illustrates the longitudinal cracking model using different regression coefficients to show the evolution of the model with the change of the factors. The calibration of the longitudinal cracking model was not considered in the NDOT MEPDG implementation as a different model is being developed and calibrated under the active NCHRP project 01-52.

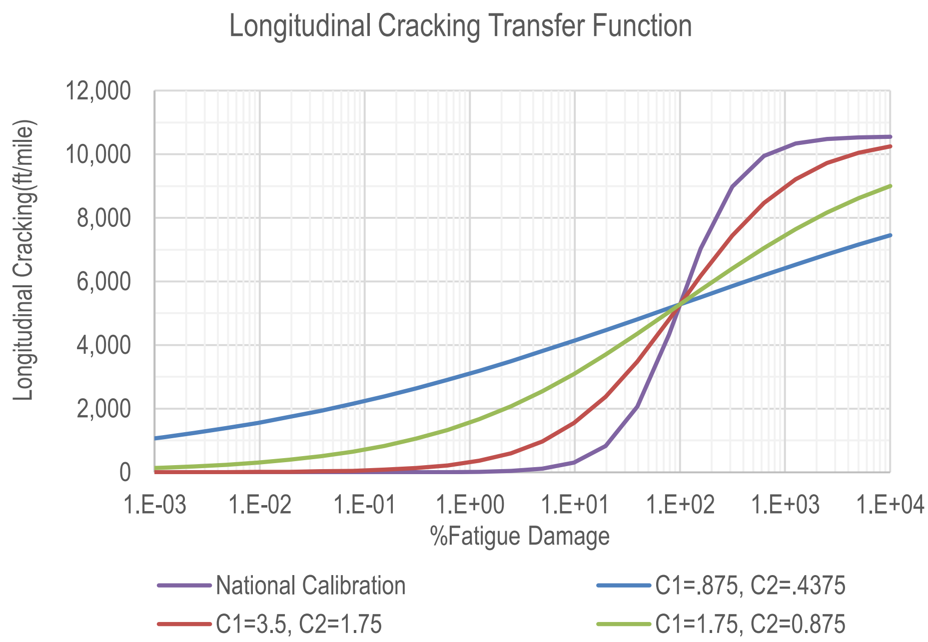

Figure 5.8- Top-Down Fatigue Cracking Transfer Function with Multiple C_1 and C_2 Combinations.

CHAPTER 6 INTERNATIONAL ROUGHNESS INDEX CALIBRATION

6.1. Overview

Roughness is considered as one of the major functional failures in asphalt pavements. This failure occurs when pavement structures are incapable of carrying out the expected function at a specified serviceability level. Roughness usually affects the ride comfort, safety, and can put additional wear on the vehicle. Additionally, roughness increases the dynamic loading of the traveling vehicles which accelerates the deterioration of the pavement. In the MEPDG roughness is defined using the IRI standards. The IRI was first introduced in Brazil by the World Bank in 1982. Sayers et al. (1986) defined the IRI as a standard statistic to correlate and calibrate roughness measurements. IRI, expressed in (in/mile), measures the cumulative vertical suspension motion of a quarter-car model and divides it by the length travelled during the test. Higher IRI values are an indication of a deteriorated pavement.

6.2. IRI Model

The MEPDG calculates the IRI using the predicted surface distresses based on the assumption that an increase in distresses leads to a rougher surface. The national MEPDG calibration used a regression analysis based on the predicted distresses to create the roughness model. Equation 6.1 shows the resulting roughness model (NCHRP 2004).

$$IRI = IRI_0 + C_1 * RD + C_2 * FC + C_3 * TC + C_4 * SF \quad (6.1)$$

where:

IRI= International Roughness Index (in. /mile),

IRI_0=Initial IRI at the time of traffic opening (in. /mile), *RD*= Mean predicted rut depth (in.),

FC=Predicted fatigue cracking combining alligator and longitudinal cracking (%),

TC= Length of transverse cracking (ft/mile),

SF=Site Factor

$$=Age\left(0.02003(PI+1)+0.007947(Rain+1)+0.000636(FI+1)\right)$$

Age = Pavement age in years,

PI = Percent plasticity index of the soil.

FI = Average annual freezing index (°F days).

Rain = Average annual rainfall (in.), and

C_1, C_2, C_3, and C_4 = Calibration factors with values of 40, 0.4, 0.008 and 0.15, respectively. These regression equation coefficients require calibration to fit the local conditions. In this study, the longitudinal and transverse cracking models were not calibrated to Nevada's conditions. Considering that the IRI predictions are based on these distresses among others; the local calibration for the IRI model was not conducted for Nevada.

CHAPTER 7 DESIGN EXAMPLES

This chapter describes the work required to conduct a pavement design using the Pavement-ME software. The detailed inputs for two sections from the calibration/validation analysis are discussed below:

7.1. District I-New Construction

This section is a new flexible pavement construction on the US 095 route in Clark County, Nevada (section US 095-39). Table 7.1 represents the general project information extracted from the TRINA software and Table 7.2 illustrates the section's thicknesses.

Table 7.1-General Project Information for US 095-39.

Route	US95N
Location Description	0.8 mi N of SR-163 (Laughlin/Davis Dam Rd)
From Street	SR-163 (Laughlin Hw)
To Street	SR-164 (Nipton Rd)
County Name	CLARK
Latitude	35.2203
Longitude	-114.86
Functional Class	3 - Principal Arterial - Other
From Mile	1.185
To Mile	20.366
Construction Year	2007
AADT Construction Year	9,300

Table 7.2-Pavement Structure and Resilient Modulus Calculations for US 095-39.

<table>
<tr><td rowspan="3">US 095-39</td><td>Year</td><td>2007</td><td>Layer Behavior</td><td>Structural Factor</td><td>Section Modeled</td><td>Modulus E (psi)</td></tr>
<tr><td rowspan="2">Structure</td><td>6" PG76-22NV</td><td>Visco-Elastic</td><td>Database</td><td>6" PG76-22NV</td><td>Database</td></tr>
<tr><td>16" Aggregate Base</td><td>Elastic</td><td>Database</td><td>16" Aggregate Base</td><td>26000</td></tr>
</table>

The design was performed for 20 years at 90% reliability. Table 3.15 provided the AADT, truck percentage, AADTT, and traffic growth. Additional traffic inputs such as vehicle classification were retrieved from Table 3.18. The climatic information inputs: longitude, latitude, elevation, and depth of water table were extracted from Table 3.24. These inputs are summarized in Table 7.3 below.

Table 7.3-Summary of Inputs for US 095-39 Example.

Input	**US 095-39**
AADT	9300
Truck Percentage (%)	19.6
AADTT	1823
Traffic Growth (%)	3
Latitude (°)	35.22
Longitude (°)	-114.86
Elevation(ft)	2545
Depth of Water Table(ft)	120

The aggregate base layer constructed was a Type I-B layer. Tables 3.27 and 3.28 define the appropriate inputs for resilient modulus and gradation limits. The web-based application developed by Zapata et al. (2010) was used to generate the subgrade layers inputs. Figures 7.1 below illustrates the soil map report. The outputs are summarized in Table 7.4. The resilient modulus of the subgrade layers was corrected using district I seasonal variation factors from Table 3.30. The corrected resilient modulus values are presented in Table 7.5 as follows.

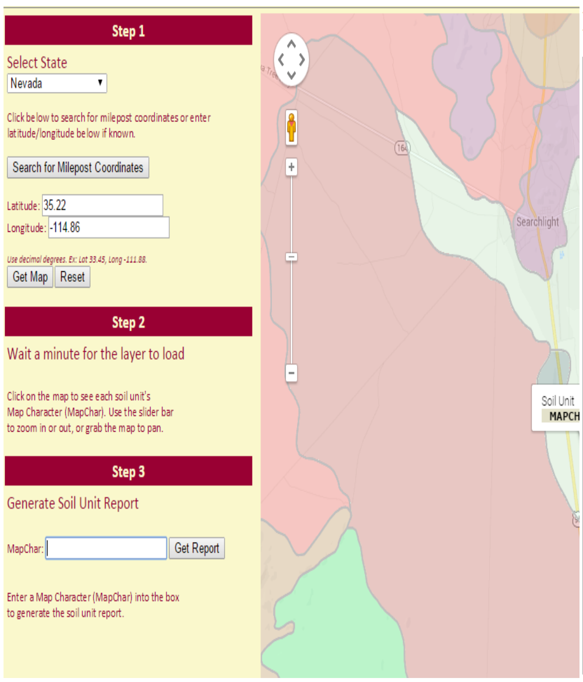

Properties of Soil Unit B83

Map Character	Map Unit Key	Map Unit Name	Component Name
B83	660591	Skyhaven-Rillito-Mead-McCullough-Ireteba-Bluepoint (s1144)	McCullough

AASHTO Classification	AASHTO Group Index	Top Depth (in)	Bottom Depth (in)	Thickness (in)	% Component	Water Table Depth Annual Min (ft)	Depth to Bedrock (ft)
A-5	0	0	7.9	7.9	25	N/A	N/A
A-2-4	0	7.9	26	18.1	25	N/A	N/A
A-1-b	0	26	59.8	33.9	25	N/A	N/A

CBR from Index Properties	Resilient Modulus from Index Properties (psi)	Passing #4 (%)	Passing #10 (%)	Passing #40 (%)	Passing #200 (%)	Passing 0.002 mm (%)	Liquid Limit (%)
17.5	15946	97.5	97.5	72.5	45	7.5	N/A
45.8	29542	95	95	60	35	13	20
26.8	20950	90	85	50	25	5	N/A

Plasticity Index (%)	Saturated Volumetric Water Content (%)	Saturated Hydraulic Conductivity (ft/hr)	Parameter af (psi)	Parameter bf	Parameter cf	Parameter hr (psi)
0	46	0.33341	9.199	4.2062	0.7016	3000
2.5	49	0.10836	1.8636	1.0594	0.9447	3000.02
0	42	1.08358	9.0803	6.005	0.759	3000

Figure 7.1- ASU Web-Based Soil Map and Report for US 095-39.

Table 7.4. ASU Soil Output Example for Soil Unit 'B83' (Section US 095-39).

	Section	US 095-39		
	Layer	**Top Layer**	**Layer 2**	**Layer 3**
Road Classification and Thicknesses	AASHTO Classification	A-5	A-2-4	A-1-b
	AASHTO Group Index	0	0	0
	Top Depth (in)	0	8	26
	Bottom Depth (in)	8	26	60
	Thickness (in)	8	18	34
	% Component	25	25	25
	Water Table Depth(ft.)	N/A (Default)	N/A (Default)	N/A (Default)
	Depth to Bedrock (ft.)	N/A (Default)	N/A (Default)	N/A (Default)
Strength Properties	CBR from Index Properties	17	46	27
	Resilient Modulus (psi)	15,946	29,542	20,950
Index Properties	Passing #4 (%)	97.5	95	90
	Passing #10 (%)	97.5	95	85
	Passing #40 (%)	72.5	60	50
	Passing #200 (%)	45	35	25
	Passing 0.002 mm (%)	7.5	13	5
	Liquid Limit (%)	N/A (Default)	20	N/A (Default)
	Plasticity Index (%)	0	2.5	0
	Saturated Volumetric Water Content (%)	46	49	42
	Saturated Hydraulic Conductivity(ft/hr)	0.3334	0.1084	1.0836
SWCC Parameters	Parameter af (psi)	9.199	1.8636	9.0803
	Parameter bf	4.2062	1.0594	6.005
	Parameter cf	0.7016	0.9447	0.759
	Parameter hr (psi)	3000	3000	3000

Table 7.5. Seasonal Resilient Modulus Input for Subgrade Layers (US 095-39).

Month	Seasonal Coefficients	Resilient Modulus (psi)		
		Top Layer	Layer 2	Layer 3
January	0.77	12,279	22,747	16,131
February	0.77	12,279	22,747	16,131
March	0.77	12,279	22,747	16,131
April	0.79	12,598	23,338	16,550
May	0.79	12,598	23,338	16,550
June	0.79	12,598	23,338	16,550
July	1.00	15,946	29,542	20,950
August	1.00	15,946	29,542	20,950
September	1.00	15,946	29,542	20,950
October	0.85	13,554	25,111	17,807
November	0.85	13,554	25,111	17,807
December	0.85	13,554	25,111	17,807

Table 7.6 presents the design inputs for the asphalt layer. The section was run using the Pavement-ME software and the appropriate calibration coefficients for District I-New sections. The IRI, total rutting, and fatigue cracking plots are exposed in Figure 7.2.

Table 7.6. Design Inputs for HMA Layer (US 095-39).

Parameter	Design Input
Asphalt Layer	
Thickness (in)	6
Mixture Volumetrics	
Unit weight (pcf)	150
Effective binder content (%)	8.5
Air voids (%)	7
Poisson's ratio	0.35
Mechanical Properties	
Dynamic Modulus	Refer to Table 3.4 (District I)
Reference temperature (deg F)	70
Asphalt Binder G* and Phase Angle	Refer to Table 3.3
Thermal	
Thermal conductivity (BTU/hr-ft-deg F)	0.67
Heat capacity (BTU/lb-deg F)	0.23

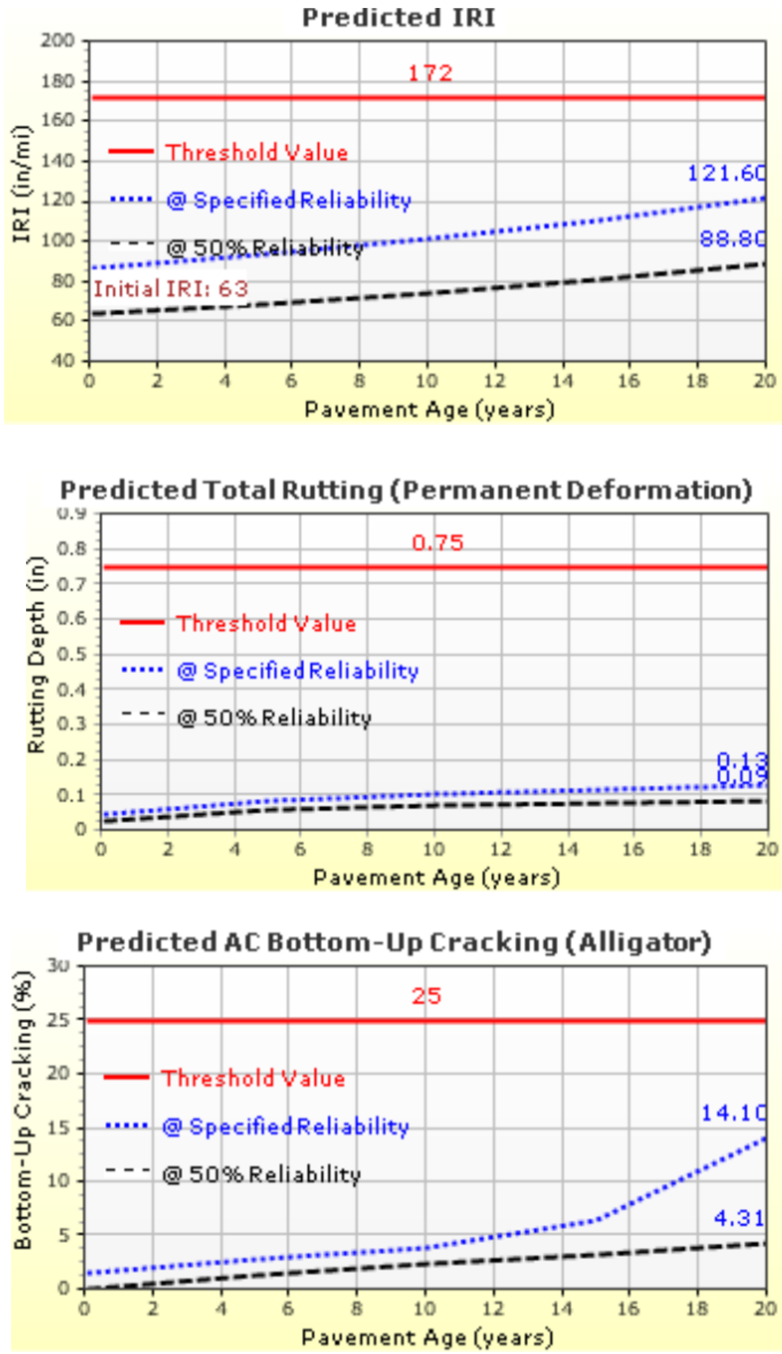

Figure 7.2. Distress Charts for New Section District I (US 095-39) (MEDesign version 2.1).

7.2. District III-Rehabilitation

This section is a new flexible pavement construction on the IR 080 interstate in Lander County, Nevada (section IR 080-140). Table 7.7 represents the general project information obtained using the TRINA software and Table 7.8 illustrates the section's thicknesses and resilient modulus calculations.

Table 7.7-General Project Information for IR 080-140.

Route	IR 080
Location Description	0.2 mi E of the E Battle Mtn Intch 'Exit 233'
From Street	SR-304 (East Battle Mtn Intch 'Exit 223')
To Street	Argenta Intch 'Exit 244'
County Name	LANDER
Latitude	40.6198
Longitude	-116.907
Functional Class	1 – Interstate
From Mile	8.124
To Mile	19.201
Construction Year	2009
AADT Construction Year	6,900

Table 7.8-Pavement Structure and Resilient Modulus Calculations for IR 080-140.

<table>
<tr><th rowspan="6">IR 80-140</th><th>Final Structure</th><th>Layer Behavior</th><th>Thickness (in)</th><th>Layer Coefficient</th><th>h*ai</th><th>Section Modeled</th><th>Modulus E (psi)</th></tr>
<tr><td></td><td></td><td></td><td></td><td></td><td>2.5" PG64-28NV</td><td>Database</td></tr>
<tr><td>2.5" PG64-28NV</td><td>Visco-Elastic</td><td>2.5</td><td>Database</td><td>Database</td><td>5.5" AC-20P</td><td>Database</td></tr>
<tr><td>5.5" AC-20P</td><td>Visco-Elastic</td><td>5.5</td><td>Database</td><td>Database</td><td>24"Aggregate Base Linear Elastic</td><td rowspan="2">28785</td></tr>
<tr><td>8" RBM</td><td>Elastic</td><td>8</td><td>0.2</td><td>1.6</td><td>0.133</td></tr>
<tr><td>16" Aggregate Base</td><td>Elastic</td><td>16</td><td>0.1</td><td>1.6</td><td>Subgrade</td><td>Database NCHRP</td></tr>
</table>

The design was performed for 20 years at 90% reliability. Table 3.17 provided the AADT, truck percentage, AADTT, and traffic growth. Additional traffic inputs such as vehicle classification were retrieved from Table 3.20. The climatic information inputs: longitude, latitude, elevation, and depth of water table were extracted from Table 3.26. These inputs are summarized in Table 7.9 below.

Table 7.9-Summary of Inputs for US 095-39 Example.

Input	IR 080-140
AADT	6900
Truck Percentage (%)	32.88
AADTT	2269
Traffic Growth (%)	3
Latitude (°)	40.62
Longitude (°)	-116.907
Elevation(ft)	4524
Depth of Water Table(ft)	74

The resulting aggregate base layer was considered a Type I-A layer with a resilient modulus of 28785 psi. Table 3.28 defined the appropriate inputs for gradation limits. The web-based application developed by Zapata et al. was used to generate the subgrade layers inputs. Figure 7.3 below illustrates the soil map report. The outputs were summarized (Table 3.29), and the resilient modulus of the subgrade layers was adjusted using district III seasonal variation factors from Table 3.30. The corrected resilient modulus values are presented in Table 7.10 as follows.

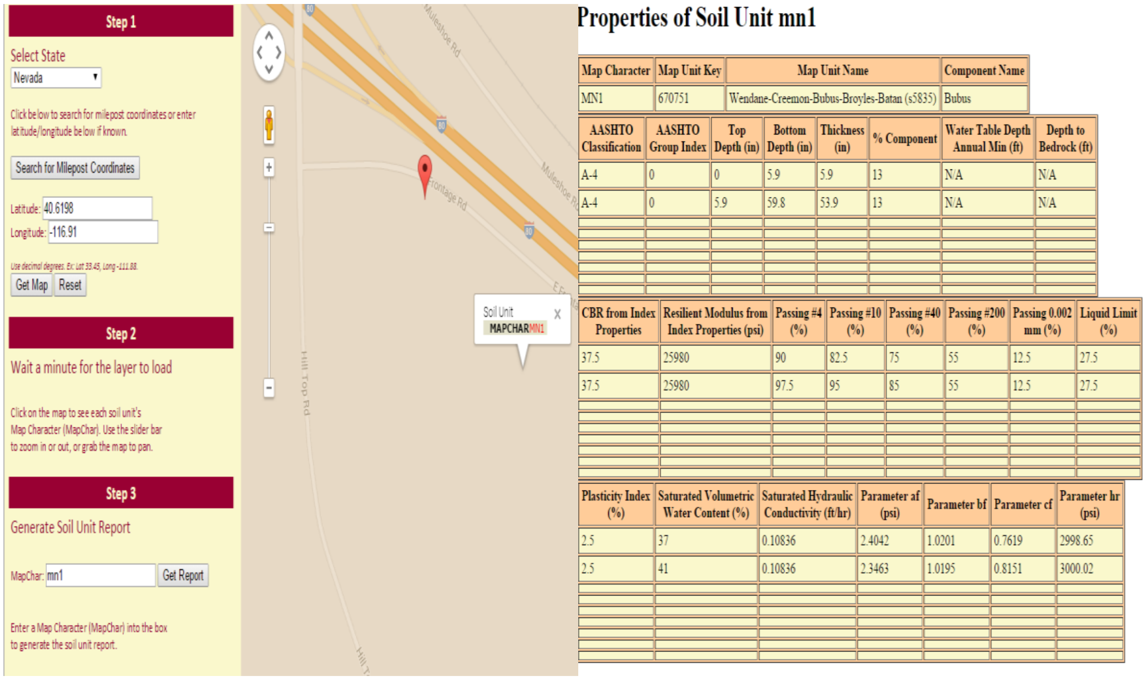

Figure 7.3- ASU Web-Based Soil Map and Report for IR 080-140.

Table 7.10. Seasonal Resilient Modulus Input for Subgrade Layers (IR 080-140).

Month	Seasonal Coefficients	Resilient Modulus (psi)	
		Top Layer	Layer 2
January	0.81	21,043	21,043
February	0.81	21,043	21,043
March	0.81	21,043	21,043
April	0.7	18,186	18,186
May	0.7	18,186	18,186
June	0.7	18,186	18,186
July	1	25,980	25,980
August	1	25,980	25,980
September	1	25,980	25,980
October	1.02	26,499	26,499
November	1.02	26,499	26,499
December	1.02	26,499	26,499

Table 7.11 presents the design inputs for the most recent asphalt layer. The existing asphalt layer properties are shown in Table 7.12 The section was run using the Pavement-ME

software and the appropriate calibration coefficients for District III-Rehabilitation sections. The AC rutting, total rutting, and fatigue cracking plots are exposed in Figure 7.4 below.

Table 7.11. Design Inputs for Overlay HMA Layer (IR 080-140).

Parameter	Design Input
Asphalt Layer	
Thickness (in)	2.5
Mixture Volumetrics	
Unit weight (pcf)	150
Effective binder content (%)	8.5
Air voids (%)	7
Poisson's ratio	0.35
Mechanical Properties	
Dynamic Modulus	Refer to Table 3.8 (District III)
Reference temperature (deg F)	70
Asphalt Binder G* and Phase Angle	Refer to Table 3.3
Thermal	
Thermal conductivity (BTU/hr-ft-deg F)	0.67
Heat capacity (BTU/lb-deg F)	0.23

Table 7.12. Design Inputs for Existing HMA Layer (IR 080-140).

Parameter	Design Input
Asphalt Layer	
Thickness (in)	5.5
Mixture Volumetrics	
Unit weight (pcf)	150
Effective binder content (%)	8.5
Air voids (%)	7
Poisson's ratio	0.35
Mechanical Properties	
Dynamic Modulus	Default
Reference temperature (deg F)	70
Asphalt Binder G* and Phase Angle	Binder Grade AC-20
Thermal	
Thermal conductivity (BTU/hr-ft-deg F)	0.67
Heat capacity (BTU/lb-deg F)	0.23

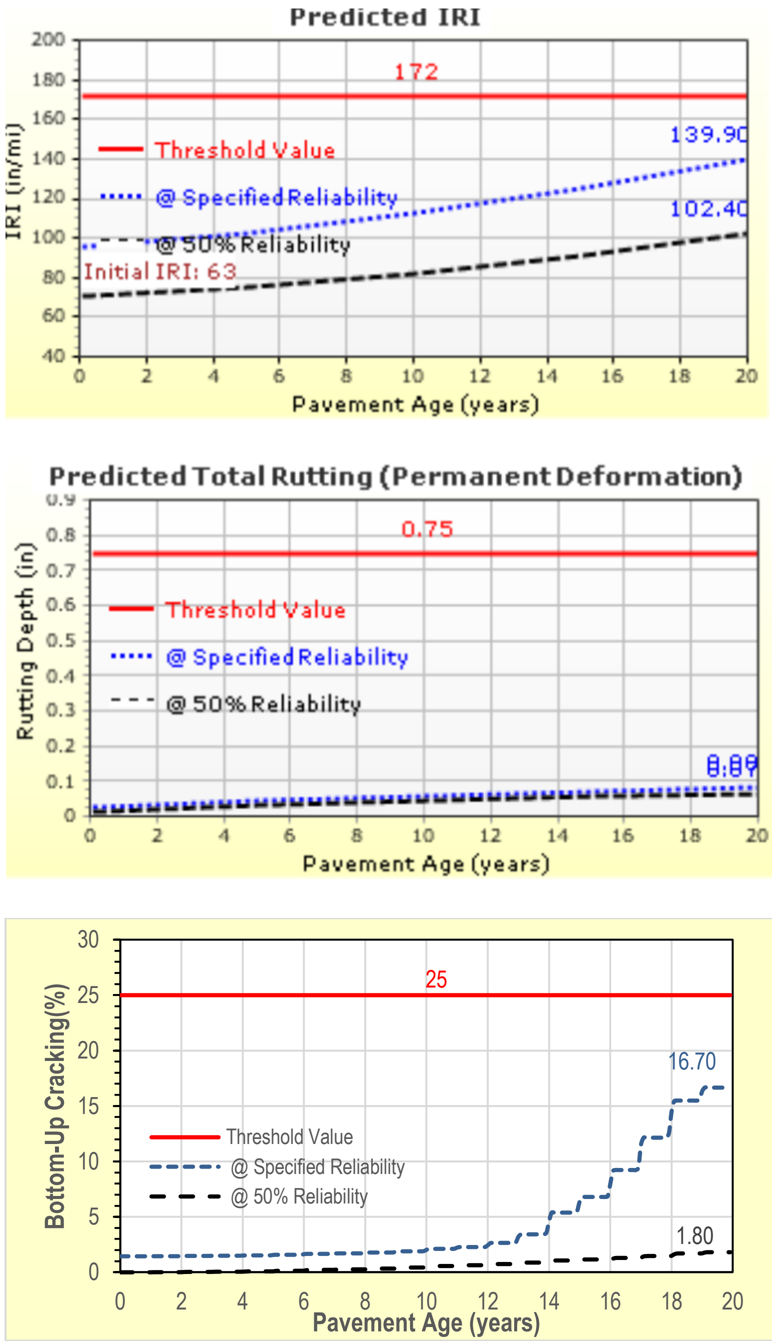

Figure 7.4. Distress Charts for Overlay Section District III (IR 080-140) (MEDesign version 2.1).

CHAPTER 8 SENSITIVITY ANALYSIS

The MEPDG analysis provided a more methodological design method for flexible and rigid pavements as predicted distresses depend on inputs parameters such as climate, traffic, materials, and design conditions. The NCHRP project 01-47 was established to determine the sensitivity of performance models to inputs variability. The design inputs evaluated in this project included traffic volume and speed, layer thicknesses, material properties (stiffness and strength for HMA and PCC, unbound materials modulus, etc.). For HMA pavements, the distress predictions were most prominently affected by the bound surface layers inputs. Four sensitivity categories were defined using a normalized sensitivity index (NSI) which relates the percentage change in any design input to the percentage change in the distress predictions. The sensitivity levels are presented in Table 8.1 below. Figure 8.1 illustrates the level of sensitivity of the different inputs used in flexible pavement design with regards to predicted distresses.

Table 8.1-Sensitivity Categories Defined in the NCHRP Project 01-47.

Sensitivity Category	**NSI Range**
Hypersensitive(HS)	>5
Very Sensitive (VS)	1-5
Sensitive (S)	0.1-1
Non-Sensitive (NS)	<0.1

HMA pavement Inputs		Level of Sensitivity for Flexible Pavement Outputs[1]				
Group	**Parameters**	**HMA Rutting**	**Total Rutting**	**Alligator Cracking**	**Long. Cracking**	**Thermal Cracking**
General	Traffic open month	NS	NS	NS	NS	NS
Traffic	Volume	VS	VS	VS	VS	NS
	Speed	VS	VS	S	S	NS
Climate	Location	VS	S	S	S	S
	Depth to groundwater table	NS	S	NS	NS	NS
Layer/General	Surface shortwave absorptivity	VS	VS	S	VS	NS
Layer/HMA	Thickness	VS	VS	VS	S	NS
	Dynamic modulus	S	S	S	S	NS
	Binder grade/stiffness	VS	S	S	S	S
	Poisson's ratio	NS	NS	NS	NS	NS
	Thermal conductivity	NS	NS	NS	NS	S
	Heat capacity	NS	NS	NS	NS	S
	Creep compliance	NS	NS	NS	NS	VS
	Tensile strength at 14°F	NS	NS	NS	NS	VS
	Aggregate coefficient of thermal contraction	NS	NS	NS	NS	VS
Layer/Base (Subbase)	Thickness	S	S	S	S	NS
	Resilient modulus	S	S	S	VS	NS
	Poisson's ratio	NS	NS	NS	NS	NS
	Soil-water characteristic curve	NS	NS	NS	NS	NS
	Permeability	NS	NS	NS	NS	NS
	Compacted/uncompacted	NS	NS	NS	NS	NS
Layer/Subgrade	Resilient modulus	NS	VS	S	S	NS
	Poisson's ratio	NS	NS	NS	NS	NS
	Soil-water characteristic curve	S	S	S	S	NS
	Permeability	NS	NS	NS	NS	NS
	Compacted/uncompacted	NS	NS	NS	NS	NS
HMA/HMA (Rehab)	Milled AC thickness	NS	NS	NS	NS	NS
	Existing AC thickness (after milling)	S	S	S	S	NS
	Existing AC binder grade	S	S	S	S	NS
	Pavement rating	VS	S	VS	VS	NS
	Total rutting	VS	VS	NS	NS	NS
HMA/JPCP (Rehab)	Existing PCC modulus of rupture	NS	NS	NS	NS	NS
	Percent slabs cracked/repaired	NS	NS	NS	NS	NS
	Monthly modulus of subgrade reaction	NS	NS	NS	NS	NS
	Month for measuring modulus	NS	NS	NS	NS	NS

[1]VS = very sensitive, S = sensitive, NS = nonsensitive.

Figure 8.1- Sensitivity Analysis Categories for Flexible Pavements Inputs.

The sensitivity of the calibrated models for Nevada's conditions was examined using the US 095 and IR 080 designs discussed in Chapter 7. The distresses calibrated in this study were HMA rutting, total rutting, and alligator cracking; thus, they were considered in the sensitivity analysis. The inputs studied in the sensitivity analysis are as follows:

- ***Traffic speed and volume***: the original design inputs were 65mph and an AADTT of 1823. The speed was changed to 55 mph and 75 mph to examine the effect of this parameter. The AADTT values used were 1641 and 2005 representing a 10% variation from the original input.

- ***Air voids (AV)***: the typical value used of in-place air voids for new bituminous layers is 7%. The effect of this input on prediction models sensitivity is not discussed in the Figure 8.1 above. The air voids values used were 5% and 9%.

- ***Volume of effective binder (Vbe)***: similar to air voids the sensitivity of this input is not shown in Figure 8.1. The typical volume of effective binder used in Nevada's mixtures is 8.5%. In this analysis Vbe values of 6.5% and 10.5% were used.

- ***Dynamic modulus (E*)***: the dynamic modulus represents the strength of an asphalt mixture. The distresses outputs are typically sensitive to this input. The dynamic modulus standard deviation (σ) values from the Nevada materials grouping for district I was used. Figure 8.2 presents the mean dynamic modulus curve from District I along with the respective standard deviation.

- ***Binder grade and stiffness***: this input is very sensitive for HMA rutting and sensitive for total rutting and alligator cracking. The G* standard deviation from district I material grouping was used in the sensitivity analysis. Figure 8.3 below illustrates the binder grade and stiffness inputs used in the sensitivity analysis.

It is noteworthy to mention that the considered variations in air voids and Vbe might not properly reflect the actual influence on predicted distresses since a change in those parameters will ultimately impact the dynamic modulus and binder stiffness. In this case, the impact of AV and Vbe fluctuations on the dynamic modulus or binder stiffness is not taken into consideration as every input is evaluated individually in order to examine its influence on the design. This type of analysis was defined in the NCHRP project 01-47 as the one-at-a-time (OAT) analysis.

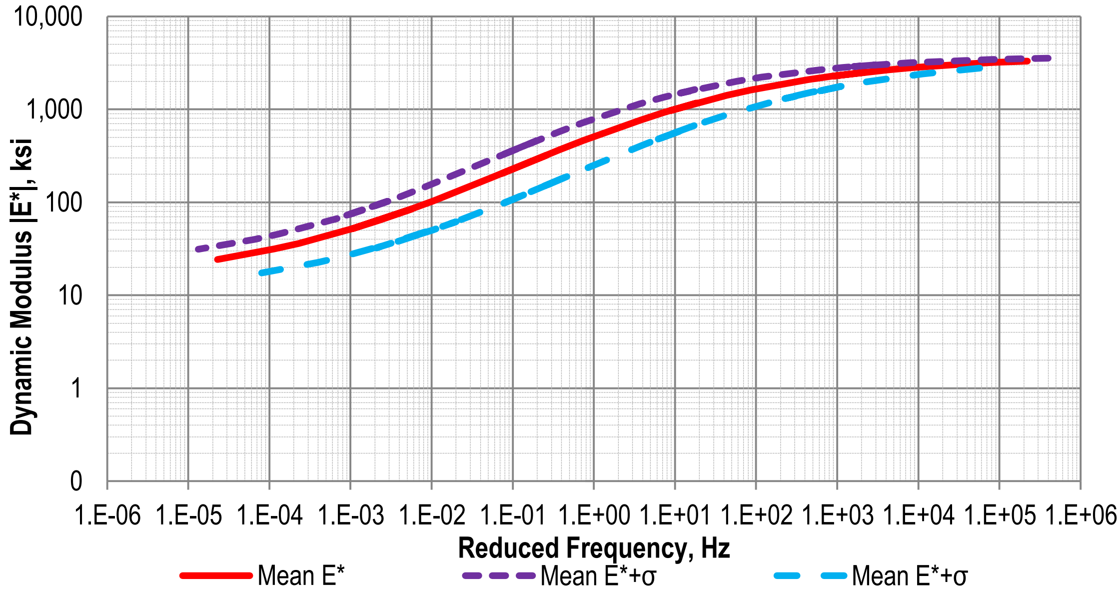

Figure 8.2- Dynamic Modulus Inputs from District I Grouping (PG76-22NV).

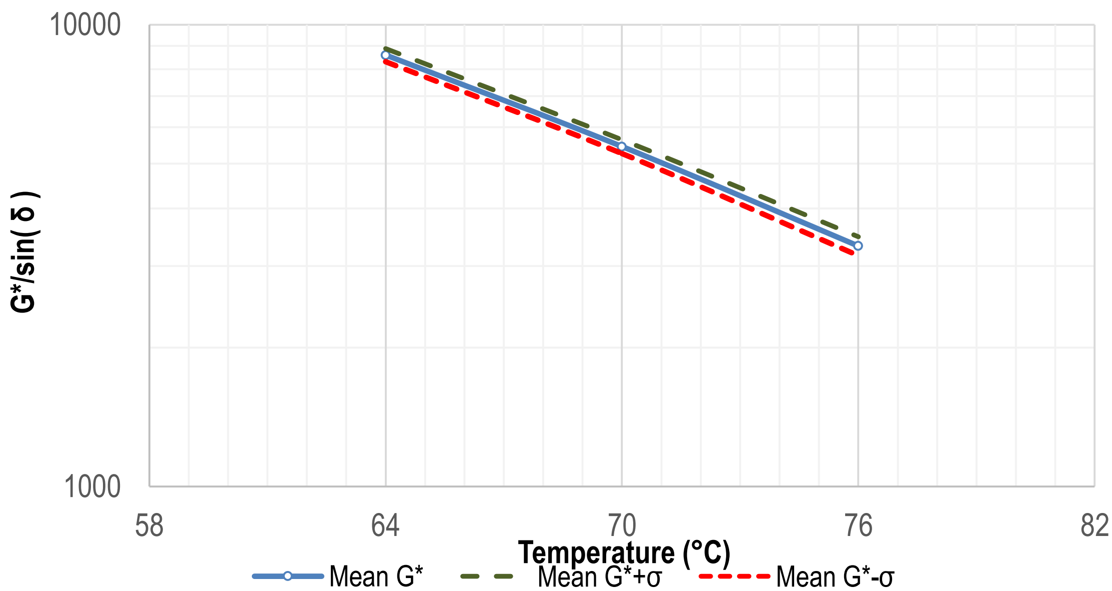

Figure 8.3- Binder Grade and Stiffness Inputs from District I Grouping (PG76-22NV).

The US 095-39 section was run using the original inputs (Section 7) at 90% reliability. Additional runs were conducted using the original inputs with the exception of one design parameter. The effect of the design inputs variation was then observed by comparing the distress levels of original and modified designs. The AC rutting results for the different runs are plotted in Figure 8.4, the total rutting results are presented in Figure 8.5, and the alligator cracking predictions are presented in Figure 8.6.

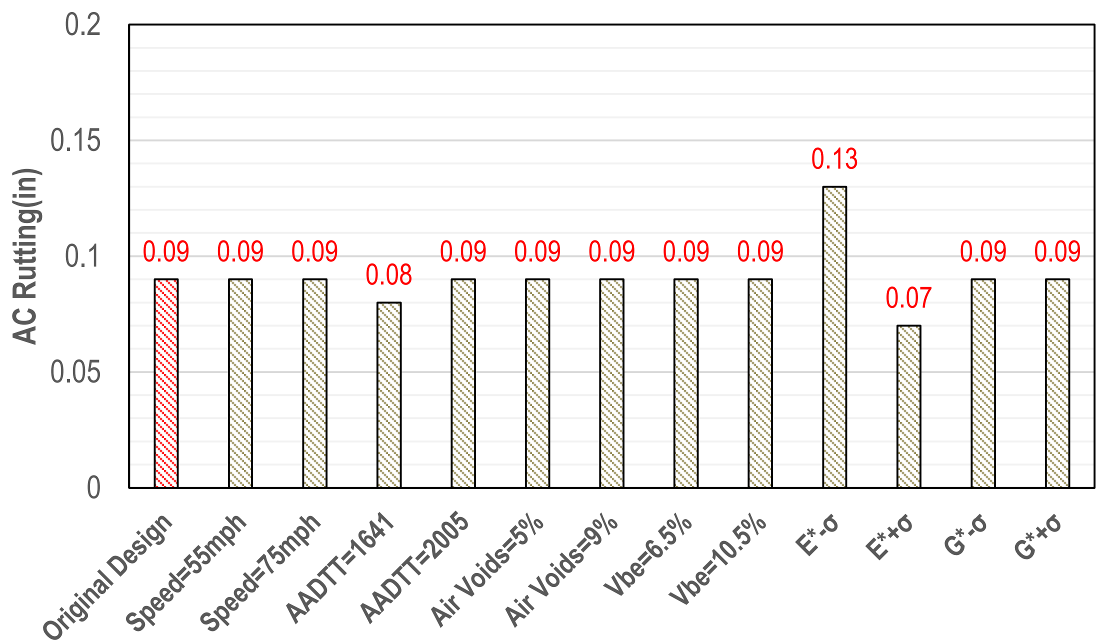

Figure 8.4- AC Rutting Results from the Sensitivity Analysis (US 095-39).

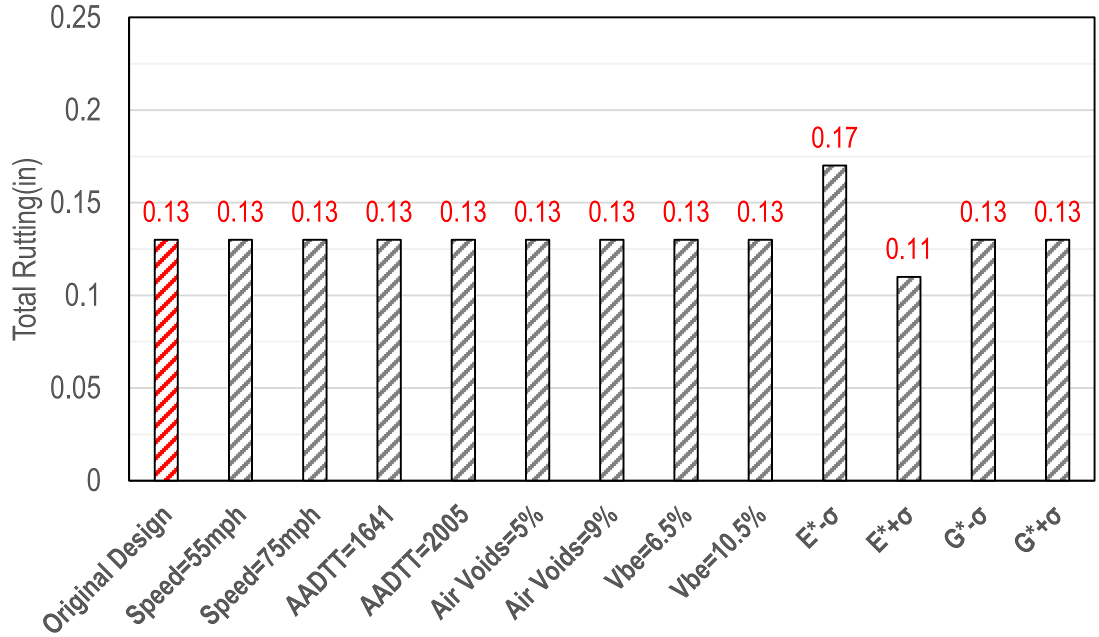

Figure 8.5- Total Rutting Results from the Sensitivity Analysis (US 095-39).

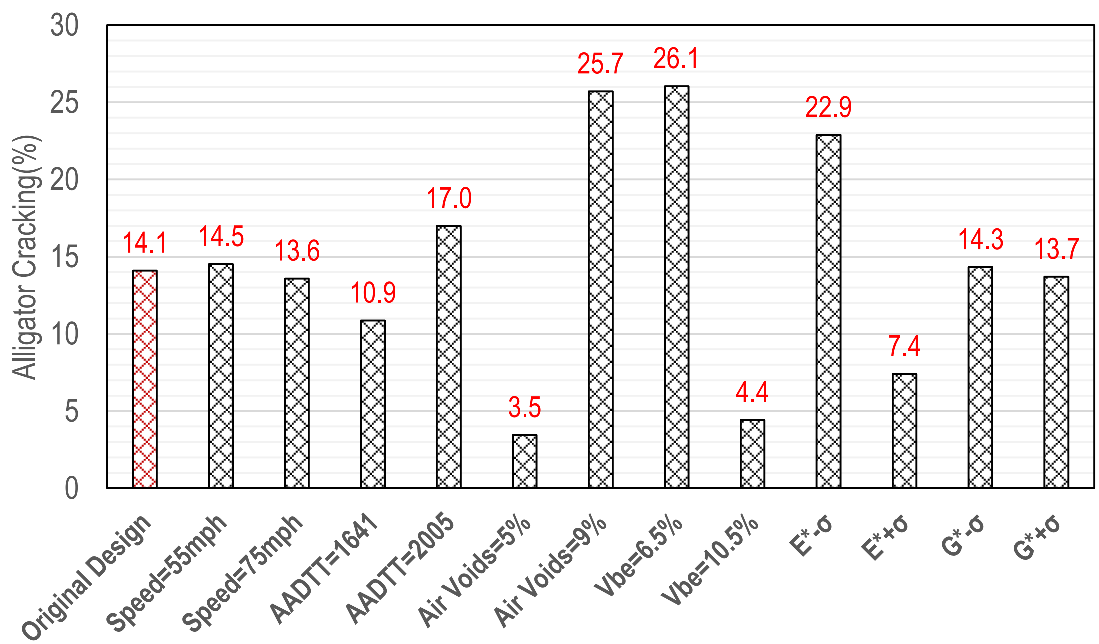

Figure 8.6- Alligator Cracking Results from the Sensitivity Analysis (US 095-39).

Results Analysis

Figure 8.4 shows that the AC rutting predictions for the different inputs were very similar: equal to 0.09 inches. The lower traffic input resulted in a reduction of the AC rutting by 0.01 inches. The variations in the dynamic modulus affected the predictions considerably as AC rutting values of 0.13 and 0.07 were predicted. The total rutting in Figure 8.5 reflects similar results to AC rutting. This was expected as the sensitivity parameters considered are mostly asphalt layer inputs with the exception of traffic volume and speed. The alligator cracking presented in Figure 8.6 above shows a lot of variability in the predictions. This calibrated model seems to be very sensitive to dynamic modulus, volume of effective binder, and air voids. The AADTT volume affects the predictions as an increase in the traffic leads to more fatigue cracking. The fatigue cracking predictions showed little variability with speed and binder stiffness modification. This can be explained by the fact that binder stiffness data had a small standard deviation (Figure 8.3).

NSI Calculations

In order to fully assess the design inputs variation for the calibrated prediction models in Nevada the NSI values were calculated for alligator fatigue cracking using the results of the sensitivity analysis of the US 095 section. The NSI is explained as a relation between the percentage changes in a design input to the percentage change in a predicted distress relative to the design limit. For example, if a 15% increase in traffic speed causes an increase in total rutting of 0.05 inches at a design limit of 0.75 inches the NSI is calculated using the Equation 8.1 below.

$$NSI = \frac{Distress\ Prediction\ Variation}{Design\ Limit * Design\ input\ variation} = \frac{+0.05}{0.75*(+0.15)} = 0.44 \qquad (8.1)$$

NSI can be positive or negative depending of the effect of the input. Typically, when an input increase causes a decrease in distress predictions the NSI is negative. The NSI calculations for alligator fatigue cracking outputs are shown in Table 8.2.

Table 8.2-NSI Calculations Example for Alligator Cracking.

Design Input	Input Variation (%)	Prediction Variation from Original Design	Calculated NSI	Category	NCHRP Recommended Category
Traffic Speed (mph)	15%	-0.4	-0.107	S	S
	-15%	0.5	-0.133	S	S
Traffic Volume	10%	-2.9	-1.16	VS	VS
	-10%	3.2	-1.28	VS	VS
HMA Air Voids (%)	28.60%	-11.6	-1.624	VS	N/A
	-28.60%	10.6	-1.484	VS	N/A
HMA Vbe (%)	23.50%	9.7	1.649	VS	N/A
	-23.50%	-12	2.04	VS	N/A
Dynamic Modulus (psi)	40%	6.7	0.67	S	S
	-40%	-8.8	0.88	S	S
Binder Stiffness (Pa)	4.20%	0.4	0.381	S	S
	-4.20%	-0.2	0.19	S	S

Note that negative values present a decrease and positive values an increase.

The results presented in Table 8.2 match the recommendations of the NCHRP project 01-47 (Figure 8.1) for the considered inputs. This indicates that the locally calibrated models perform similarly to the national models for inputs sensitivity.

CHAPTER 9 SUMMARY, CONCLUSIONS AND RECOMMENDATIONS

9.1. Summary and Conclusions

The MEPDG implementation in Nevada has been an ongoing project since 2005. The Nevada Department of Transportation (NDOT) in cooperation with the researchers at the University of Nevada, Reno developed a plan to utilize the MEPDG procedure. Some of the tasks completed in this study are presented below:

- Dense graded mixtures characterization including 100% virgin HMA mixtures, mixtures with 15% recycled asphalt pavement (RAP), and warm mix asphalt (WMA) mixtures. This is an ongoing activity as mixtures are sampled regularly.
- Collecting project related information (traffic, climate, and materials) and converting NDOT PMS data to match the MEPDG format.
- Conducting sensitivity analysis using the NCHRP project 1-47 to identify the significant input variables while creating an input database specific of NDOT's pavements.
- Developing a procedure for designing pavement sections using the AASHTOWare Pavement-ME software. This was accomplished through the Nevada Pavement-ME manual. This manual provides guidance for inputs collection and design methods.

These tasks were conducted to ensure that the MEPDG software accurately predicted pavement performance within the state of Nevada. Considering that he majority of the newly constructed pavements have polymer modified binders, the need for a local calibration became significant. In this study, the rutting and bottom-up fatigue cracking models were calibrated to fit Nevada's conditions. The calibration/validation was conducted using data from 58 sections. These sections included 24 sampled mixtures tested for dynamic modulus, binder stiffness, rutting, and fatigue. The materials inputs for the remaining 34 sections were computed using averages from every district. Level 1 data inputs were prominently used in the calibration. Whereas level 2 inputs were mostly used as part of the validation process. The detailed rutting and bottom-up fatigue cracking calibration/validation are discussed below.

9.1.1. Rutting Calibration

The rutting calibration conducted in this study can be summarized as follows:

- Initial runs were made using the NDOT rutting regression factors (Table 3.10) to assess the necessity of additional local calibration.
- Optimization runs were done using the appropriate regression factors for every section and different sets of the power coefficients β_{r2} and β_{r3} for a total of 16 combinations for every district.
- The individual measured layers rutting were calculated by multiplying the total PMS measured rutting by the appropriate proportions from the software predictions.
- The asphalt rutting was optimized using the linear multiplier β_{r1} to reduce the sum of square errors between measured and predicted AC rutting. The rutting predictions for new sections behaved distinctively from their rehabilitated counterparts. Resulting in the separation of new and rehabilitated sections within every district, thus increasing the number of calibration sets from 3 to 6.

- The total rutting was optimized using the β_{r1} from the previous steps and simultaneously optimizing the base and subgrade linear calibration factors β_{base} and $\beta_{subgrade}$. The optimization method used the Microsoft excel solver to minimize the sum of squared errors between total measured and predicted rutting.
- The calibration factors initial selection was based on the regression analysis of the optimized models. The calibration sets with the best fit and the highest R-squared values for AC and total rutting were selected for verification. Once the verification was completed the models with the highest precision were chosen.
- The standard deviation models were calibrated to fit NDOT's PMS data observations to get a better representation of the state's reliability parameters.

The final locally calibrated AC rutting model is:

$$\frac{\varepsilon_p}{\varepsilon_r} = k_z * \beta_{r1} * 10^{k1} T^{k2*\beta_{r2}} N^{k3*\beta_{r3}}$$

The final locally calibrated unbound layers rutting model is:

$$\delta_a(N) = \beta_{s1} k_1 * \varepsilon_v * h \left(\frac{\varepsilon_0}{\varepsilon_y}\right) e^{-\left(\frac{\rho}{N}\right)^{\beta}}$$

Throughout this study it was clear that the nationally calibrated models for AC and unbound materials were over predicting the rutting. The local calibration significantly improved the correlation between predicted and measured rutting by reducing the software predictions. The local calibration factors for every district and construction type are presented in Table 9.1 below.

Table 9.1-Final Rutting Calibration Factors for Nevada's Pavements.

Calibration Factor	District I - Overlay	District I - New	District II - Overlay	District II - New	District III - Overlay	District III - New
K_{r1}	-2.9708	-2.9708	-3.2605	-3.2605	-3.4717	-3.4717
K_{r2}	1.7435	1.7435	2.0054	2.0054	2.0258	2.0258
K_{r3}	0.3547	0.3547	0.3161	0.3161	0.3946	0.3946
β_{r1}	0.0794	0.1045	0.3741	0.1698	0.0797	0.1365
β_{r2}	1.0	1.0	0.7	1.0	1.0	0.9
β_{r3}	1.0	1.0	0.9	0.9	1.0	0.8
β_b	0.1280	0.0901	0.3775	0.0838	0.1220	0.1463
β_{sg}	0.0145	0.1073	0.1661	0.2411	0.0100	0.1776

9.1.2. Fatigue Calibration

As part of the MEPDG implementation for the state of Nevada, this research focused on the bottom-up fatigue cracking calibration. The top-down fatigue cracking calibration was not considered in this study because the current models were outdated. For this purpose, the fatigue measurements in the NDOT PMS were converted to match the Pavement-ME outputs (section 3.2). The summary of the steps followed in this calibration are shown as follows:

- Initial runs were made using the NDOT rutting regression factors (Table 3.11) to assess the need of additional local calibration.
- Optimization runs were made for sections using the appropriate regression factors and different sets of the power coefficients β_{f2} and β_{f3} for a total of 9 combinations.
- For every combination the excel solver was run to minimize the sum of squared errors between measured and predicted values. Transfer function parameters C_1 and C_2 equal to 0.8 improved the precision of the predictions.
- Using the calibrated transfer function the linear β_{f1} multiplier was optimized to reduce the sum of square errors between measured and predicted fatigue cracking.

Similar to rutting calibration, new and rehabilitated sections were considered separately. However, due to the lack of fatigue cracking distresses (the pavements considered in the calibration were still at a relatively early age) the sections from district II and III were combined. As a result, four sets of calibration groups were considered.

- For every set of data, the combination resulting in the lowest errors was validated using the Pavement-ME software. In this case, the beta 1 was adjusted as a function of the AC thickness which properly represented the thick vs thin section behavior of the bottom-up fatigue cracking model.

The final locally calibrated fatigue cracking model is:

$$N_f = 0.00432 * \beta_{f1} * K_1 * C * \left(\frac{1}{\varepsilon_t}\right)^{\beta_{f2} * K_2} * \left(\frac{1}{E}\right)^{\beta_f * K_3}$$

The final locally calibrated bottom-up cracking transfer function is:

$$FC = \left(\frac{6000}{1+e^{0.8*C'1+0.8*C'2Log(Damage)}}\right) * \frac{1}{60}$$

The calibration factors for every district and construction type are presented in Table 9.2 below. The local calibration of the fatigue models significantly improved the distresses predictions as the nationally calibrated model was found to be underestimating the fatigue cracking. Furthermore, the sensitivity analysis conducted on the calibrated models exhibited consistent results when compared to the national model which further validated the calibration.

Table 9.2-Final Bottom-Up Fatigue Cracking Calibration Factors for Nevada's Pavements.

Calibration Factor	District I - Overlay	District I - New	District II-III - Overlay	District II-III - New
K_{f1}	214.176	214.176	30.0794	30.0794
K_{f2}	5.0284	5.0284	5.0537	5.0537
K_{f3}	2.3072	2.3072	2.8904	2.8904
β'_{f1} [1]	0.2	0.005	0.015	50
β_{f2}	1.0	1.0	0.7	1.0
β_{f3}	1.0	1.0	0.9	0.9

[1] *Note that* $\beta_{f1} = K'_1 * \beta'_{f1} = \left(0.000398 + \frac{0.003602}{1+e^{11.02-3.49*h_{ac}}}\right) * \left(\frac{1}{0.004}\right) * \beta'_{f1}$.

9.2. Recommendations

The MEPDG implementation is still an ongoing process as additional states are looking into adopting the new design method. Some of the models integrated in the current Pavement-ME software such as the binder aging or the longitudinal cracking are still being reviewed. The work completed in this study improved the predictions for rutting and bottom-up fatigue cracking. However, further improvements can be made as some distress models were not calibrated (longitudinal cracking, thermal cracking, and reflective cracking). This study recommends that the following tasks need to be completed in order to improve the prediction models:

- The characterization of additional asphalt mixtures to expand the materials database and cover new paving technologies such as RAP, WMA, or cold in-place recycling (CIR). CIR materials characterization is becoming important as states are looking into transitioning to more cost efficient rehabilitation strategies.

- Increase the number of calibration/validation sections while monitoring the currently studied sections for distresses evolution. This is important mainly because bottom-up fatigue cracking develops in the late stages of the pavement.
- Conduct nondestructive testing such as falling weigh Deflectometer (FWD) to better evaluate the existing pavement conditions before making decisions concerning the rehabilitation strategy. Core samples can also be collected to more accurately determine the existing pavement structure.
- Perform trench studies to appropriately measure the rutting in each layer of the pavement structure. The data obtained would improve the accuracy of the rutting calibration as estimates will no longer be used to calculate the proportion of rutting in each layer.
- Further recalibration/validation is recommended as more data inputs are collected. Calibrations using extended data pool typically lead to more accurate results.

REFERENCES

AASHTO, 1993. AASHTO Guide for Design of Pavement Structures 1993. Washington, D.C.

AASHTO, 2008. Manual of Practice for the Mechanistic–Empirical Pavement Design Guide. American Association of State Highway and Transportation Officials, Washington, D.C.

AASHTO, 2010. Manual of Practice for Local Calibration of the Mechanistic-Empirical Pavement Design Guide. American Association of State Highway and Transportation Officials, Washington, D.C.

AASHTO, 2013. Standard Specifications for Transportation Materials and Methods of Sampling and Testing, 33rd Edition, American Association of State Highway and Transportation Officials, Washington D.C.

AASHTOWare, 2013. AASHTOWare Pavement ME Design, American Association of State Highway and Transportation Officials, Washington, D.C.

American Society for Testing and Materials (ASTM). Determining Fatigue Failure of Compacted Asphalt Concrete Subjected to Repeated Flexural Bending. D 7640. American Society for Testing and Materials. 2010 Annual Book of ASTM Standards.

Ceylan, H., Kim, S., Gopalakrishnan, K., & Ma, D., 2013. *Iowa Calibration of MEPDG Performance Prediction Models*. InTrans Project Nb. 11-401. Iowa State University, Ames, IA.

Darter, M., Titus-Glover, L., & Von Quintus, H., 2009. *Draft User's Guide for UDOT Mechanistic-Empirical Pavement Design*. ERES Division of ARA Inc., Champaign, IL.

Darter, M., Titus-Glover, L., & Von Quintus, H., 2014. *Calibration and Implementation of the AASHTO Mechanistic-Empirical Pavement Design Guide in Arizona*. ERES Division of ARA Inc., Champaign, IL.

El-Basyouny, M.M., 2004. *Calibration and Validation of Asphalt Pavement Distress Models for 2002 Design Guide.* Ph.D. Dissertation, Arizona State University, Tempe, AZ.

El-Basyouny, M.M., & Witczak, M.W., 2005. *Development of the Fatigue Cracking Models for the 2002 Design Guide*. Paper presented at the Annual Meeting of the Transportation Research Board, Washington, D.C.

Feaster, C., & Hajj, E.Y., 2012. *Characterization of Field-Produced HMA Mixtures from Nevada for Mechanistic-Empirical Pavement Design*. MSc. Dissertation, University of Nevada, Reno, NV.

Jadoun, F., & Hou, M., 2011. *Calibration of the Flexible Pavement Distress Prediction Models in the Mechanistic-Empirical Pavement Design Guide for North Carolina*. Ph.D. Dissertation, North Carolina State University, Raleigh, N.C.

Kim, Y. R., Jadoun, F. M., Hou, T., & Muthadi, N., 2011. *Local calibration of the MEPDG for flexible pavement design.* Report No. FHWA/NC/2007-07. North Carolina Department of Transportation, Raleigh, N.C.

Lasdon, L.S., Waren. A. D., Jain, A., & Ratner, M., 1978. *Design and Testing of a Generalized Reduced Gradient Code for Nonlinear Programming.* In ACM Transactions on Mathematical Software, Vol. 4, No. 1, pp. 34-49.

Li, J., Pierce, L. M., & Uhlmeyer, J., 2009. *Calibration of Flexible Pavement in Mechanistic-Empirical Pavement Design Guide for Washington State*. Transportation Research Record: Journal of the Transportation Research Board, 2095, 73-83. Washington, D.C.

Mallela, J., Titus-Glover, L., Sadasivam, S., Bhattacharya, B., Darter, M., & Von Quintus, H., 2013. *Implementation of the AASHTO Mechanistic-Empirical Pavement Design Guide for Colorado.* Report no. CDOT-2013-4. Colorado Department of Transportation, Denver, CO.

NCHRP 1-37A, 2002. *Guide for Mechanistic-Empirical the Design of New and Rehabilitated Pavement Structures*. ERES Division of ARA Inc., Champaign, IL.

NCHRP Research Results Digest No. 283, 2003. *Jackknife Testing-An Experimental Approach to Refine Model Calibration and Validation*. National Cooperative Highway Research Program, Transportation Research Board, National Research Council. Washington, D.C.

NCHRP 1-40B, 2009. *User Manual and Local Calibration Guide for the Mechanistic-Empirical Pavement Design Guide and Software*. ERES Division of ARA Inc., Champaign, IL.

NCHRP 1-42A, 2010. *Top-Down Cracking of Hot-Mix Asphalt Layers: Models for Initiation and Propagation*. National Cooperative Highway Research Program, Transportation Research Board, National Research Council. Washington, D.C.

NCHRP 1-47, 2011. *Sensitivity Evaluation of MEPDG Performance Prediction*. National Cooperative Highway Research Program, Transportation Research Board, National Research Council. Washington, D.C.

Nevada Department of Transportation, 2010. *Pavement Management System Overview.* Material Division, Carson City, NV.

Nevada Department of Transportation, 2012. *Roadbed Structural History*. Carson City, NV.

Nevada Department of Transportation, 2014. *Standard Specifications for Road and Bridge Construction*. Carson City, NV.

SAYERS, M.W et al., 1986. *Guidelines for Conducting and Calibrating Road Roughness Measurements*. World Bank Technical Paper Number 46. The World Bank, Washington, D.C.

Sebaaly, P.E., Schoener, P., Siddharthan, R., and Epps, J., 1994. *Implementation of Nevada's Overlay Design Procedure*. In proceedings, 4th International Conference on the Bearing Capacity of Roads and Airfields, University of Minnesota, MN.

Sebaaly, P. E., Bemanian, S., & Lani, S., 2000. *Nevada's Approach to the Backcalculation Process*. Nondestructive Testing of Pavements and Backcalculation of Moduli: Third Volume, ASTM STP 1375, S. D. Tayabji and E. O. Lukanen, Eds., American Society for Testing and Materials, West Conshohocken, PA.

Souliman, M. I., Mamlouk, M. S., El-Basyouny, M., &Zapata, C. E., 2010. *Calibration of the AASHTO MEPDG for Designing Flexible Pavements in Arizona Conditions*. In International Journal of Pavements, Volume 9, Issue 1-2-3, 2010, pp. 2-13.

The AASHO Road Test, 1962. *Pavement Research, Highway Research Board Special Report 61E.* National Research Council. Washington, D.C.

Scott Fortmann-Roe, 2012. *Understanding the Bias-Variance Tradeoff*. Available on the World Wide Web: http://scott.fortmann-roe.com/docs/BiasVariance.html

Williams, C., & Shaidur, R., 2013. *Mechanistic-Empirical Pavement Design Guide Calibration for Pavement Rehabilitation*. Final Report SPR 718, Institute of Transportation Iowa State University, Ames, IA.

Witczak, M.W., Andrei, D., & Mirza, W., 1999. *Development of Revised Predictive Model for the Dynamic (Complex) Modulus of Asphalt Mixtures*. Interteam Technical Report, NCHRP Project 1-37A, University of Maryland, College Park, MD.

Zapata et al., 2010. *A National Catalog of Subgrade Soil–Water Characteristic Curves and Selected Soil Properties for Use with the MEPDG*. C.E. Research Results Digest 347, Transportation Research Board, Washington, D.C.

CHAPTER 10 APPENDIX A: DISTRESSES PLOTS

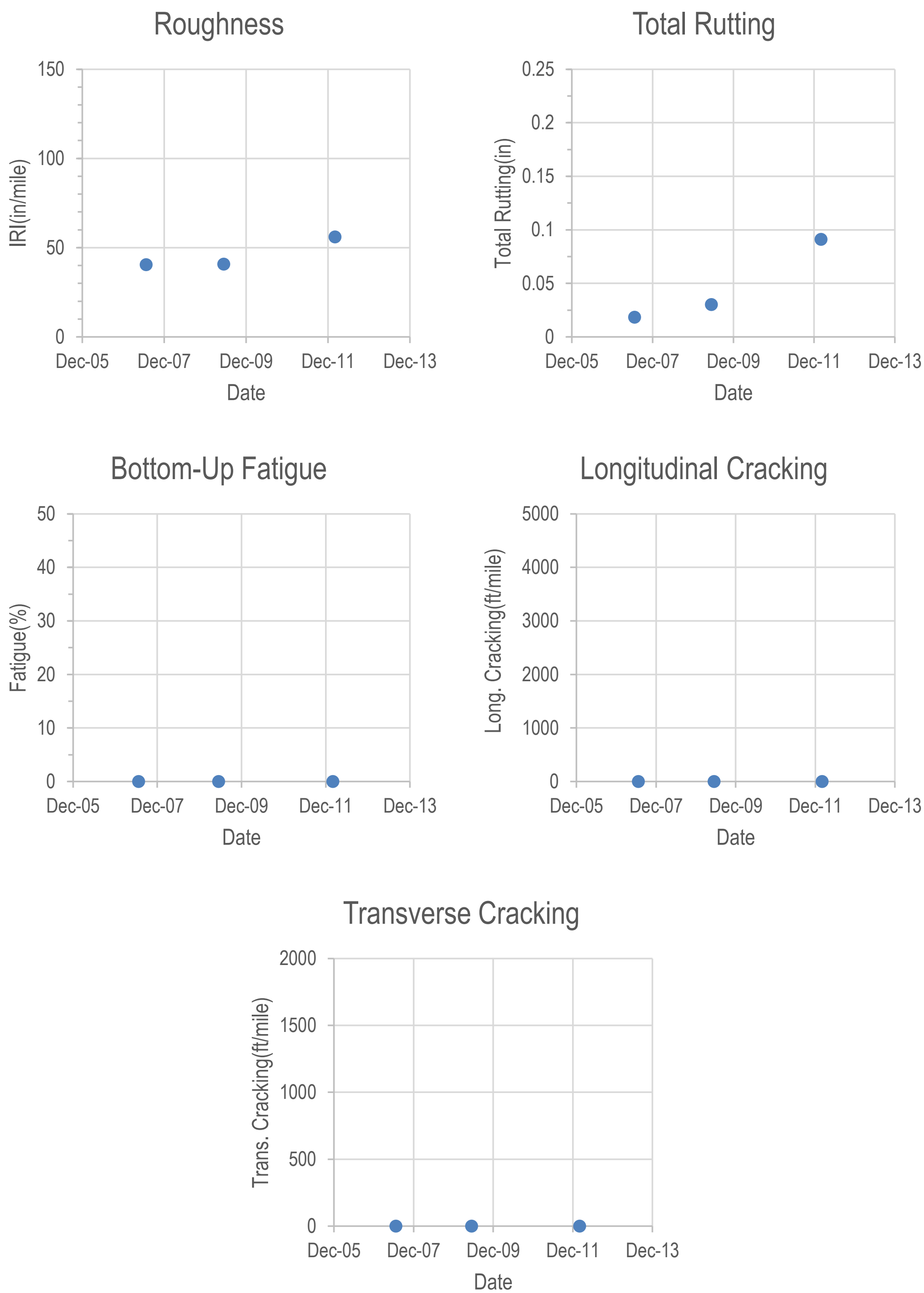

Figure 10.1-Distresses Plots for IR 080-107.

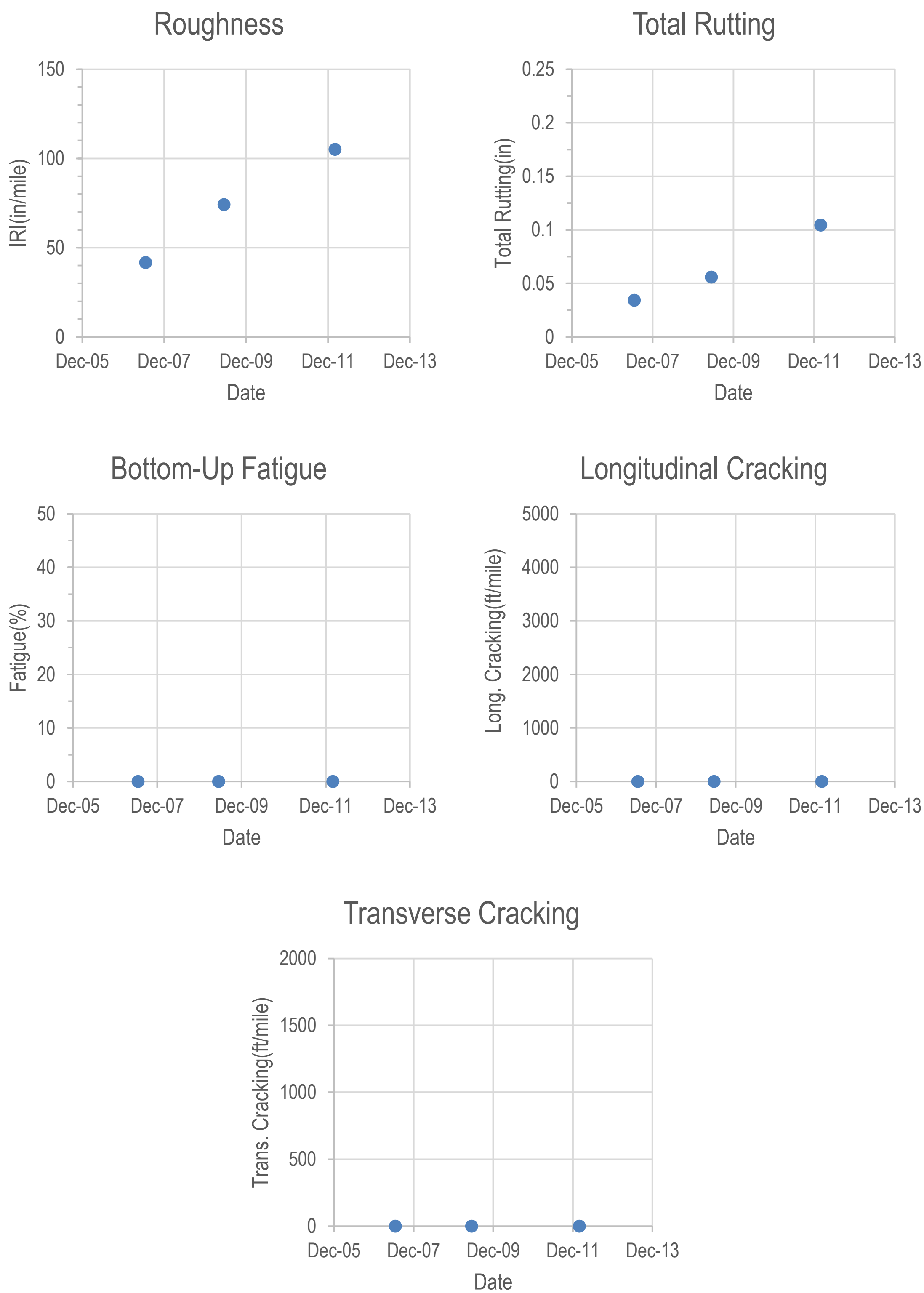

Figure 10.2-Distresses Plots for IR 080-109.

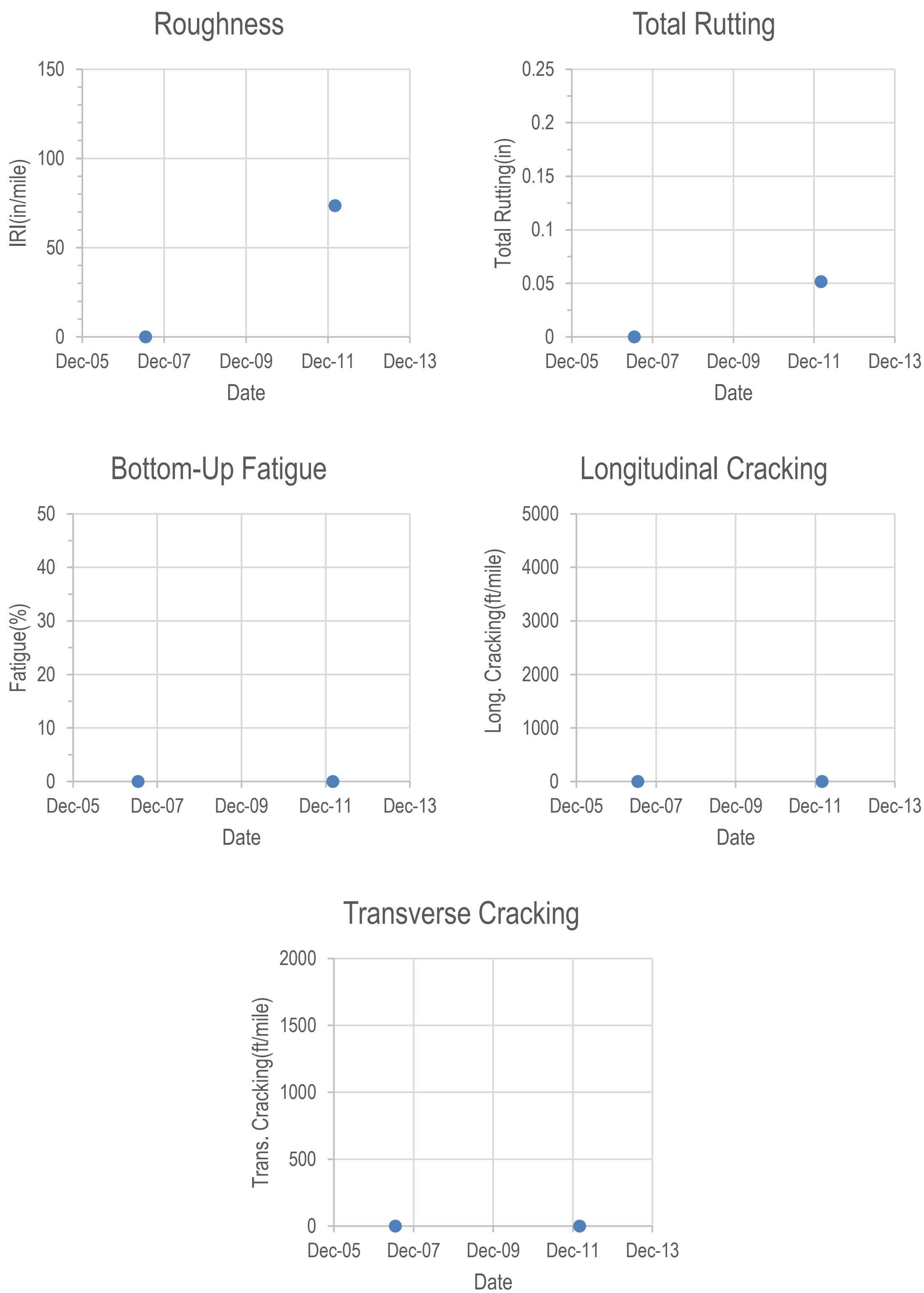

Figure 10.3-Distresses Plots for IR 080-111.

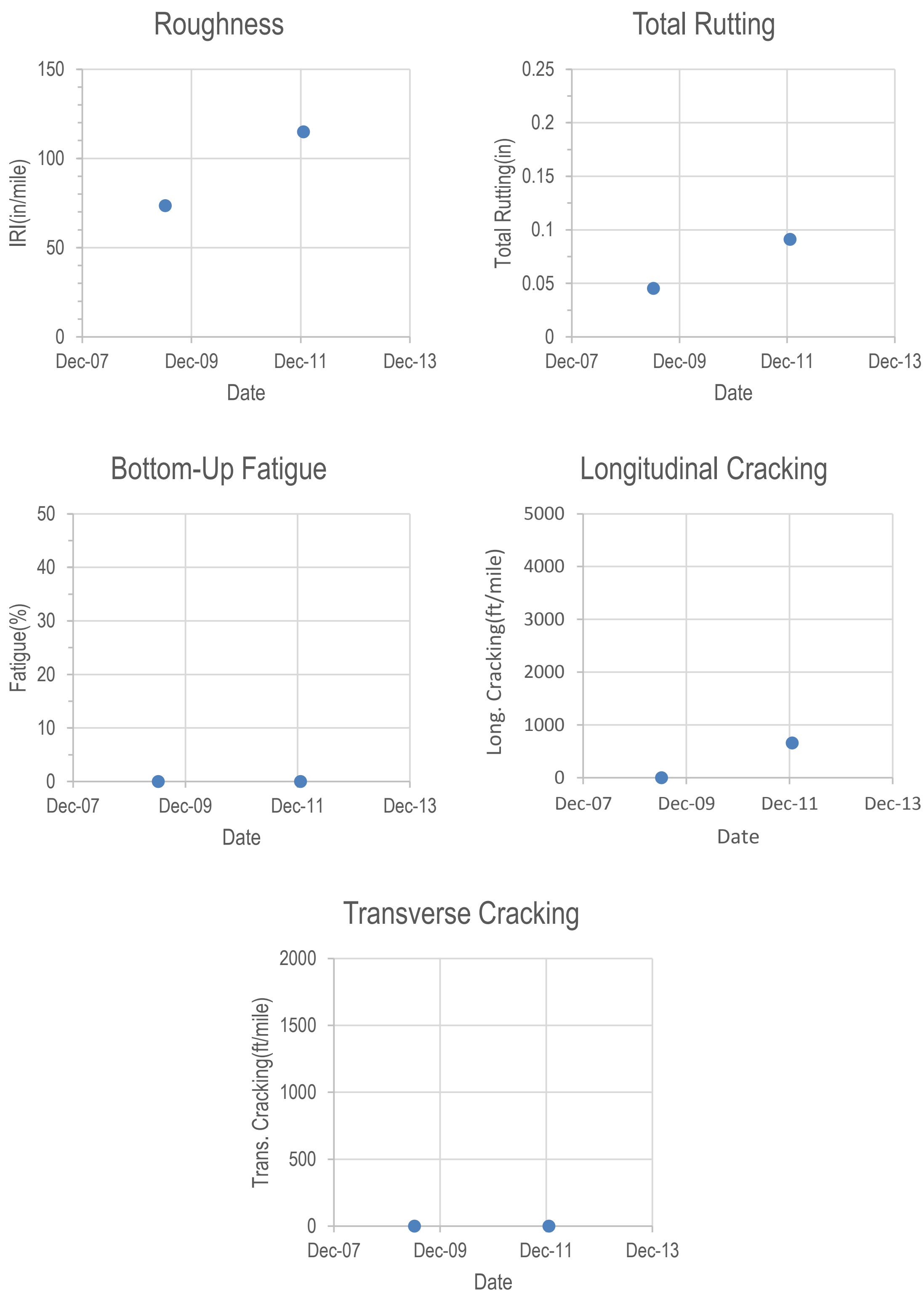

Figure 10.4-Distresses Plots for IR 080-116.

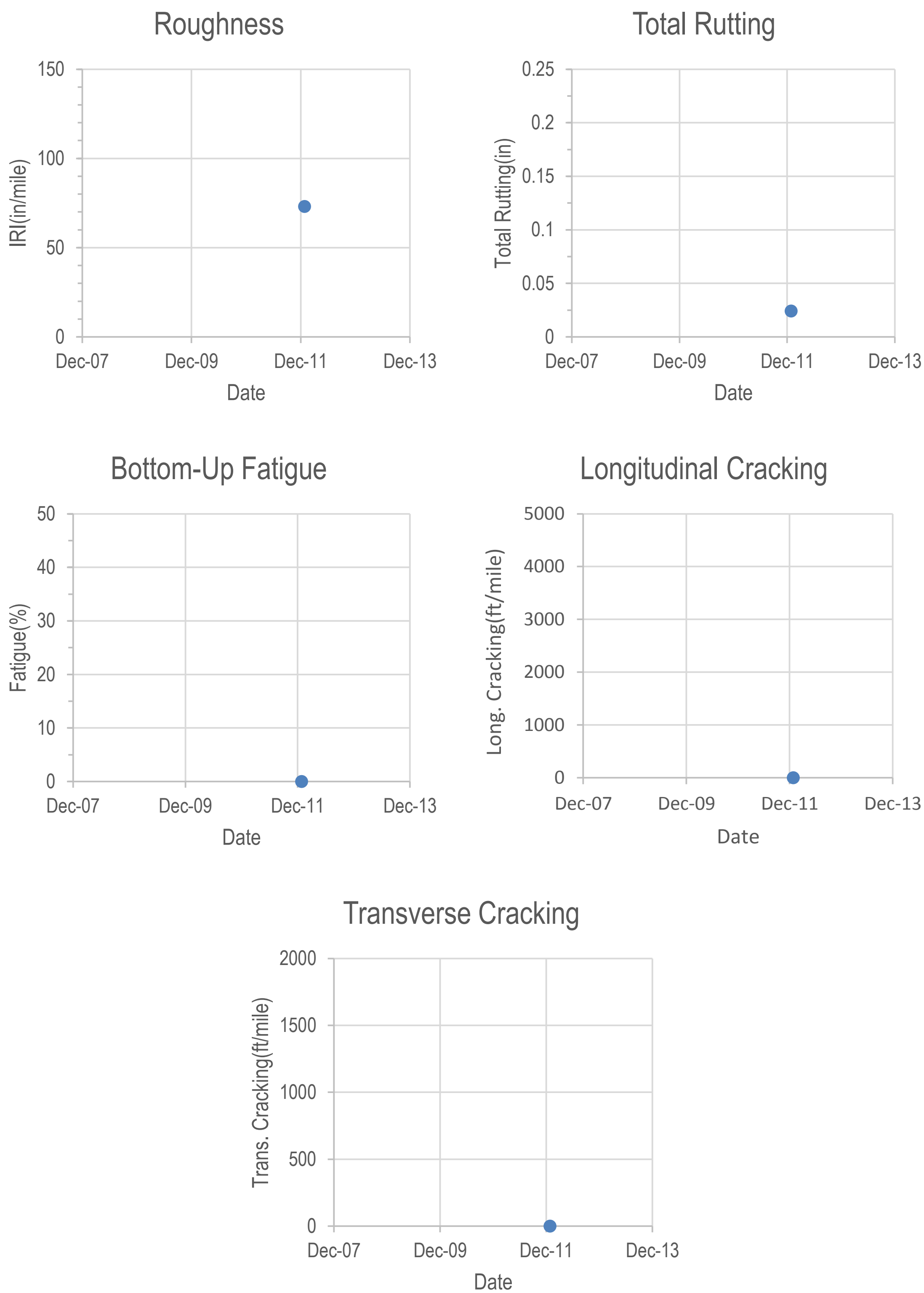

Figure 10.5-Distresses Plots for IR 080-118.

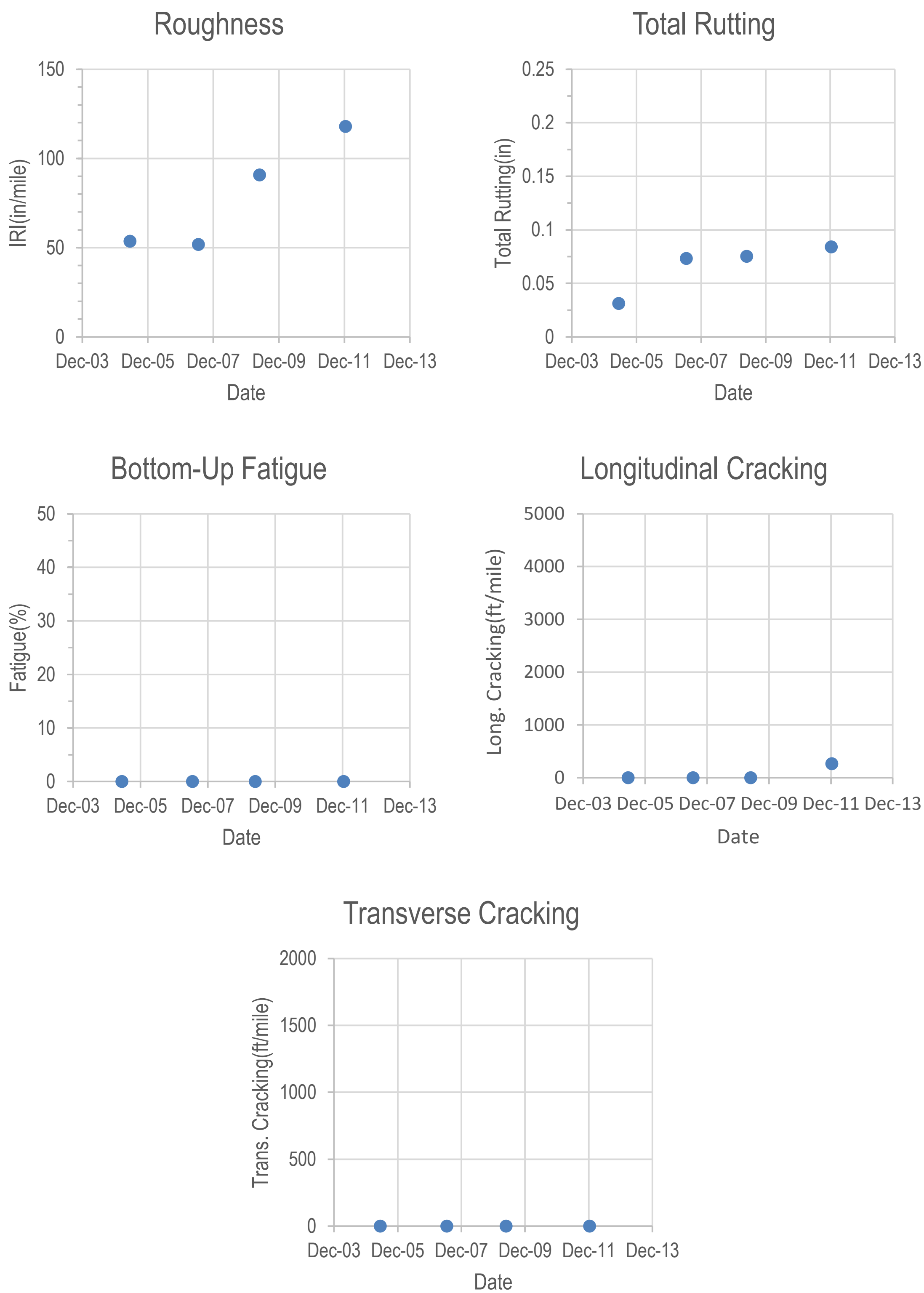

Figure 10.6-Distresses Plots for IR 080-120.

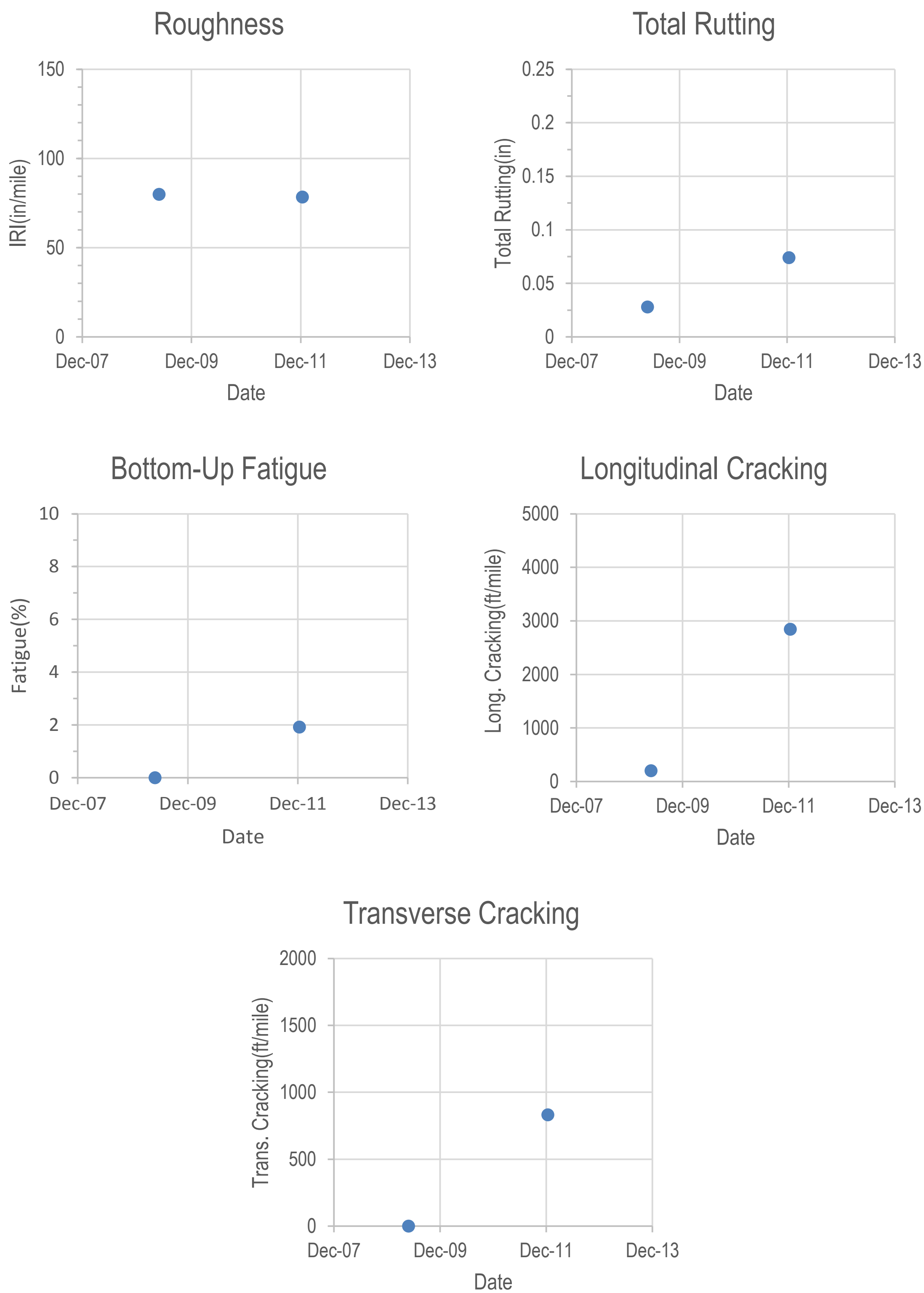

Figure 10.7-Distresses Plots for IR 080-121.

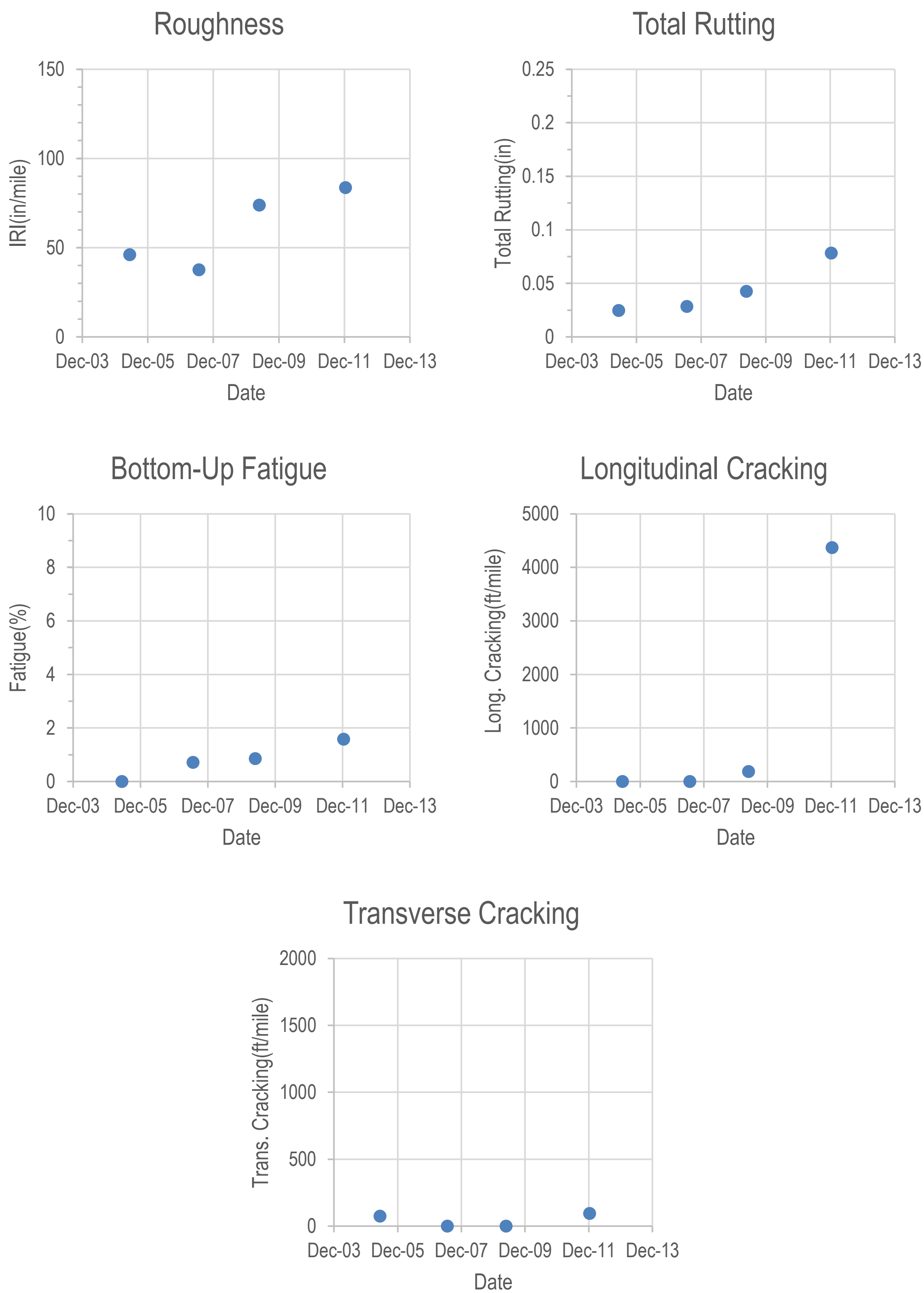

Figure 10.8-Distresses Plots for IR 080-122.

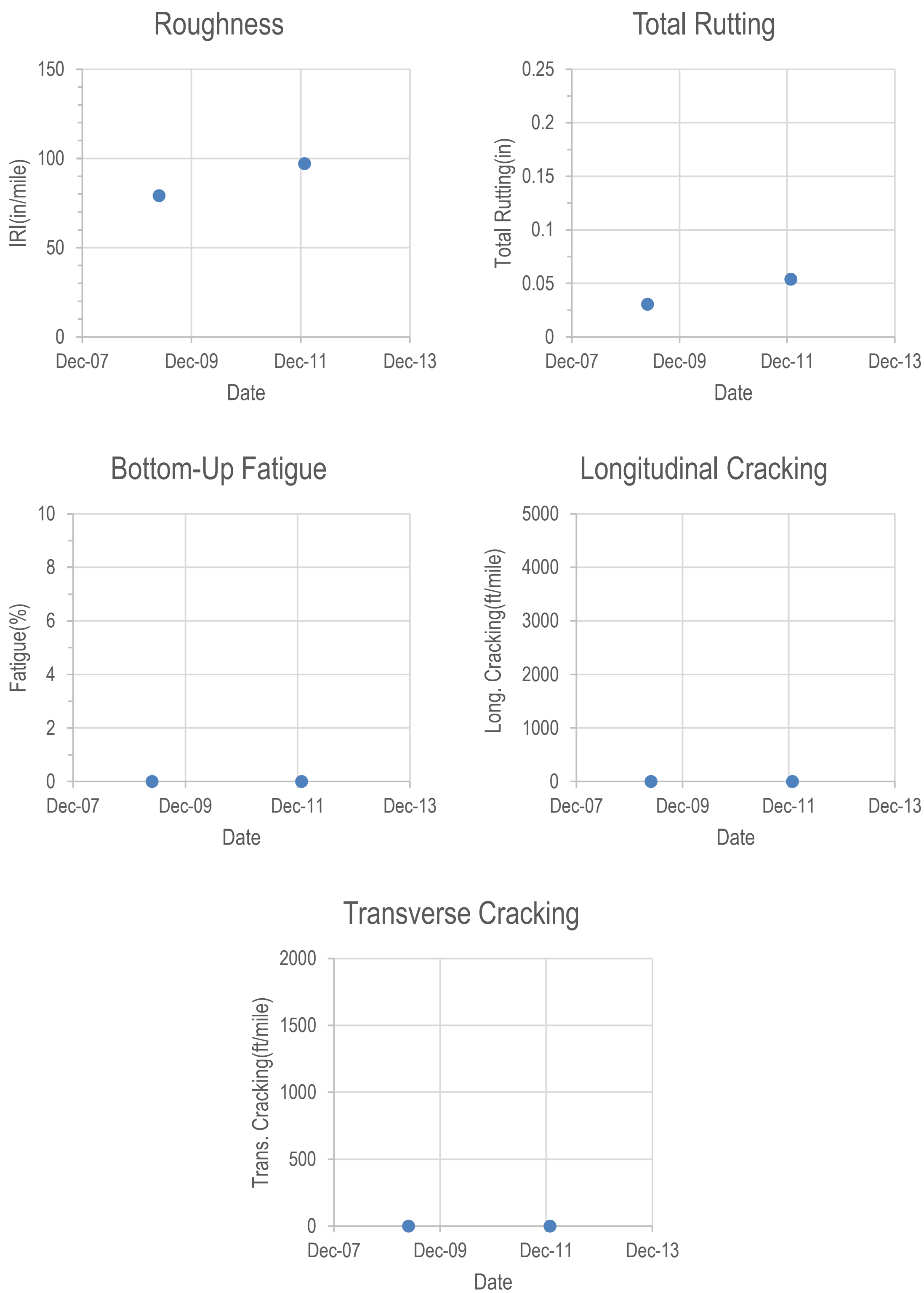

Figure 10.9-Distresses Plots for IR 080-124.

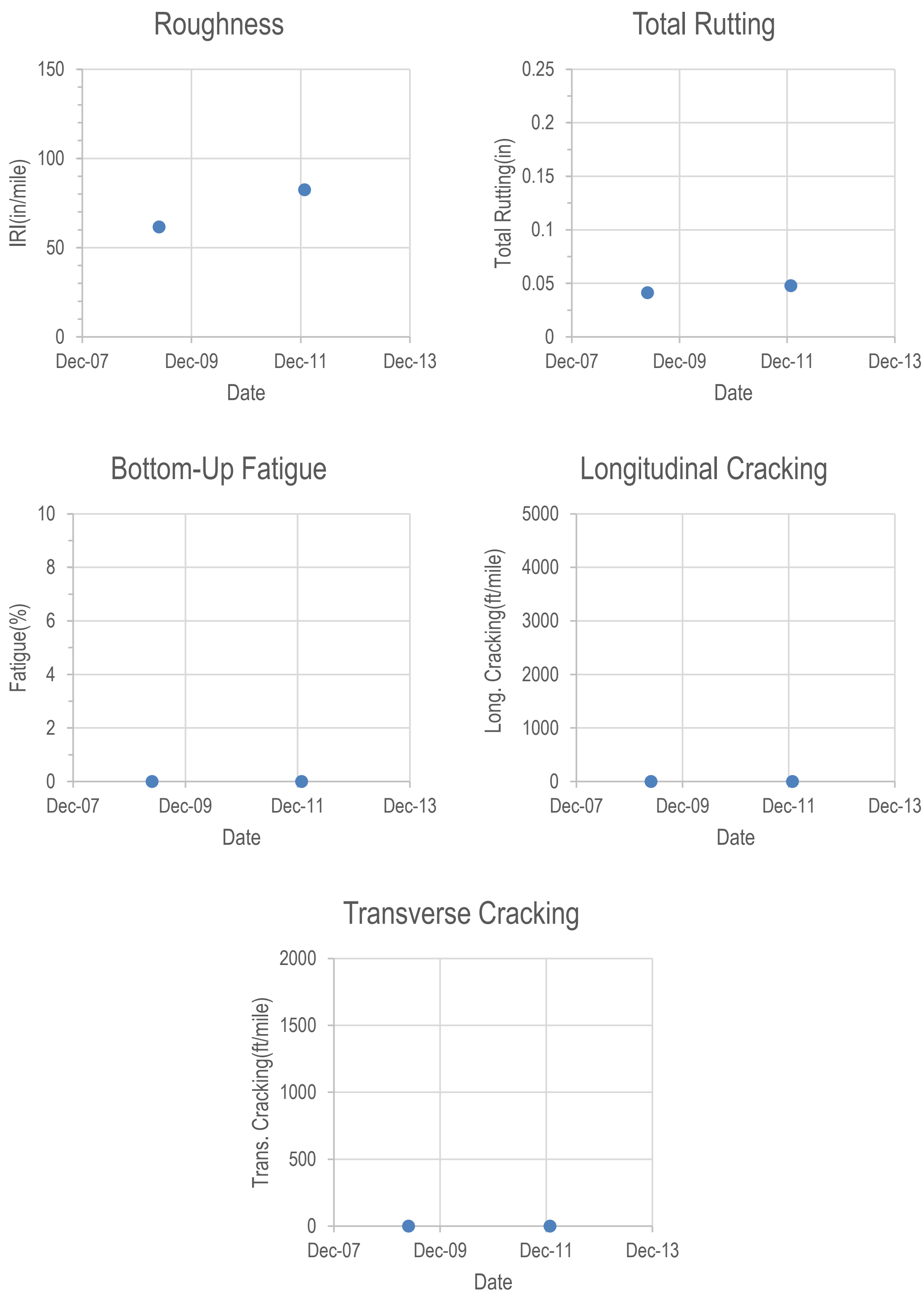

Figure 10.10-Distresses Plots for IR 080-128.

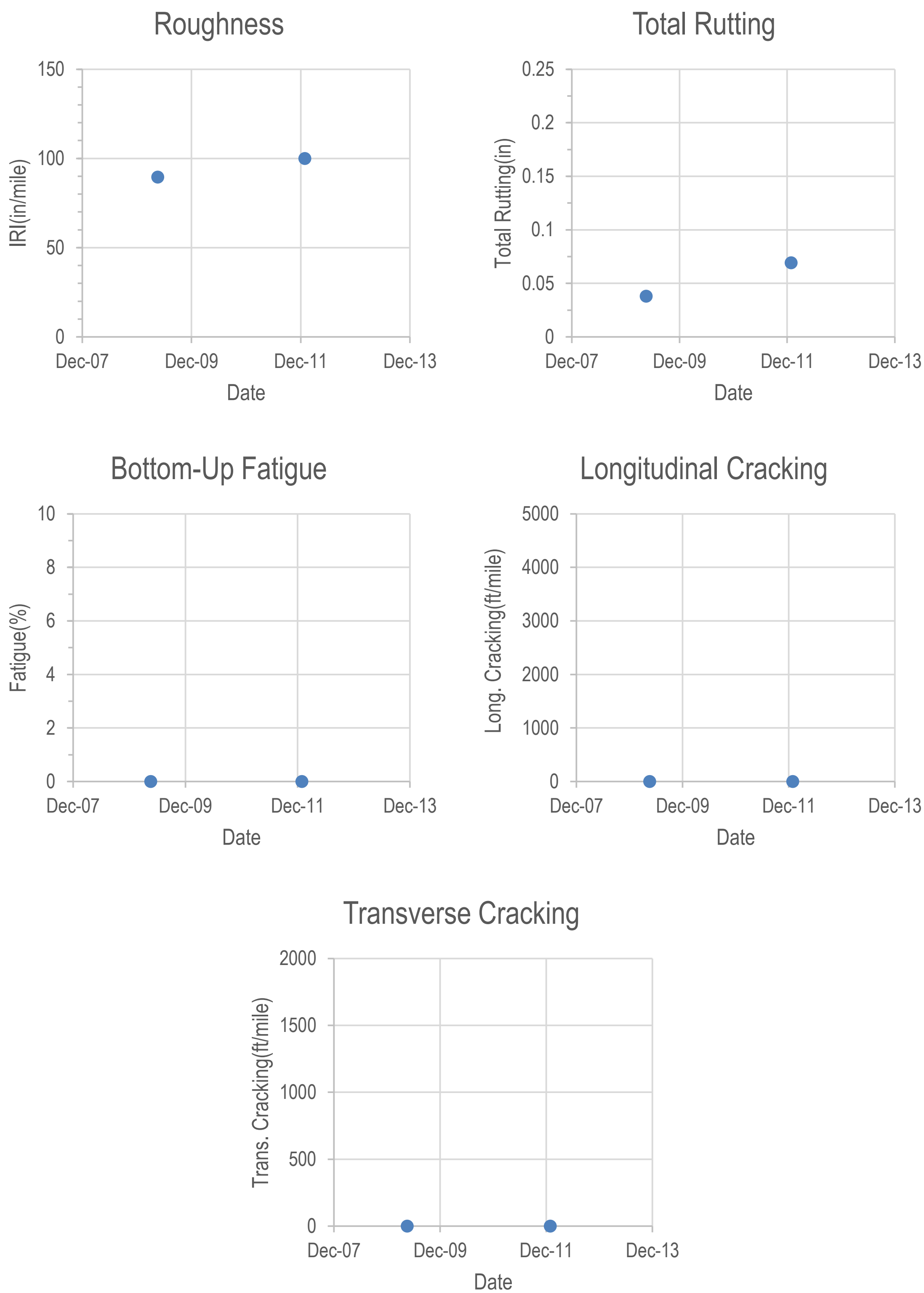

Figure 10.11-Distresses Plots for IR 080-129.

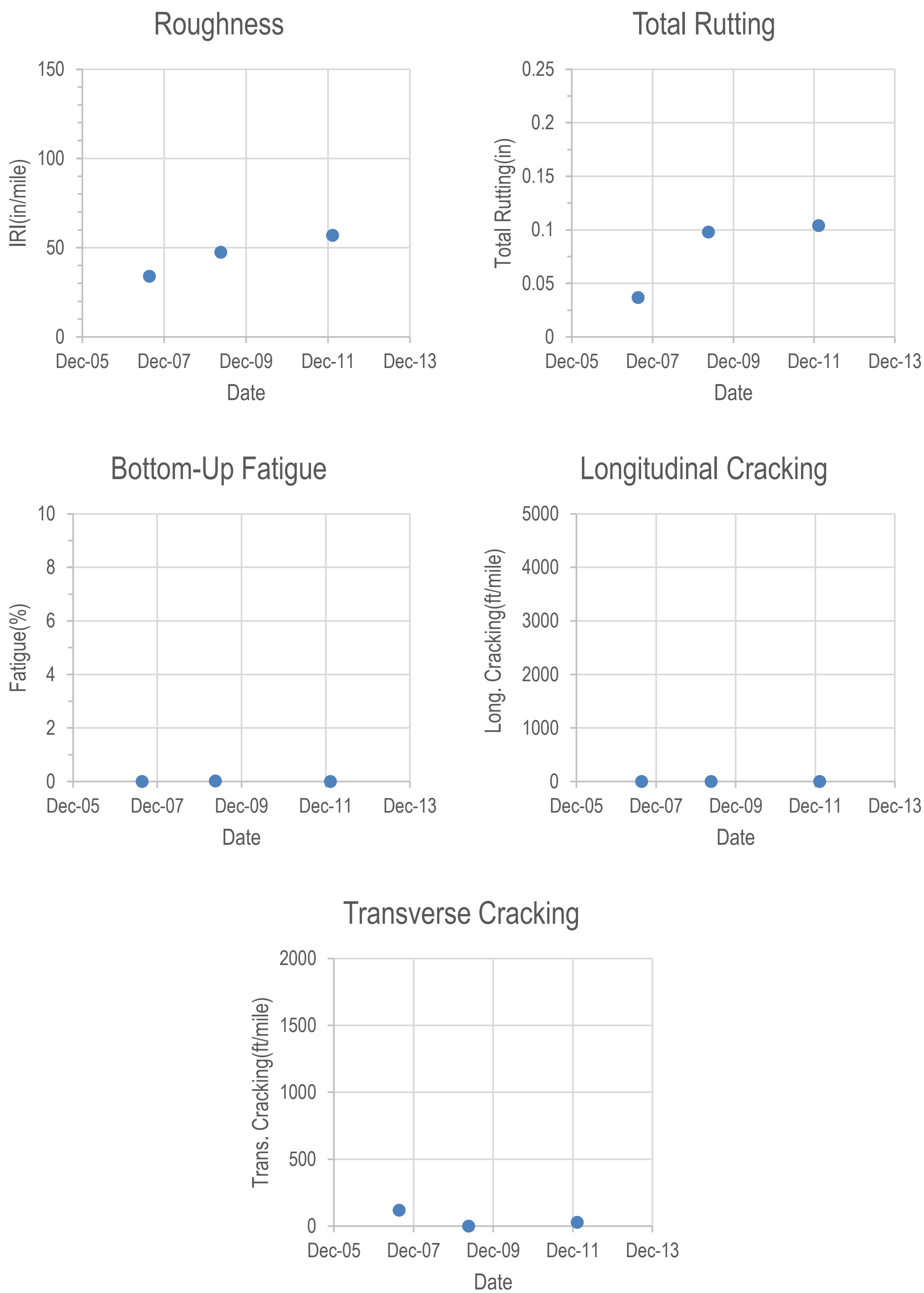

Figure 10.12-Distresses Plots for IR 080-132.

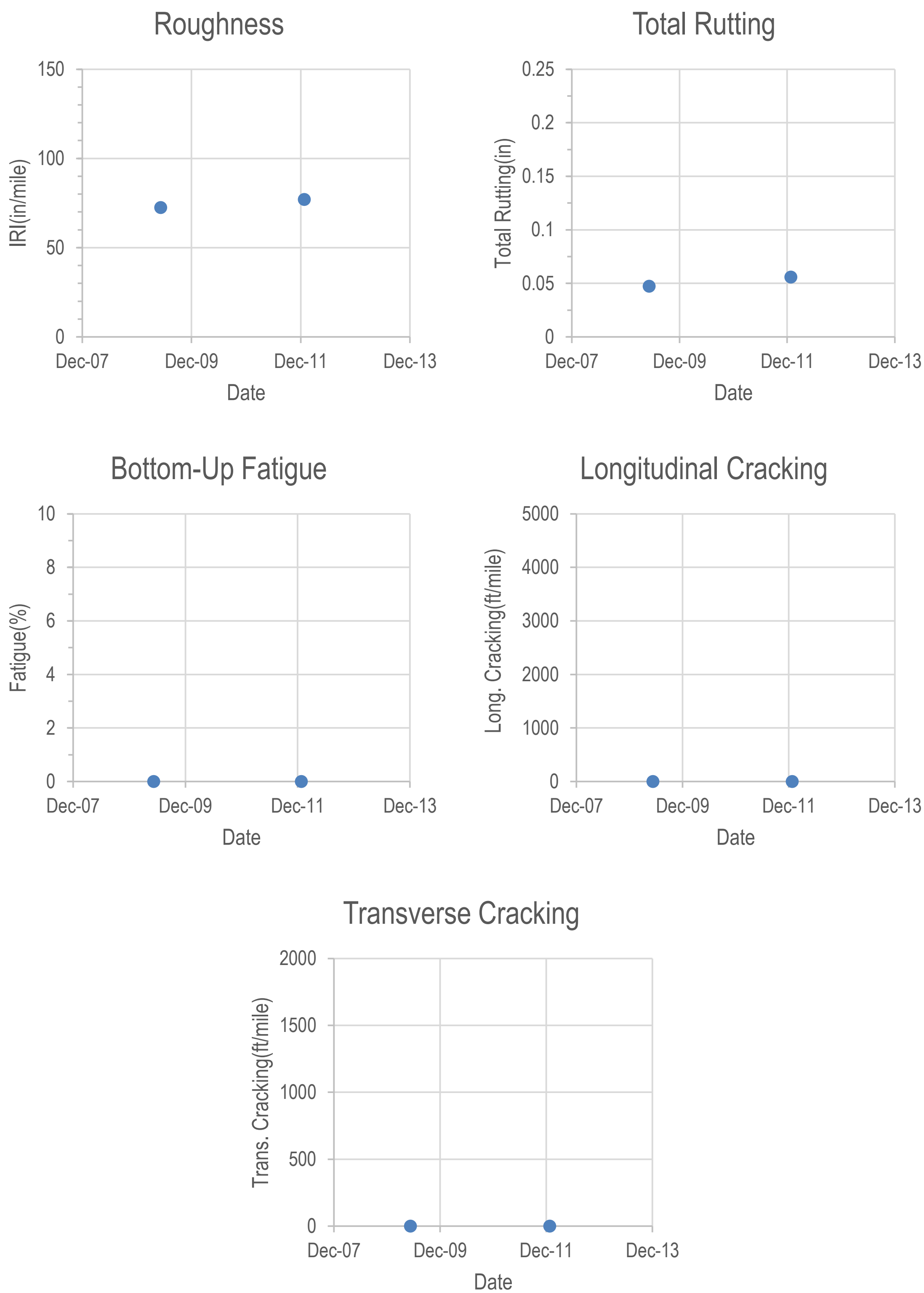

Figure 10.13-Distresses Plots for IR 080-134.

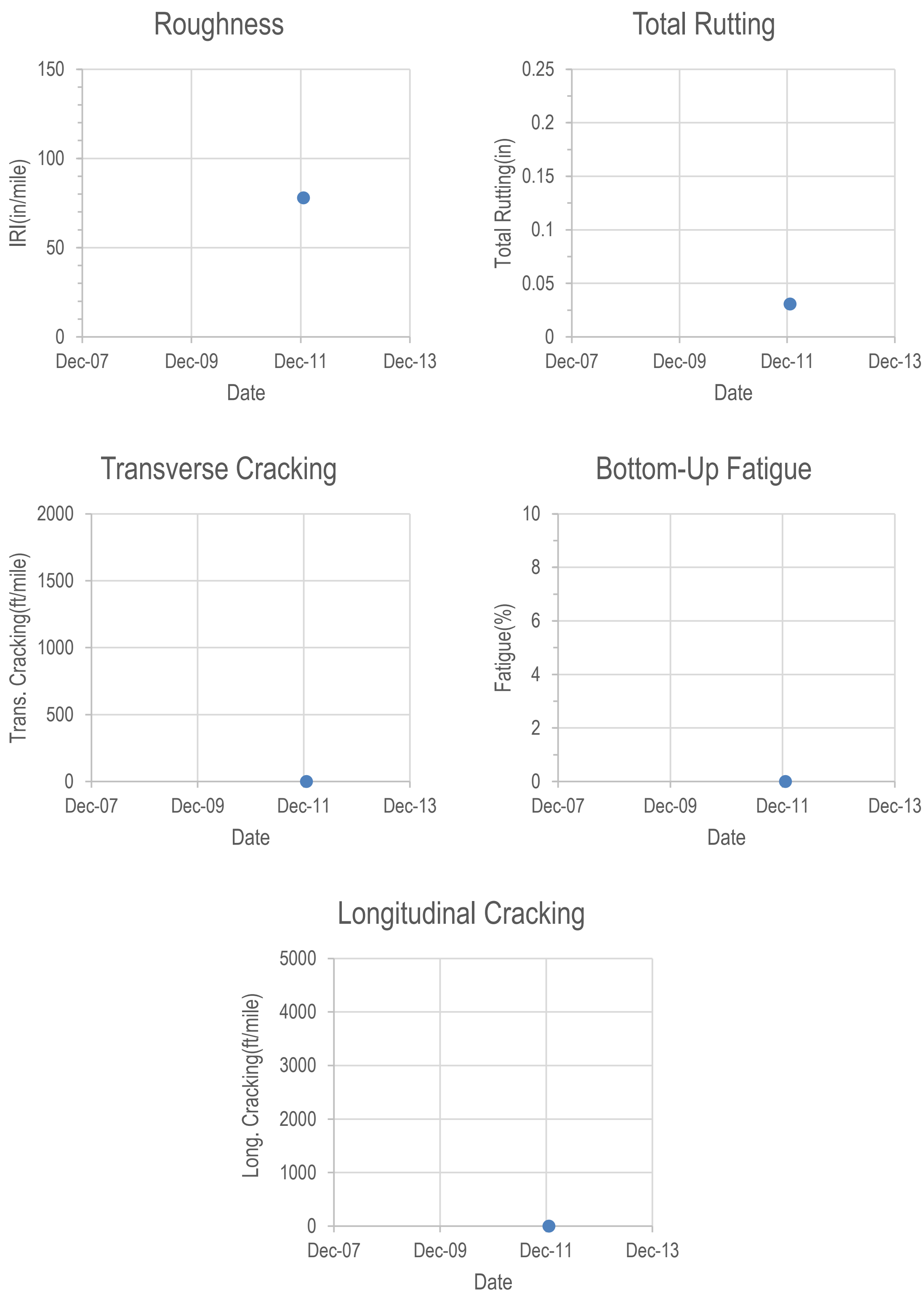

Figure 10.14-Distresses Plots for IR 080-138.

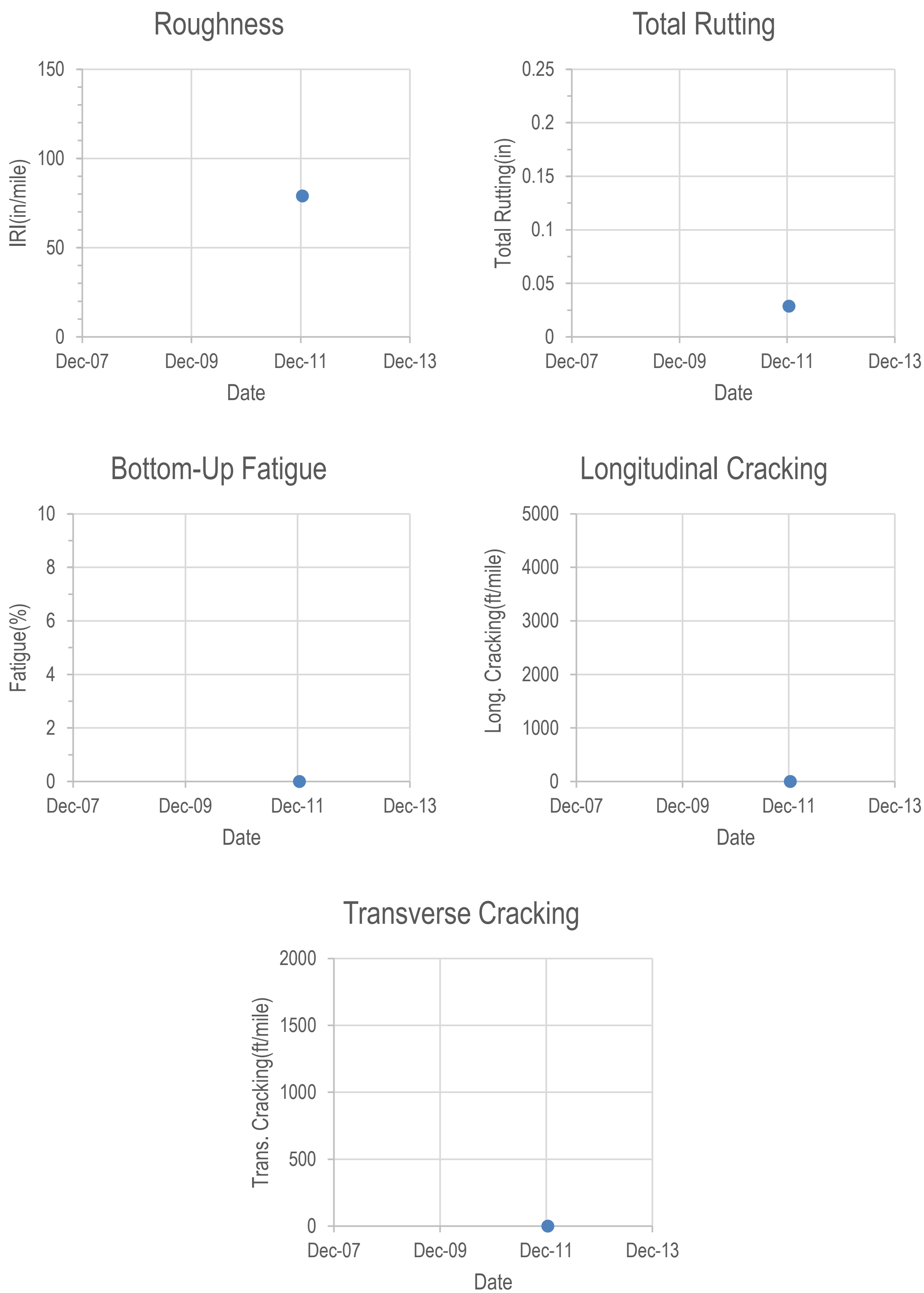

Figure 10.15-Distresses Plots for IR 080-139.

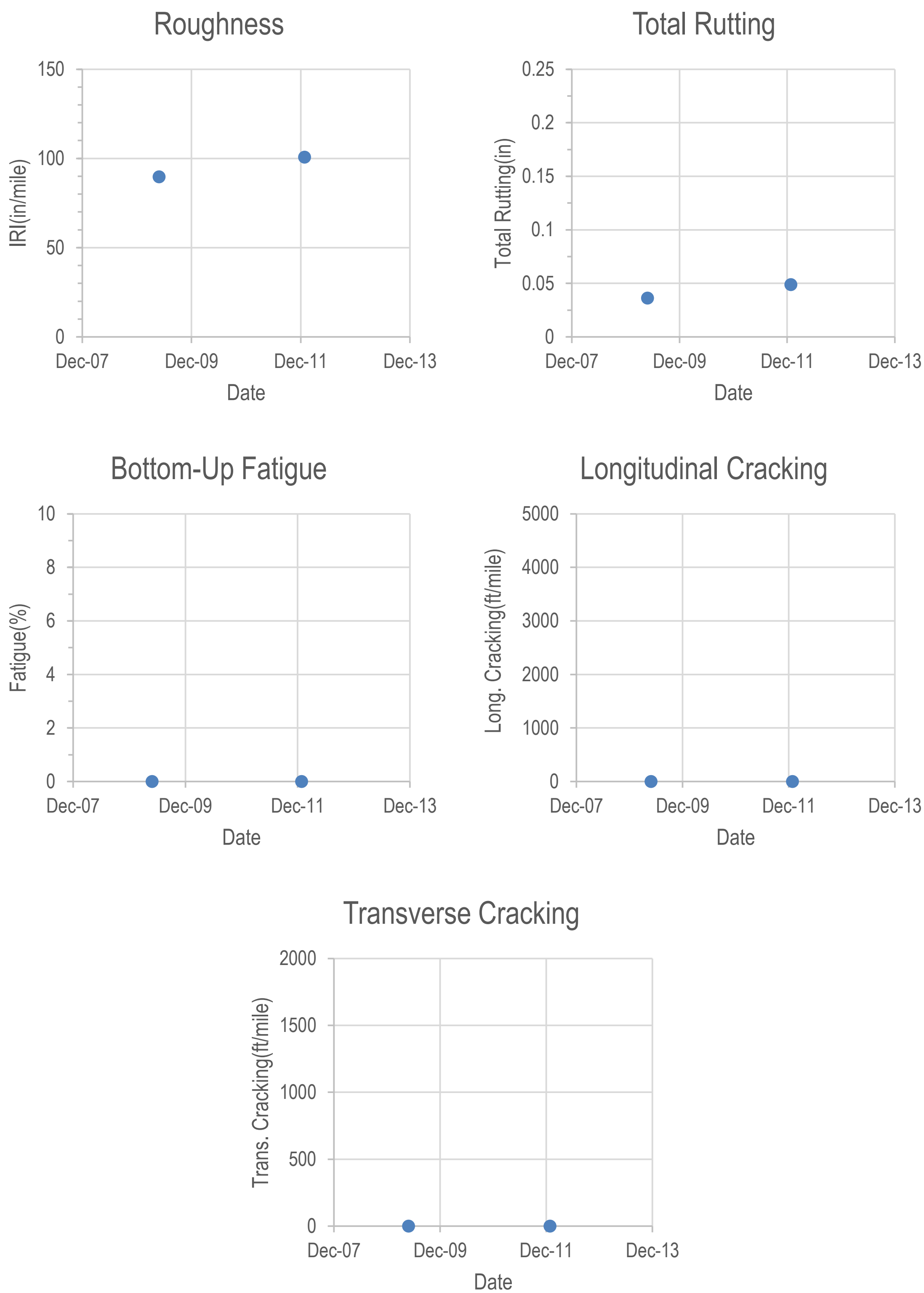

Figure 10.16-Distresses Plots for IR 080-140.

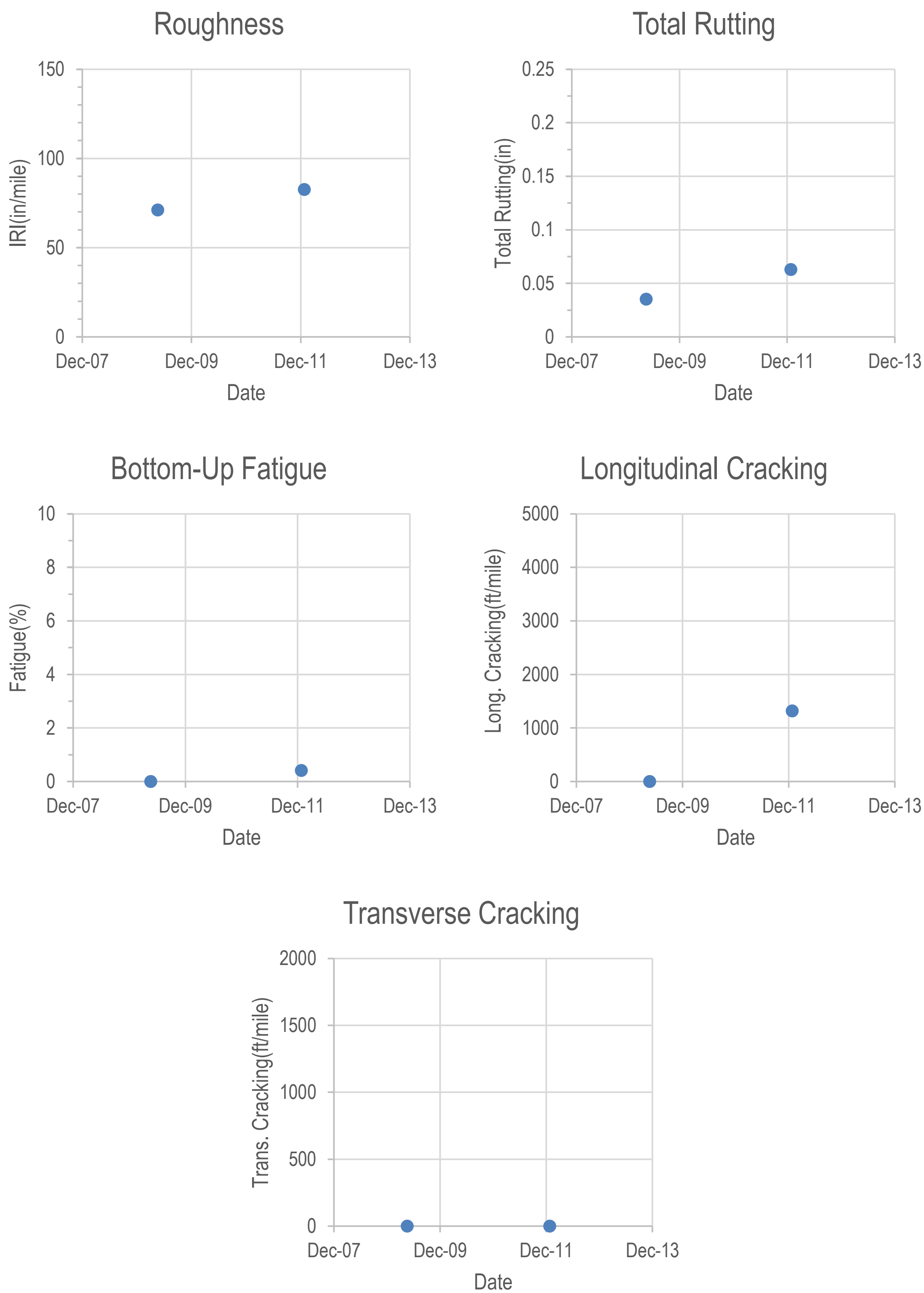

Figure 10.17-Distresses Plots for IR 080-141.

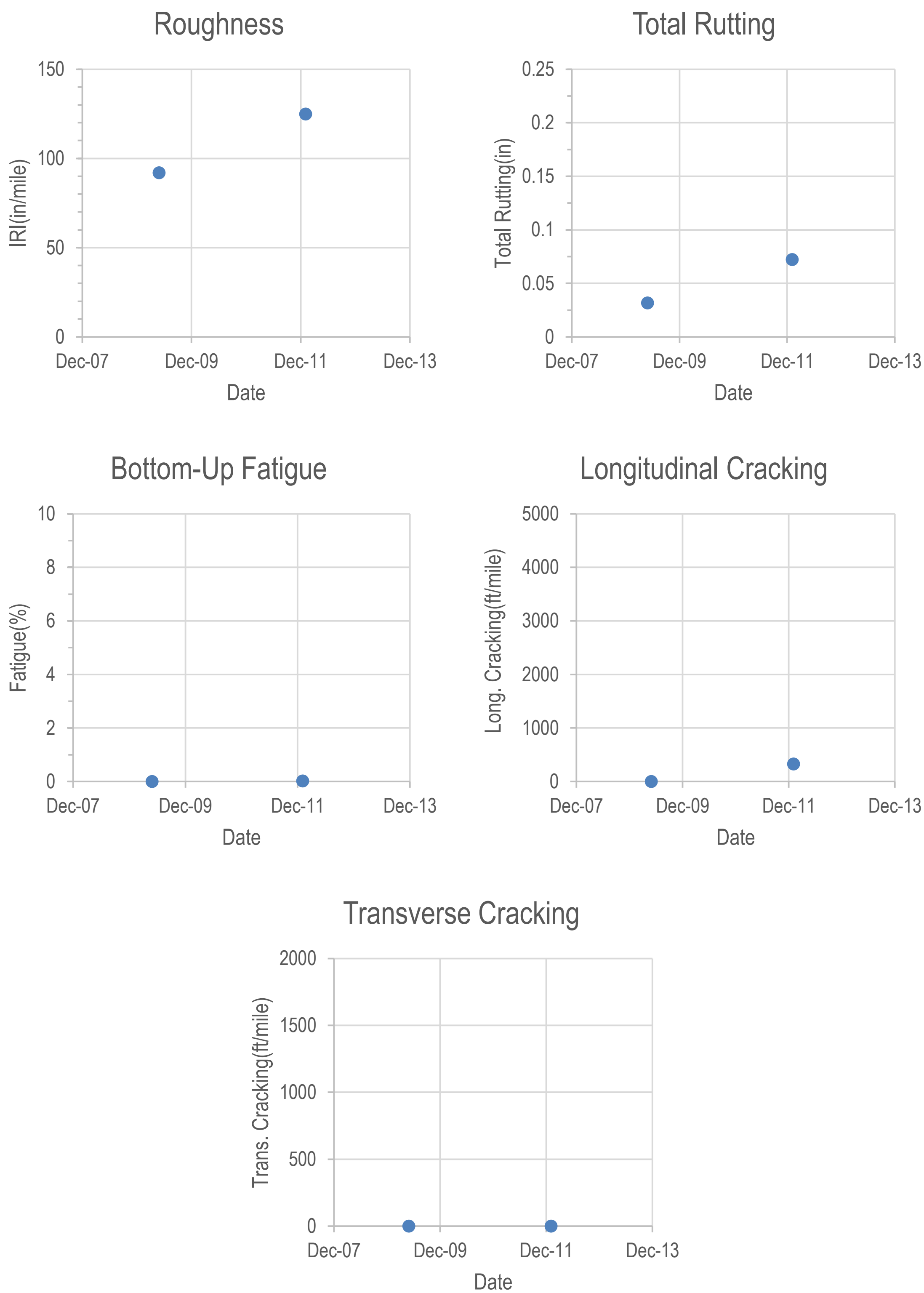

Figure 10.18-Distresses Plots for IR 080-142.

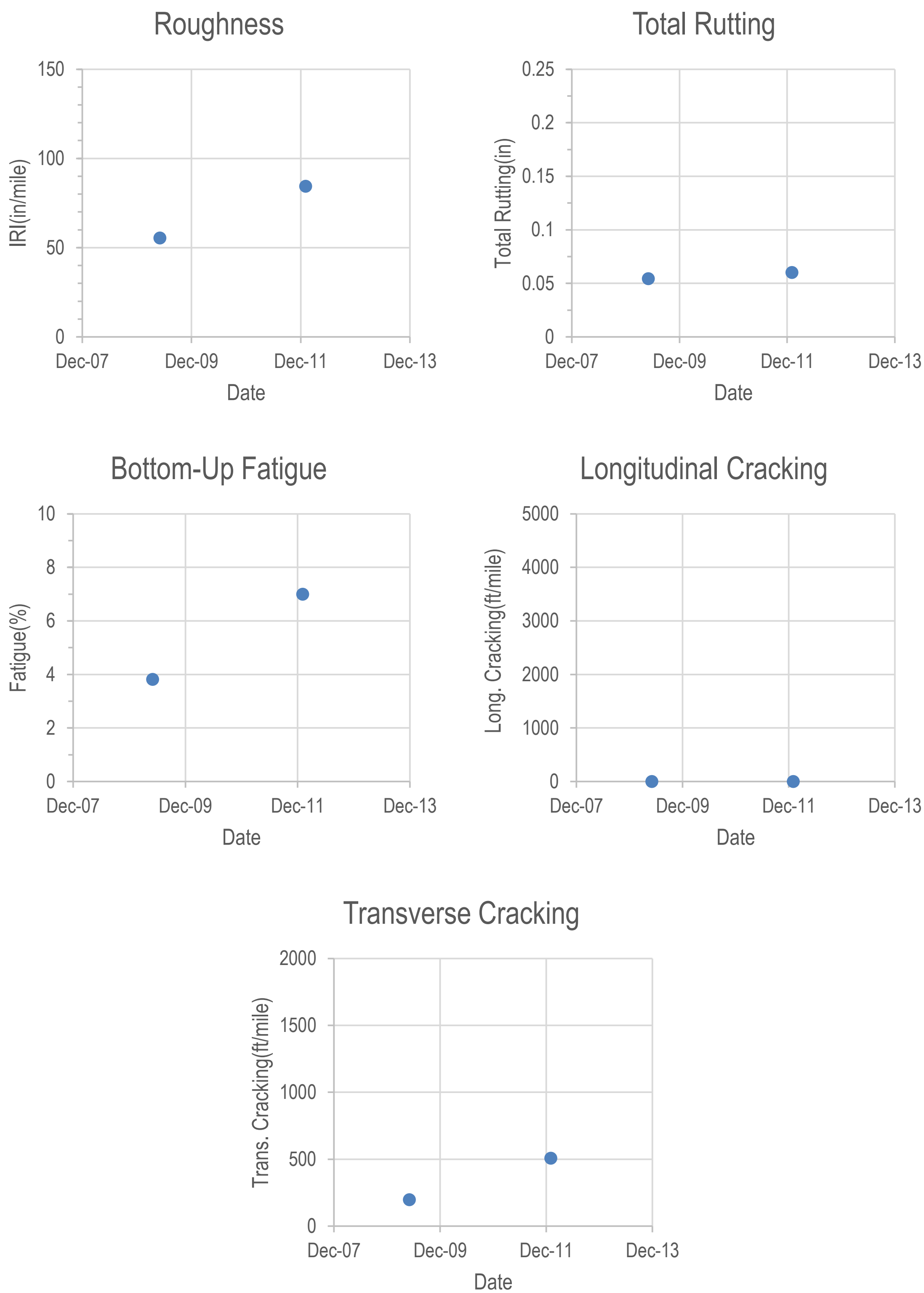

Figure 10.19-Distresses Plots for IR 015-95.

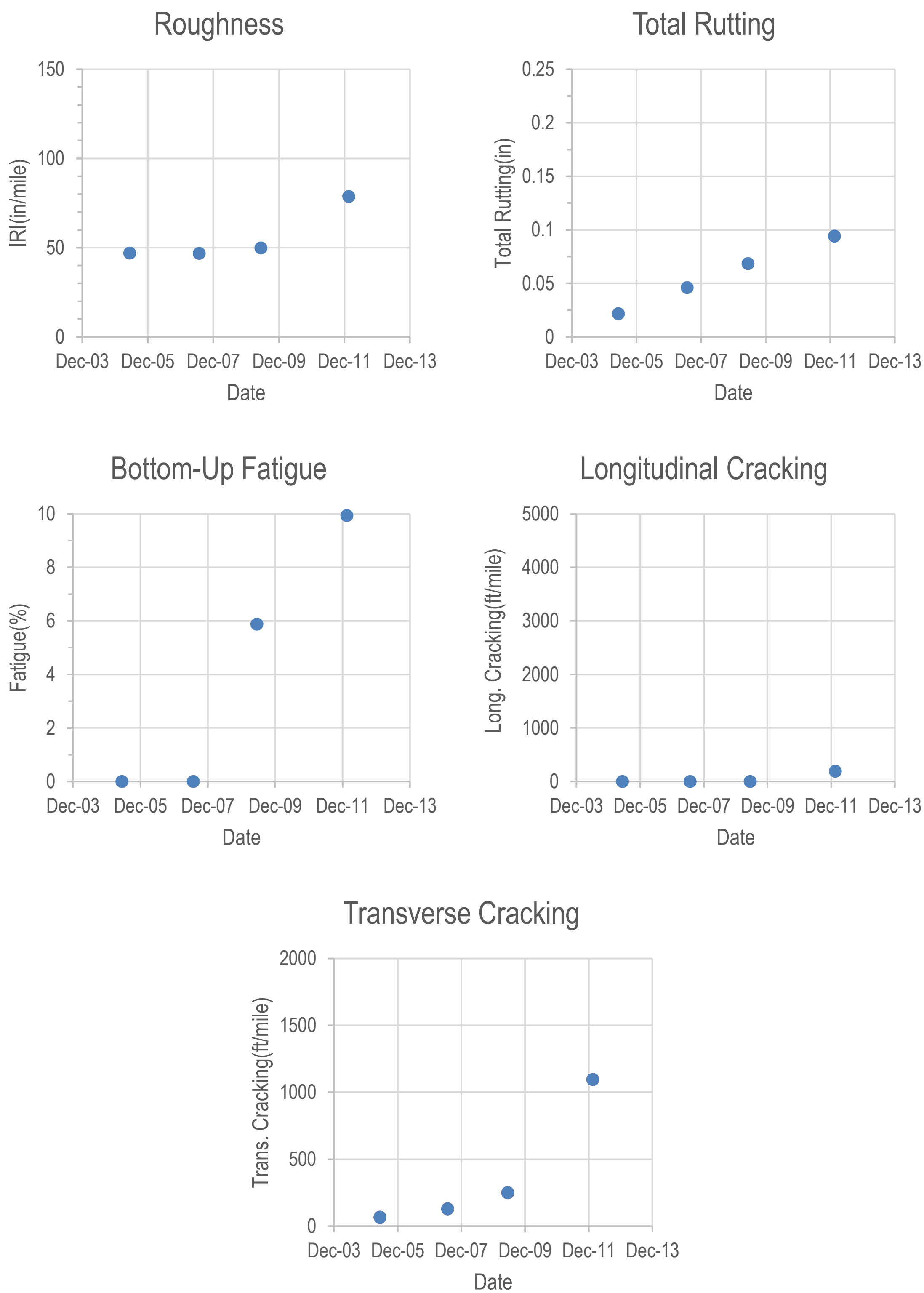

Figure 10.20-Distresses Plots for IR 015-99A.

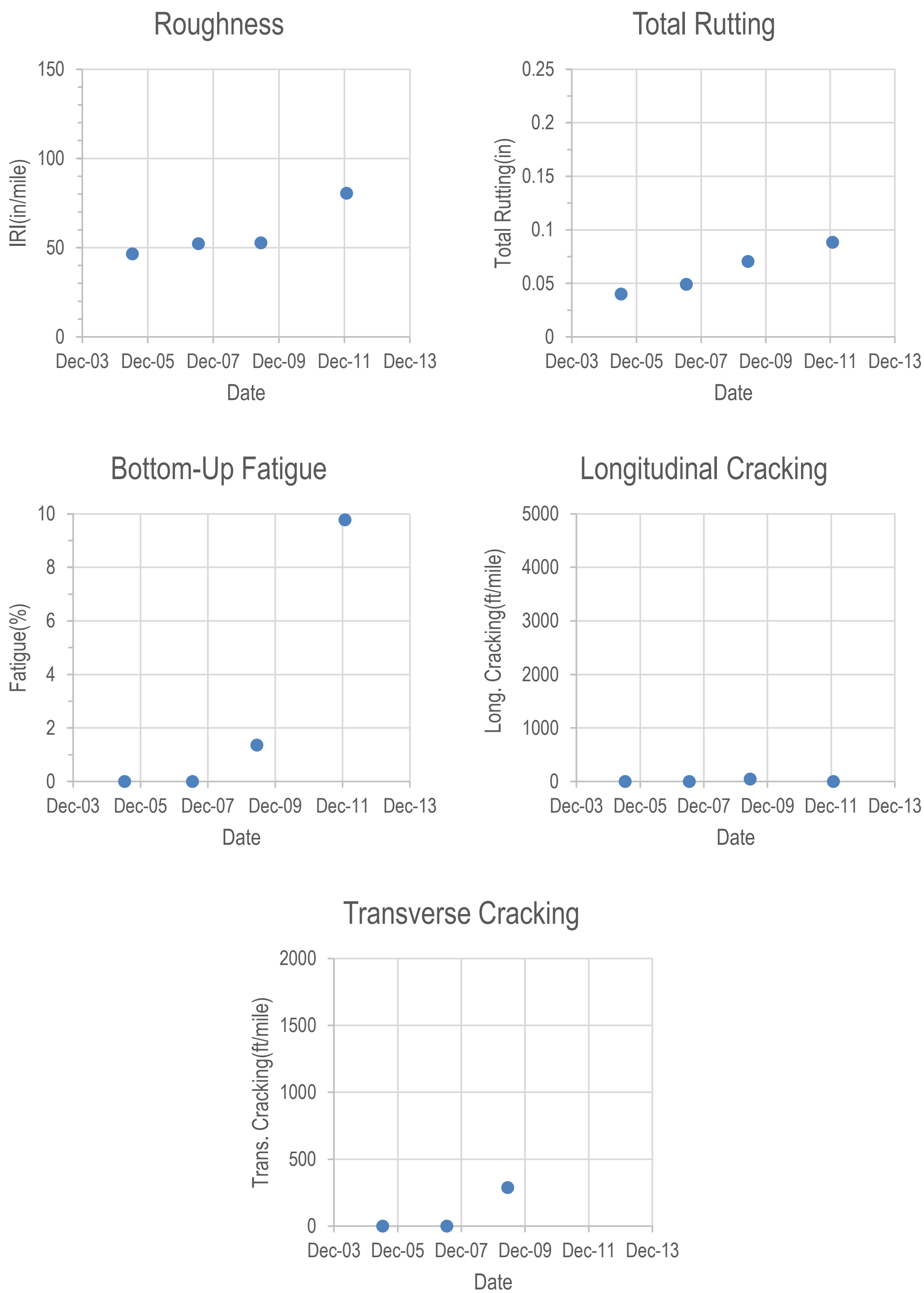

Figure 10.21-Distresses Plots for IR 015-99B.

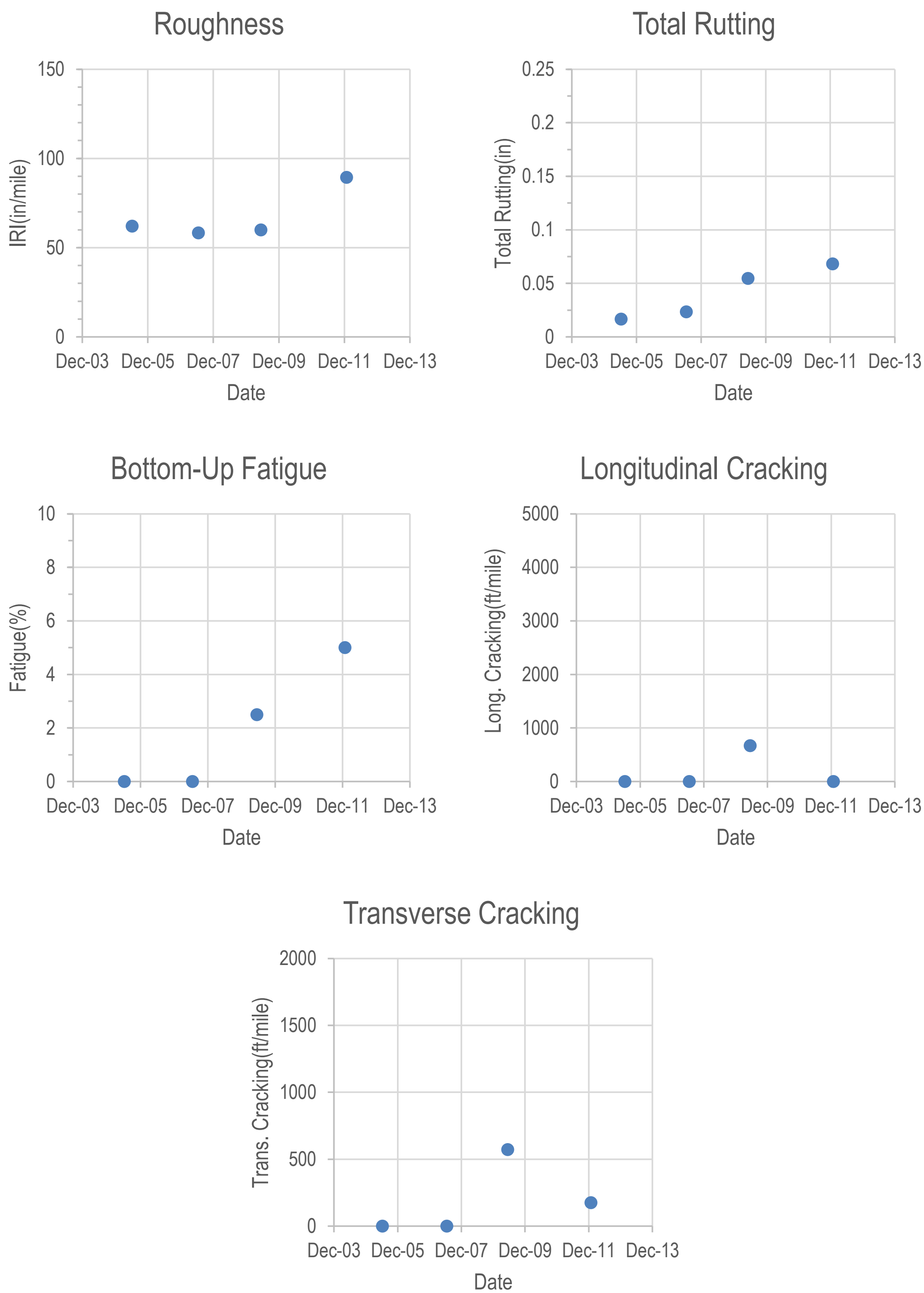

Figure 10.22-Distresses Plots for IR 015-100.

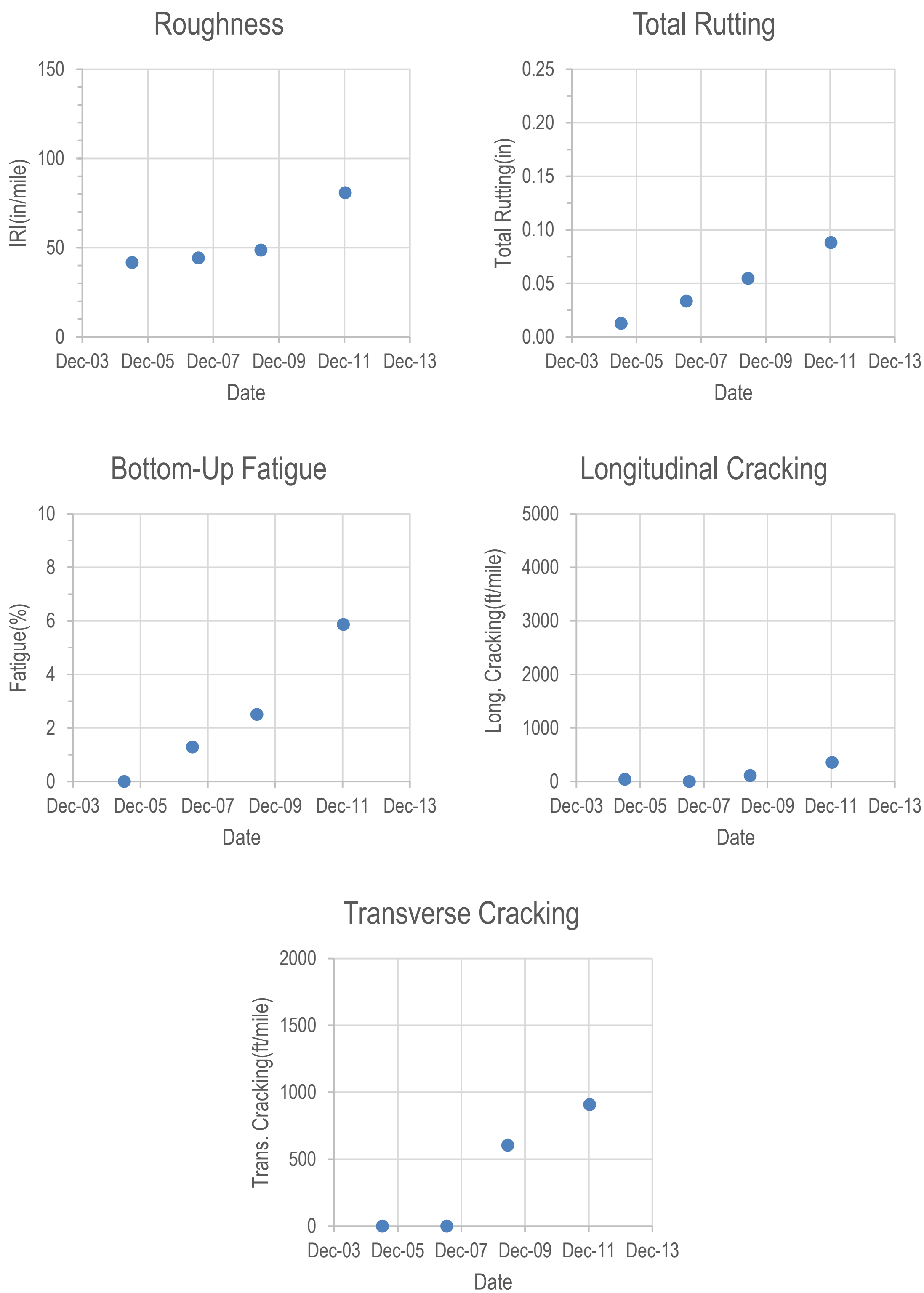

Figure 10.23-Distresses Plots for IR 015-101.

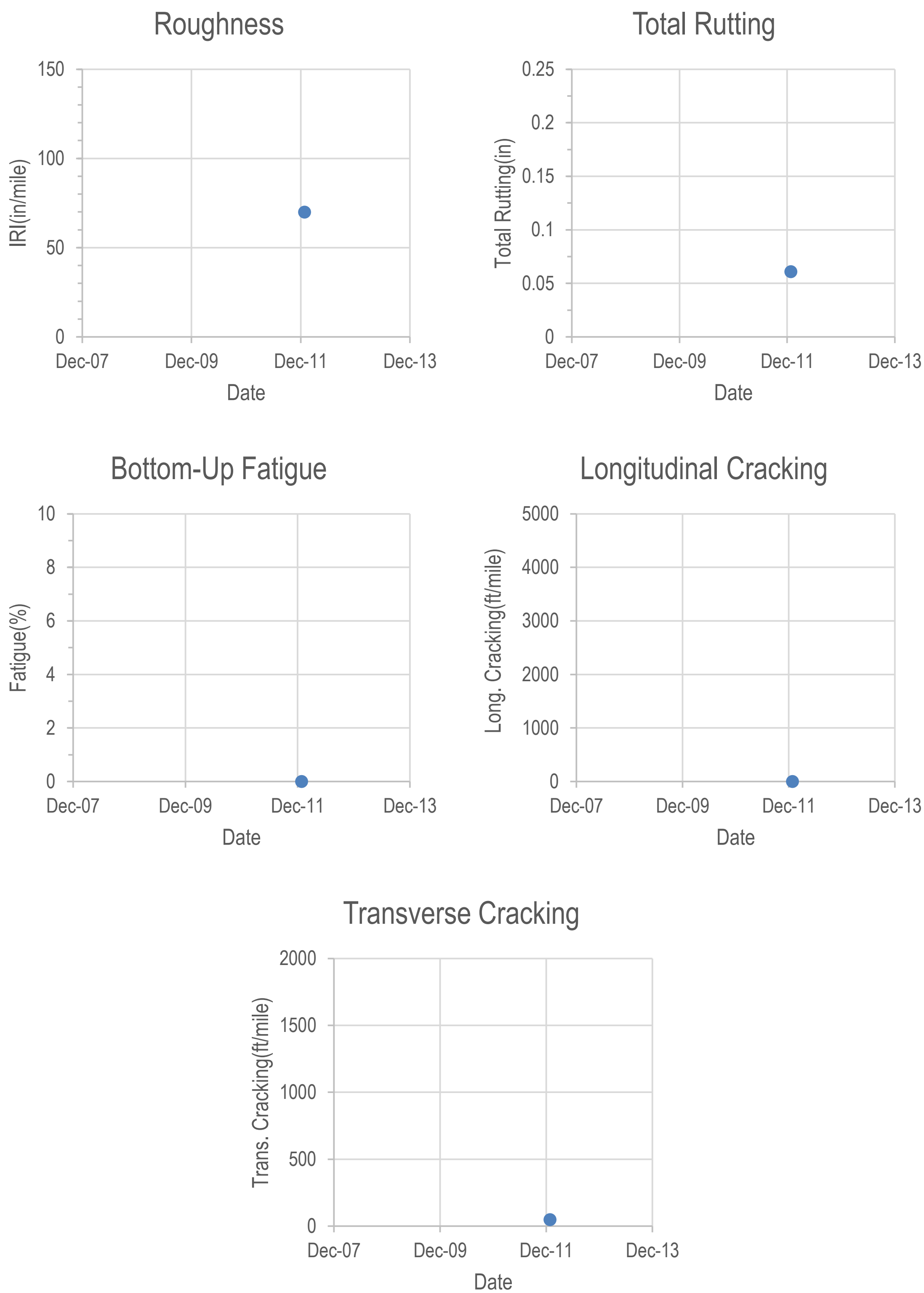

Figure 10.24-Distresses Plots for IR 015-102.

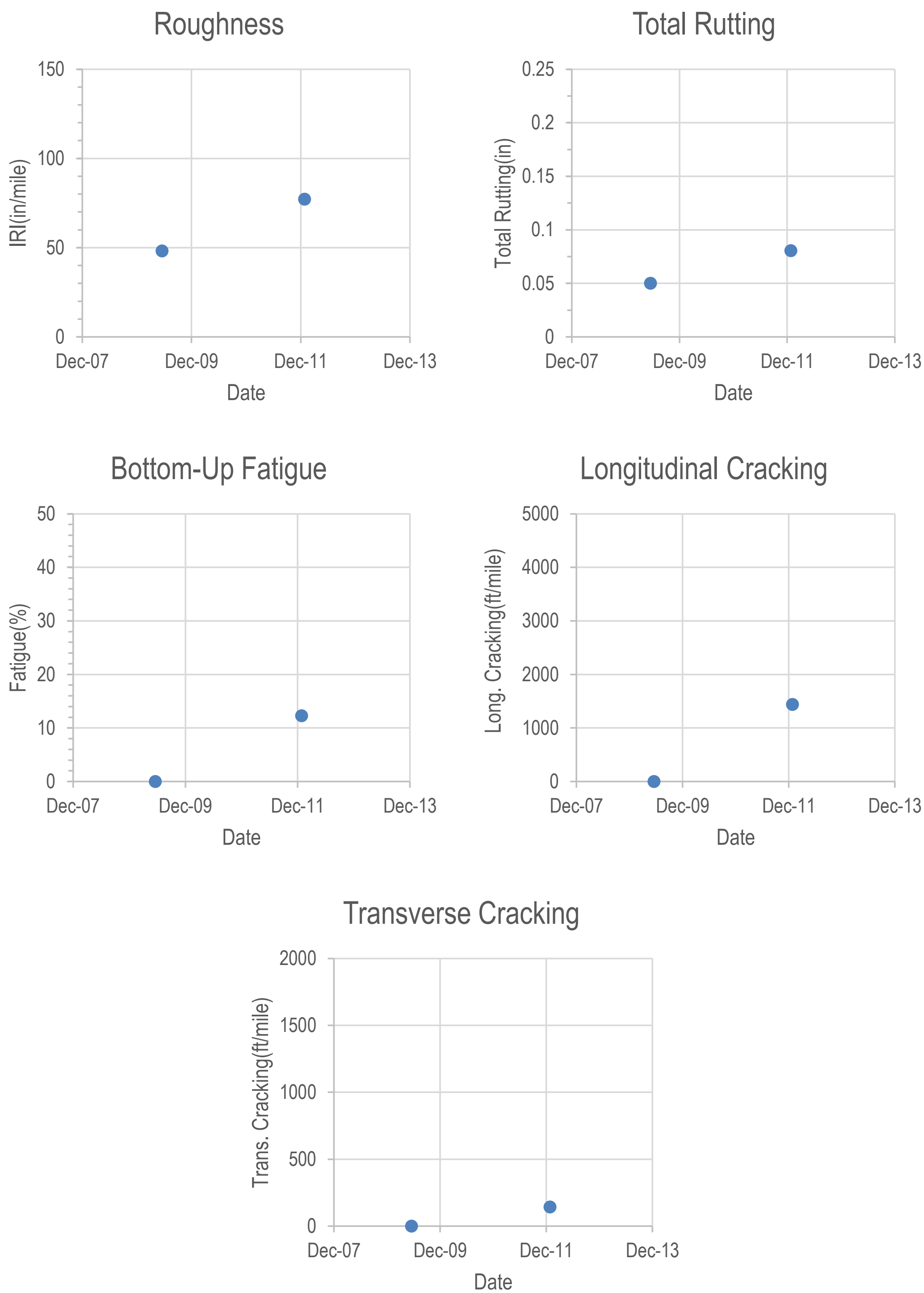

Figure 10.25-Distresses Plots for IR 015-103.

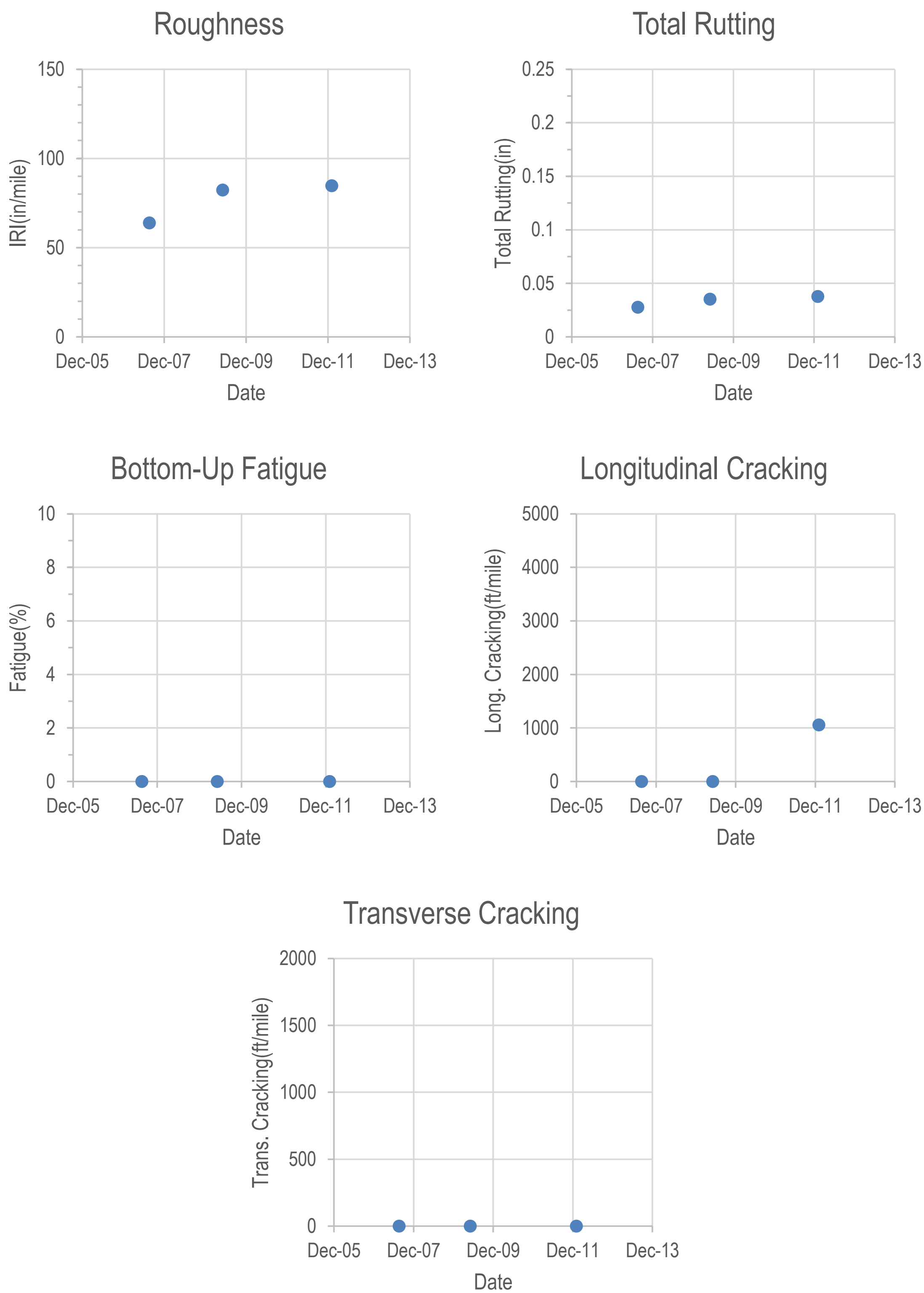

Figure 10.26-Distresses Plots for SR 160-8.

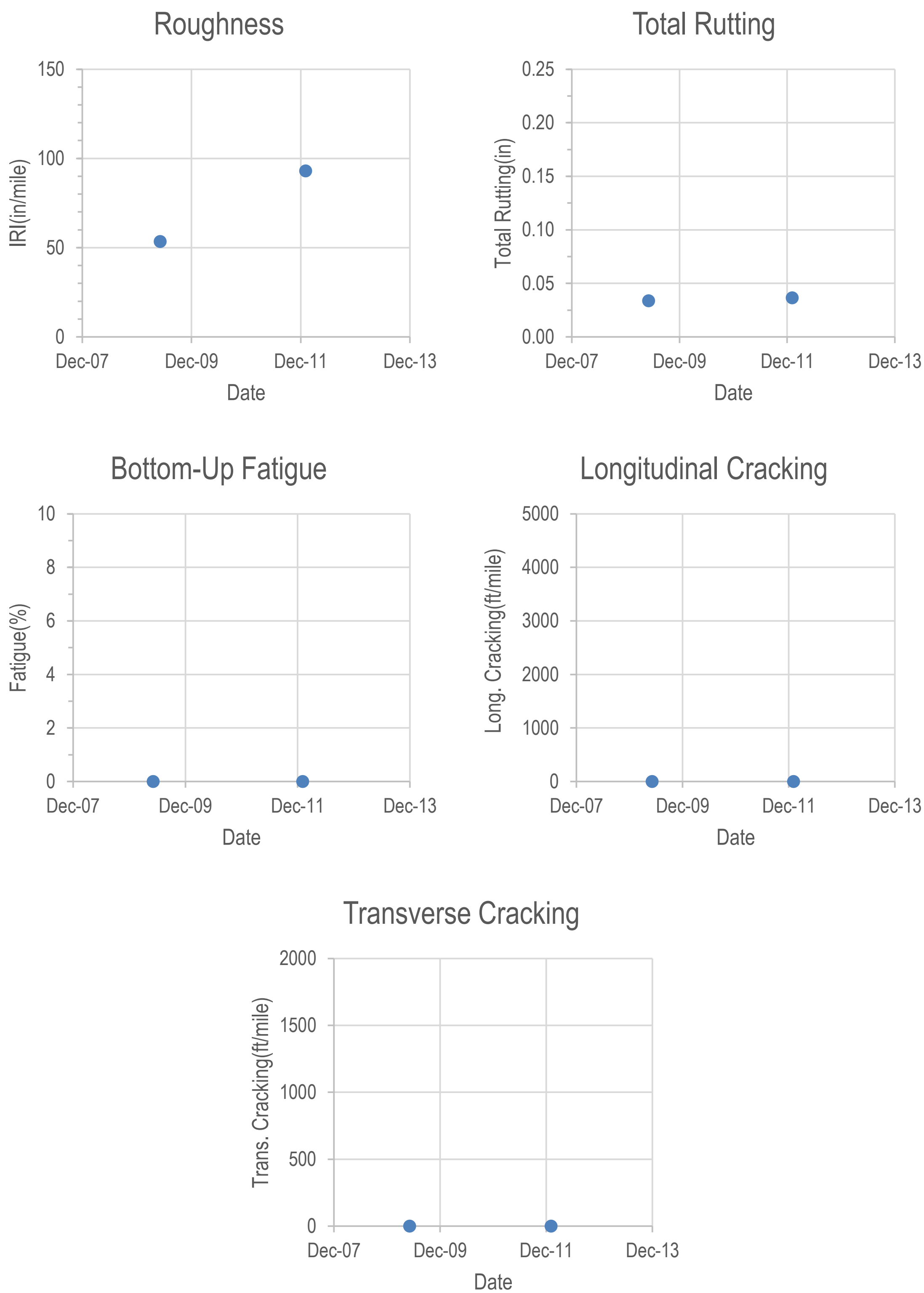

Figure 10.27-Distresses Plots for SR 160-9.

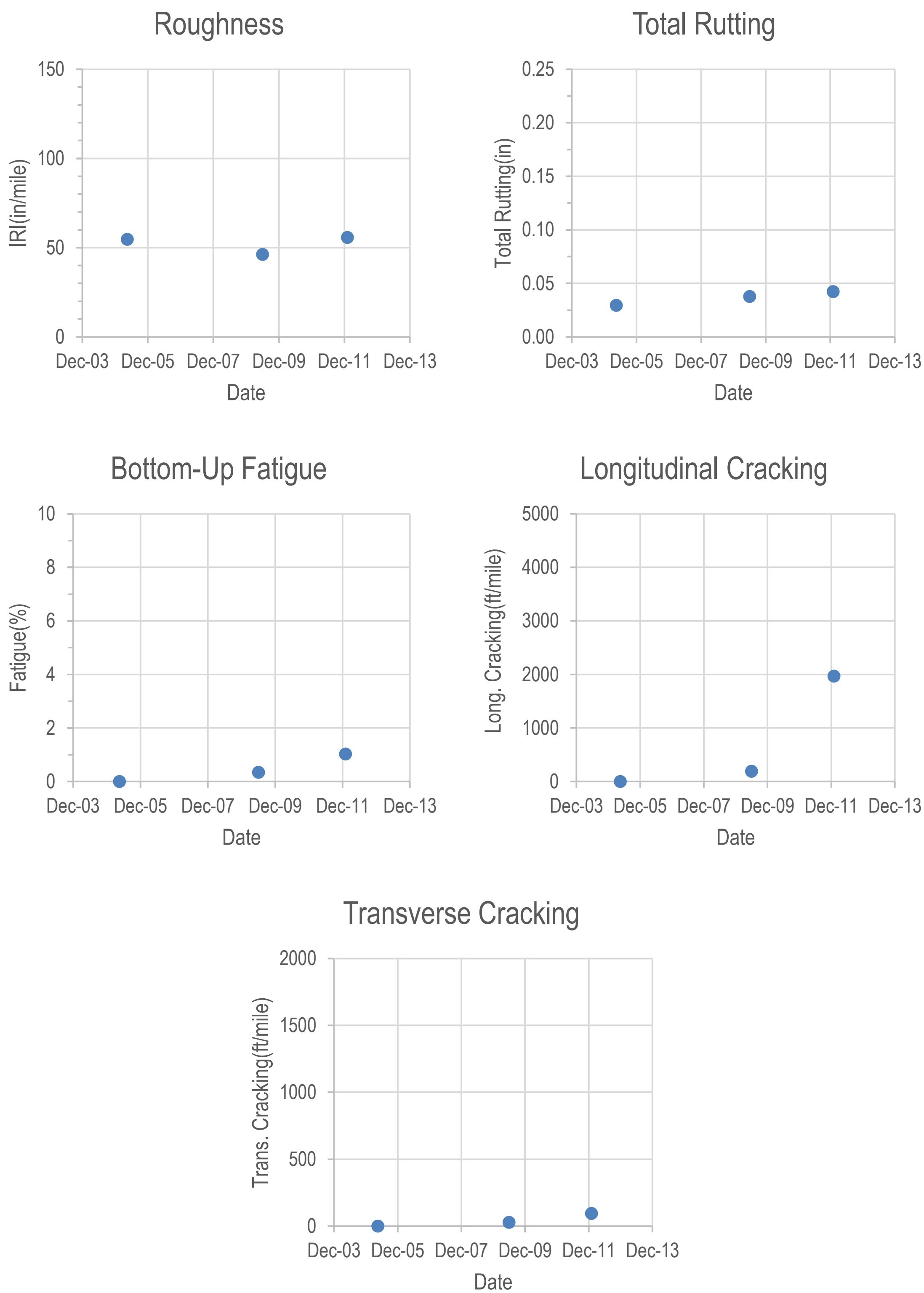

Figure 10.28-Distresses Plots for SR 160-11.

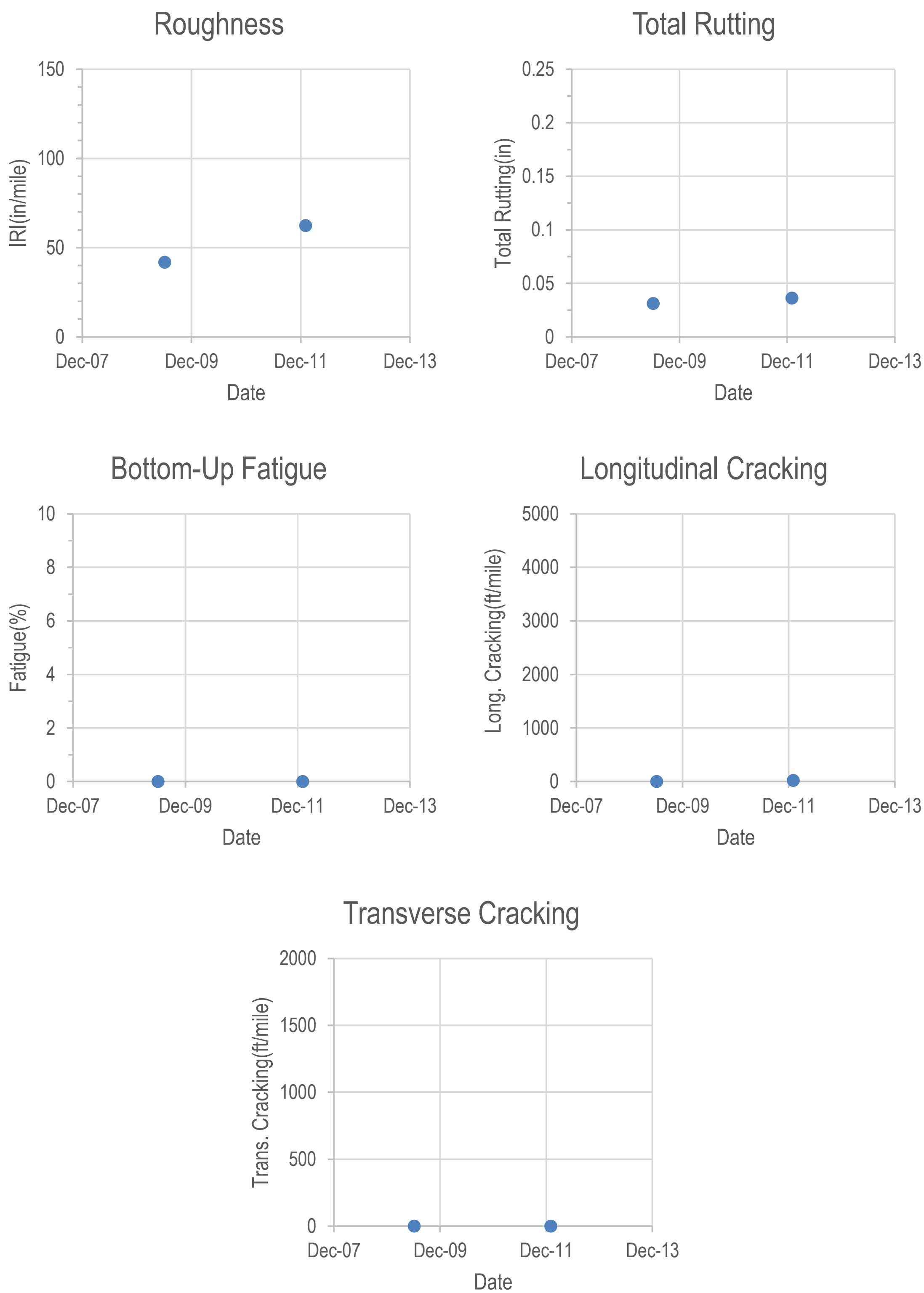

Figure 10.29-Distresses Plots for SR 160-12A.

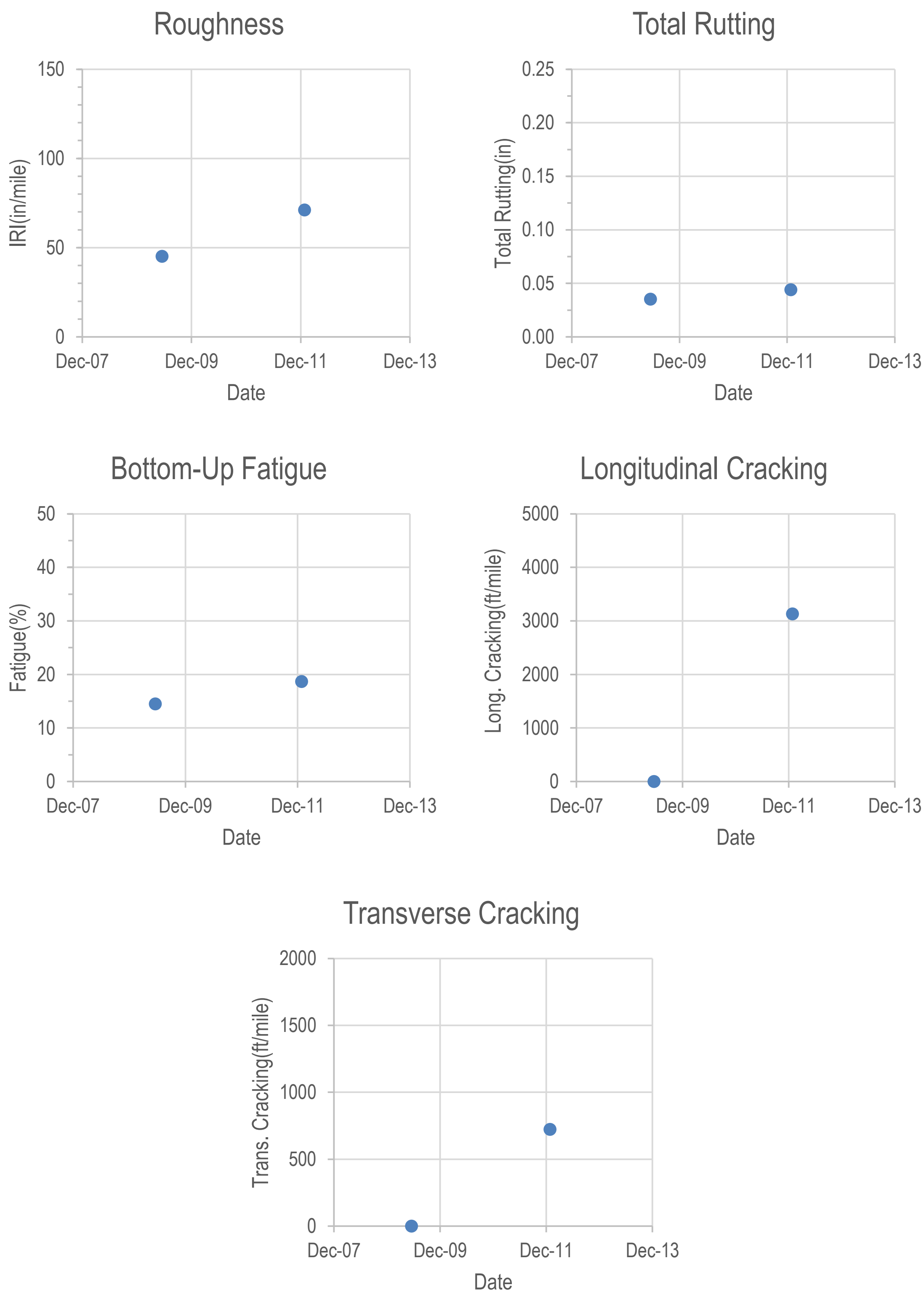

Figure 10.30-Distresses Plots for SR 160-12B.

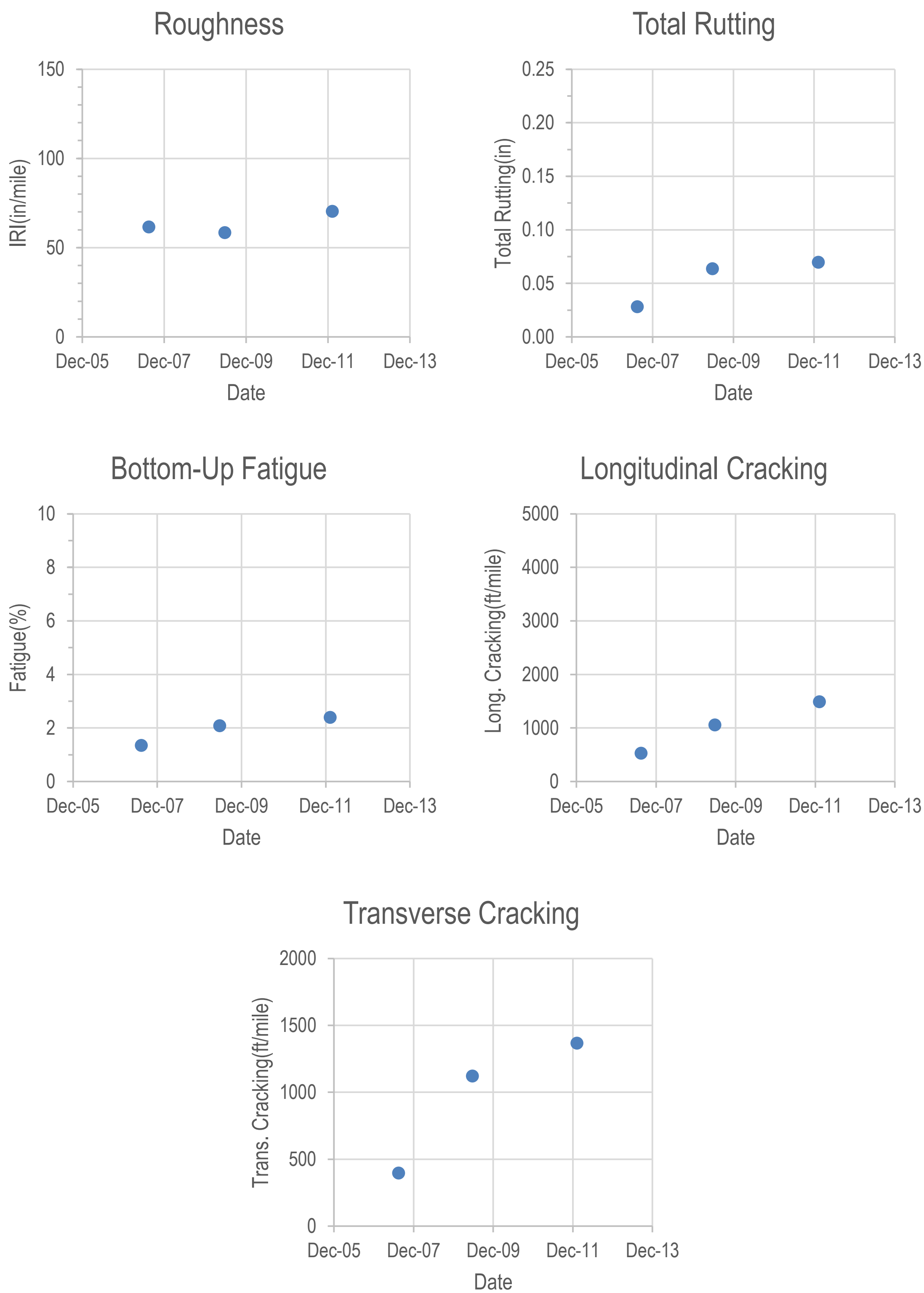

Figure 10.31-Distresses Plots for SR 160-13.

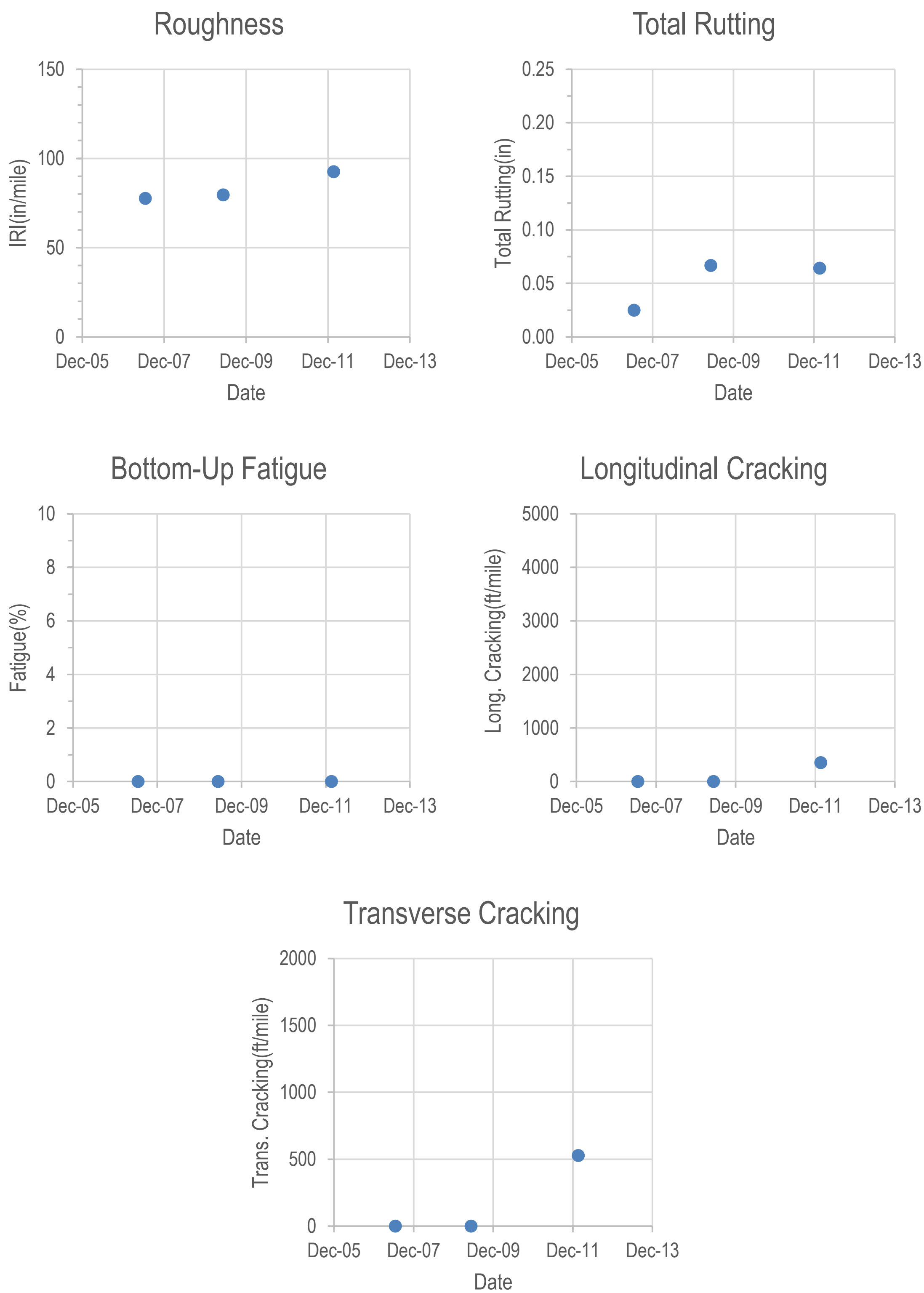

Figure 10.32-Distresses Plots for SR 159-6.

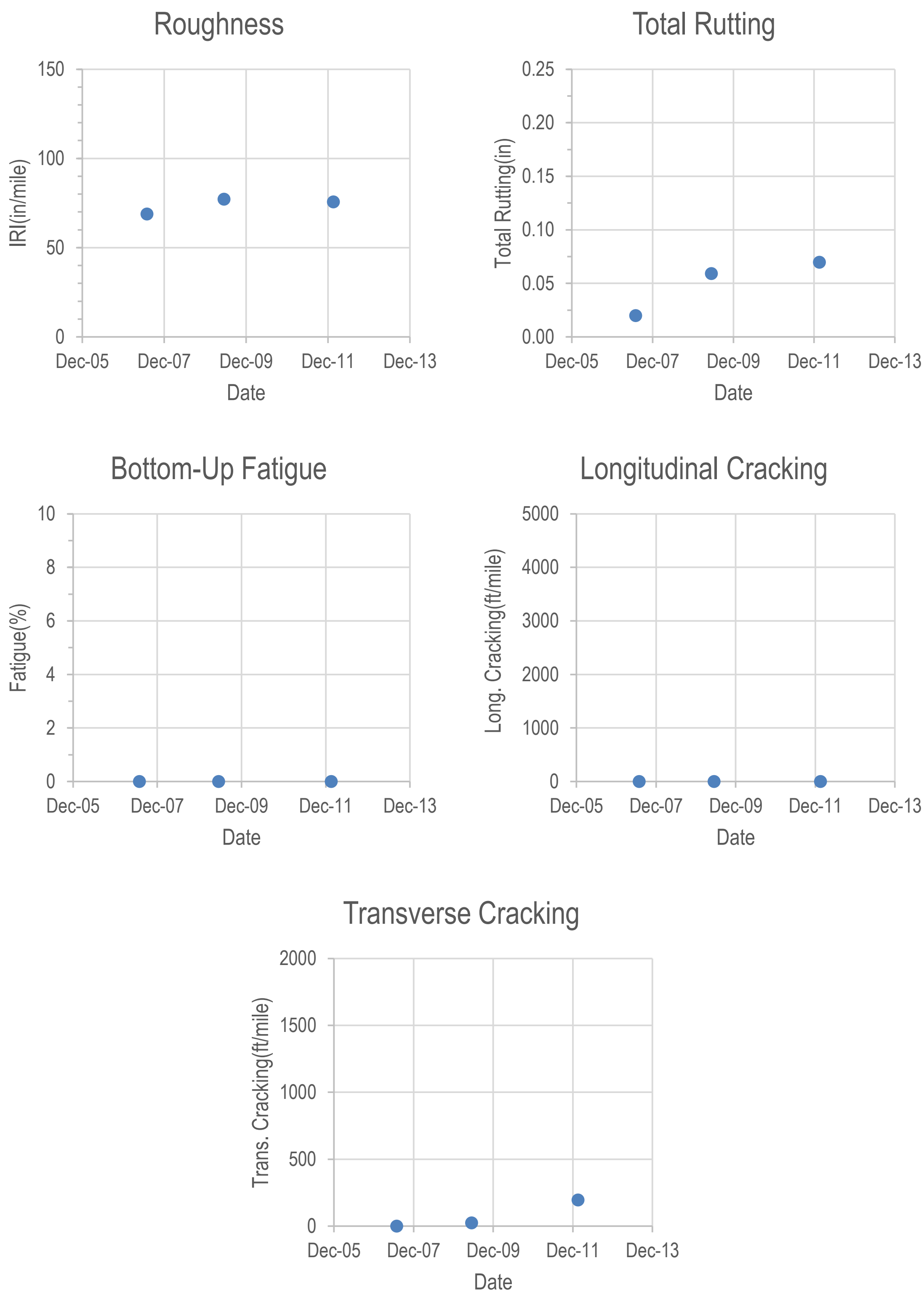

Figure 10.33-Distresses Plots for SR 117-1.

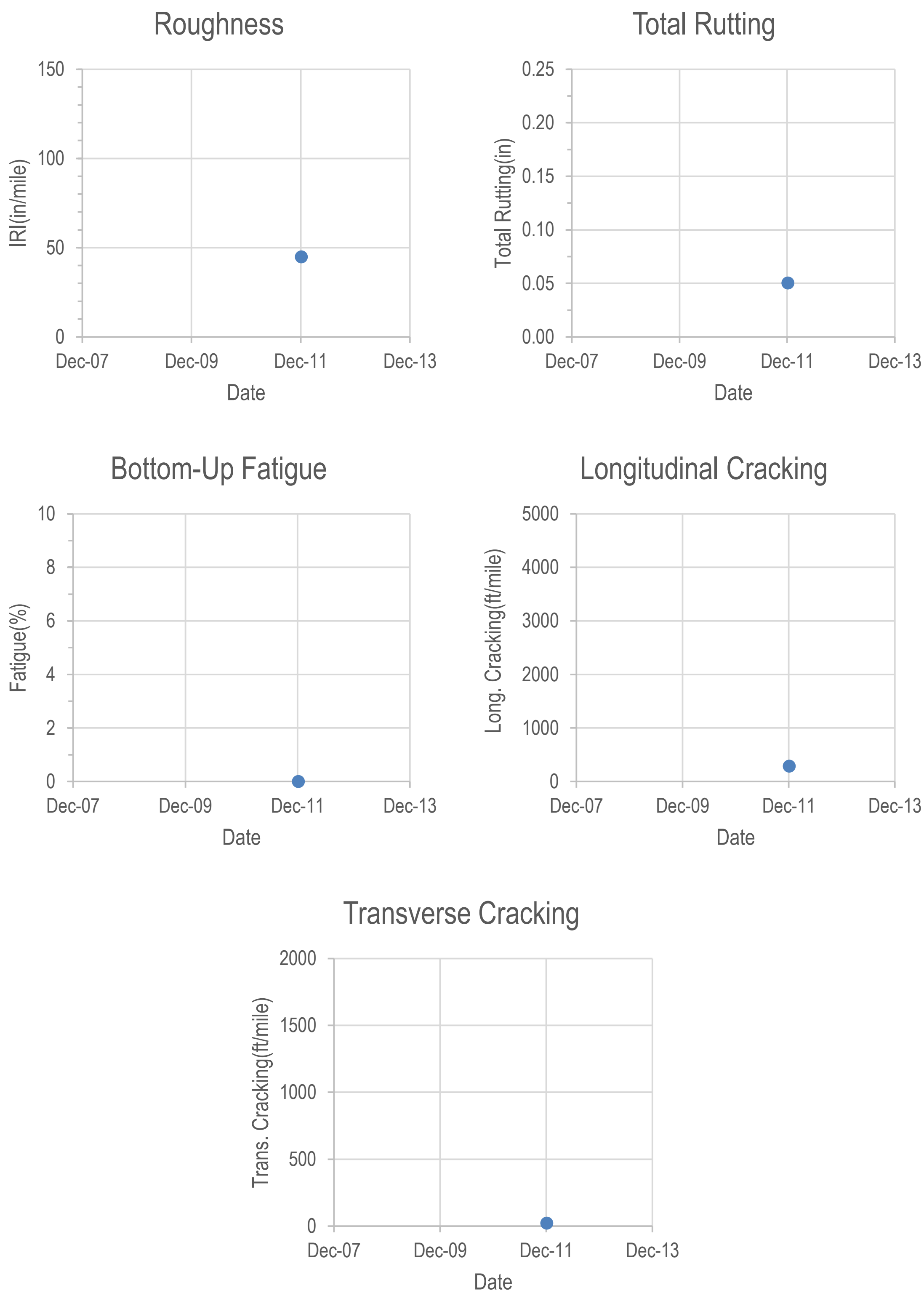

Figure 10.34-Distresses Plots for SR 208-22.

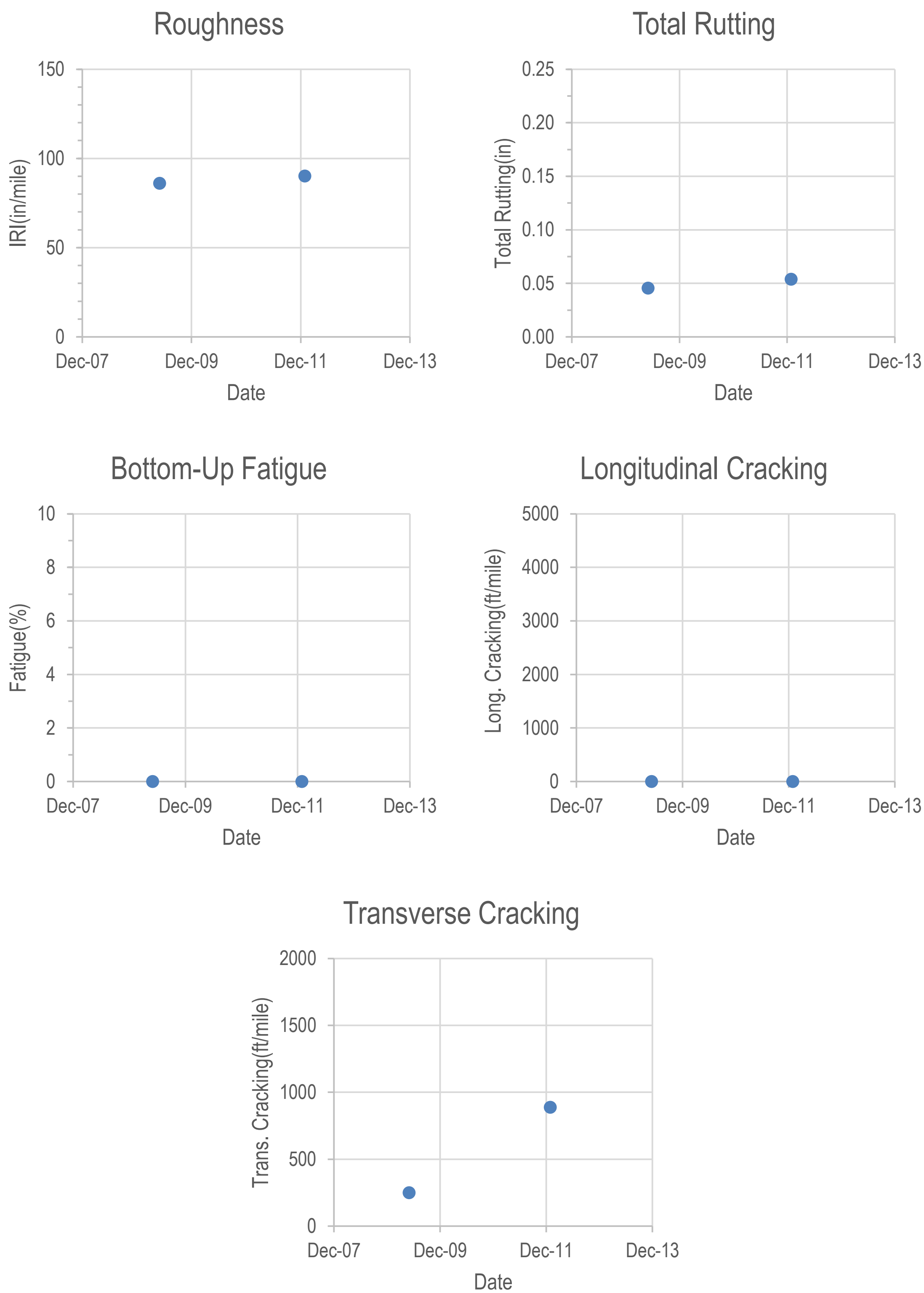

Figure 10.35-Distresses Plots for SR 208-23.

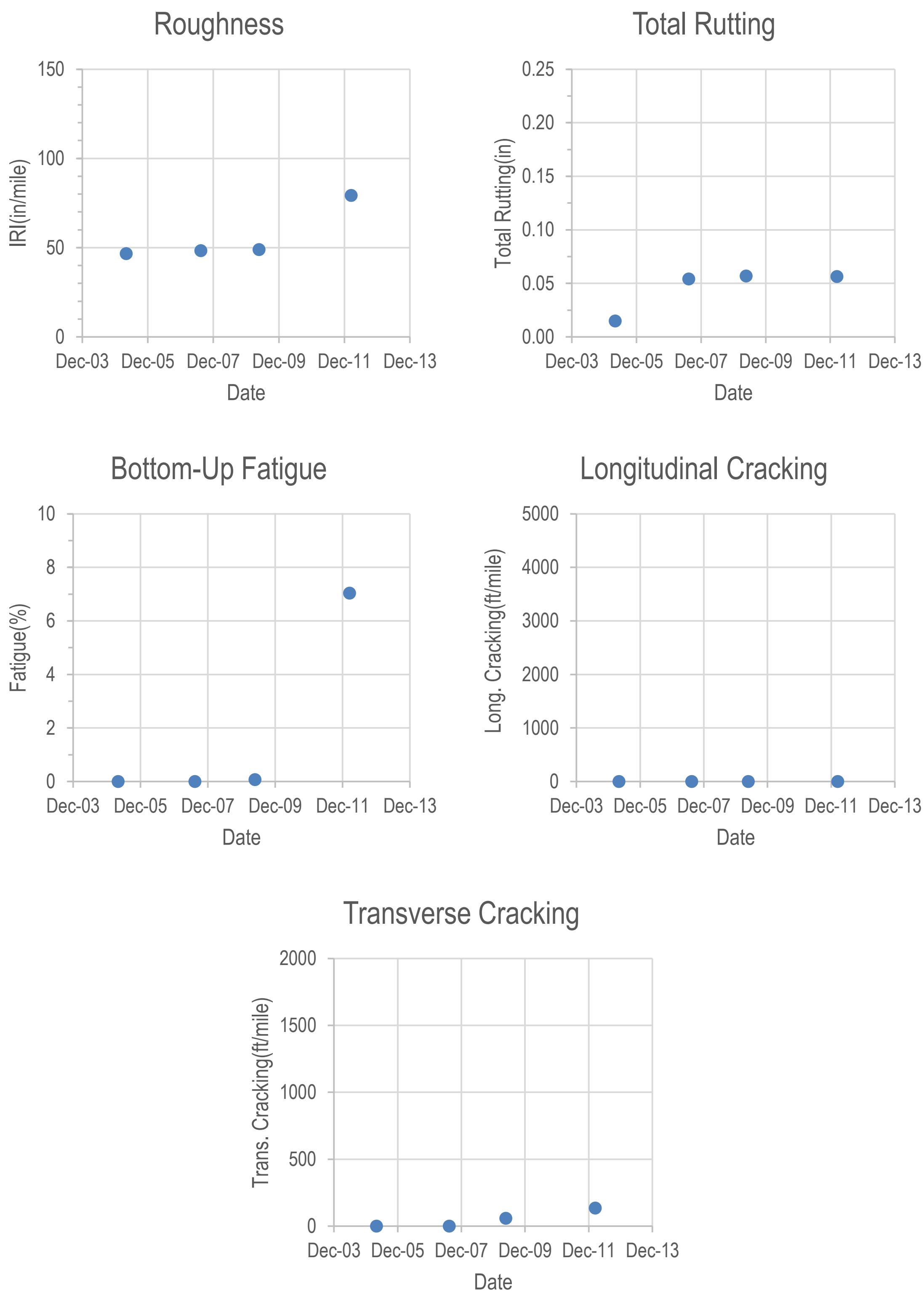

Figure 10.36-Distresses Plots for SR 225-26.

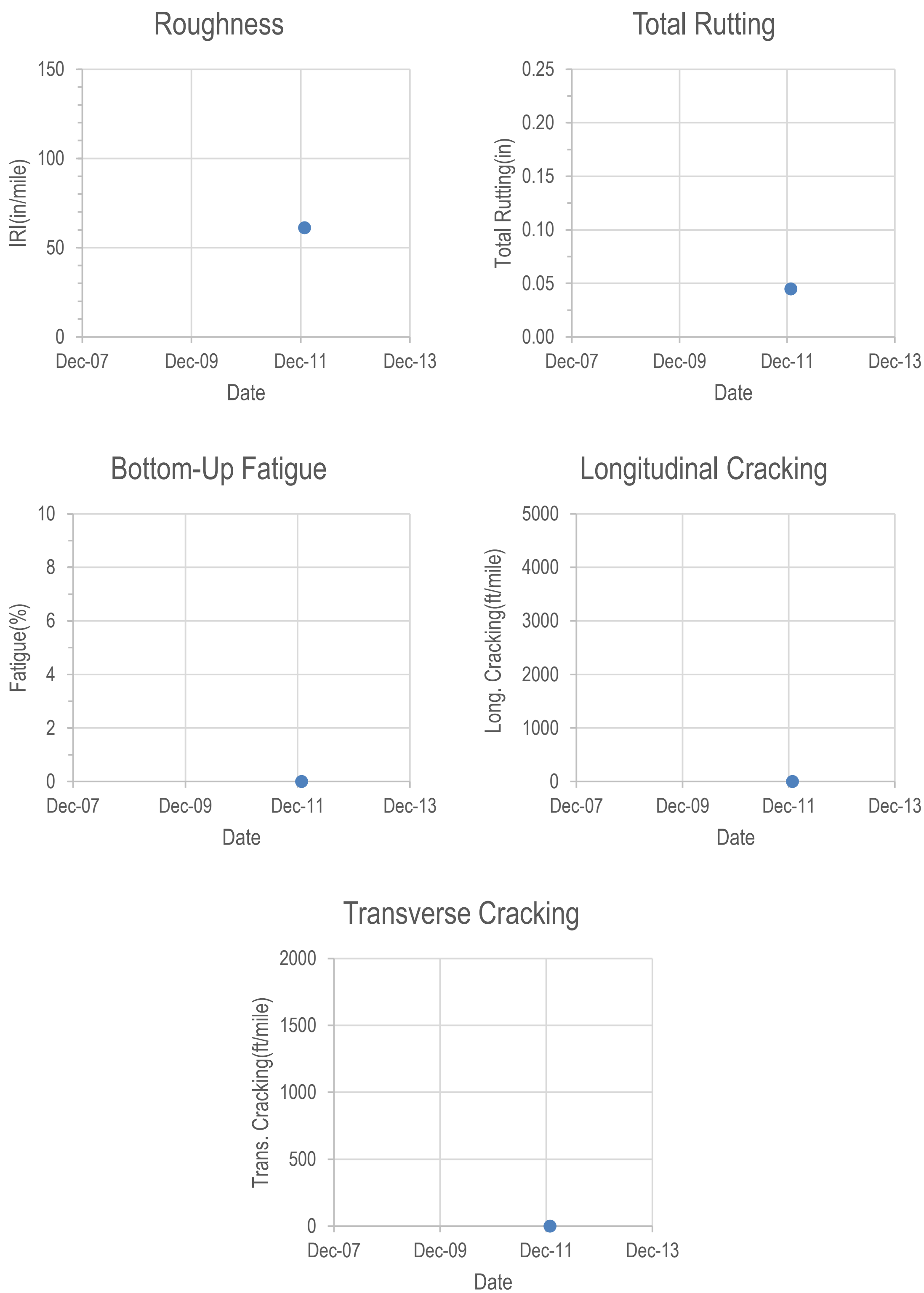

Figure 10.37-Distresses Plots for SR 318-143.

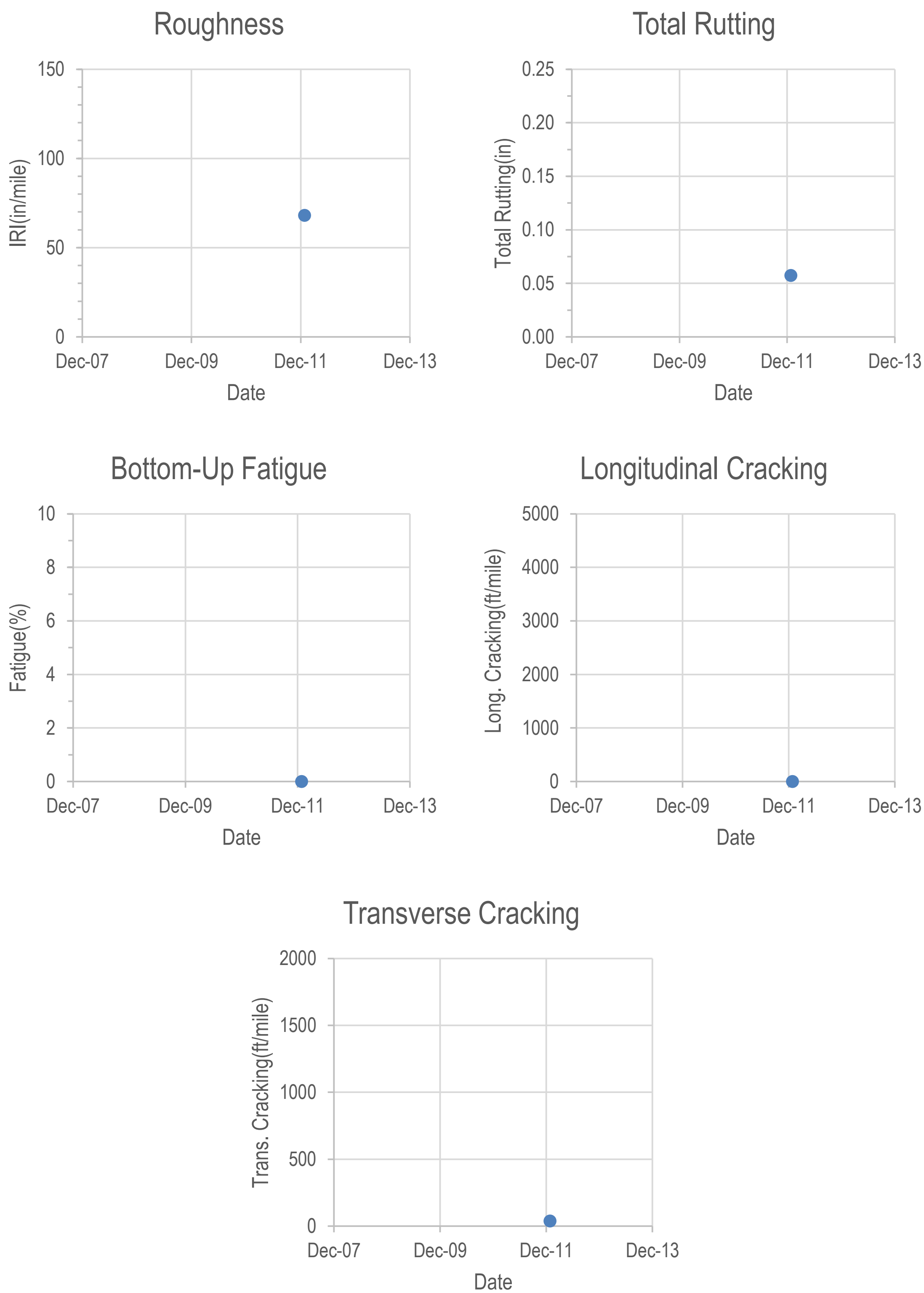

Figure 10.38-Distresses Plots for SR 318-145.

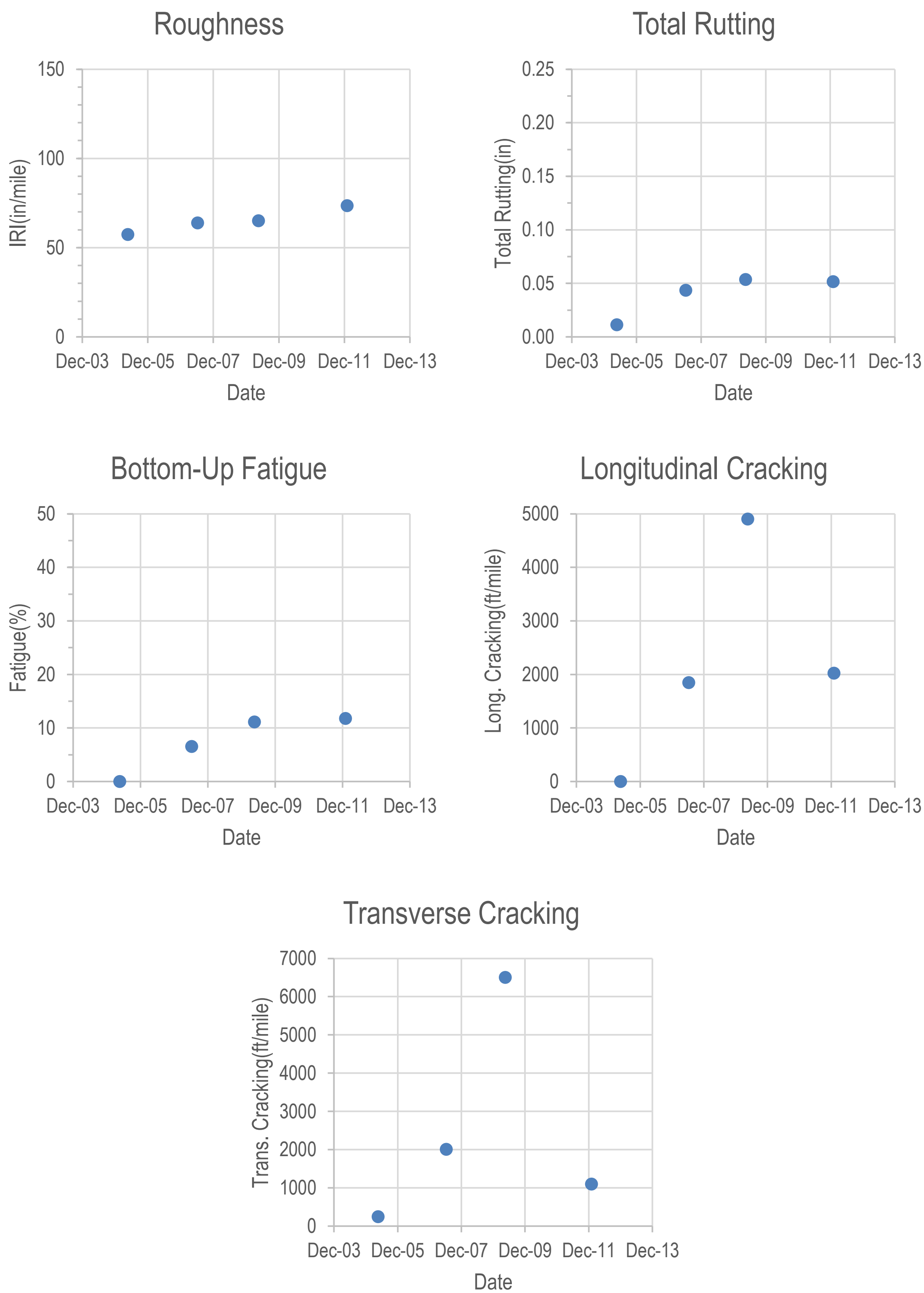

Figure 10.39-Distresses Plots for SR 582-35.

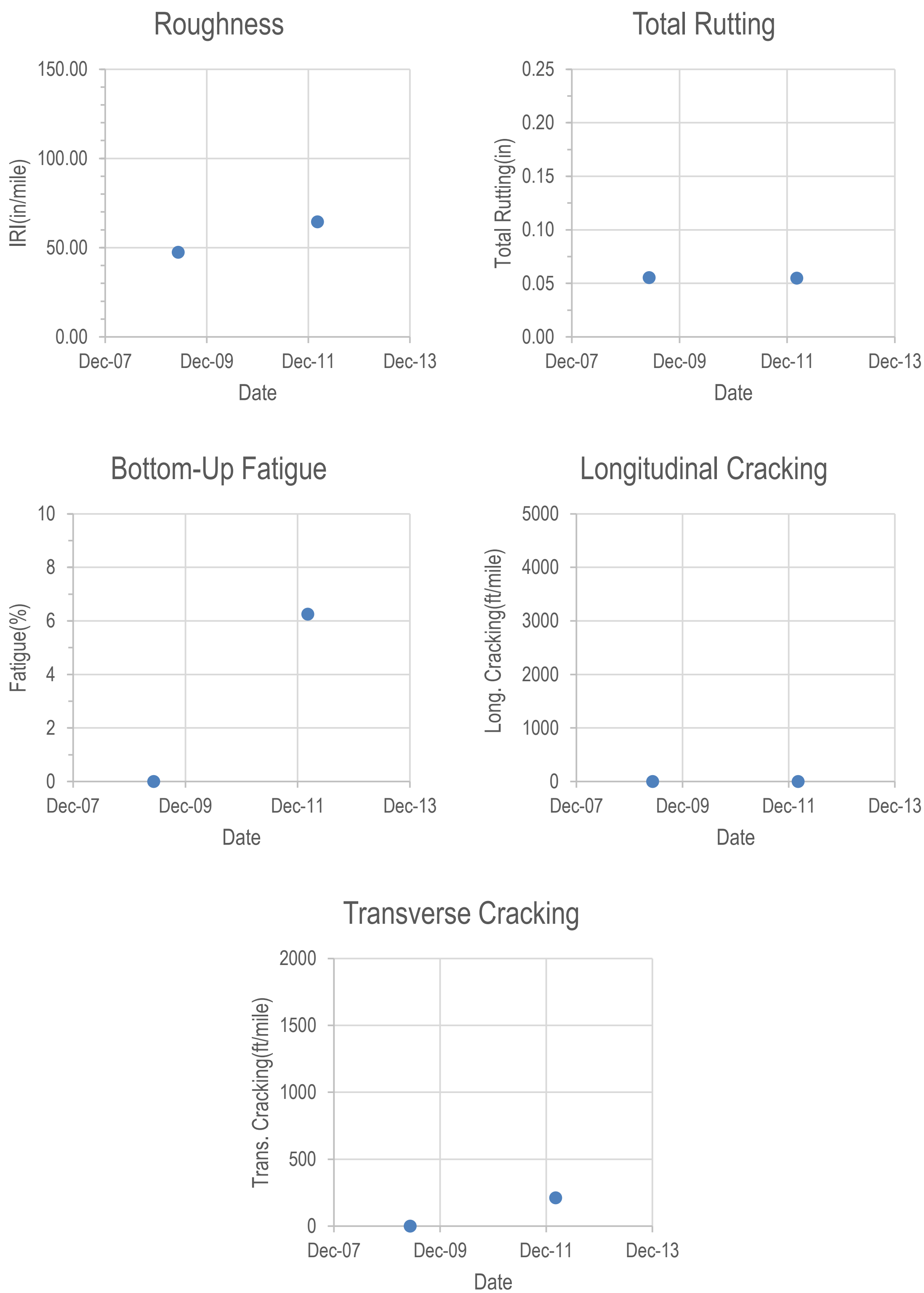

Figure 10.40-Distresses Plots for US 050A-72.

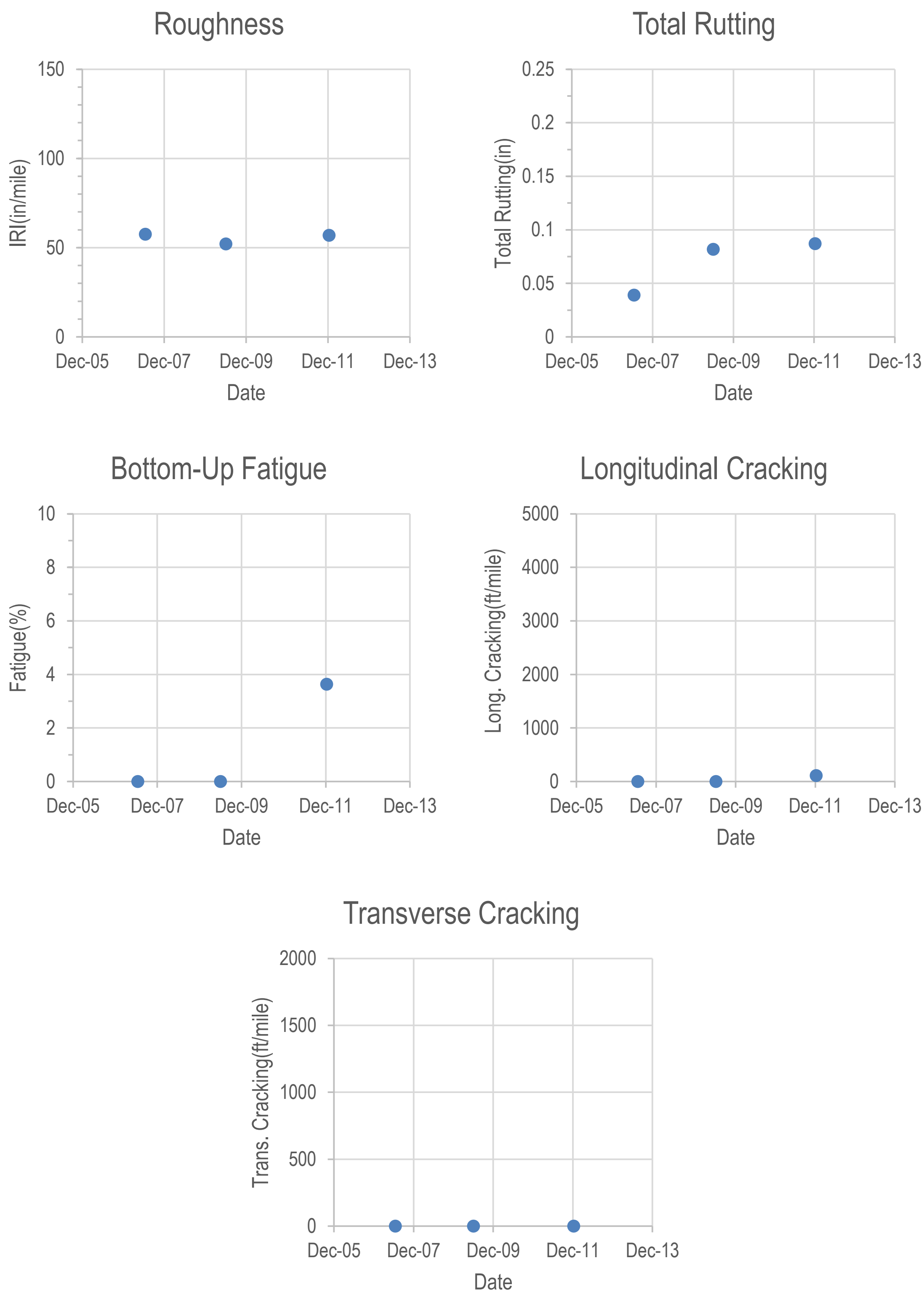

Figure 10.41-Distresses Plots for US 395-74A.

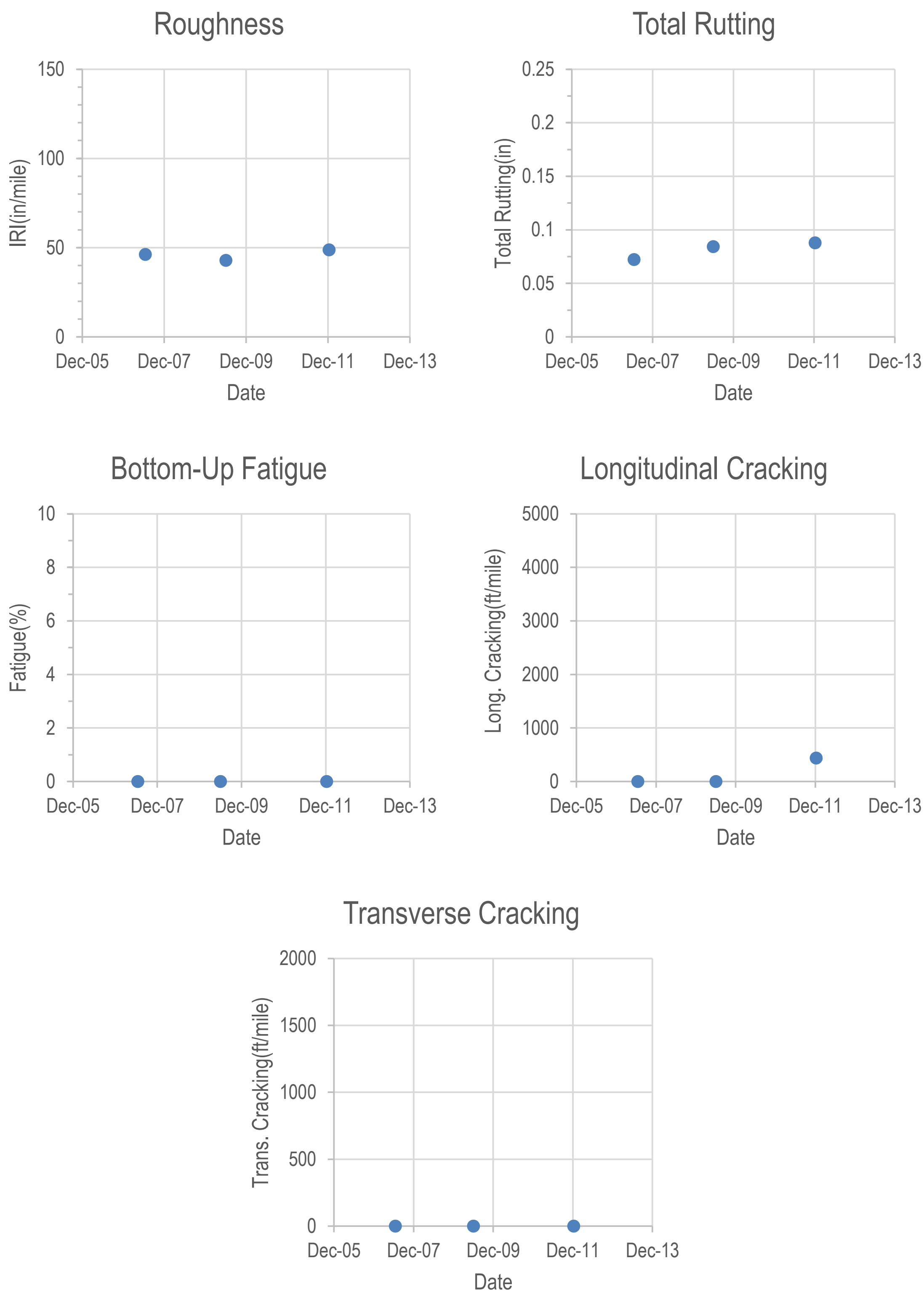

Figure 10.42-Distresses Plots for US 395-74B.

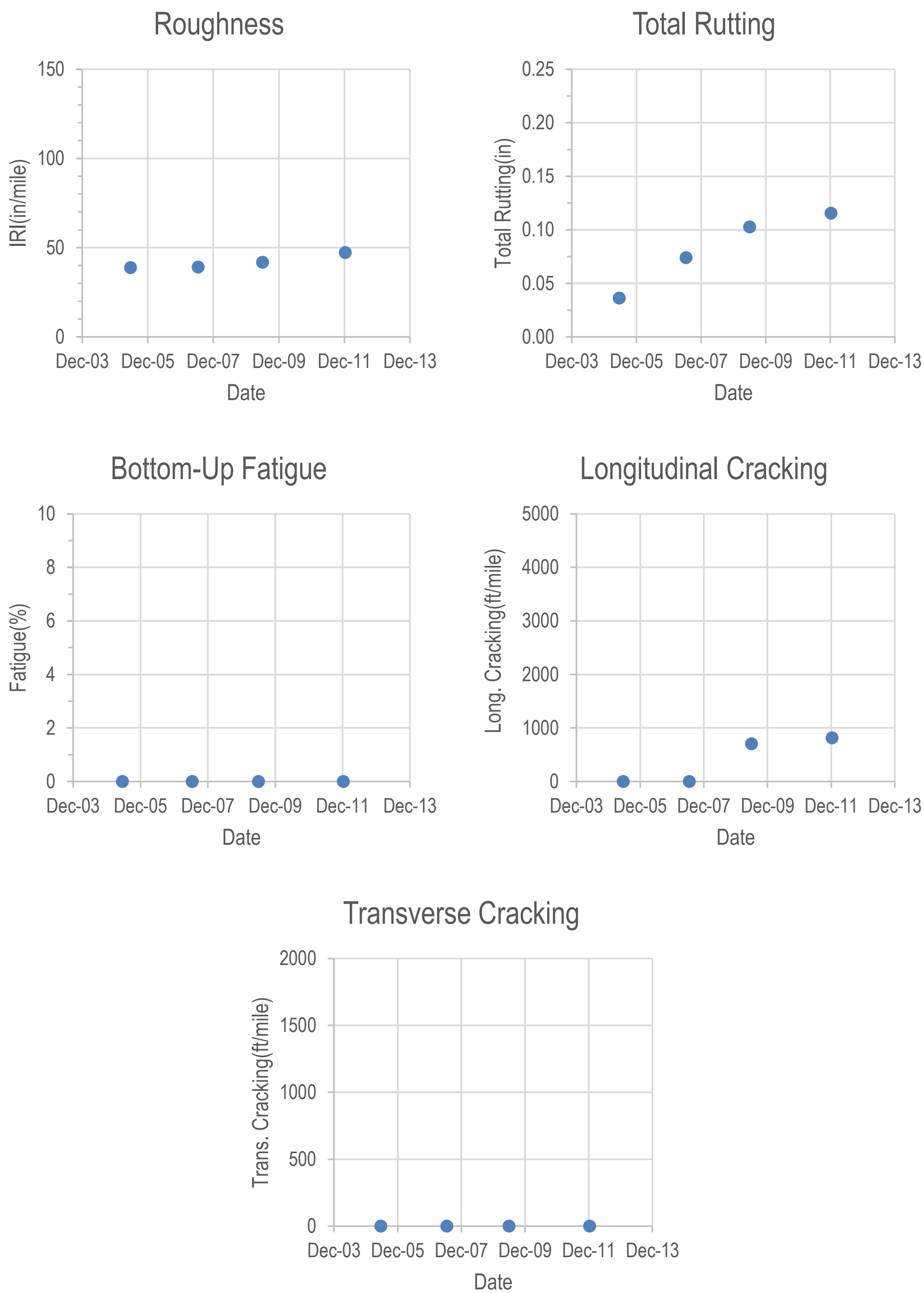

Figure 10.43-Distresses Plots for US 395-76.

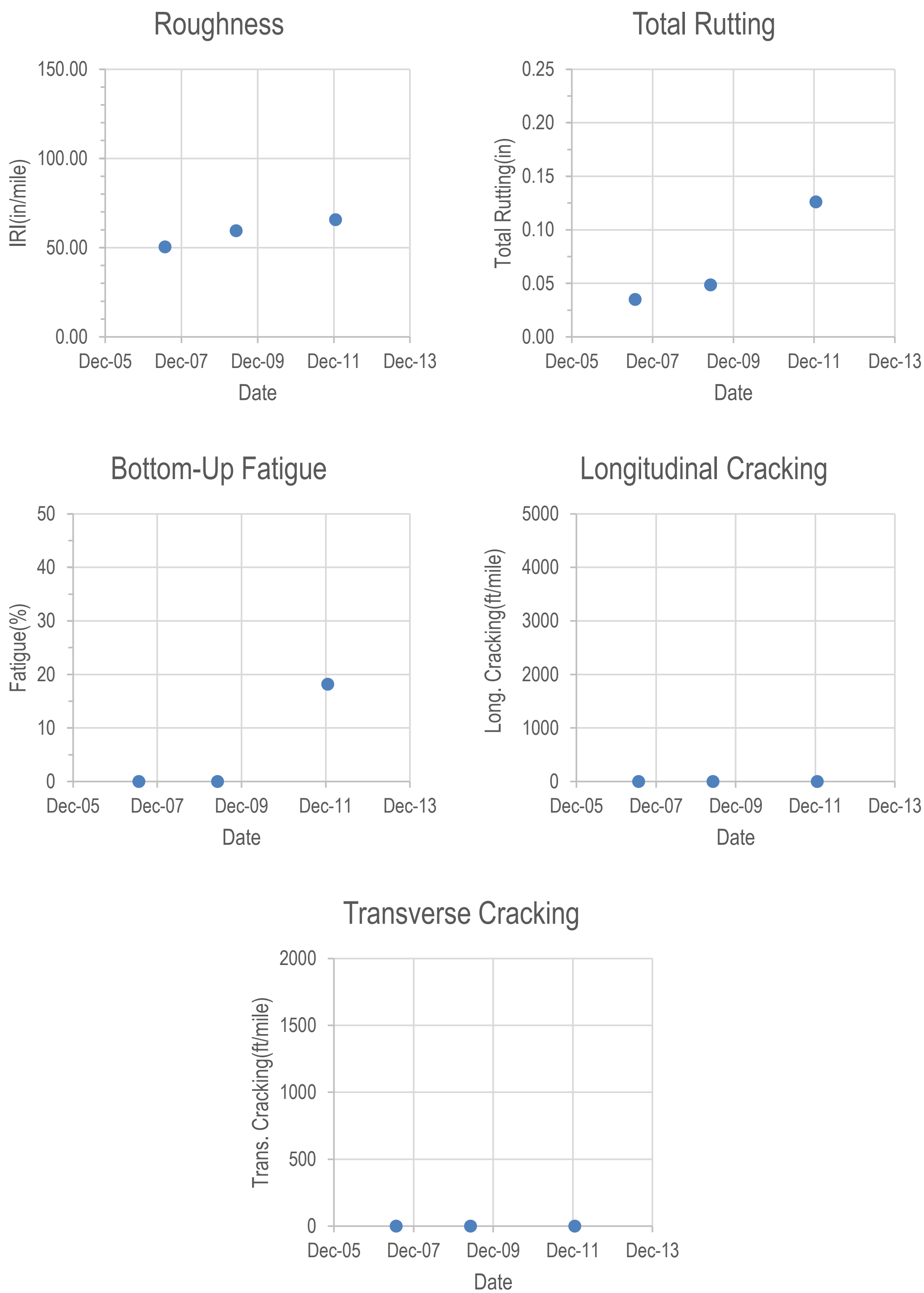

Figure 10.44-Distresses Plots for US 395-80.

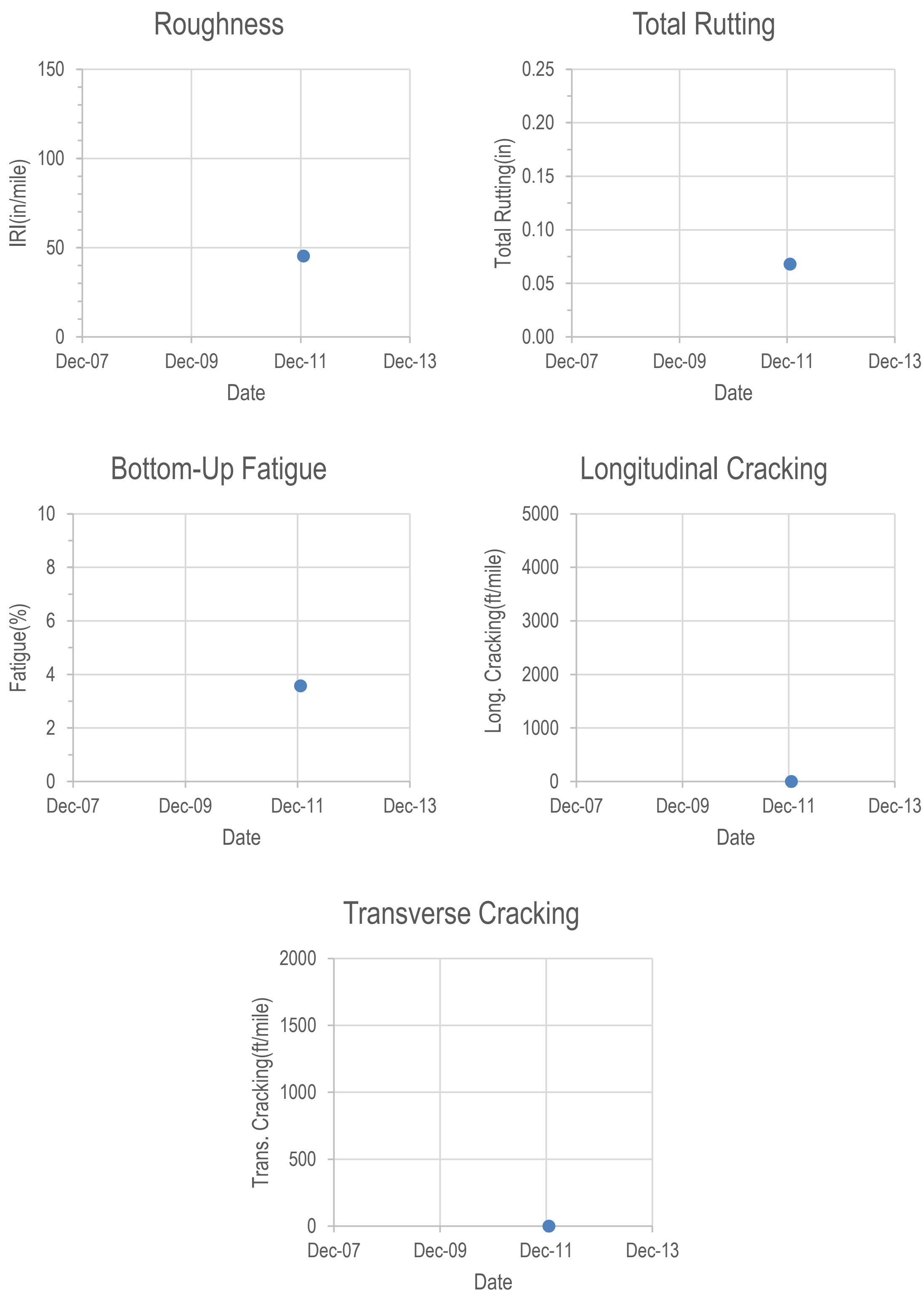

Figure 10.45-Distresses Plots for US 395-83.

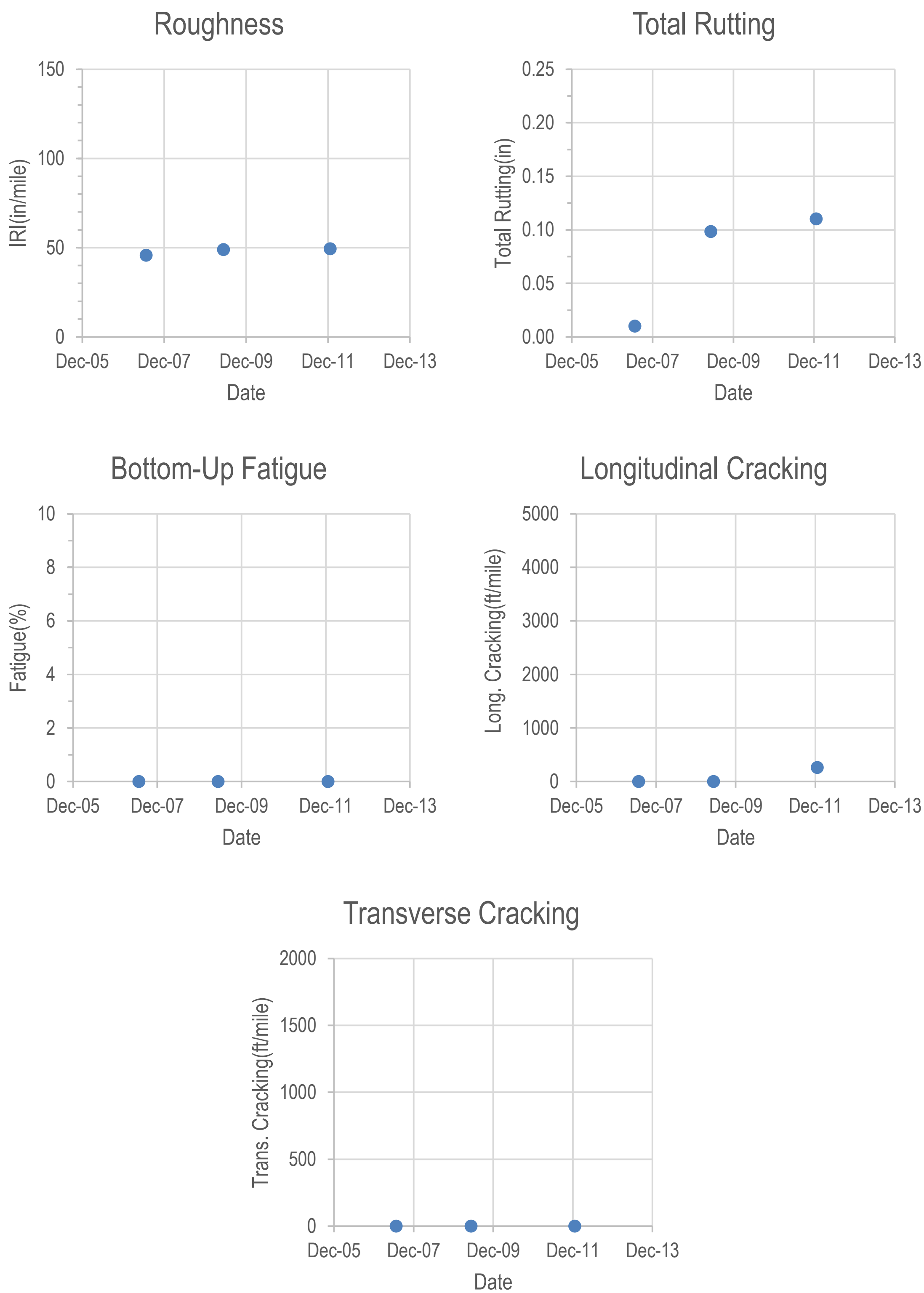

Figure 10.46-Distresses Plots for US 395-86.

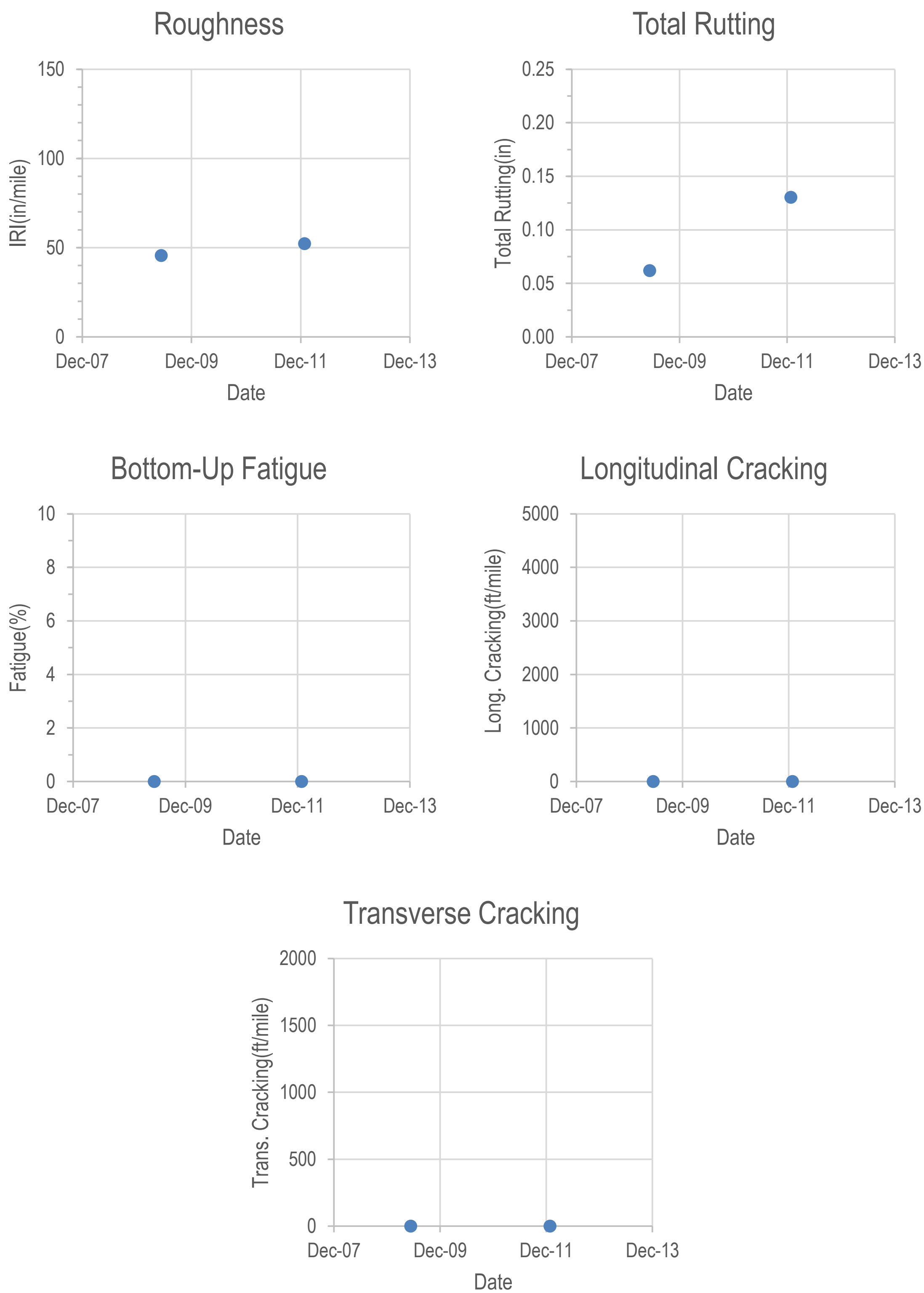

Figure 10.47-Distresses Plots for US 395-89.

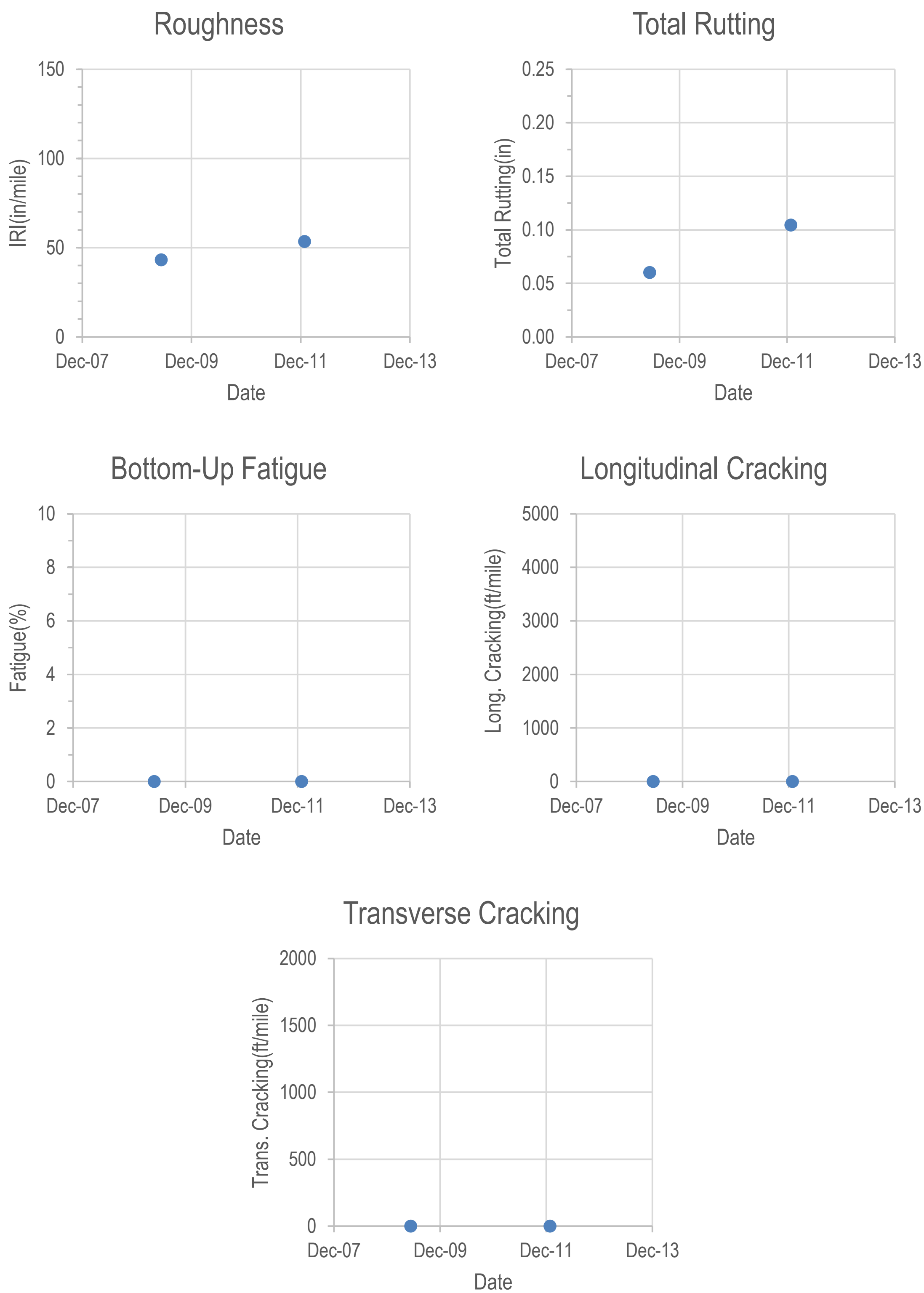

Figure 10.48-Distresses Plots for US 395-90.

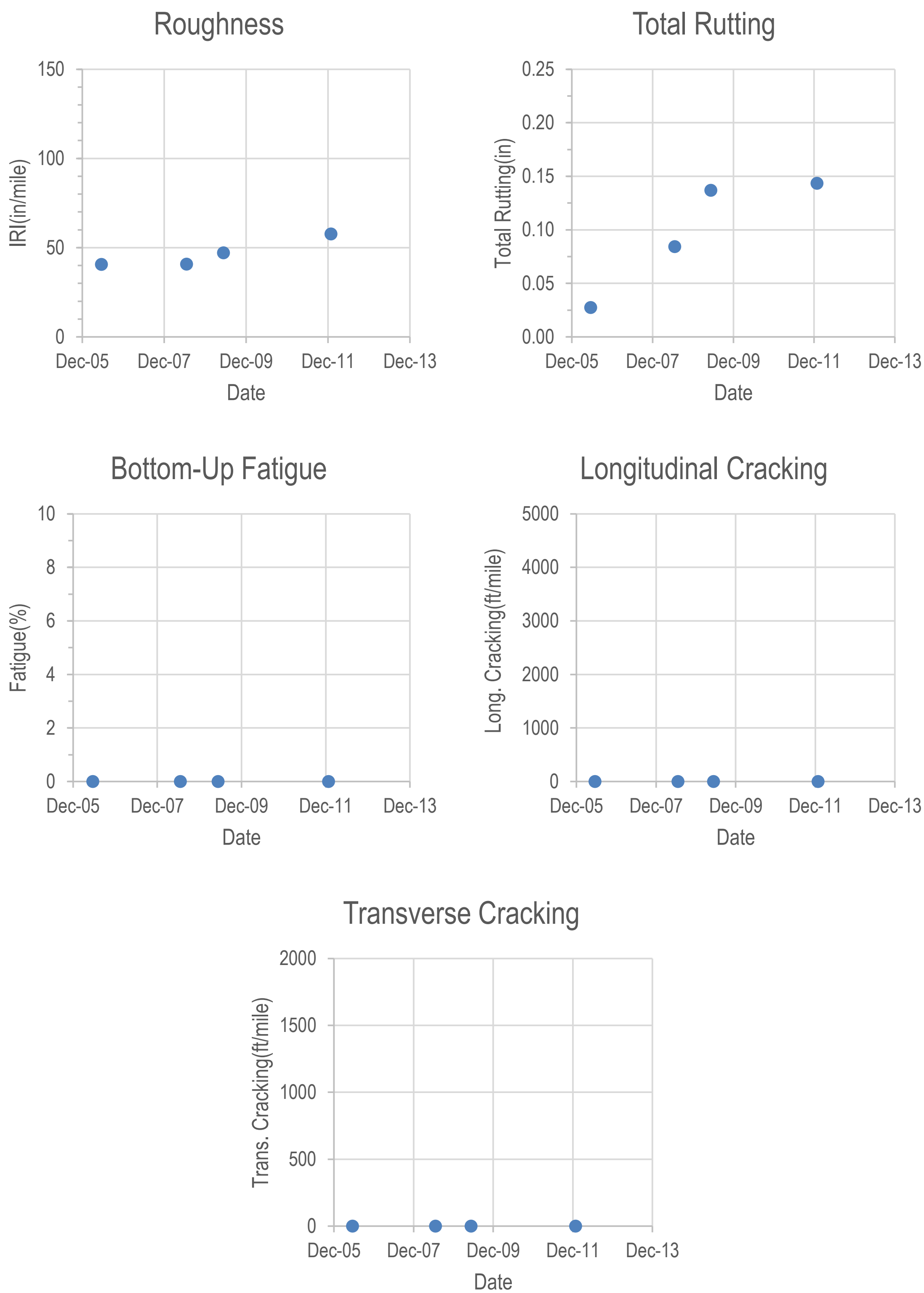

Figure 10.49-Distresses Plots for US 395-91.

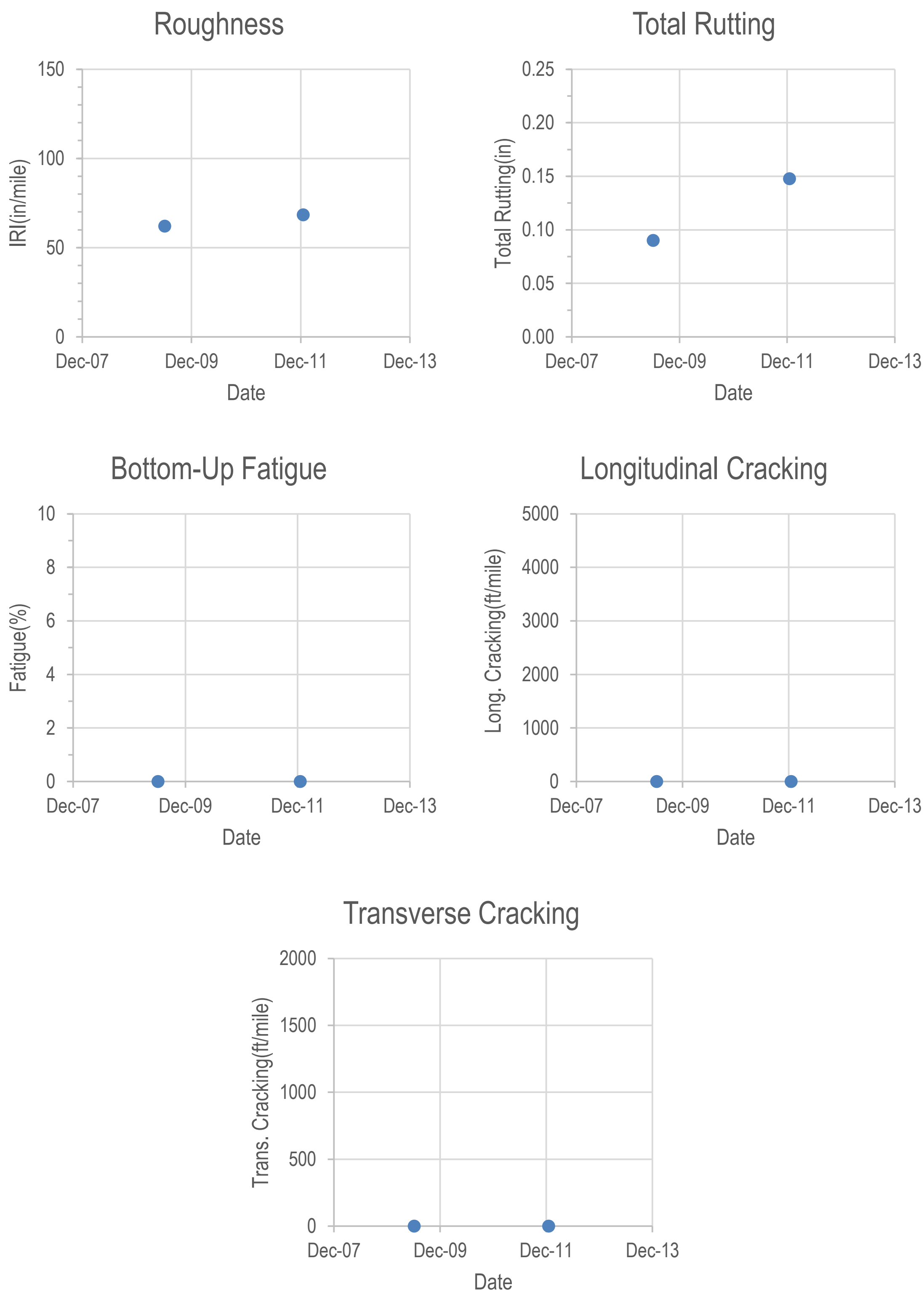

Figure 10.50-Distresses Plots for US 050-56.

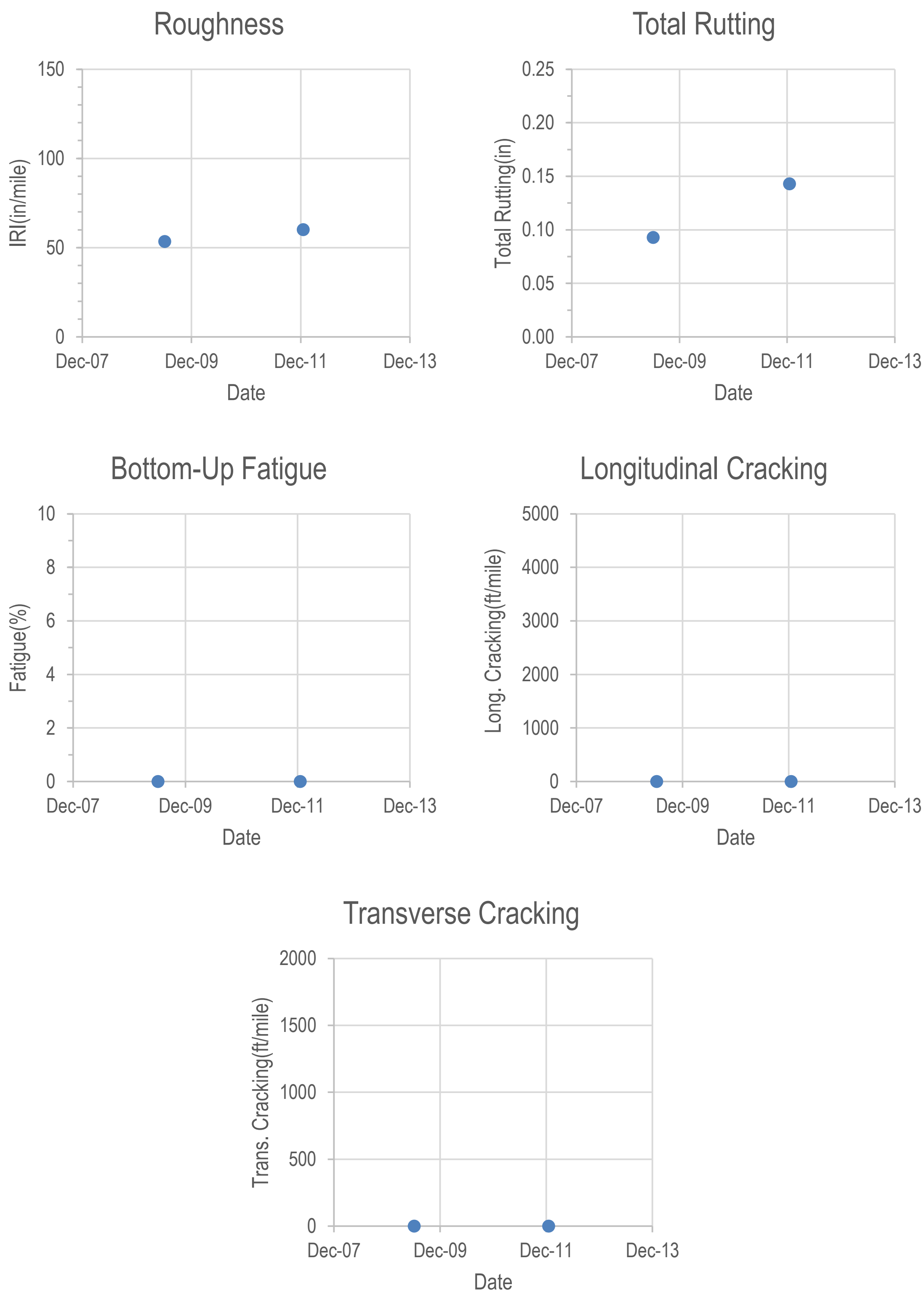

Figure 10.51-Distresses Plots for US 050-58.

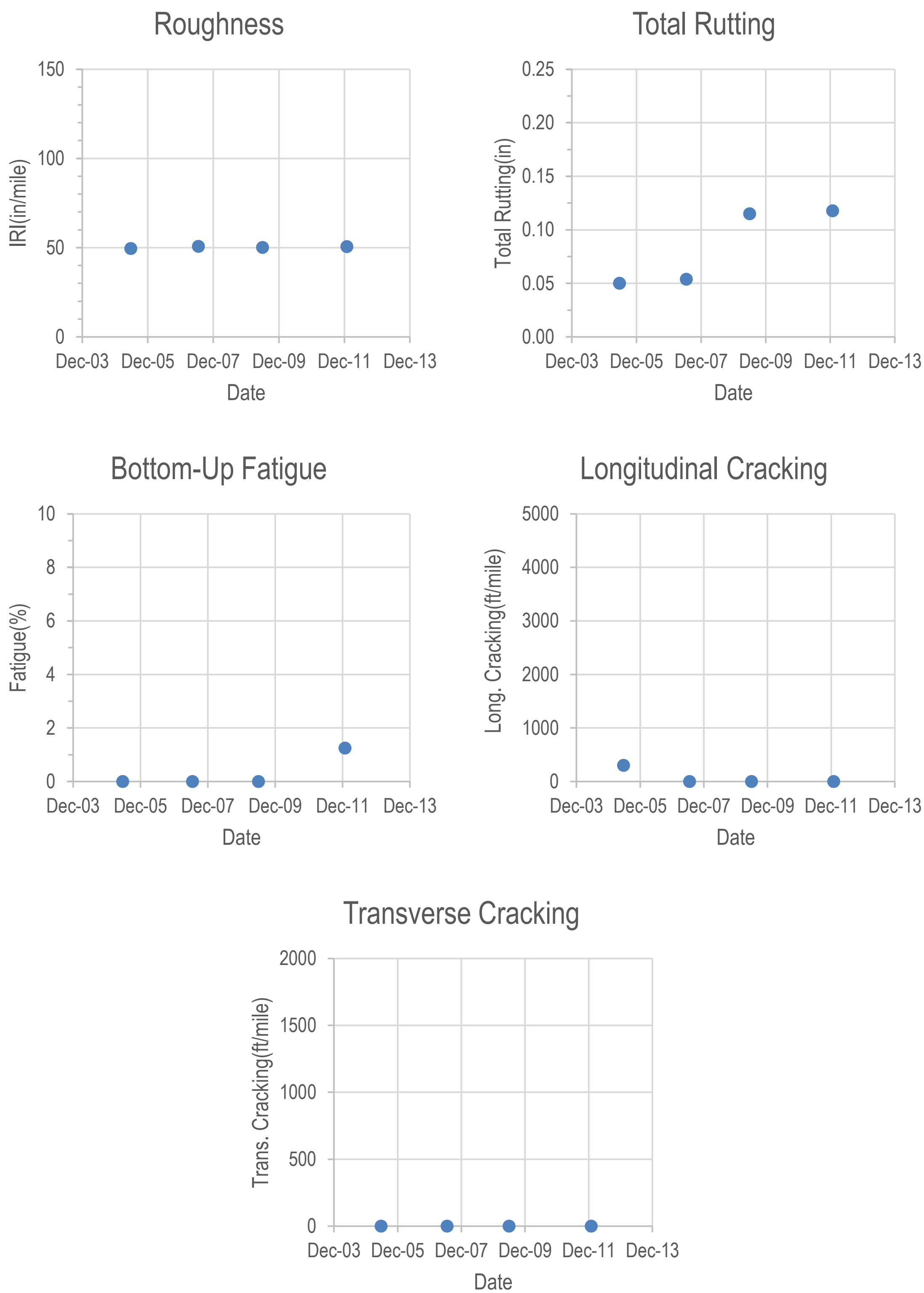

Figure 10.52-Distresses Plots for US 050-59.

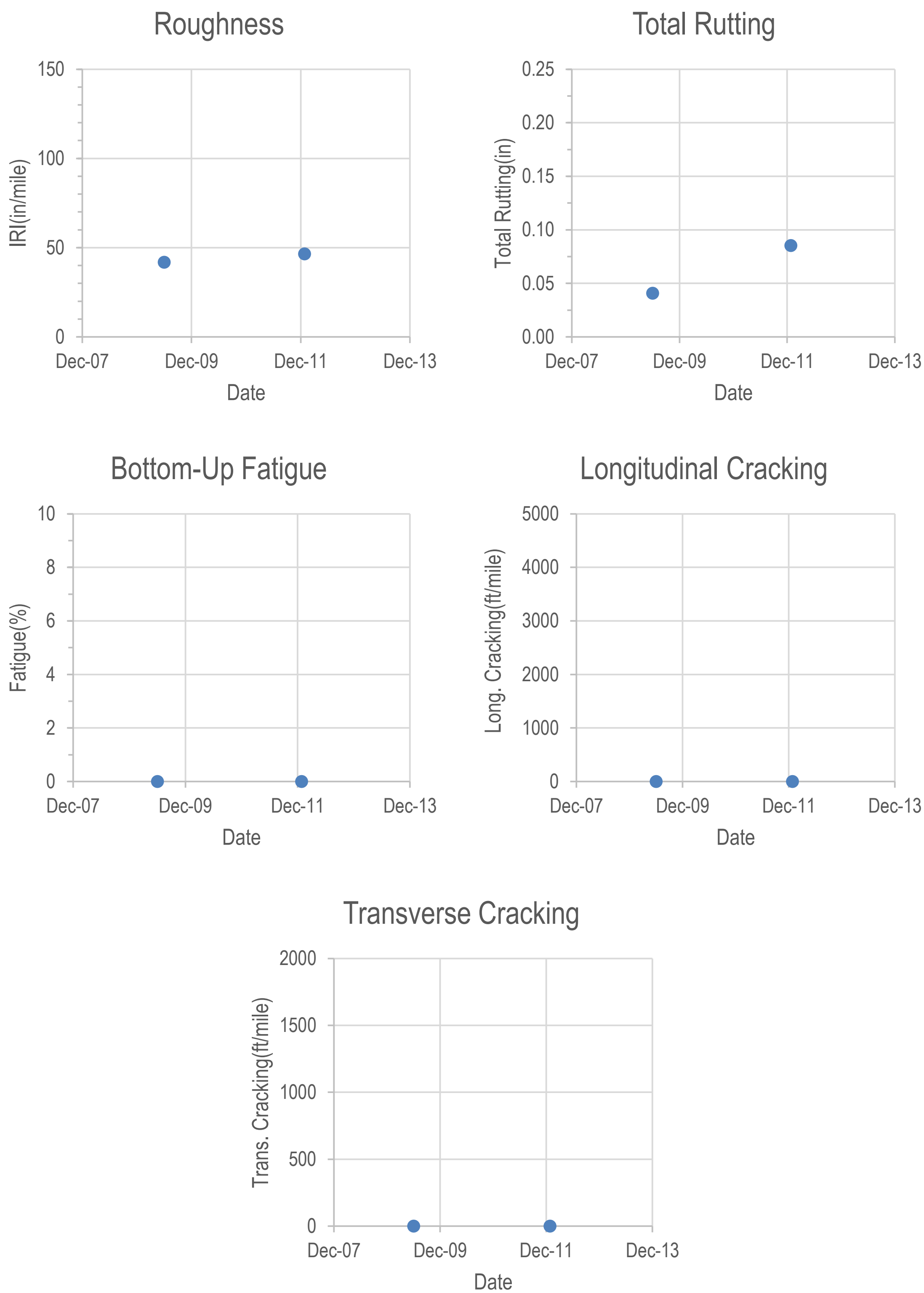

Figure 10.53-Distresses Plots for US 050-66.

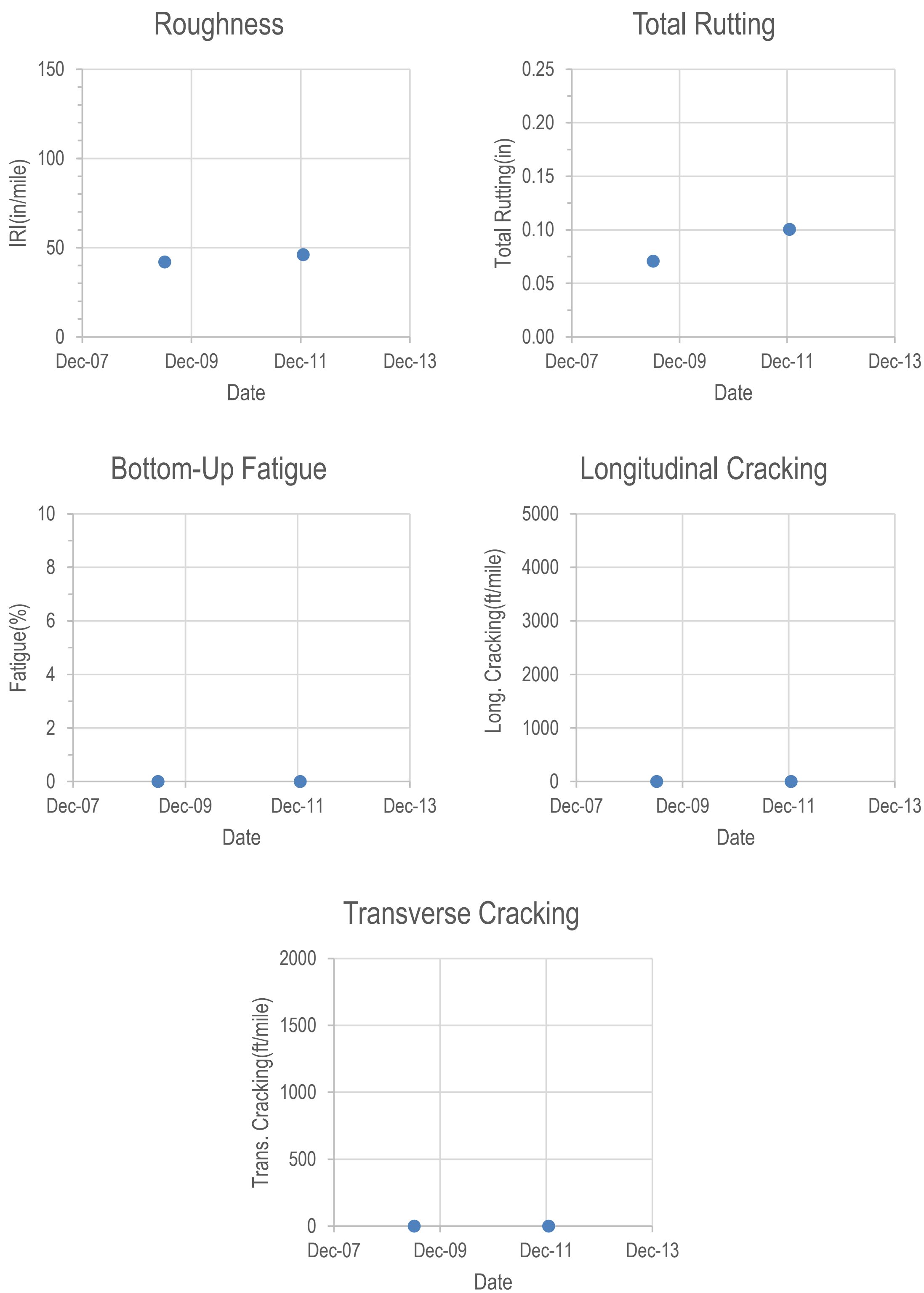

Figure 10.54-Distresses Plots for US 050-136.

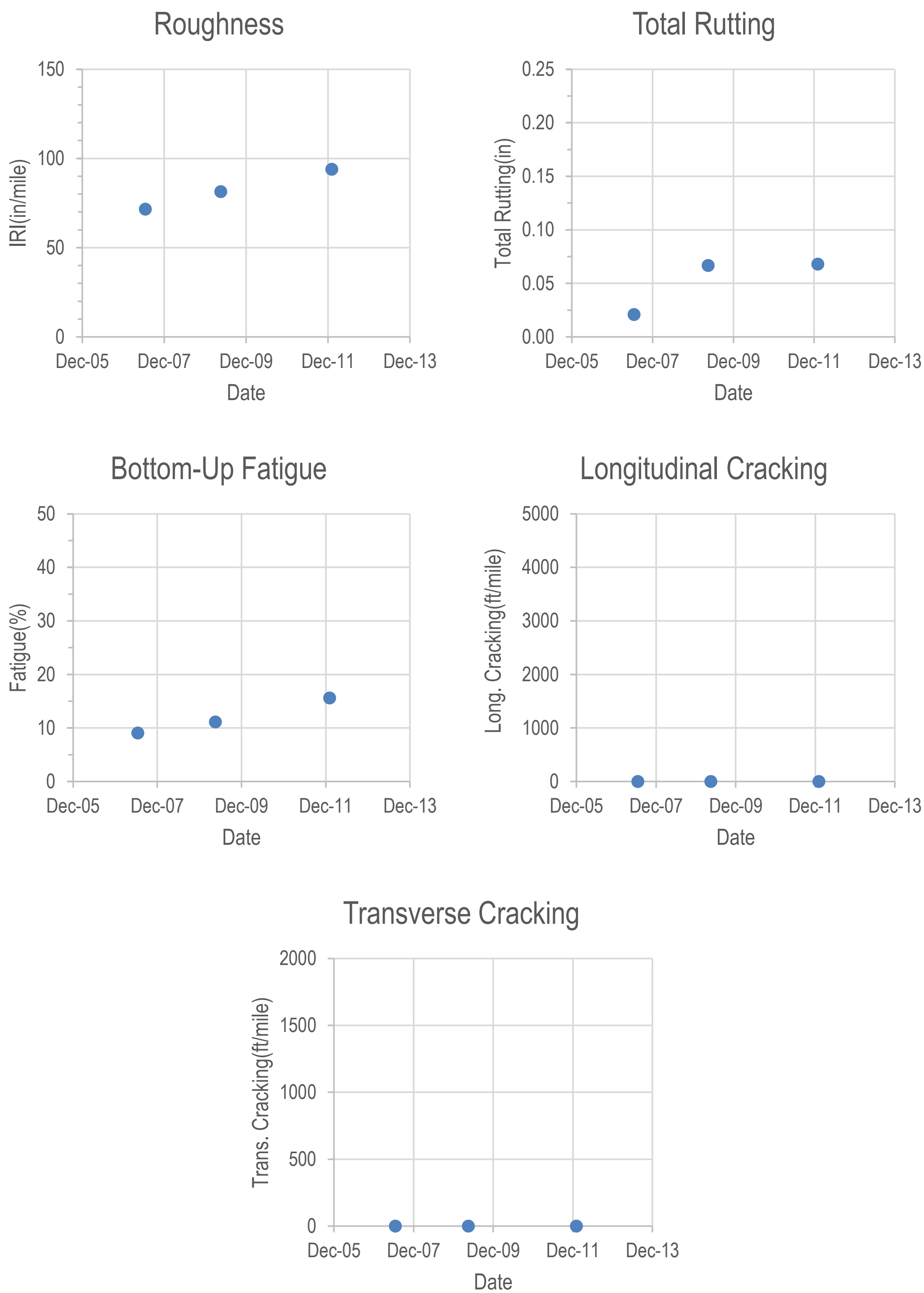

Figure 10.55-Distresses Plots for US 093-40.

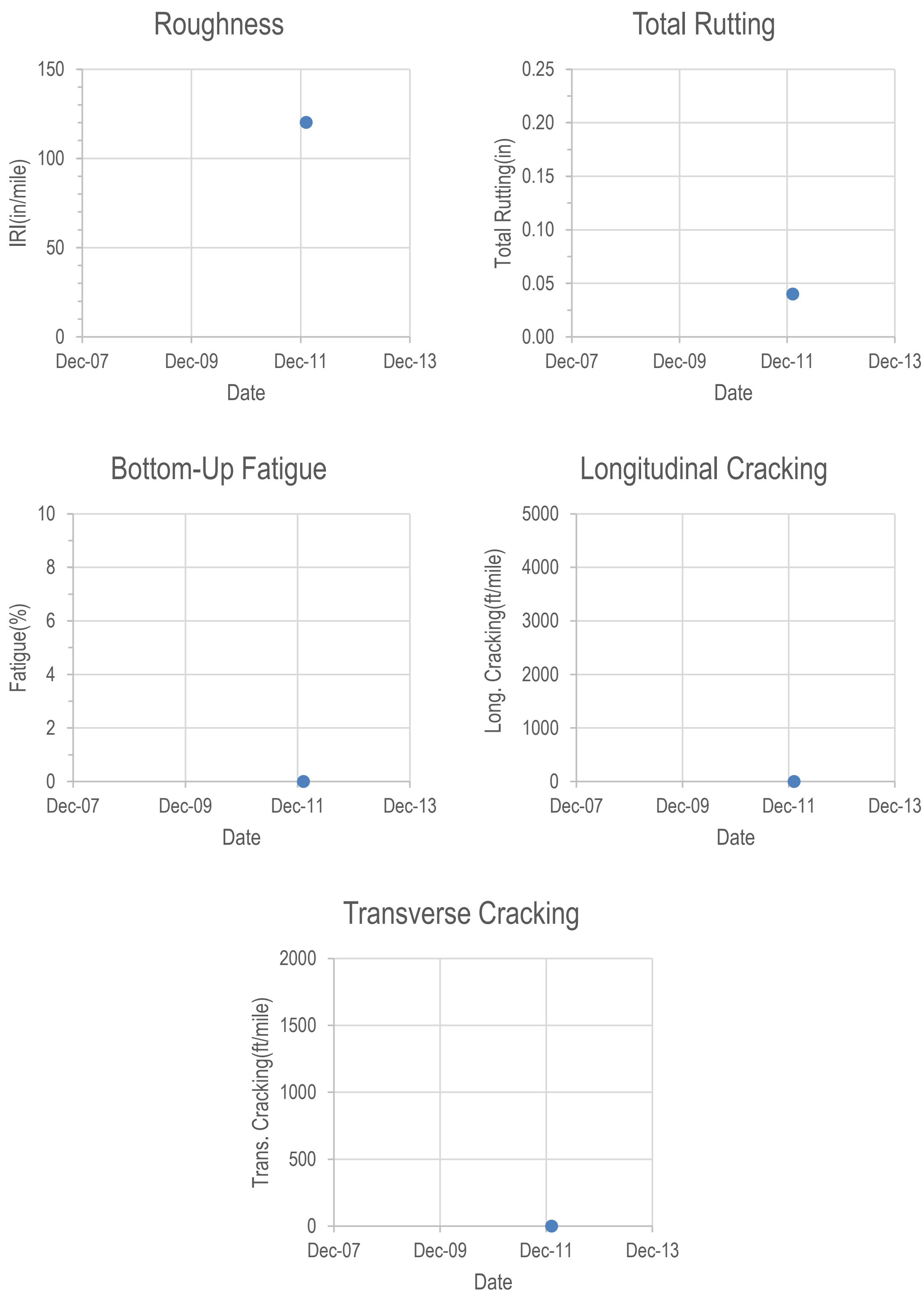

Figure 10.56-Distresses Plots for US 095-39.

CHAPTER 11 APPENDIX B: SECTION THICKNESSES

Table 11.1-Pavement Structure and Resilient Modulus Calculations for IR 080-107.

	Year	1927	1941	1991	1999	2006
IR 080-107	Structure					
					4" AC-20P	
			2.5" Plantmix Surface	2" AC-20P	2" AC-20P	6" PG64-28NV
			9" Aggregate Base	9" Aggregate Base	9" Aggregate Base	8" RBM
		5" Aggregate Base	5" Aggregate Base	5" Aggregate Base	5" Aggregate Base	8" Aggregate Base

	Final Structure	Layer Behavior	Thickness(in)	Layer Coefficient	h*ai	Section Modeled	Modulus E (psi)
IR 080-107						6"PG 76-22NV	Database
						16"Aggregate Base Linear Elastic	26650
	6" PG64-28NV	Visco-Elastic	6	Database	Database		
	8" RBM	Elastic	8	0.15	1.2	0.125	
	8" Aggregate Base	Elastic	8	0.1	0.8	Subgrade	Database NCHRP

Table 11.2-Pavement Structure and Resilient Modulus Calculations for IR 080-109.

	Year	1938	1967	1991	1999	2006
IR 80-109	Structure			2" AC-20P	2" AC-20P	
			4" 120-150 PEN	2" 120-150 PEN	2" 120-150 PEN	
			6" Aggregate Base	6" Aggregate Base	6" Aggregate Base	6" PG64-28NV
		1.5" Plantmix Surface	1.5" Plantmix Surface	1.5" Plantmix Surface	1.5" Plantmix Surface	8" RBM
		10" Aggregate Base	10" Aggregate Base	10" Aggregate Base	10" Aggregate Base	10" Aggregate Base

	Final Structure	Layer Behavior	Thickness(in)	Layer Coefficient	h*ai	Section Modeled	Modulus E (psi)
IR 80-109						6"PG 76-22NV	Database
						18"Aggregate Base Linear Elastic	25974
	6" PG64-28NV	Visco-Elastic	6	Database	Database		
	8" RBM	Elastic	8	0.15	1.2	0.122	
	10" Aggregate Base	Elastic	10	0.1	1	Subgrade	Database NCHRP

Table 11.3-Pavement Structure and Resilient Modulus Calculations for IR 080-111.

	Year	1938	1963	1975	1990	2001	2009
IR 80-111	Structure						
							3"PG64-28NV
				2" AR-2000	2" AC-20P	3.5" AC-20P	2" AC-20P
			3.5" Plantmix Surface	3.5" Plantmix Surface	3.5" Plantmix Surface	3.5" Plantmix Surface	3.5" Plantmix Surface
			8" Aggregate Base	8" Aggregate Base	8" Aggregate Base	8" Aggregate Base	8" Aggregate Base
		1.5" Plantmix Surface	1.5" Plantmix Surface	1.5" Plantmix Surface	1.5" Plantmix Surface	1.5" Plantmix Surface	1.5" Plantmix Surface
		10" Aggregate Base	10" Aggregate Base	10" Aggregate Base	10" Aggregate Base	10" Aggregate Base	10" Aggregate Base

	Final Structure	Layer Behavior	Thickness(in)	Layer Coefficient	h*ai	Section Modeled	Modulus E (psi)
IR 80-111						3"PG 64-28NV	Database
	3"PG64-28NV	Visco-Elastic	3	Database	Database	2" AC-20P	Database
	2" AC-20P	Visco-Elastic	2	Database	Database	23" Aggregate Base Linear Elastic	28593
	3.5" Plantmix Surface	Elastic	3.5	0.25	0.875		
	8" Aggregate Base	Elastic	8	0.1	0.8	0.133	
	1.5" Plantmix Surface	Elastic	1.5	0.25	0.375	Subgrade	Database NCHRP
	10" Aggregate Base	Elastic	10	0.1	1		

Table 11.4-Pavement Structure and Resilient Modulus Calculations for IR 080-116.

	Year	1962	1975	1982	1990	2001	2008
IR 80-116	**Structure**						2.5" PG64-28NV
					3.5" AC-20P	5.5" AC-20P	4" AC-20P
				8" PCC	6" PCC	RBM 8"	RBM 8"
				6" Cement Treated Base	6" Cement Treated Base	6" Cement Treated Base	6" Cement Treated Base
			1.5" Plantmix Surface	1.5" Plantmix Surface	1.5" Plantmix Surface	1.5" Plantmix Surface	1.5" Plantmix Surface
		4" Plantmix Surface	4" Plantmix Surface	4" Plantmix Surface	4" Plantmix Surface	4" Plantmix Surface	4" Plantmix Surface
		10" Aggregate Base	10" Aggregate Base	10" Aggregate Base	10" Aggregate Base	10" Aggregate Base	10" Aggregate Base

	Final Structure	Layer Behavior	Thickness(in)	Layer Coefficient	h*ai	Section Modeled	Modulus E (psi)
IR 80-116	2.5" PG64-28NV	Visco-Elastic	2.5	Database	Database	2.5" PG64-28NV	Database
	4" AC-20P	Visco-Elastic	4	Database	Database	4" AC-20P	Database
	RBM 8"	Elastic	8	0.15	1.2	29.5 "Aggregate Base Linear Elastic	34112
	6" Cement Treated Base	Elastic	6	0.15	0.9		
	1.5" Plantmix Surface	Elastic	1.5	0.25	0.375	0.152	
	4" Plantmix Surface	Elastic	4	0.25	1	Subgrade	Database NCHRP
	10" Aggregate Base	Elastic	10	0.1	1		

Table 11.5-Pavement Structure and Resilient Modulus Calculations for IR 080-118.

	Year	1925	1980	1991	2001	2009
IR 80-118	Structure					
						2.5" PG64-28NV
			2" AR-8000		2.5" AC-20P	1" AC-20P
		3" Plantmix Surface	3" Plantmix Surface	5" AC-20P	4" AC-20P	4" AC-20P
		5" Aggregate Base	5" Aggregate Base	5" Aggregate Base	5" Aggregate Base	5" Aggregate Base

	Final Structure	Layer Behavior	Thickness (in)	Layer Coefficient	h*ai	Section Modeled	Modulus E (psi)
IR 80-118						2.5" PG64-28NV	Database
	2.5" PG64-28NV	Visco-Elastic	2.5	Database	Database	1" AC-20P	39178
	1" AC-20P	Visco-Elastic	1	Database	Database	9"Aggregate Base Linear Elastic	
	4" AC-20P	Elastic	4	0.25	1	0.167	
	5" Aggregate Base	Elastic	5	0.1	0.5	Subgrade	Database NCHRP

Table 11.6-Pavement Structure and Resilient Modulus Calculations for IR 080-120.

	Year	1976	1981	1993	1999	2006
IR 80-120	Structure					2" PG64-28NV
					6.5" AC-20P	5" AC-20P
				9" PCC	9" PCC Rubblized	9" PCC Rubblized
			8" PCC	4" Cement Treated Base	4" Cement Treated Base	4" Cement Treated Base
			6" Cement Treated Base	6" Aggregate Base	6" Aggregate Base	6" Aggregate Base
		10" AR-2000	10" AR-2000	5" AR-2000	5" AR-2000	5" AR-2000
		5" Aggregate Base	5" Aggregate Base	5" Aggregate Base	5" Aggregate Base	5" Aggregate Base

	Final Structure	Layer Behavior	Thickness(in)	Layer Coefficient	h*ai	Section Modeled	Modulus E (psi)
IR 80-120	2" PG64-28NV	Visco-Elastic	2	Database	Database	2" PG64-28NV	Database
	5" AC-20P	Visco-Elastic	5	Database	Database	5" AC-20P	Database
	9" PCC Rubblized	Elastic	9	0.2	1.8	29"Aggregate Base Linear Elastic	35793
	4" Cement Treated Base	Elastic	4	0.1	0.4		
	6" Aggregate Base	Elastic	6	0.1	0.6	0.157	
	5" AR-2000	Elastic	5	0.25	1.25	Subgrade	Database NCHRP
	5" Aggregate Base	Elastic	5	0.1	0.5		

Table 11.7-Pavement Structure and Resilient Modulus Calculations for IR 080-121.

	Year	1925	1941	1967	1991	2001	2009
IR 80-121	Structure						2.5" PG 64-28NV
						2" AC-20P	.5" AC-20P
					5.5" AC-20P	4.5" AC-20P	4.5" AC-20P
					5.5" 60-70 PEN	5.5" 60-70 PEN	5.5" 60-70 PEN
				4" 120-150 PEN	2.5" 120-150 PEN	2.5" 120-150 PEN	2.5" 120-150 PEN
				6" Cement Treated Base	6" Cement Treated Base	6" Cement Treated Base	6" Cement Treated Base
				12" Aggregate Base	12" Aggregate Base	12" Aggregate Base	12" Aggregate Base
			2.5" Plantmix Surface	2.5" Plantmix Surface	2.5" Plantmix Surface	2.5" Plantmix Surface	2.5" Plantmix Surface
			7" Aggregate Base	7" Aggregate Base	7" Aggregate Base	7" Aggregate Base	7" Aggregate Base
		5" Aggregate Base	5" Aggregate Base	5" Aggregate Base	5" Aggregate Base	5" Aggregate Base	5" Aggregate Base

	Final Structure	Layer Behavior	Thickness(in)	Layer Coefficient	h*ai	Section Modeled	Modulus E (psi)
IR 80-121	2.5" PG 64-28NV	Visco-Elastic	**2.5**	Database	Database	2.5" PG 64-28NV	Database
	.5" AC-20P	Visco-Elastic	0.5	Database	Database	5" AC-20P	Database
	4.5" AC-20P	Elastic	4.5	0.25	1.125	40.5" Aggregate Base Linear Elastic	32451
	5.5" 60-70 PEN	Elastic	5.5	0.25	1.375		
	2.5" 120-150 PEN	Elastic	2.5	0.25	0.625		
	6" Cement Treated Base	Elastic	6	0.15	0.9		
	12" Aggregate Base	Elastic	12	0.1	1.2		
	2.5" Plantmix Surface	Elastic	2.5	0.25	0.625	0.146	
	7" Aggregate Base	Elastic	7	0.1	0.7	Subgrade	Database NCHRP
	5" Aggregate Base	Elastic	5	0.1	0.5		

Table 11.8-Pavement Structure and Resilient Modulus Calculations for IR 080-122.

	Year	1931	1947	1961	1974	1989	1997	2005
IR 80-122	Structure							4" PG64-28NV
					2.5" 120-150 PEN	2" AC-20P	3.5" AC-20P	3.5" CIR
				4" Plantmix Surface	4" Plantmix Surface	4" Plantmix Surface	4" Plantmix Surface	4" Plantmix Surface
				4" Aggregate Base	4" Aggregate Base	4" Aggregate Base	4" Aggregate Base	4" Aggregate Base
			2.5" 200-300 PEN	2.5" 200-300 PEN	2.5" 200-300 PEN	2.5" 200-300 PEN	2.5" 200-300 PEN	2.5" 200-300 PEN
			9.5" Aggregate Base	9.5" Aggregate Base	9.5" Aggregate Base	9.5" Aggregate Base	9.5" Aggregate Base	9.5" Aggregate Base
		3" Plantmix Surface	3" Plantmix Surface	3" Plantmix Surface	3" Plantmix Surface	3" Plantmix Surface	3" Plantmix Surface	3" Plantmix Surface
		6" Aggregate Base	6" Aggregate Base	6" Aggregate Base	6" Aggregate Base	6" Aggregate Base	6" Aggregate Base	6" Aggregate Base

	Final Structure	Layer Behavior	Thickness(in)	Layer Coefficient	h*ai	Section Modeled	Modulus E (psi)
IR 80-122	4" PG64-28NV	Visco-Elastic	**4**	Database	Database	4"PG 64-28NV	Database
	3.5" CIR	Elastic	3.5	0.3	1.05	32.5" Aggregate Base Linear Elastic	38716
	4" Plantmix Surface	Elastic	4	0.25	1		
	4" Aggregate Base	Elastic	4	0.1	0.4		
	2.5" 200-300 PEN	Elastic	2.5	0.25	0.625		
	9.5" Aggregate Base	Elastic	9.5	0.1	0.95	0.165	
	3" Plantmix Surface	Elastic	3	0.25	0.75	Subgrade	Database NCHRP
	6" Aggregate Base	Elastic	6	0.1	0.6		

Table 11.9-Pavement Structure and Resilient Modulus Calculations for IR 080-124.

	Year	1922	1929	1963	1992	2001	2009
IR 80-124	Structure						
					2" AC-20P		2.5"PG64-28NV
				3.5" Plantmix Surface	1.5" Plantmix Surface	5.5" AC-20P	4" AC-20P
				8" CTB	8" CTB	8" RBM	8" RBM
				4" Aggregate Base	4" Aggregate Base	4" Aggregate Base	4" Aggregate Base
			3" Aggregate Base	3" Aggregate Base	3" Aggregate Base	3" Aggregate Base	3" Aggregate Base
		5" Aggregate Base	5" Aggregate Base	5" Aggregate Base	5" Aggregate Base	5" Aggregate Base	5" Aggregate Base

<table>
<tr><th rowspan="8">IR 80-124</th><th>Final Structure</th><th>Layer Behavior</th><th>Thickness(in)</th><th>Layer Coefficient</th><th>h*ai</th><th>Section Modeled</th><th>Modulus E (psi)</th></tr>
<tr><td></td><td></td><td></td><td></td><td></td><td>2.5"PG 64-28NV</td><td>Database</td></tr>
<tr><td>2.5"PG64-28NV</td><td>Visco-Elastic</td><td>2.5</td><td>Database</td><td>Database</td><td>4" AC-20P</td><td>Database</td></tr>
<tr><td>4" AC-20P</td><td>Visco-Elastic</td><td>4</td><td>Database</td><td>Database</td><td rowspan="2">20" Aggregate Base Linear Elastic</td><td rowspan="3">25446</td></tr>
<tr><td>8" RBM</td><td>Elastic</td><td>8</td><td>0.15</td><td>1.2</td></tr>
<tr><td>4" Aggregate Base</td><td>Elastic</td><td>4</td><td>0.1</td><td>0.4</td><td>0.120</td></tr>
<tr><td>3" Aggregate Base</td><td>Elastic</td><td>3</td><td>0.1</td><td>0.3</td><td rowspan="2">Subgrade</td><td rowspan="2">Database NCHRP</td></tr>
<tr><td>5" Aggregate Base</td><td>Elastic</td><td>5</td><td>0.1</td><td>0.5</td></tr>
</table>

Table 11.10-Pavement Structure and Resilient Modulus Calculations for IR 080-128.

	Year	1965	1984	1992	2001	2009
IR 80-128	Structure				2" AC-20P	2.5" PG64-28NV
			5" AR-4000	5" AC-20P	5" AC-20P	5" AC-20P
		3.5" Plantmix Surface	2.5" Plantmix Surface	8" RBM	8" RBM	8" RBM
		14" Aggregate Base	14" Aggregate Base	14" Aggregate Base	14" Aggregate Base	14" Aggregate Base

	Final Structure	Layer Behavior	Thickness(in)	Layer Coefficient	h*ai	Section Modeled	Modulus E (psi)
IR 80-128	2.5" PG64-28NV	Visco-Elastic	2.5	Database	Database	2.5" PG64-28NV	Database
						5" AC-20P	Database
	5" AC-20P	Visco-Elastic	5	Database	Database	22" Aggregate Base Linear Elastic	25022
	8" RBM	Elastic	8	0.15	1.2	0.118	
	14" Aggregate Base	Elastic	14	0.1	1.4	Subgrade	Database NCHRP

Table 11.11-Pavement Structure and Resilient Modulus Calculations for IR 080-129.

	Year	1965	1984	2001	2009
IR 80-129	Structure				
				2" AC-20P	2.5" PG64-28NV
			5" AR-4000	5" AR-4000	5" AR-4000
		3.5" Plantmix Surface	2.5" Plantmix Surface	2.5" Plantmix Surface	2.5" Plantmix Surface
		14" Aggregate Base	14" Aggregate Base	14" Aggregate Base	14" Aggregate Base

	Final Structure	Layer Behavior	Thickness (in)	Layer Coefficie nt	h*ai	Section Modeled	Modulus E (psi)
IR 80-129						2.5" PG64-28NV	Database
	2.5" PG64-28NV	Visco-Elastic	2.5	Database	Database	21.5" Aggregate Base Linear Elastic	34312
	5" AR-4000	Elastic	5	0.25	1.25		
	2.5" Plantmix Surface	Elastic	2.5	0.25	0.625	0.152	
	14" Aggregate Base	Elastic	14	0.1	1.4	Subgrade	Database NCHRP

Table 11.12-Pavement Structure and Resilient Modulus Calculations for IR 080-132.

<table>
<tr><td rowspan="5">IR 80-132</td><td>Year</td><td>1981</td><td>1995</td><td>2006</td></tr>
<tr><td rowspan="4">Structure</td><td></td><td></td><td></td></tr>
<tr><td></td><td>5" AC-20P</td><td>5.5" PG64-28NV</td></tr>
<tr><td>8" PCC</td><td>9" Crack and Seat</td><td>8" Crack and Seat</td></tr>
<tr><td>9"' CTB</td><td>9"' CTB</td><td>9"' CTB</td></tr>
</table>

<table>
<tr><td rowspan="5">IR 80-132</td><td>Final Structure</td><td>Layer Behavior</td><td>Thickness(in)</td><td>Layer Coefficient</td><td>h*ai</td><td>Section Modeled</td><td>Modulus E (psi)</td></tr>
<tr><td></td><td></td><td></td><td></td><td></td><td>5.5"PG 64-28NV</td><td>Database</td></tr>
<tr><td>5.5" PG64-28NV</td><td>Visco-Elastic</td><td>5.5</td><td>Database</td><td>Database</td><td>17" Aggregate Base Linear Elastic</td><td rowspan="2">41745</td></tr>
<tr><td>8" Crack and Seat</td><td>Elastic</td><td>8</td><td>0.2</td><td>1.6</td><td>0.174</td></tr>
<tr><td>9"' CTB</td><td>Elastic</td><td>9</td><td>0.15</td><td>1.35</td><td>Subgrade</td><td>Database NCHRP</td></tr>
</table>

Table 11.13-Pavement Structure and Resilient Modulus Calculations for IR 080-134A.

	Year	1925	1947	1968	1989	2001	2008
IR 80-134A	Structure						4"PG 64-28NV
							3.5" CIR
					5" AC-20P	7" AC-20P	3.5" AC-20P
				4" 120-150 PEN	RBM 5"	RBM 5"	RBM 5"
				8" Cement Treated Base	7" Cement Treated Base	7" Cement Treated Base	7" Cement Treated Base
				12" Aggregate Base	12" Aggregate Base	12" Aggregate Base	12" Aggregate Base
			2.5" Plantmix Surface	2.5" Plantmix Surface	2.5" Plantmix Surface	2.5" Plantmix Surface	2.5" Plantmix Surface
			15.5" Aggregate Base	15.5" Aggregate Base	15.5" Aggregate Base	15.5" Aggregate Base	15.5" Aggregate Base
		5" Aggregate Base	5" Aggregate Base	5" Aggregate Base	5" Aggregate Base	5" Aggregate Base	5" Aggregate Base

	Final Structure	Layer Behavior	Thickness(in)	Layer Coefficient	h*ai	Section Modeled	Modulus E (psi)
IR 80-134A	4"PG 64-28NV	Visco-Elastic	4	Database	Database	4"PG 64-28NV	Database
	3.5" CIR	Elastic	3.5	0.25	0.875	55 "Aggregate Base Linear Elastic	29916
	3.5" AC-20P	Elastic	3.5	0.25	0.875		
	RBM 5"	Elastic	5	0.15	0.75		
	7" Cement Treated Base	Elastic	7	0.15	1.05		
	12" Aggregate Base	Elastic	12	0.1	1.2		
	2.5" Plantmix Surface	Elastic	2.5	0.25	0.625	0.138	
	15.5" Aggregate Base	Elastic	15.5	0.1	1.55	Subgrade	Database NCHRP
	5" Aggregate Base	Elastic	5	0.1	0.5		

Table 11.14-Pavement Structure and Resilient Modulus Calculations for IR 080-134B.

	Year	1932	1949	1974	1997	2000	2008
IR 80-134B	Structure						4"PG 64-28NV
							3.5" CIR
					2" AC-20P	4" AC-20P	0.5" AC-20P
				4" 120-150 PEN	2" 120-150 PEN	2" 120-150 PEN	2" 120-150 PEN
				5" Aggregate Base	5" Aggregate Base	5" Aggregate Base	5" Aggregate Base
			2.5" Plantmix Surface	2.5" Plantmix Surface	2.5" Plantmix Surface	2.5" Plantmix Surface	2.5" Plantmix Surface
			9.5" Aggregate Base	9.5" Aggregate Base	9.5" Aggregate Base	9.5" Aggregate Base	9.5" Aggregate Base
		3" Plantmix Surface	3" Plantmix Surface	3" Plantmix Surface	3" Plantmix Surface	3" Plantmix Surface	3" Plantmix Surface
		6" Aggregate Base	6" Aggregate Base	6" Aggregate Base	6" Aggregate Base	6" Aggregate Base	6" Aggregate Base

	Final Structure	Layer Behavior	Thickness(in)	Layer Coefficient	h*ai	Section Modeled	Modulus E (psi)
IR 80-134B	4"PG 64-28NV	Visco-Elastic	4	Database	Database	4"PG 64-28NV	Database
	3.5" CIR	Elastic	3.5	0.25	0.875	32" Aggregate Base Linear Elastic	34817
	0.5" AC-20P	Elastic	0.5	0.25	0.125		
	2" 120-150 PEN	Elastic	2	0.25	0.5		
	5" Aggregate Base	Elastic	5	0.1	0.5		
	2.5" Plantmix Surface	Elastic	2.5	0.25	0.625		
	9.5" Aggregate Base	Elastic	9.5	0.1	0.95	0.154	
	3" Plantmix Surface	Elastic	3	0.25	0.75	Subgrade	Database NCHRP
	6" Aggregate Base	Elastic	6	0.1	0.6		

Table 11.15-Pavement Structure and Resilient Modulus Calculations for IR 080-138.

IR 80-138	Year	1966	1982	2001	2009
	Structure				2.5" PG 64-28NV
				2" AC-20P	1" AC-20P
			3.5" Plantmix Surface	1" Plantmix Surface	1" Plantmix Surface
		4" Plantmix Surface	4" Plantmix Surface	4" Plantmix Surface	4" Plantmix Surface
		12" Aggregate Base	12" Aggregate Base	12" Aggregate Base	12" Aggregate Base

	Final Structure	Layer Behavior	Thickness(in)	Layer Coefficient	h*ai	Section Modeled	Modulus E (psi)
IR 80-138	2.5" PG 64-28NV	Visco-Elastic	2.5	Database	Database	2.5"PG 64-28NV	Database
	1" AC-20P	Visco-Elastic	1	Database	Database	1" AC-20P	Database
	1" Plantmix Surface	Elastic	1	0.25	0.25	17" Aggregate Base Linear Elastic	31804
	4" Plantmix Surface	Elastic	4	0.25	1	0.144	
	12" Aggregate Base	Elastic	12	0.1	1.2	Subgrade	Database NCHRP

Table 11.16-Pavement Structure and Resilient Modulus Calculations for IR 080-139.

	Year	1925	1941	1992	2001	2009
IR 80-139	**Structure**					2" PG64-28NV
				3.5" AC-20P	4.5" AC-20P	3.5" AC-20P
			2.5" Plantmix Surface	1" Plantmix Surface	1" Plantmix Surface	1" Plantmix Surface
			7" Aggregate Base	7" Aggregate Base	7" Aggregate Base	7" Aggregate Base
		5" Aggregate Base	5" Aggregate Base	5" Aggregate Base	5" Aggregate Base	5" Aggregate Base

	Final Structure	Layer Behavior	Thickness(in)	Layer Coefficient	h*ai	Section Modeled	Modulus E (psi)
IR 80-139	2" PG64-28NV	Visco-Elastic	2	Database	Database	2" PG64-28NV	Database
	3.5" AC-20P	Visco-Elastic	3.5	Database	Database	3.5" AC-20P	23531
	1" Plantmix Surface	Elastic	1	0.25	0.25	13"Aggregate Base Linear Elastic	
	7" Aggregate Base	Elastic	7	0.1	0.7	0.112	
	5" Aggregate Base	Elastic	5	0.1	0.5	Subgrade	Database NCHRP

Table 11.17-Pavement Structure and Resilient Modulus Calculations for IR 080-140.

	Year	1965	1984	1992	2001	2009
IR 80-140	Structure					
					2" AC-20P	2.5" PG64-28NV
			5" AR-4000	5" AC-20P	5" AC-20P	5.5" AC-20P
		3.5" Plantmix Surface	2.5" Plantmix Surface	8" RBM	8" RBM	8" RBM
		16" Aggregate Base	16" Aggregate Base	16" Aggregate Base	16" Aggregate Base	16" Aggregate Base

	Final Structure	Layer Behavior	Thickness(in)	Layer Coefficient	h*ai	Section Modeled	Modulus E (psi)
IR 80-140						2.5" PG64-28NV	Database
	2.5" PG64-28NV	Visco-Elastic	2.5	Database	Database	5.5" AC-20P	Database
	5.5" AC-20P	Visco-Elastic	5.5	Database	Database	24"Aggregate Base Linear Elastic	28785
	8" RBM	Elastic	8	0.2	1.6	0.133	
	16" Aggregate Base	Elastic	16	0.1	1.6	Subgrade	Database NCHRP

Table 11.18-Pavement Structure and Resilient Modulus Calculations for IR 080-141.

	Year	**1965**	**1984**	**1989**	**2000**	**2009**
IR 80-141	**Structure**					
					2" AC-20P	2.5" PG64-28NV
			5" AR-4000	5" AC-20P	5" AC-20P	5.5" AC-20P
		3.5" Plantmix Surface	2.5" Plantmix Surface	8"RBM	8"RBM	8"RBM
		20" Aggregate Base	20" Aggregate Base	20" Aggregate Base	20" Aggregate Base	20" Aggregate Base

	Final Structure	**Layer Behavior**	**Thickness(in)**	**Layer Coefficient**	**h*ai**	**Section Modeled**	**Modulus E (psi)**
IR 80-141						2.5" PG64-28NV	Database
	2.5" PG64-28NV	Visco-Elastic	2.5	Database	Database	5.5" AC-20P	Database
	5.5" AC-20P	Visco-Elastic	5.5	Database	Database	28"Aggregate Base Linear Elastic	24136
	8"RBM	Elastic	8	0.15	1.2	0.114	
	20" Aggregate Base	Elastic	20	0.1	2	Subgrade	Database NCHRP

Table 11.19-Pavement Structure and Resilient Modulus Calculations for IR 080-142.

	Year	1925	1941	1981	1999	2007
IR 80-142	Structure					
						2" PG64-28NV
			2.5" Plantmix Surface		5" AC-20P	3.5" AC-20P
			7" Aggregate Base	8" PCC	8" Rubblized PCC	8" Rubblized PCC
		5" Aggregate Base	5" Aggregate Base	6" CTB	6" CTB	6" CTB

	Final Structure	Layer Behavior	Thickness (in)	Layer Coefficient	h*ai	Section Modeled	Modulus E (psi)
IR 80-142						2" PG64-28NV	Database
	2" PG64-28NV	Visco-Elastic	2	Database	Database	3.5" AC-20P	Database
	3.5" AC-20P	Visco-Elastic	3.5	Database	Database	14"Aggregate Base Linear Elastic	43737
	8" Rubblized PCC	Elastic	8	0.2	1.6	0.179	
	6" CTB	Elastic	6	0.15	0.9	Subgrade	Database NCHRP

Table 11.20-Pavement Structure and Resilient Modulus Calculations for IR 015-95.

	Year	1963	1999	2006
IR 15-95	Structure			
				2" PG76-22NV
		3.5" 85-100 PEN	6.3" AC-30P	3.5" AC-30P
		16" Aggregate Base	24" Aggregate Base	24" Aggregate Base

	Final Structure	Layer Behavior	Thickness(in)	Layer Coefficient	h*ai	Section Modeled	Modulus E (psi)
IR 15-95						2" PG76-22NV	Database
						3.5" AC-20P	Database
	2" PG76-22NV	Visco-Elastic	2	Database	Database	24" Aggregate Base Linear Elastic	21150
	3.5" AC-30P	Visco-Elastic	3.5	Database	Database	0.100	
	24" Aggregate Base	Elastic	24	0.1	2.4	Subgrade	Database NCHRP

Table 11.21-Pavement Structure and Resilient Modulus Calculations for IR 015-99A.

IR 15-99A	Year	1965	1980	1992	2003
	Structure				
					2"PG 76-22NV
			3.5" AR-8000	4" AC-30P	3" AC-30P
		3.5" 85-100 PEN	3.5" 85-100 PEN	3" 85-100 PEN	3" 85-100 PEN
		16" Aggregate Base	16" Aggregate Base	16" Aggregate Base	16" Aggregate Base

	Final Structure	Layer Behavior	Thickness(in)	Layer Coefficient	h*ai	Section Modeled	Modulus E (psi)
IR 15-99A						2"PG 76-22NV	Database
	2"PG 76-22NV	Visco-Elastic	1	Database	Database	3" AC-30P	Database
	3" AC-30P	Visco-Elastic	1	Database	Database	19" Aggregate Base Linear Elastic	26328
	3" 85-100 PEN	Elastic	3	0.25	0.75	0.124	
	16" Aggregate Base	Elastic	16	0.1	1.6	Subgrade	Database NCHRP

Table 11.22-Pavement Structure and Resilient Modulus Calculations for IR 015-99B.

	Year	1946	1972	1995	2003
IR 15-99B	Structure				
					2"PG 76-22NV
			2.5" 60-70 PEN	4" AC-30P	3" AC-30P
		2.5" 200-300 PEN	2.5" 200-300 PEN	2.5" 200-300 PEN	2.5" 200-300 PEN
		12.5" Aggregate Base	12.5" Aggregate Base	12.5" Aggregate Base	12.5" Aggregate Base

	Final Structure	Layer Behavior	Thickness(in)	Layer Coefficient	h*ai	Section Modeled	Modulus E (psi)
IR 15-99B						2"PG 76-22NV	Database
	2"PG 76-22NV	Visco-Elastic	2	Database	Database	3" AC-30P	Database
	3" AC-30P	Visco-Elastic	3	Database	Database	15" Aggregate Base Linear Elastic	26650
	2.5" 200-300 PEN	Elastic	2.5	0.25	0.625	0.125	
	12.5" Aggregate Base	Elastic	12.5	0.1	1.25	Subgrade	Database NCHRP

Table 11.23-Pavement Structure and Resilient Modulus Calculations for IR 015-100.

	Year	1923	1946	1959	1972	1995	2003
IR 15-100	**Structure**						2"PG 76-22NV
						4" AC-30P	4" AC-30P
					5.5" 60-70 PEN	3" 60-70 PEN	3" 60-70 PEN
					3" Aggregate Base	3" Aggregate Base	3" Aggregate Base
				3.5" Plantmix Surface	3.5" Plantmix Surface	3.5" Plantmix Surface	3.5" Plantmix Surface
				10" Aggregate Base	10" Aggregate Base	10" Aggregate Base	10" Aggregate Base
			2.5" Plantmix Surface	2.5" Plantmix Surface	2.5" Plantmix Surface	2.5" Plantmix Surface	2.5" Plantmix Surface
			12.5" Aggregate Base	12.5" Aggregate Base	12.5" Aggregate Base	12.5" Aggregate Base	12.5" Aggregate Base
		5" Aggregate Base	5" Aggregate Base	5" Aggregate Base	5" Aggregate Base	5" Aggregate Base	5" Aggregate Base

	Final Structure	Layer Behavior	Thickness(in)	Layer Coefficient	h*ai	Section Modeled	Modulus E (psi)
IR 15-100	2"PG 76-22NV	Visco-Elastic	2	Database	Database	4"PG 64-28NV	Database
	4" AC-30P	Visco-Elastic	4	Database	Database	4" AC-30P	Database
	3" 60-70 PEN	Elastic	3	0.25	0.75	39.5" Aggregate Base Linear Elastic	29011
	3" Aggregate Base	Elastic	3	0.1	0.3		
	3.5" Plantmix Surface	Elastic	3.5	0.25	0.875		
	10" Aggregate Base	Elastic	10	0.1	1		
	2.5" Plantmix Surface	Elastic	2.5	0.25	0.625	0.134	
	12.5" Aggregate Base	Elastic	12.5	0.1	1.25	Subgrade	Database NCHRP
	5" Aggregate Base	Elastic	5	0.1	0.5		

Table 11.24-Pavement Structure and Resilient Modulus Calculations for IR 015-101.

	Year	1925	1959	1972	1995	2004
IR 15-101	Structure					
						2"PG 76-22NV
				2.5" 60-70 PEN	4" AC-30P	3" AC-30P
			3.5" Plantmix Surface	3.5" Plantmix Surface	3.5" Plantmix Surface	3.5" Plantmix Surface
			4" Aggregate Base	4" Aggregate Base	4" Aggregate Base	4" Aggregate Base
		5" Aggregate Base	5" Aggregate Base	5" Aggregate Base	5" Aggregate Base	5" Aggregate Base

	Final Structure	Layer Behavior	Thickness (in)	Layer Coefficient	h*ai	Section Modeled	Modulus E (psi)
IR 15-101						2"PG 76-22NV	Database
						3" AC-30P	Database
	2"PG 76-22NV	Visco-Elastic	2	Database	Database	12.5" Aggregate Base Linear Elastic	31187
	3" AC-30P	Visco-Elastic	3	Database	Database		
	3.5" Plantmix Surface	Elastic	3.5	0.25	0.875	0.142	
	4" Aggregate Base	Elastic	4	0.1	0.4	Subgrade	Database NCHRP
	5" Aggregate Base	Elastic	5	0.1	0.5		

Table 11.25-Pavement Structure and Resilient Modulus Calculations for IR 015-102.

	Year	1925	1953	1966	1994	2002	2010
IR 15-102	Structure					2.5" AC-30P	2.5"PG 76-22NV
					4" AC-20P	3" AC-20P	2.5" AC-20P
				4" 85-100 PEN	2.5" 85-100 PEN	2.5" 85-100 PEN	2.5" 85-100 PEN
				6" Aggregate Base	6" Aggregate Base	6" Aggregate Base	6" Aggregate Base
			4" 120-150 PEN	4" 120-150 PEN	4" 120-150 PEN	4" 120-150 PEN	4" 120-150 PEN
			3" Aggregate Base	3" Aggregate Base	3" Aggregate Base	3" Aggregate Base	3" Aggregate Base
		5" Aggregate Base	5" Aggregate Base	5" Aggregate Base	5" Aggregate Base	5" Aggregate Base	5" Aggregate Base

	Final Structure	Layer Behavior	Thickness(in)	Layer Coefficient	h*ai	Section Modeled	Modulus E (psi)
IR 15-102	2.5"PG 76-22NV	Visco-Elastic	2.5	Database	Database	2.5"PG 76-22NV	Database
	2.5" AC-20P	Elastic	2.5	0.25	0.625		Database
	2.5" 85-100 PEN	Elastic	2.5	0.25	0.625	23" Aggregate Base Linear Elastic	36394
	6" Aggregate Base	Elastic	6	0.1	0.6		
	4" 120-150 PEN	Elastic	4	0.25	1	0.159	
	3" Aggregate Base	Elastic	3	0.1	0.3	Subgrade	Database NCHRP
	5" Aggregate Base	Elastic	5	0.1	0.5		

Table 11.26-Pavement Structure and Resilient Modulus Calculations for IR 015-103.

	Year	1955	1967	1975	1991	2000	2007
IR 15-103	Structure						2" PG76-22NV
						2" PG76-22NV	1" PG76-22NV
				4" AR-8000	6.5" AC-20P	5.5" AC-20P	5.5" AC-20P
				7" Aggregate Base	RBM 8"	RBM 8"	RBM 8"
			4" 60-70 PEN	4" 60-70 PEN	4" 60-70 PEN	4" 60-70 PEN	4" 60-70 PEN
			14" Aggregate Base	14" Aggregate Base	14" Aggregate Base	14" Aggregate Base	14" Aggregate Base
		2.5" Plantmix Surface	2.5" Plantmix Surface	2.5" Plantmix Surface	2.5" Plantmix Surface	2.5" Plantmix Surface	2.5" Plantmix Surface
		6" Aggregate Base	6" Aggregate Base	6" Aggregate Base	6" Aggregate Base	6" Aggregate Base	6" Aggregate Base

	Final Structure	Layer Behavior	Thickness(in)	Layer Coefficient	h*ai	Section Modeled	Modulus E (psi)
IR 15-103	2" PG76-22NV	Visco-Elastic	2	Database	Database	2" PG76-22NV	Database
	1" PG76-22NV	Visco-Elastic	1	Database	Database	1" PG76-22NV	Database
	5.5" AC-20P	Elastic	5.5	Database	Database	5.5" AC-20P	Database
	RBM 8"	Elastic	8	0.15	1.2	34.5" Aggregate Base Linear Elastic	30574
	4" 60-70 PEN	Elastic	4	0.25	1		
	14" Aggregate Base	Elastic	14	0.1	1.4	0.140	
	2.5" Plantmix Surface	Visco-Elastic	2.5	0.25	0.625	Subgrade	Database NCHRP
	6" Aggregate Base	Visco-Elastic	6	0.1	0.6		

Table 11.27-Pavement Structure and Resilient Modulus Calculations for SR 160-8.

	Year	1944	1974	1995	2004
SR 160-8	Structure				
					4"PG 64-28NV
			2" AR-8000		3" CIR
		2" Plantmix Surface	2" Plantmix Surface	4" AC-30P	1" AC-30P

	Final Structure	Layer Behavior	Thickness(in)	Layer Coefficient	h*ai	Section Modeled	Modulus E (psi)
SR 160-8						4"PG 64-28NV	Database
						4"Aggregate Base Linear Elastic	84666
	4"PG 64-28NV	Visco-Elastic	4	Database	Database	0.250	
	3" CIR	Elastic	3	0.25	0.75	Subgrade	Database NCHRP
	1" AC-30P	Elastic	1	0.25	0.25		

Table 11.28-Pavement Structure and Resilient Modulus Calculations for SR 160-9.

	Year	**1944**	**1974**	**1992**	**2009**
SR 160-9	**Structure**				
				2" AC-20P	
				6" Cement Treated Base	
			2" AR-8000	2" AR-8000	6"PG 76-22NV
		2.5" 200-300 PEN	2.5" 200-300 PEN	2.5" 200-300 PEN	24" Aggregate Base

	Final Structure	**Layer Behavior**	**Thickness(in)**	**Layer Coefficient**	**h*ai**	**Section Modeled**	**Modulus E (psi)**
SR 160-9						6"PG 76-22NV	Database
							22100
						24" Aggregate Base Linear Elastic	
	6"PG 76-22NV	Visco-Elastic	6	Database	Database	0.100	
	24" Aggregate Base	Elastic	24	0.1	2.4	Subgrade	Database NCHRP

Table 11.29-Pavement Structure and Resilient Modulus Calculations for SR 160-11.

SR 160-11	Year	1952	1995	2005
	Structure			
				3" PG76-22NV
		2" Plantmix Surface	4" AC-20P	3" AC-20P
		9" Aggregate Base	10" Aggregate Base	10" Aggregate Base

	Final Structure	Layer Behavior	Thickness(in)	Layer Coefficient	h*ai	Section Modeled	Modulus E (psi)
SR 160-11						3" PG76-22NV	Database
						3" AC-20P	Database
	3" PG76-22NV	Visco-Elastic	3	Database	Database	10" Aggregate Base Linear Elastic	21150
	3" AC-20P	Visco-Elastic	3	Database	Database	0.100	
	10" Aggregate Base	Elastic	10	0.1	1	Subgrade	Database NCHRP

Table 11.30-Pavement Structure and Resilient Modulus Calculations for SR 160-12A.

	Year	1952	1997	2007
SR 160-12A	Structure			
			2" PG 70-16	5" PG76-22NV
		6" Gravel Surface	6" Gravel Surface	RBM 8"
		6" Aggregate Base	6" Aggregate Base	6" Aggregate Base

	Final Structure	Layer Behavior	Thickness(in)	Layer Coefficient	h*ai	Section Modeled	Modulus E (psi)
SR 160-12A						5" PG76-22NV	Database
	5" PG76-22NV	Visco-Elastic	5	Database	Database	14" Aggregate Base Linear Elastic	23352
	RBM 8"	Elastic	8	0.15	0.75	0.111	
	6" Aggregate Base	Elastic	6	0.1	0.8	Subgrade	Database NCHRP

Table 11.31-Pavement Structure and Resilient Modulus Calculations for SR 160-12B.

<table>
<tr><td rowspan="6">SR 160-12B</td><td>Year</td><td>1952</td><td>1999</td><td>2007</td></tr>
<tr><td rowspan="5">Structure</td><td></td><td></td><td>5" PG76-22NV</td></tr>
<tr><td></td><td></td><td>RBM 8"</td></tr>
<tr><td></td><td>12" Aggregate Base</td><td>4" Aggregate Base</td></tr>
<tr><td>6" Gravel Surface</td><td>6" Gravel Surface</td><td>6" Gravel Surface</td></tr>
<tr><td>6" Aggregate Base</td><td>6" Aggregate Base</td><td>6" Aggregate Base</td></tr>
</table>

<table>
<tr><td rowspan="6">SR 160-12B</td><td>Final Structure</td><td>Layer Behavior</td><td>Thickness(in)</td><td>Layer Coefficient</td><td>h*ai</td><td>Section Modeled</td><td>Modulus E (psi)</td></tr>
<tr><td>5" PG76-22NV</td><td>Visco-Elastic</td><td>5</td><td>Database</td><td>Database</td><td>5" PG76-22NV</td><td>Database</td></tr>
<tr><td>RBM 8"</td><td>Elastic</td><td>8</td><td>0.15</td><td>0.75</td><td rowspan="2">24" Aggregate Base Linear Elastic</td><td rowspan="3">22408</td></tr>
<tr><td>4" Aggregate Base</td><td>Elastic</td><td>4</td><td>0.1</td><td>0.8</td></tr>
<tr><td>6" Gravel Surface</td><td>Elastic</td><td>6</td><td>0.1</td><td>0.4</td><td>0.106</td></tr>
<tr><td>6" Aggregate Base</td><td>Elastic</td><td>6</td><td>0.1</td><td>0.6</td><td>Subgrade</td><td>Database NCHRP</td></tr>
</table>

Table 11.32-Pavement Structure and Resilient Modulus Calculations for SR 160-13.

	Year	1953	1996	2007
SR 160-13	Structure			5" PG76-22NV
			3.5" AC-30P	RBM 8"
			10" Aggregate Base	5.5" Aggregate Base
		2" Plantmix Surface	2" Plantmix Surface	2" Plantmix Surface

	Final Structure	Layer Behavior	Thickness(in)	Layer Coefficient	h*ai	Section Modeled	Modulus E (psi)
SR 160-13	5" PG76-22NV	Visco-Elastic	5	Database	Database	5"PG 76-222NV	Database
	RBM 8"	Elastic	8	0.15	0.75	15.5" Aggregate Base Linear Elastic	48036
	5.5" Aggregate Base	Elastic	5.5	0.1	0.8	0.189	
	2" Plantmix Surface	Elastic	2	0.25	1.375	Subgrade	Database NCHRP

Table 11.33-Pavement Structure and Resilient Modulus Calculations for SR 159-6.

	Year	1944	1990	2006
SR 159-6	Structure		2" AR-4000	
		2.5" 200-300 PEN	1" 200-300 PEN	3" PG76-22NV
		3.5" Aggregate Base	3.5" Aggregate Base	3.5" Aggregate Base

	Final Structure	Layer Behavior	Thickness(in)	Layer Coefficient	h*ai	Section Modeled	Modulus E (psi)
SR 159-6						3" PG76-22NV	Database
	3" PG76-22NV	Visco-Elastic	3	Database	Database	3.5"Aggregate Base Linear Elastic	21150
	3.5" Aggregate Base	Elastic	3.5	0.1	0.35	0.100	
						Subgrade	Database NCHRP

Table 11.34-Pavement Structure and Resilient Modulus Calculations for SR 117-1.

SR 117-1	**Year**	**1960**	**1971**	**1992**	**2005**
	Structure			2"AC-20P	2" PG64-28NV
			1.5" Plantmix Surface	1.5" Plantmix Surface	1" Plantmix Surface
		2.5" Plantmix Surface	2.5" Plantmix Surface	2.5" Plantmix Surface	2.5" Plantmix Surface
		6.5" Aggregate Base	6.5" Aggregate Base	6.5" Aggregate Base	6.5" Aggregate Base

	Final Structure	**Layer Behavior**	**Thickness(in)**	**Layer Coefficient**	**h*ai**	**Section Modeled**	**Modulus E (psi)**
SR 117-1	2" PG64-28NV	Visco-Elastic	2	Database	Database	2" PG64-28NV	Database
	1" Plantmix Surface	Elastic	1	0.25	0.25	10"Aggregate Base Linear Elastic	34367
	2.5" Plantmix Surface	Elastic	2.5	0.25	0.625	0.153	
	6.5" Aggregate Base	Elastic	6.5	0.1	0.65	Subgrade	Database NCHRP

Table 11.35-Pavement Structure and Resilient Modulus Calculations for SR 208-22.

SR 208-22	**Year**	**1972**	**1995**	**2006**
	Structure			
			2.5" AC-20P	3"PG 64-28NV
		2.5" Plantmix Surface	2.5" Plantmix Surface	2.5" Plantmix Surface
		4" Aggregate Base	4" Aggregate Base	4" Aggregate Base

	Final Structure	**Layer Behavior**	**Thickness(in)**	**Layer Coefficient**	**h*ai**	**Section Modeled**	**Modulus E (psi)**
SR 208-22						3"PG 64-28NV	Database
	3"PG 64-28NV	Visco-Elastic	3	Database	Database	6.5" Aggregate Base Linear Elastic	36058
	2.5" Plantmix Surface	Elastic	2.5	0.25	0.625	0.158	
	4" Aggregate Base	Elastic	4	0.1	0.4	Subgrade	Database NCHRP

Table 11.36-Pavement Structure and Resilient Modulus Calculations for SR 208-23.

	Year	**1972**	**1995**	**2006**
SR 208-23	**Structure**			
			2.5" AC-20P	3"PG 64-28NV
		1.5" Plantmix Surface	1.5" Plantmix Surface	1" Plantmix Surface
		4" Aggregate Base	4" Aggregate Base	4" Aggregate Base

	Final Structure	**Layer Behavior**	**Thickness(in)**	**Layer Coefficient**	**h*ai**	**Section Modeled**	**Modulus E (psi)**
SR 208-23						3"PG 64-28NV	Database
	3"PG 64-28NV	Visco-Elastic	3	Database	Database	5" Aggregate Base Linear Elastic	27911
	1" Plantmix Surface	Elastic	1	0.25	0.25	0.130	
	4" Aggregate Base	Elastic	4	0.1	0.4	Subgrade	Database NCHRP

Table 11.37-Pavement Structure and Resilient Modulus Calculations for SR 225-26.

	Year	1937	1940	1949	1966	1994	2002
SR 225-26	**Structure**					1.5"AC-20P	
					3" 120-150 PEN	3" 120-150 PEN	3.5"PG 64-28NV
					7" Aggregate Base	7" Aggregate Base	RBM 8"
				2" Plantmix Surface	2" Plantmix Surface	2" Plantmix Surface	2" Plantmix Surface
			2.5" Plantmix Surface	2.5" Plantmix Surface	2.5" Plantmix Surface	2.5" Plantmix Surface	2.5" Plantmix Surface
			9" Aggregate Base	9" Aggregate Base	9" Aggregate Base	9" Aggregate Base	9" Aggregate Base
		6" Aggregate Base	6" Aggregate Base	6" Aggregate Base	6" Aggregate Base	6" Aggregate Base	6" Aggregate Base

	Final Structure	Layer Behavior	Thickness(in)	Layer Coefficient	h*ai	Section Modeled	Modulus E (psi)
SR 225-26							
	3.5"PG 64-28NV	Visco-Elastic	3.5	Database	Database	3.5" PG 64-28NV	Database
	RBM 8"	Elastic	8	0.15	1.2	27.5" Aggregate Base Linear Elastic	30359
	2" Plantmix Surface	Elastic	2	0.25	0.5		
	2.5" Plantmix Surface	Elastic	2.5	0.25	0.625	0.139	
	9" Aggregate Base	Elastic	9	0.1	0.9	Subgrade	Database NCHRP
	6" Aggregate Base	Elastic	6	0.1	0.6		

Table 11.38-Pavement Structure and Resilient Modulus Calculations for SR 318-143.

SR 318-143	Year	1981	1999	2010
	Structure			
			2" AC-20P	4"PG 64-28NV
		3.5" AR-4000	3.5" AR-4000	RBM 8"
		6" Aggregate Base	6" Aggregate Base	4" Aggregate Base

	Final Structure	Layer Behavior	Thickness(in)	Layer Coefficient	h*ai	Section Modeled	Modulus E (psi)
SR 318-143						4"PG 64-28NV	Database
	4"PG 64-28NV	Visco-Elastic	4	Database	Database	12" Aggregate Base Linear Elastic	24674
	RBM 8"	Elastic	8	0.15	0.6	0.117	
	4" Aggregate Base	Elastic	4	0.1	0.8	Subgrade	Database NCHRP

Table 11.39-Pavement Structure and Resilient Modulus Calculations for SR 318-145.

	Year	1975	1983	1999	2010
SR 318-145	Structure				3"PG 64-28NV
				2" AC-20P	3" CIR
			2" AR-4000	2" AR-4000	1" AR-4000
		3" 120-150 PEN	3" 120-150 PEN	3" 120-150 PEN	3" 120-150 PEN
		4" Aggregate Base	4" Aggregate Base	4" Aggregate Base	4" Aggregate Base

	Final Structure	Layer Behavior	Thickness(in)	Layer Coefficient	h*ai	Section Modeled	Modulus E (psi)
SR 318-145	3"PG 64-28NV	Visco-Elastic	3	Database	Database	3"PG 64-28NV	Database
	3" CIR	Elastic	3	0.25	0.75	11"Aggregate Base Linear Elastic	51127
	1" AR-4000	Elastic	1	0.25	0.25	0.195	
	3" 120-150 PEN	Elastic	3	0.25	0.75	Subgrade	Database NCHRP
	4" Aggregate Base	Elastic	4	0.1	0.4		

Table 11.40-Pavement Structure and Resilient Modulus Calculations for SR 582-35.

	Year	1931	1957	1996	2002
SR 582-35	Structure				2" PG76-22NV
				5" AC 30 Asphalt	2.25" AC 30 Asphalt
				16" Aggregate Base	16" Aggregate Base
			3.5" Plantmix Surface	3.5" Plantmix Surface	3.5" Plantmix Surface
			8" Aggregate Base	8" Aggregate Base	8" Aggregate Base
		3" Asphalt Roadmix	3" Asphalt Roadmix	3" Asphalt Roadmix	3" Asphalt Roadmix
		6" Aggregate Base	6" Aggregate Base	6" Aggregate Base	6" Aggregate Base

	Final Structure	Layer Behavior	Thickness(in)	Layer Coefficient	h*ai	Section Modeled	Modulus E (psi)
SR 582-35	2" PG76-22NV	Visco-Elastic	2	Database	Database	2" PG76-22NV	Database
	2.25" AC-30	Visco-Elastic	2.25	Database	Database	2.25" AC 30	Database
	16" Aggregate Base	Elastic	16	0.1	1.6	36.5" Aggregate Base Linear Elastic	27076
	3.5" Plantmix Surface	Elastic	3.5	0.25	0.875		
	8" Aggregate Base	Elastic	8	0.1	0.8	0.127	
	3" Asphalt Roadmix	Elastic	3	0.25	0.75	Subgrade	Database NCHRP
	6" Aggregate Base	Elastic	6	0.1	0.6		

Table 11.41-Pavement Structure and Resilient Modulus Calculations for US 050A-72.

	Year	1922	1930	1941	1958	1979	1986	1999	2007
US 50A -72	Structure							0.2" PG64-28	3" PG64-28NV
							3" AR-4000	2.8" AR-4000	1" AR-4000
						2" Plantmix Surface	2" Plantmix Surface	2" Plantmix Surface	2" Plantmix Surface
					1.5" 120-150 PEN	1.5" 120-150 PEN	1.5" 120-150 PEN	1.5" 120-150 PEN	1.5" 120-150 PEN
				2.5" Plantmix Surface	2.5" Plantmix Surface	2.5" Plantmix Surface	2.5" Plantmix Surface	2.5" Plantmix Surface	2.5" Plantmix Surface
			3" Plantmix Surface	3" Plantmix Surface	3" Plantmix Surface	3" Plantmix Surface	3" Plantmix Surface	3" Plantmix Surface	3" Plantmix Surface
		6" Aggregate Base	6" Aggregate Base	6" Aggregate Base	6" Aggregate Base	6" Aggregate Base	6" Aggregate Base	6" Aggregate Base	6" Aggregate Base

	Final Structure	Layer Behavior	Thickness(in)	Layer Coefficient	h*ai	Section Modeled	Modulus E (psi)
US 50A-72	3" PG64-28NV	Visco-Elastic	3	Database	Database	3" PG64-28NV	Database
	1" AR-4000	Elastic	1	0.25	0.25	16" Aggregate Base Linear Elastic	42316
	2" Plantmix Surface	Elastic	2	0.1	0.2		
	1.5" 120-150 PEN	Elastic	1.5	0.25	0.375	0.175	
	2.5" Plantmix Surface	Elastic	2.5	0.25	0.625	Subgrade	Database NCHRP
	3" Plantmix Surface	Elastic	3	0.25	0.75		
	6" Aggregate Base	Elastic	6	0.1	0.6		

Table 11.42-Pavement Structure and Resilient Modulus Calculations for US 395-74A.

	Year	1929	1949	1989	1995	2005
US 395-74A	Structure					3"PG 64-28NV
				2.5" Plantmix Surface	4" AC-20P	1" AC-20P
			2.5" Plantmix Surface	2.5" Plantmix Surface	RBM 8"	RBM 8"
			9" Aggregate Base	9" Aggregate Base	6" Aggregate Base	6" Aggregate Base
		4" Plantmix Surface	4" Plantmix Surface	4" Plantmix Surface	4" Plantmix Surface	4" Plantmix Surface
		4" Aggregate Base	4" Aggregate Base	4" Aggregate Base	4" Aggregate Base	4" Aggregate Base

	Final Structure	Layer Behavior	Thickness(in)	Layer Coefficient	h*ai	Section Modeled	Modulus E (psi)
US 395-74A	3"PG 64-28NV	Visco-Elastic	3	Database	Database	3"PG 64-28NV	Database
	1" AC-20P	Visco-Elastic	1	Database	Database	1" AC-20P	Database
	RBM 8"	Elastic	8	0.15	1.2	22" Aggregate Base Linear Elastic	32200
	6" Aggregate Base	Elastic	6	0.1	0.6	0.145	
	4" Plantmix Surface	Elastic	4	0.25	1	Subgrade	Database NCHRP
	4" Aggregate Base	Elastic	4	0.1	0.4		

Table 11.43-Pavement Structure and Resilient Modulus Calculations for US 395-74B.

	Year	1931	1940	1966	1978	1989	1995	2005
US 395-74B	Structure					2.5" Plantmix Surface		
					4.5" AR-2000	4.5" AR-2000		3"PG 64-28NV
					2" Aggregate Base	2" Aggregate Base	4" AC-20P	1" AC-20P
				1.5" Plantmix Surface	1.5" Plantmix Surface	1.5" Plantmix Surface	RBM 8"	RBM 8"
			2.5" Plantmix Surface	2.5" Plantmix Surface	2.5" Plantmix Surface	2.5" Plantmix Surface	2.5" Plantmix Surface	2.5" Plantmix Surface
			9.5" Aggregate Base	9.5" Aggregate Base	9.5" Aggregate Base	9.5" Aggregate Base	9.5" Aggregate Base	9.5" Aggregate Base
		3" Plantmix Surface	3" Plantmix Surface	3" Plantmix Surface	3" Plantmix Surface	3" Plantmix Surface	3" Plantmix Surface	3" Plantmix Surface
		9" Aggregate Base	9" Aggregate Base	9" Aggregate Base	9" Aggregate Base	9" Aggregate Base	9" Aggregate Base	9" Aggregate Base

	Final Structure	Layer Behavior	Thickness(in)	Layer Coefficient	h*ai	Section Modeled	Modulus E (psi)
US 395-74B							
	3"PG 64-28NV	Visco-Elastic	3	Database	Database	3"PG 64-28NV	Database
	1" AC-20P	Visco-Elastic	1	Database	Database	1" AC-20P	Database
	RBM 8"	Elastic	8	0.15	1.2	32" Aggregate Base Linear Elastic	29643
	2.5" Plantmix Surface	Elastic	2.5	0.25	0.625		
	9.5" Aggregate Base	Elastic	9.5	0.1	0.95	0.137	
	3" Plantmix Surface	Elastic	3	0.25	0.75	Subgrade	Database NCHRP
	9" Aggregate Base	Elastic	9	0.1	0.9		

Table 11.44-Pavement Structure and Resilient Modulus Calculations for US 395-76.

US 395-76	Year	1928	1941	1962	1966	1969	1994	2004
	Structure							3"PG 64-28NV
					1.5" Plantmix Surface		5" AC-20P	4" AC-20P
				1.5" Plantmix Surface	1.5" Plantmix Surface	5" 200-300 PEN	3" 200-300 PEN	3" 200-300 PEN
			2.5" Plantmix Surface	2.5" Plantmix Surface	2.5" Plantmix Surface	8" Cement Treated Base	8" Cement Treated Base	8" Cement Treated Base
			6.5" Aggregate Base	6.5" Aggregate Base	6.5" Aggregate Base	4" Aggregate Base	4" Aggregate Base	4" Aggregate Base
		3" Plantmix Surface	3" Plantmix Surface	3" Plantmix Surface	3" Plantmix Surface	3" Plantmix Surface	3" Plantmix Surface	3" Plantmix Surface
		9.5" Aggregate Base	9.5" Aggregate Base	9.5" Aggregate Base	9.5" Aggregate Base	9.5" Aggregate Base	9.5" Aggregate Base	9.5" Aggregate Base

US 395-76	Final Structure	Layer Behavior	Thickness(in)	Layer Coefficient	h*ai	Section Modeled	Modulus E (psi)
	3"PG 64-28NV	Visco-Elastic	3	Database	Database	3"PG 64-28NV	Database
	4" AC-20P	Visco-Elastic	4	Database	Database	4" AC-20P	Database
	3" 200-300 PEN	Elastic	3	0.25	0.75	27.5" Aggregate Base Linear Elastic	32745
	8" Cement Treated Base	Elastic	8	0.15	1.2		
	4" Aggregate Base	Elastic	4	0.1	0.4	0.147	
	3" Plantmix Surface	Elastic	3	0.25	0.75	Subgrade	Database NCHRP
	9.5" Aggregate Base	Elastic	9.5	0.1	0.95		

Table 11.45-Pavement Structure and Resilient Modulus Calculations for US 395-80.

US 395-80	**Year**	**1964**	**1979**	**1995**	**2006**
	Structure				1"PG 64-28NV
				3" AC-20P	2" AC-20P
			4" AR-4000	1" AR-4000	1" AR-4000
		2.5" 120-150 PEN	2.5" 120-150 PEN	2.5" 120-150 PEN	2.5" 120-150 PEN
		15" Aggregate Base	15" Aggregate Base	15" Aggregate Base	15" Aggregate Base

	Final Structure	Layer Behavior	Thickness(in)	Layer Coefficient	h*ai	Section Modeled	Modulus E (psi)
US 395-80	1"PG 64-28NV	Visco-Elastic	1	Database	Database	1" PG64-28NV	Database
	2" AC-20P	Visco-Elastic	2	Database	Database	2" AC-20P	Database
	1" AR-4000	Elastic	1	0.25	0.25	18.5" Aggregate Base Linear Elastic	27496
	2.5" 120-150 PEN	Elastic	2.5	0.25	0.625	0.128	
	15" Aggregate Base	Elastic	15	0.1	1.5	Subgrade	Database NCHRP

Table 11.46-Pavement Structure and Resilient Modulus Calculations for US 395-83.

	Year	1970	1995	2009
US 395-83	Structure			
			4" AC-20P	3"PG 64-28NV
		4" 60-70 PEN	2" 60-70 PEN	2" 60-70 PEN
		7" Aggregate Base	7" Aggregate Base	7" Aggregate Base

	Final Structure	Layer Behavior	Thickness(in)	Layer Coefficient	h*ai	Section Modeled	Modulus E (psi)
US 395-83						3" PG64-28NV	Database
						9" Aggregate Base Linear Elastic	28785
	3"PG 64-28NV	Visco-Elastic	3	Database	Database		
	2" 60-70 PEN	Elastic	2	0.25	0.5	0.133	
	7" Aggregate Base	Elastic	7	0.1	0.7	Subgrade	Database NCHRP

Table 11.47-Pavement Structure and Resilient Modulus Calculations for US 395-86.

	Year	1921	1931	1956	1972	1985	1997	2004
US 395-86	Structure							2"PG 64-28NV
							6" AC-20P	4" AC-20P
					1" 120-150 PEN	4.5" AR-4000	1.5" AR-4000	1.5" AR-4000
				4" 120-150 PEN	4" 120-150 PEN	2" 120-150 PEN	2" 120-150 PEN	2" 120-150 PEN
				8" Aggregate Base	8" Aggregate Base	8" Aggregate Base	8" Aggregate Base	8" Aggregate Base
			3" Plantmix Surface	3" Plantmix Surface	3" Plantmix Surface	3" Plantmix Surface	3" Plantmix Surface	3" Plantmix Surface
		6" Cement Treated Base	6" Cement Treated Base	6" Cement Treated Base	6" Cement Treated Base	6" Cement Treated Base	6" Cement Treated Base	6" Cement Treated Base

	Final Structure	Layer Behavior	Thickness(in)	Layer Coefficient	h*ai	Section Modeled	Modulus E (psi)
US 395-86	2"PG 64-28NV	Visco-Elastic	2	Database	Database	2"PG 64-28NV	Database
	4" AC-20P	Visco-Elastic	4	Database	Database	4" AC-20P	Database
	1.5" AR-4000	Elastic	1.5	0.25	0.375	20.5" Aggregate Base Linear Elastic	37591
	2" 120-150 PEN	Elastic	2	0.25	0.5		
	8" Aggregate Base	Elastic	8	0.1	0.8	0.162	
	3" Plantmix Surface	Elastic	3	0.25	0.75	Subgrade	Database NCHRP
	6" Cement Treated Base	Elastic	6	0.15	0.9		

Table 11.48-Pavement Structure and Resilient Modulus Calculations for US 395-89.

	Year	1943	1971	1989	1999	2008
US 395-89	**Structure**					2" PG64-28NV
					3" Plantmix Surface AC-20P	2" Plantmix Surface AC-20P
				4" Plantmix Surface AR-4000	1" Plantmix Surface AR-4000	1" Plantmix Surface AR-4000
			1.5" 200-300 PEN	1.5" 200-300 PEN	1.5" 200-300 PEN	1.5" 200-300 PEN
		5" Plantmix Surface	5" Plantmix Surface	5" Plantmix Surface	5" Plantmix Surface	5" Plantmix Surface
		6.5" Aggregate Base	6.5" Aggregate Base	6.5" Aggregate Base	6.5" Aggregate Base	6.5" Aggregate Base

	Final Structure	Layer Behavior	Thickness(in)	Layer Coefficient	h*ai	Section Modeled	Modulus E (psi)
US 395-89	2" PG64-28NV	Visco-Elastic	2	Database	Database	2" PG64-28NV	Database
	2" AC-20P	Visco-Elastic	2	Database	Database	2" AC-20P	Database
	1" Plantmix Surface AR-4000	Elastic	1	0.25	0.25	14" Aggregate Base Linear Elastic	44465
	1.5" 200-300 PEN	Elastic	1.5	0.25	0.375	0.180	
	5" Plantmix Surface	Elastic	5	0.25	1.25	Subgrade	Database NCHRP
	6.5" Aggregate Base	Elastic	6.5	0.1	0.65		

Table 11.49-Pavement Structure and Resilient Modulus Calculations for US 395-90.

<table>
<tr><th rowspan="6">US 395-90</th><th>Year</th><th>1961</th><th>1989</th><th>1999</th><th>2009</th></tr>
<tr><th rowspan="5">Structure</th><td></td><td></td><td></td><td>2"PG 64-28NV</td></tr>
<tr><td></td><td></td><td>2" AC-20P</td><td>1" AC-20P</td></tr>
<tr><td></td><td>4" AR-4000</td><td>1" AR-4000</td><td>1" AR-4000</td></tr>
<tr><td>4" Plantmix Surface</td><td>4" Plantmix Surface</td><td>4" Plantmix Surface</td><td>4" Plantmix Surface</td></tr>
<tr><td>8" Aggregate Base</td><td>8" Aggregate Base</td><td>8" Aggregate Base</td><td>8" Aggregate Base</td></tr>
</table>

<table>
<tr><th rowspan="6">US 395-90</th><th>Final Structure</th><th>Layer Behavior</th><th>Thickness(in)</th><th>Layer Coefficient</th><th>h*ai</th><th>Section Modeled</th><th>Modulus E (psi)</th></tr>
<tr><td>2"PG 64-28NV</td><td>Visco-Elastic</td><td>2</td><td>Database</td><td>Database</td><td>2"PG 64-28NV</td><td>Database</td></tr>
<tr><td>1" AC-20P</td><td>Visco-Elastic</td><td>1</td><td>Database</td><td>Database</td><td>1" AC-20P</td><td>Database</td></tr>
<tr><td>1" AR-4000</td><td>Elastic</td><td>1</td><td>0.25</td><td>0.25</td><td>13" Aggregate Base Linear Elastic</td><td rowspan="2">36058</td></tr>
<tr><td>4" Plantmix Surface</td><td>Elastic</td><td>4</td><td>0.25</td><td>1</td><td>0.158</td></tr>
<tr><td>8" Aggregate Base</td><td>Elastic</td><td>8</td><td>0.1</td><td>0.8</td><td>Subgrade</td><td>Database NCHRP</td></tr>
</table>

Table 11.50-Pavement Structure and Resilient Modulus Calculations for US 395-91.

US 395-91	**Year**	**1976**	**1995**	**2005**
	Structure			
		8.5" AR-4000	4" AC-20P	6"PG 64-28NV
		3" Aggregate Base	RBM 8"	RBM 8"

	Final Structure	Layer Behavior	Thickness(in)	Layer Coefficient	h*ai	Section Modeled	Modulus E (psi)
US 395-91						6" PG64-28NV	Database
						8" Aggregate Base Linear Elastic	33582
	6"PG 64-28NV	Visco-Elastic	6	Database	Database	0.150	
	RBM 8"	Elastic	8	0.15	1.2	Subgrade	Database NCHRP

Table 11.51-Pavement Structure and Resilient Modulus Calculations for US 050-56.

	Year	1953	1962	1966	1974	1982	2000	2008
US 50-56	Structure					2.5" AR-4000		
					1.5" Plantmix Surface	1.5" Plantmix Surface	3" AC-20P	2"PG 64-28NV
				3"120-150 PEN	3"120-150 PEN	3"120-150 PEN	3"120-150 PEN	3"120-150 PEN
			4"120-150 PEN	4"120-150 PEN	4"120-150 PEN	4"120-150 PEN	4"120-150 PEN	4"120-150 PEN
			6" Cement Treated Base	6" Cement Treated Base	6" Cement Treated Base	6" Cement Treated Base	6" Cement Treated Base	6" Cement Treated Base
		1.5" Plantmix Surface	1.5" Plantmix Surface	1.5" Plantmix Surface	1.5" Plantmix Surface	1.5" Plantmix Surface	1.5" Plantmix Surface	1.5" Plantmix Surface

	Final Structure	Layer Behavior	Thickness(in)	Layer Coefficient	h*ai	Section Modeled	Modulus E (psi)
US 50-56						2"PG 64-28NV	Database
	2"PG 64-28NV	Visco-Elastic	2	Database	Database		
	3"120-150 PEN	Elastic	3	0.25	0.75	14.5" Aggregate Base Linear Elastic	57747
	4"120-150 PEN	Elastic	4	0.25	1	0.209	
	6" Cement Treated Base	Elastic	6	0.15	0.9	Subgrade	Database NCHRP
	1.5" Plantmix Surface	Elastic	1.5	0.25	0.375		

Table 11.52-Pavement Structure and Resilient Modulus Calculations for US 050-58.

US 50-58	**Year**	**1970**	**1982**	**2000**	**2008**
	Structure				
			2.5" AR-4000	2" AC-20P	2" PG64-28NV
		3" 85-100 PEN	3" 85-100 PEN	3" 85-100 PEN	2" 85-100 PEN
		6" Cement Treated Base	6" Cement Treated Base	6" Cement Treated Base	6" Cement Treated Base

	Final Structure	**Layer Behavior**	**Thickness(in)**	**Layer Coefficient**	**h*ai**	**Section Modeled**	**Modulus E (psi)**
US 50-58						2"PG 64-28NV	Database
						8" Aggregate Base Linear Elastic	42316
	2" PG64-28NV	Visco-Elastic	2	Database	Database	0.175	
	2" 85-100 PEN	Elastic	2	0.25	0.5	Subgrade	Database NCHRP
	6" Cement Treated Base	Elastic	6	0.15	0.9		

Table 11.53-Pavement Structure and Resilient Modulus Calculations for US 050-66.

	Year	1934	1954	1974	1985	1997	2009
US 50-66	**Structure**				2" AR-4000		2"PG 64-28NV
				2" AR-1000	2" AR-1000	4" AC-20P	4" AC-20P
			2.5" Plantmix Surface	2.5" Plantmix Surface	2.5" Plantmix Surface	RBM 8"	RBM 8"
			5.5" Aggregate Base	5.5" Aggregate Base	5.5" Aggregate Base	4" Aggregate Base	4" Aggregate Base
		4" Plantmix Surface	4" Plantmix Surface	4" Plantmix Surface	4" Plantmix Surface	4" Plantmix Surface	4" Plantmix Surface
		3" Aggregate Base	3" Aggregate Base	3" Aggregate Base	3" Aggregate Base	3" Aggregate Base	3" Aggregate Base

	Final Structure	Layer Behavior	Thickness(in)	Layer Coefficient	h*ai	Section Modeled	Modulus E (psi)
US 50-66	2"PG 64-28NV	Visco-Elastic	2	Database	Database	2"PG 64-28NV	Database
	4" AC-20P	Visco-Elastic	4	Database	Database	4" AC-20P	Database
	RBM 8"	Elastic	8	0.15	1.2	19" Aggregate Base Linear Elastic	34409
	4" Aggregate Base	Elastic	4	0.1	0.4	0.153	
	4" Plantmix Surface	Elastic	4	0.25	1	Subgrade	Database NCHRP
	3" Aggregate Base	Elastic	3	0.1	0.3		

Table 11.54-Pavement Structure and Resilient Modulus Calculations for US 050-136.

	Year	1957	1961	1978	1980	1990	2008
US 50-136	Structure						2"PG64-28NV
					3" AR-4000	7" AC-20P	4" AC-20P
					4" Aggregate Base	4" Aggregate Base	4" Aggregate Base
				1.5" AR-2000	1.5" AR-2000	1.5" AR-2000	1.5" AR-2000
			2" Plantmix Surface	2" Plantmix Surface	2" Plantmix Surface	2" Plantmix Surface	2" Plantmix Surface
			2" Plantmix Base	2" Plantmix Base	2" Plantmix Base	2" Plantmix Base	2" Plantmix Base
		4" Asphalt Roadmix	4" Asphalt Roadmix	4" Asphalt Roadmix	4" Asphalt Roadmix	4" Asphalt Roadmix	4" Asphalt Roadmix
		8" Aggregate Base	8" Aggregate Base	8" Aggregate Base	8" Aggregate Base	8" Aggregate Base	8" Aggregate Base

	Final Structure	Layer Behavior	Thickness(in)	Layer Coefficient	h*ai	Section Modeled	Modulus E (psi)
US 50-136	2"PG64-28NV	Visco-Elastic	2	Database	Database	2"PG64-28NV	Database
	4" AC-20P	Visco-Elastic	4	Database	Database	4" AC-20P	Database
	4" Aggregate Base	Elastic	4	0.1	0.4	21.5" Aggregate Base Linear Elastic	39038
	1.5" AR-2000	Elastic	1.5	0.25	0.375		
	2" Plantmix Surface	Elastic	2	0.25	0.5	0.166	
	2" Plantmix Base	Elastic	2	0.25	0.5	Subgrade	Database NCHRP
	4" Asphalt Roadmix	Elastic	4	0.25	1		
	8" Aggregate Base	Elastic	8	0.1	0.8		

Table 11.55-Pavement Structure and Resilient Modulus Calculations for US 093-40.

	Year	1932	1961	Sep-92	Aug-95	Aug-05
US 93-40	**Structure**				2" AC-30P	2"PG 76-22NV
				2.5" AR-8000	2.5" AR-8000	2" AR-8000
			4" 85-100 PEN	4" 85-100 PEN	4" 85-100 PEN	4" 85-100 PEN
			8" Aggregate Base	8" Aggregate Base	8" Aggregate Base	8" Aggregate Base
		6" Aggregate Base	6" Aggregate Base	6" Aggregate Base	6" Aggregate Base	6" Aggregate Base

	Final Structure	Layer Behavior	Thickness(in)	Layer Coefficient	h*ai	Section Modeled	Modulus E (psi)
US 93-40	2"PG 76-22NV	Visco-Elastic	2	Database	Database	2"PG 76-22NV	Database
	2" AR-8000	Elastic	2	0.25	0.5	20" Aggregate Base Linear Elastic	32064
	4" 85-100 PEN	Elastic	4	0.25	1		
	8" Aggregate Base	Elastic	8	0.1	0.8	0.145	
	6" Aggregate Base	Elastic	6	0.1	0.6	Subgrade	Database NCHRP

CHAPTER 12 APPENDIX C: RUTTING CALIBRATION

Table 12.1-Optimization Results for District I-New.

	βr2	βr3	βr1	βbase	βsg	R-squared Total Rutting	R-square Asphalt Rutting
District I-New	0.7	0.7	0.1873	0.1618	0.1822	0.1000	0.1332
	0.7	0.8	0.1810	0.1603	0.1806	0.1011	0.1896
	0.7	0.9	0.1962	0.2359	0.1388	0.1582	0.6941
	0.7	1.0	0.1735	0.1540	0.1748	0.1060	0.3345
	0.8	0.7	0.1793	0.1564	0.1777	0.1008	0.1481
	0.8	0.8	0.1731	0.1534	0.1744	0.1029	0.2092
	0.8	0.9	0.1708	0.1478	0.1690	0.1142	0.2493
	0.8	1.0	0.1599	0.1424	0.1625	0.1119	0.3336
	0.9	0.7	0.1684	0.1468	0.1680	0.1015	0.1515
	0.9	0.8	0.1610	0.1404	0.1612	0.1052	0.2090
	0.9	0.9	0.1511	0.1319	0.1520	0.1110	0.2671
	0.9	1.0	0.1359	0.1218	0.1406	0.1195	0.3207
	1.0	0.7	0.1481	0.1288	0.1497	0.1005	0.1496
	1.0	0.8	0.1361	0.1181	0.1383	0.1059	0.2004
	1.0	0.9	0.1189	0.1062	0.1254	0.1133	0.2491
	1.0	1.0	0.1045	0.0900	0.1073	0.1223	0.2893

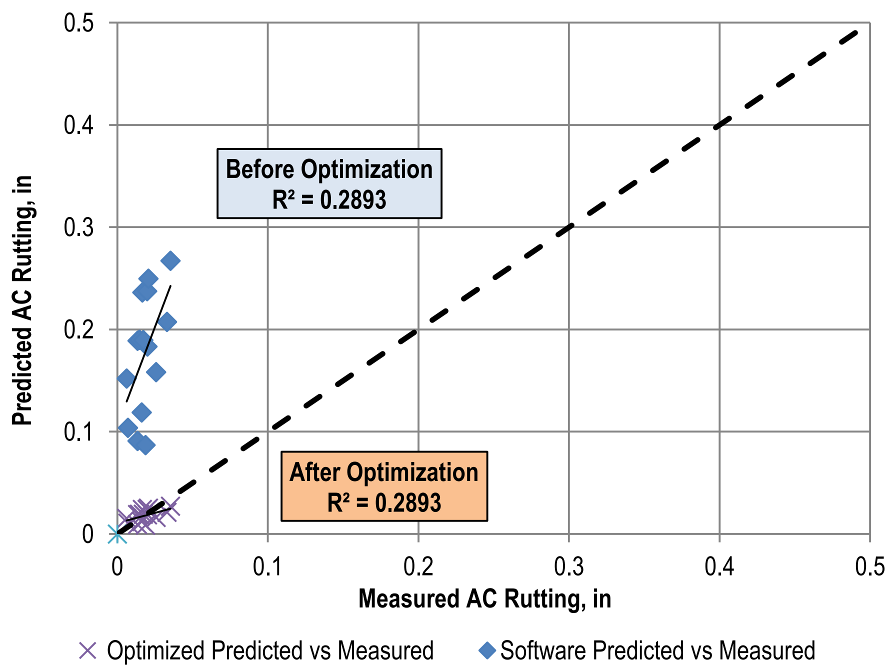

Figure 12.1-AC Rutting Optimization District I-New (β_{r1} =0.1045, β_{r2}=β_{r3}=1.0).

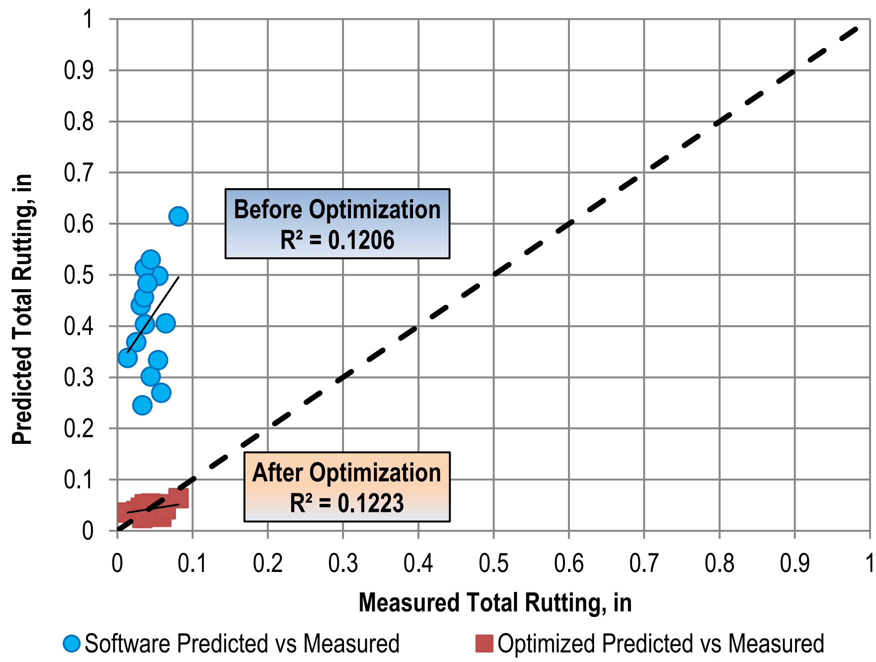

Figure 12.2-Total Rutting Optimization District I (β_b =0.0900, β_{sg}=0.1073).

Table 12.2-Optimization Results for District II-Overlay.

	βr2	βr3	βr1	βbase	βsg	R-squared Total Rutting	R-square Asphalt Rutting
District II-Overlay	0.7	0.7	0.3359	0.4317	0.1469	0.1959	0.0582
	0.7	0.8	0.3437	0.4261	0.1460	0.2788	0.1582
	0.7	0.9	0.3741	0.3775	0.1661	0.3037	0.7927
	0.7	1.0	0.3521	0.4057	0.1429	0.2957	0.4893
	0.8	0.7	0.3323	0.4205	0.1385	0.2833	0.2339
	0.8	0.8	0.2967	0.3516	0.1902	0.2911	0.2356
	0.8	0.9	0.3191	0.3878	0.1344	0.3029	0.4284
	0.8	1.0	0.2988	0.3611	0.1360	0.3222	0.5832
	0.9	0.7	0.2951	0.3852	0.1240	0.2940	0.1764
	0.9	0.8	0.2793	0.3598	0.1224	0.3110	0.3629
	0.9	0.9	0.2527	0.3262	0.1265	0.3376	0.5099
	0.9	1.0	0.2141	0.2867	0.1319	0.3346	0.5452
	1.0	0.7	0.2320	0.3197	0.1051	0.3183	0.2802
	1.0	0.8	0.2016	0.2823	0.1067	0.3234	0.3756
	1.0	0.9	0.1661	0.2399	0.1145	0.3077	0.3797
	1.0	1.0	0.1298	0.1970	0.1276	0.2562	0.3186

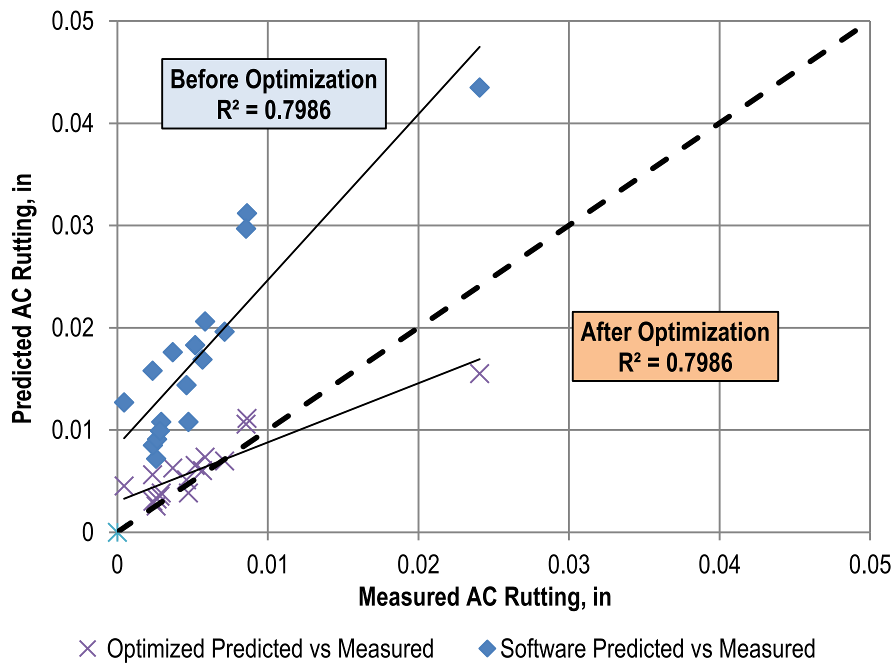

Figure 12.3-AC Rutting Optimization District II-Overlay (β_{r1} =0.3741, β_{r2}=0.7, and β_{r3}=0.9).

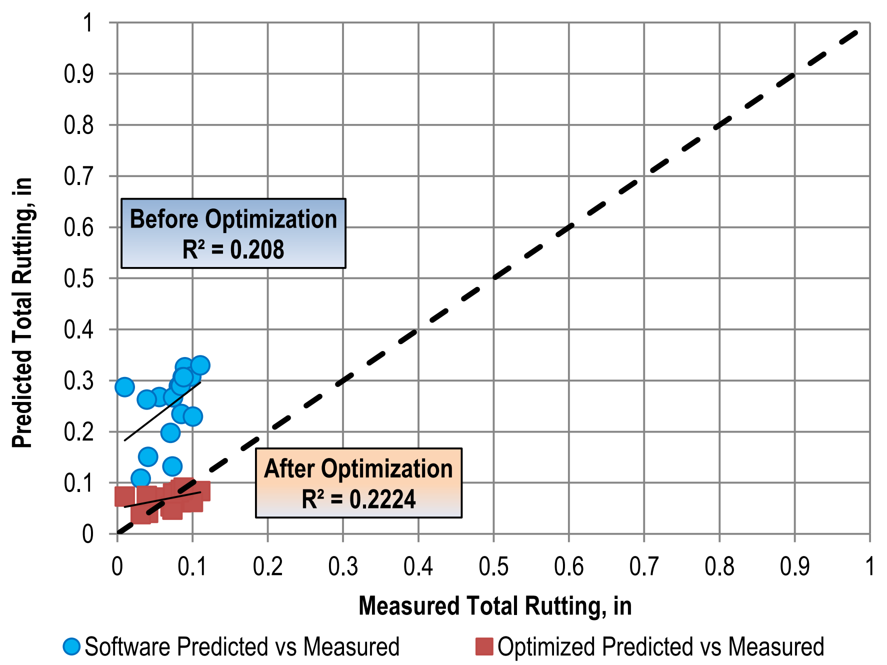

Figure 12.4-Total Rutting Optimization District II-Overlay (β_b =0.3775, β_{sg}=0.1661).

Table 12.3-Optimization Results for District II-New.

	βr2	βr3	βr1	βbase	βsg	R-squared Total Rutting	R-square Asphalt Rutting
District II- New	0.7	0.7	0.2609	0.1553	0.3224	0.1107	0.3860
	0.7	0.8	0.2621	0.1260	0.3368	0.074	0.4121
	0.7	0.9	0.2471	0.1286	0.3310	0.0681	0.3480
	0.7	1.0	0.2560	0.1255	0.3285	0.0797	0.4330
	0.8	0.7	0.2524	0.1238	0.3310	0.078	0.3821
	0.8	0.8	0.2512	0.1220	0.3264	0.0852	0.4143
	0.8	0.9	0.2479	0.1195	0.3201	0.0956	0.4429
	0.8	1.0	0.2418	0.1159	0.3113	0.1109	0.4691
	0.9	0.7	0.2354	0.1165	0.3137	0.0951	0.3832
	0.9	0.8	0.2287	0.1123	0.3040	0.1089	0.4111
	0.9	0.9	0.2186	0.1083	0.2910	0.1235	0.4510
	0.9	1.0	0.2053	0.1000	0.2746	0.1549	0.4626
	1.0	0.7	0.2017	0.1007	0.2787	0.1236	0.3727
	1.0	0.8	0.1876	0.0931	0.2615	0.1433	0.3956
	1.0	0.9	0.1698	0.0838	0.2411	0.1655	0.4138
	1.0	1.0	0.1359	0.0252	0.2827	0.0788	0.4594

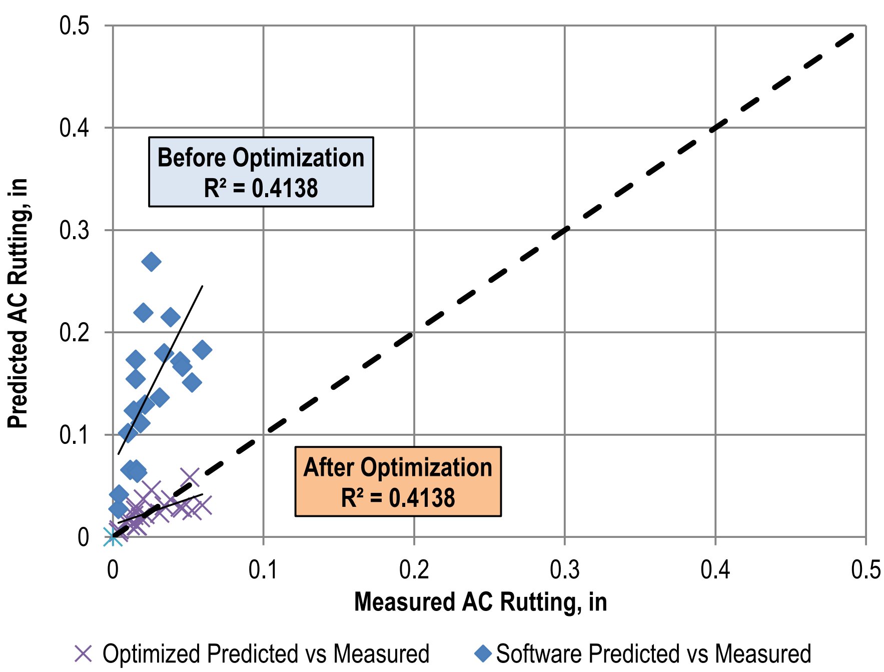

Figure 12.5-AC Rutting Optimization District II-New (β_{r1} =0.1698, β_{r2}=1.0, and β_{r3}=0.9).

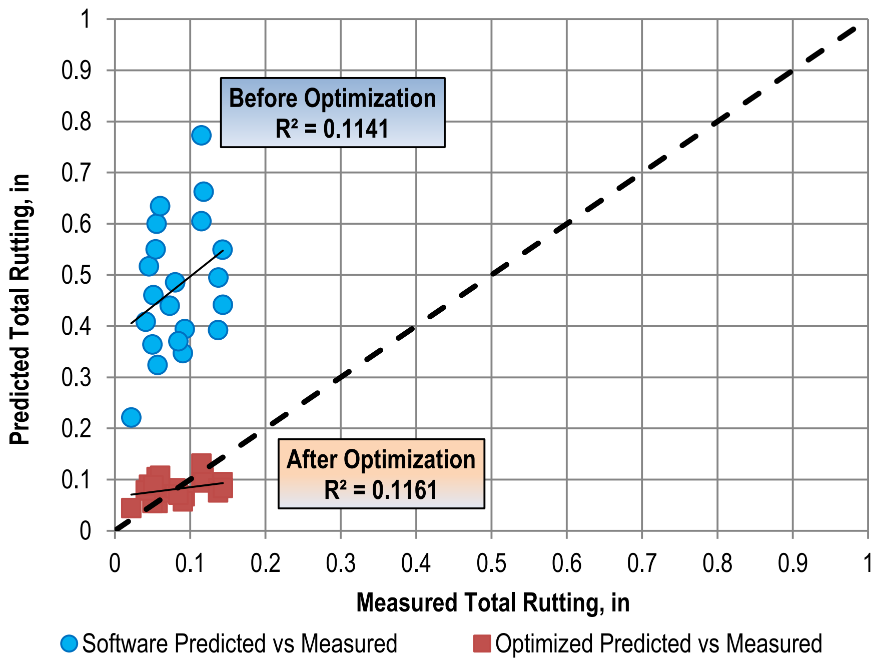

Figure 12.6-Total Rutting Optimization District II-New (β_b =0.0838, β_{sg}=0.2411).

Table 12.4-Optimization Results for District III-Overlay.

	βr2	βr3	βr1	βbase	βsg	R-squared Total Rutting	R-square Asphalt Rutting
District III -Overlay	0.7	0.7	0.2724	0.4490	0.0100	0.0199	0.0301
	0.7	0.8	0.2686	0.4398	0.0100	0.0258	0.0613
	0.7	0.9	0.3630	0.3924	0.0100	0.1959	0.9046
	0.7	1.0	0.2546	0.4019	0.0100	0.0668	0.1791
	0.8	0.7	0.2580	0.4240	0.0100	0.0323	0.0459
	0.8	0.8	0.2497	0.4022	0.0100	0.0522	0.1050
	0.8	0.9	0.2355	0.3706	0.0100	0.1012	0.1970
	0.8	1.0	0.2158	0.3375	0.0100	0.1851	0.3487
	0.9	0.7	0.2221	0.3609	0.0100	0.1234	0.1770
	0.9	0.8	0.2086	0.3271	0.0100	0.3125	0.7622
	0.9	0.9	0.1791	0.2779	0.0100	0.2923	0.3707
	0.9	1.0	0.1442	0.2233	0.0100	0.4321	0.4839
	1.0	0.7	0.1732	0.2718	0.0100	0.2499	0.3271
	1.0	0.8	0.1416	0.2205	0.0100	0.3929	0.4463
	1.0	0.9	0.1092	0.1688	0.0100	0.5064	0.5392
	1.0	1.0	0.0797	0.1218	0.0100	0.5747	0.6055

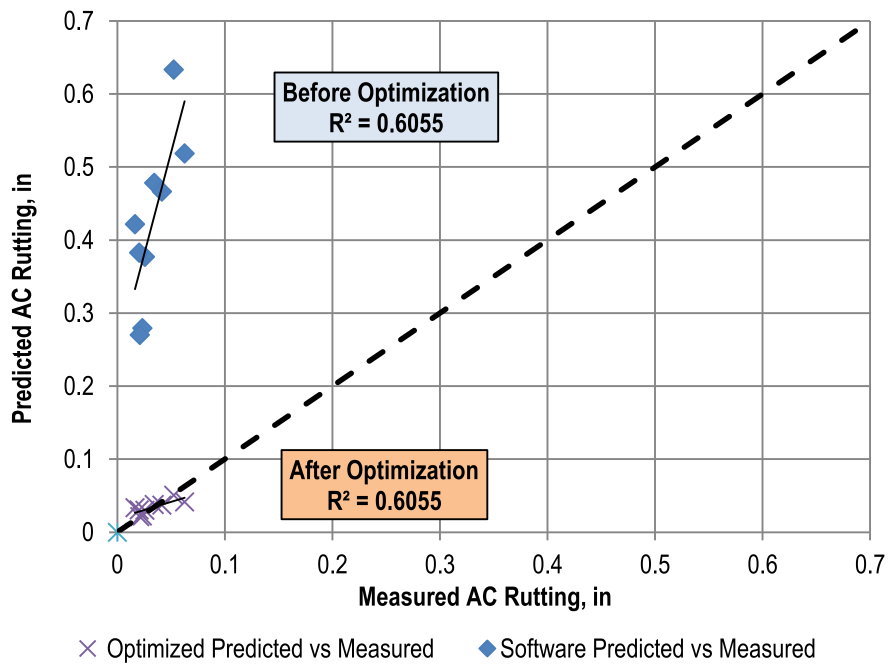

Figure 12.7-AC Rutting Optimization District III-Overlay (β_{r1} =0.0797, β_{r2}=1.0, and β_{r3}=1.0).

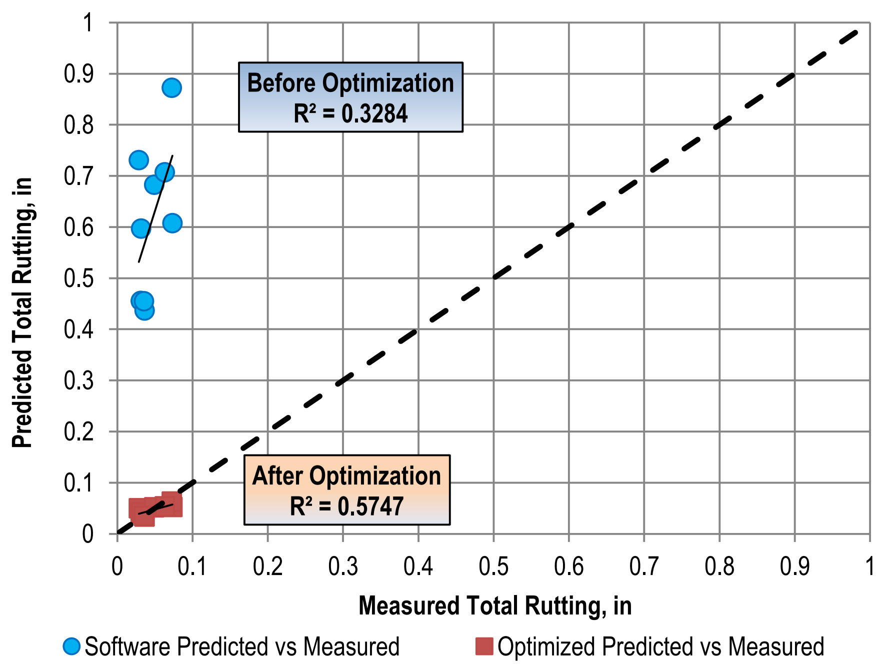

Figure 12.8-Total Rutting Optimization District III-Overlay (β_b =0.1218, β_{sg}=0.0100).

Table 12.5-Optimization Results for District III-New.

	βr2	βr3	βr1	βbase	βsg	R-squared Total Rutting	R-square Asphalt Rutting
District III -New	0.7	0.7	0.1694	0.1777	0.1968	0.5821	0.9774
	0.7	0.8	0.1674	0.1759	0.1956	0.5745	0.9759
	0.7	0.9	0.1527	0.2047	0.1320	0.5324	0.9909
	0.7	1.0	0.1604	0.1698	0.1914	0.5558	0.9708
	0.8	0.7	0.1619	0.1703	0.1926	0.5562	0.9725
	0.8	0.8	0.1675	0.1681	0.1910	0.5407	0.9695
	0.8	0.9	0.1510	0.1608	0.1860	0.5270	0.9649
	0.8	1.0	0.1427	0.1534	0.1811	0.5074	0.9571
	0.9	0.7	0.1454	0.1543	0.1832	0.5071	0.9602
	0.9	0.8	0.1365	0.1463	0.1776	0.4868	0.9512
	0.9	0.9	0.1253	0.1364	0.1706	0.4646	0.9373
	0.9	1.0	0.1118	0.1244	0.1623	0.4421	0.9153
	1.0	0.7	0.1157	0.1252	0.1656	0.437	0.9232
	1.0	0.8	0.1192	0.0212	0.3933	0.4908	0.8003
	1.0	0.9	0.0879	0.0998	0.1476	0.3984	0.8598
	1.0	1.0	0.0728	0.0862	0.1373	0.3825	0.8072

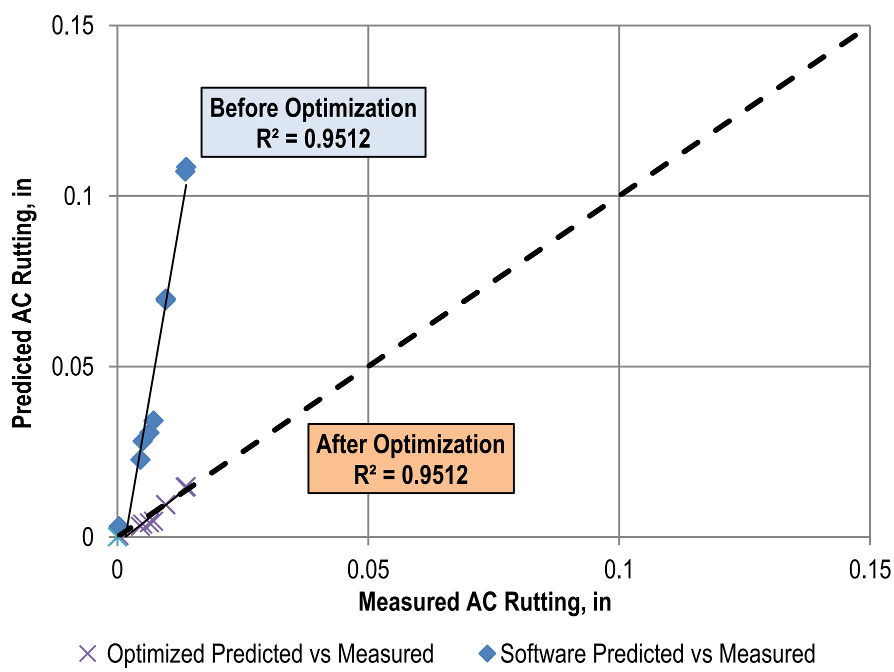

Figure 12.9-AC Rutting Optimization District III-New (β_{r1} =0.1365, β_{r2}=0.9, and β_{r3}=0.8).

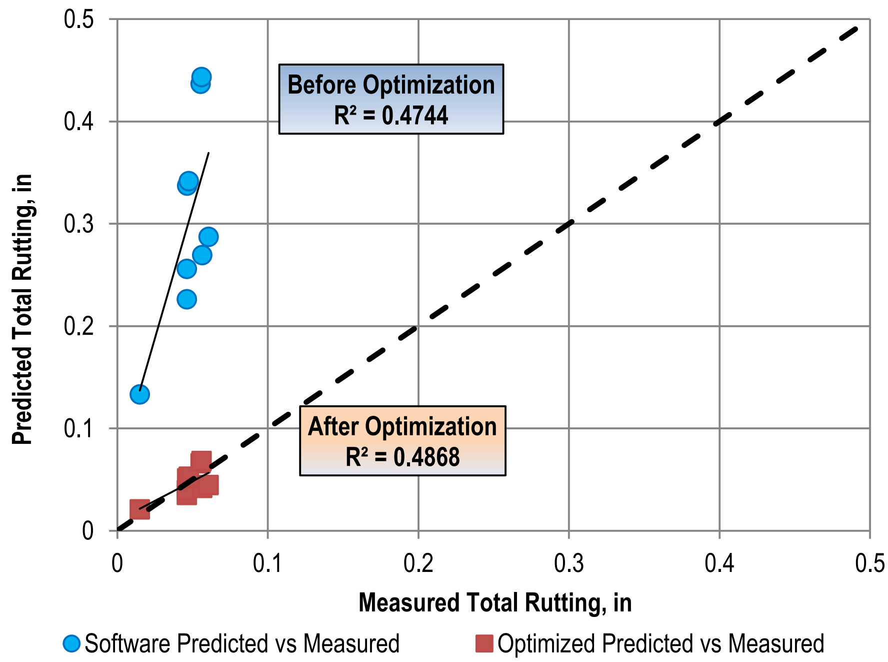

Figure 12.10-Total Rutting Optimization District III-New (β_b =0.1463, β_{sg}=0.1776).

CHAPTER 13 APPENDIX D: RUTTING VALIDATION/VERIFICATION PLOTS

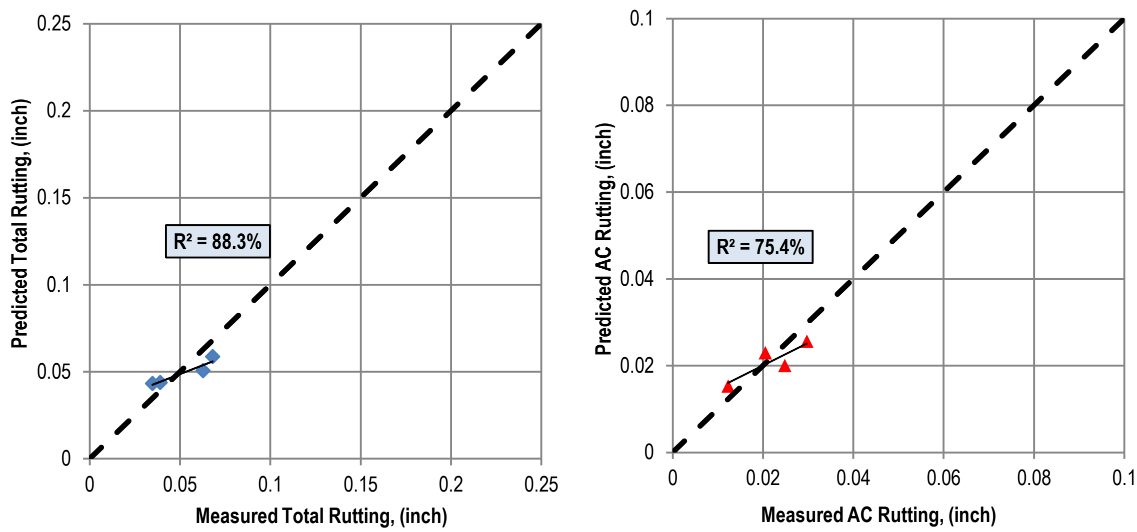

Figure 13.1-Rutting Validation Plots District I -New.

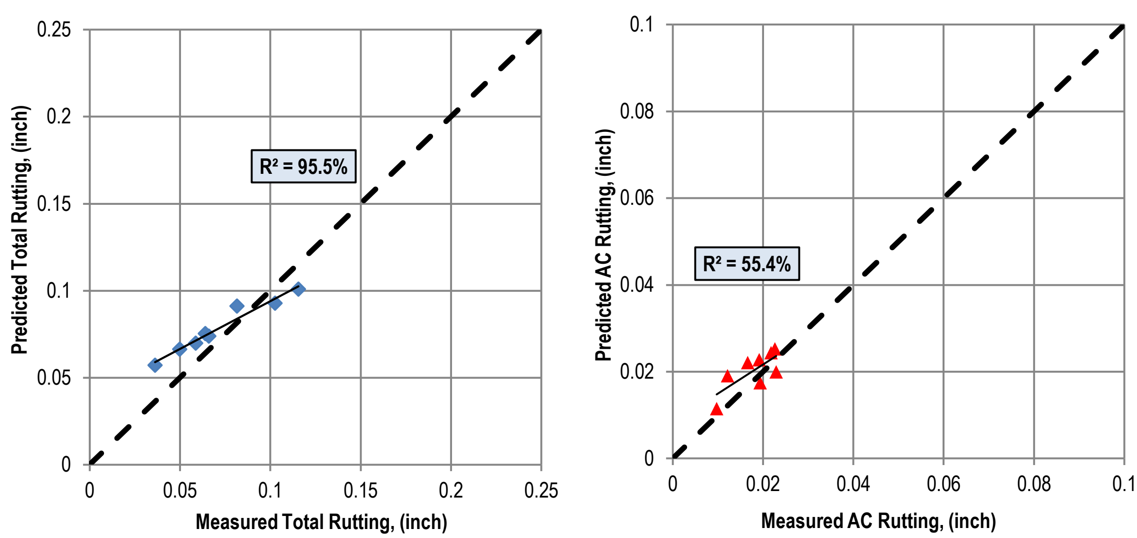

Figure 13.2-Rutting Validation Plots District II -Overlay.

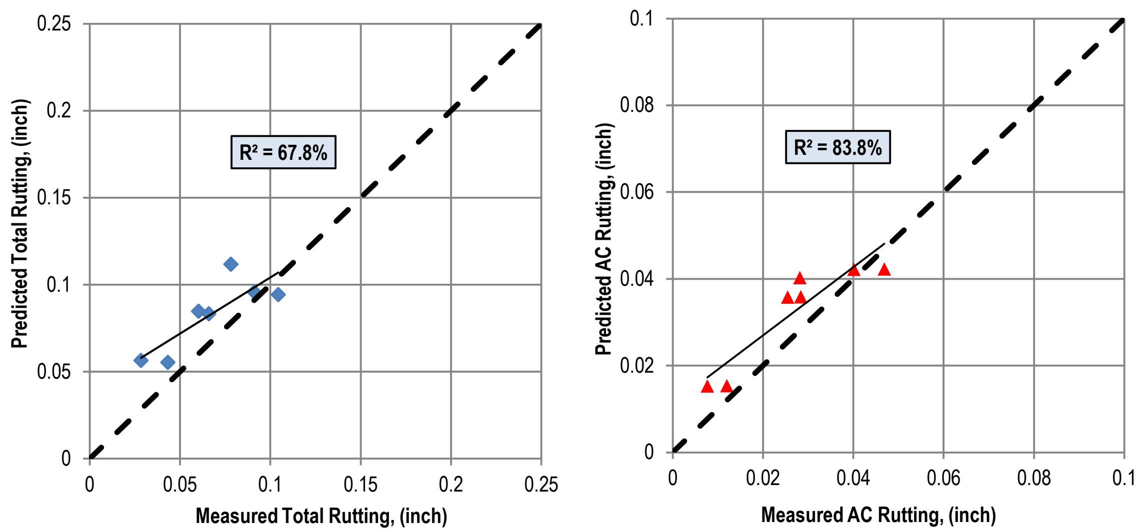

Figure 13.3-Rutting Validation Plots District II -New.

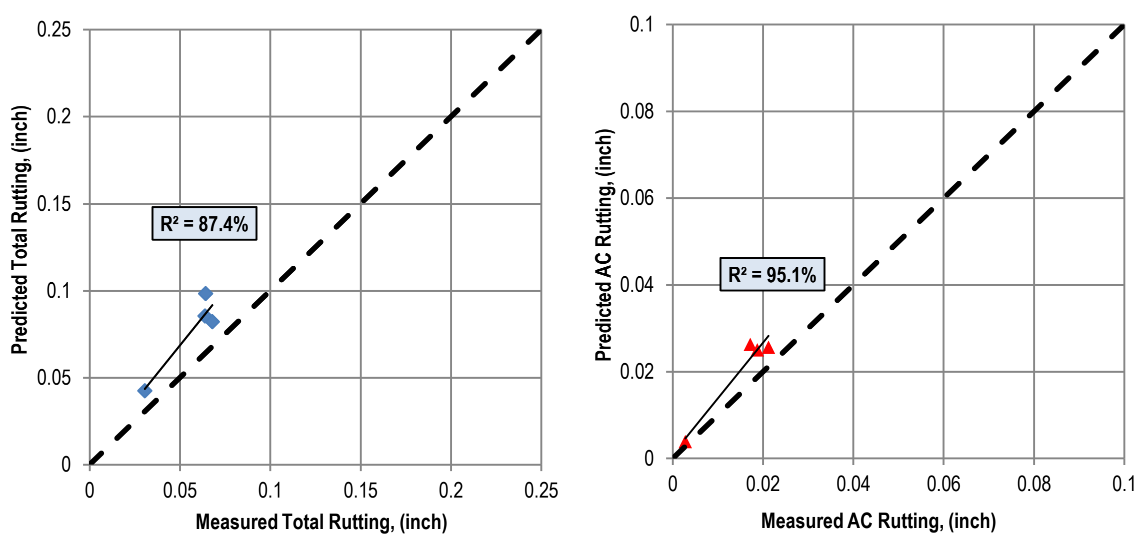

Figure 13.4-Rutting Validation Plots District III -Overlay.

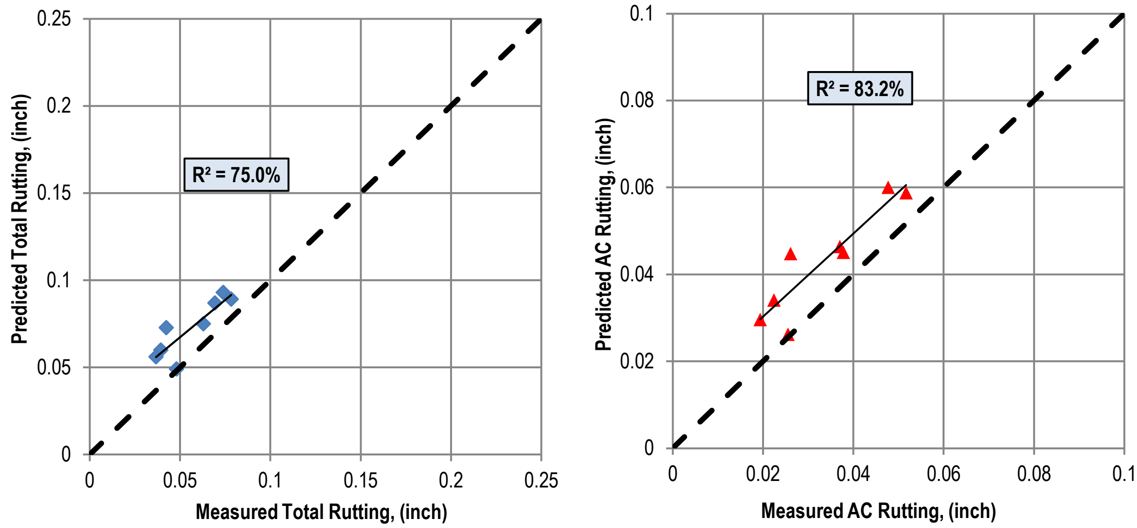

Figure 13.5-Rutting Validation Plots District III -New.

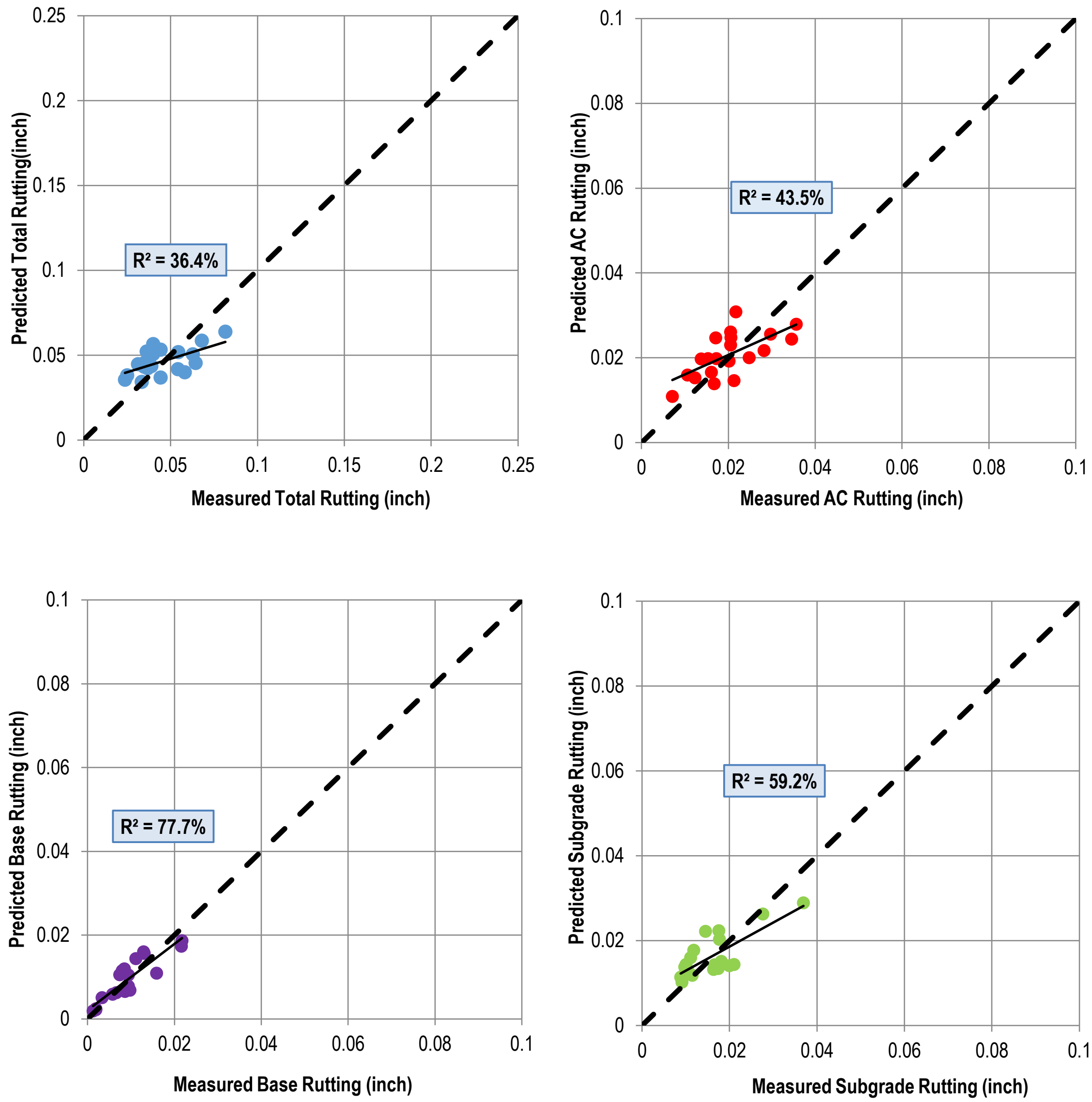

Figure 13.6-Rutting Verification Plots District I - New.

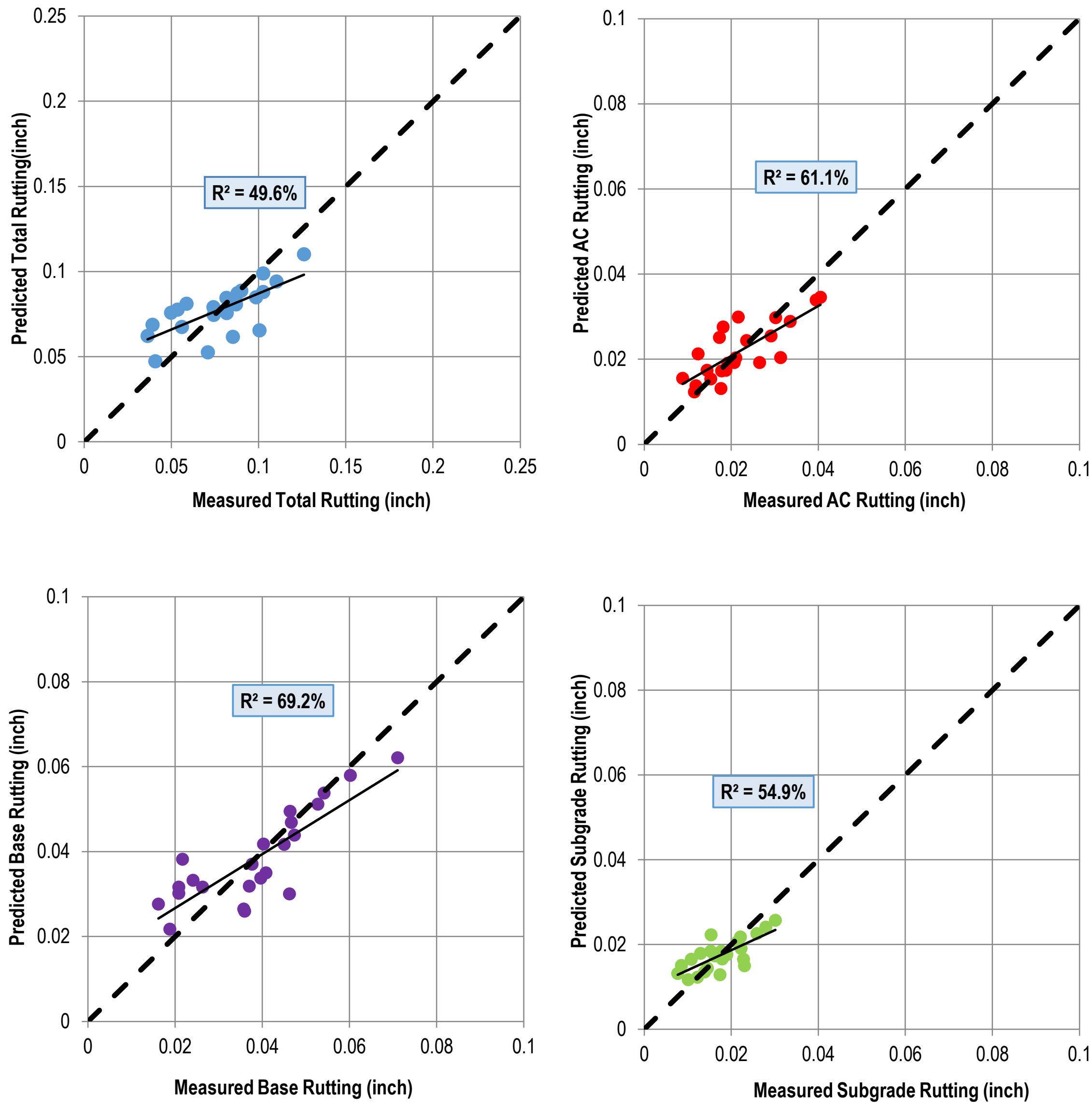

Figure 13.7-Rutting Verification Plots District II - Overlay.

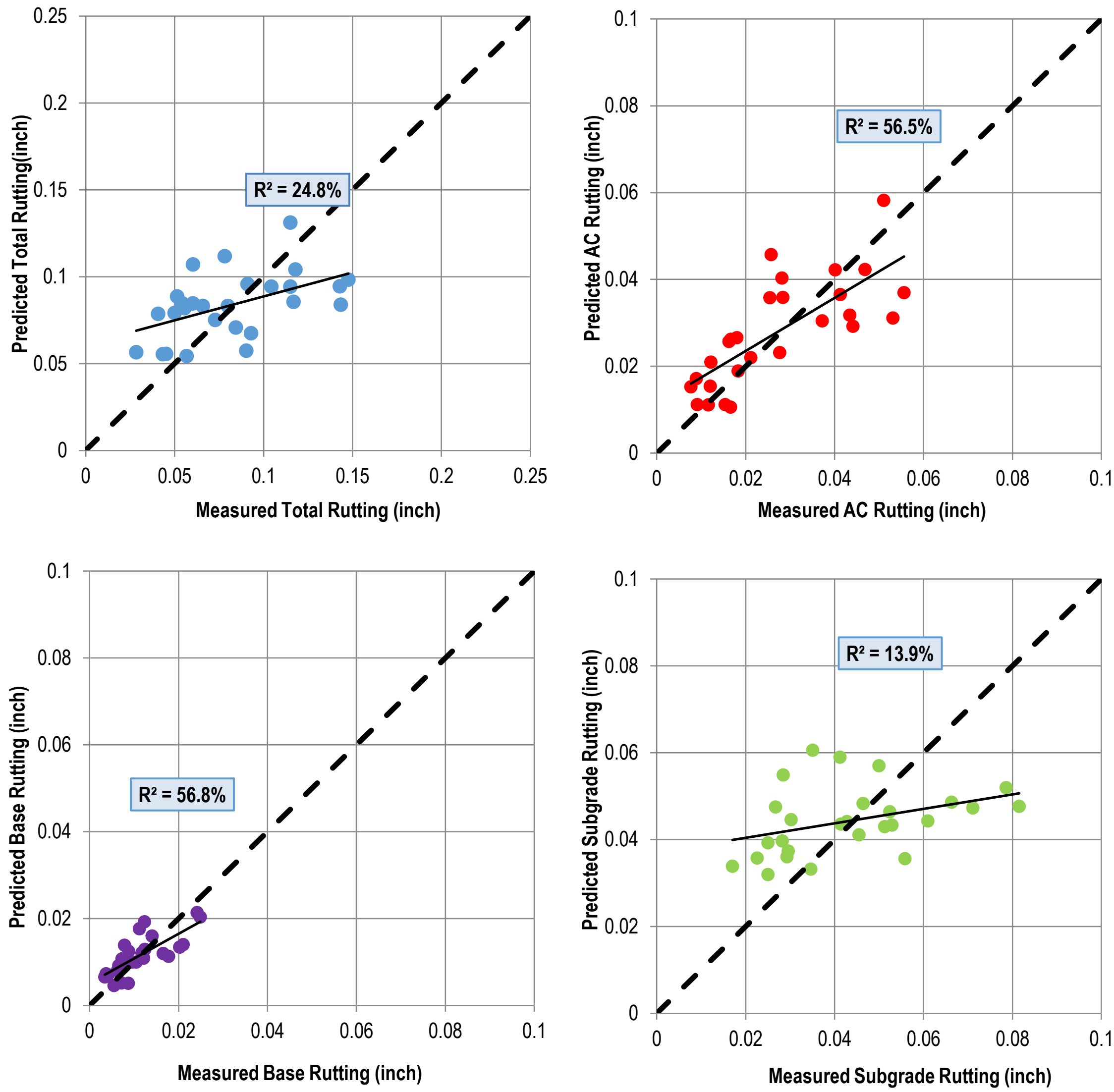

Figure 13.8-Rutting Verification Plots District II - New.

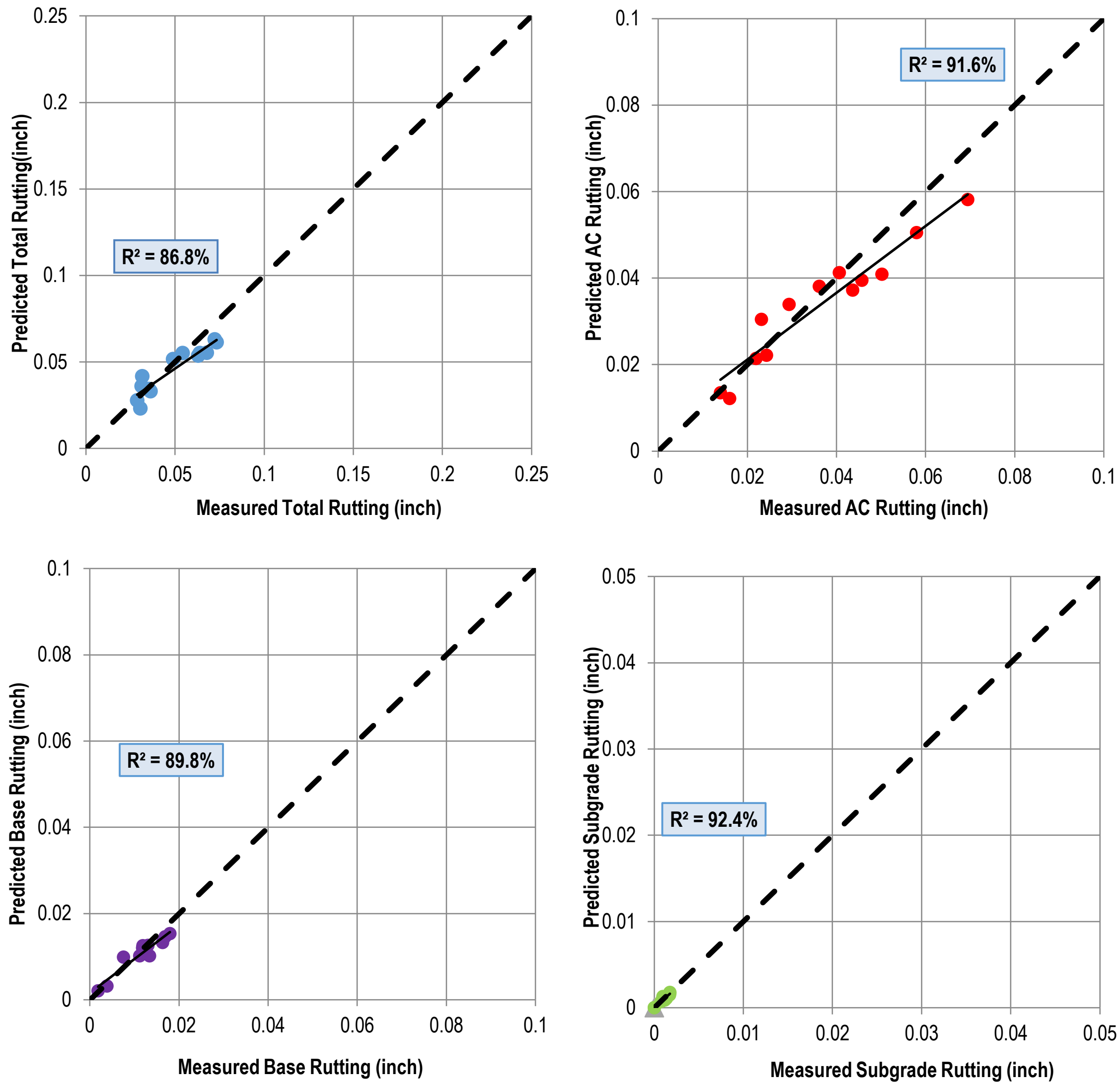

Figure 13.9-Rutting Verification Plots District III - Overlay.

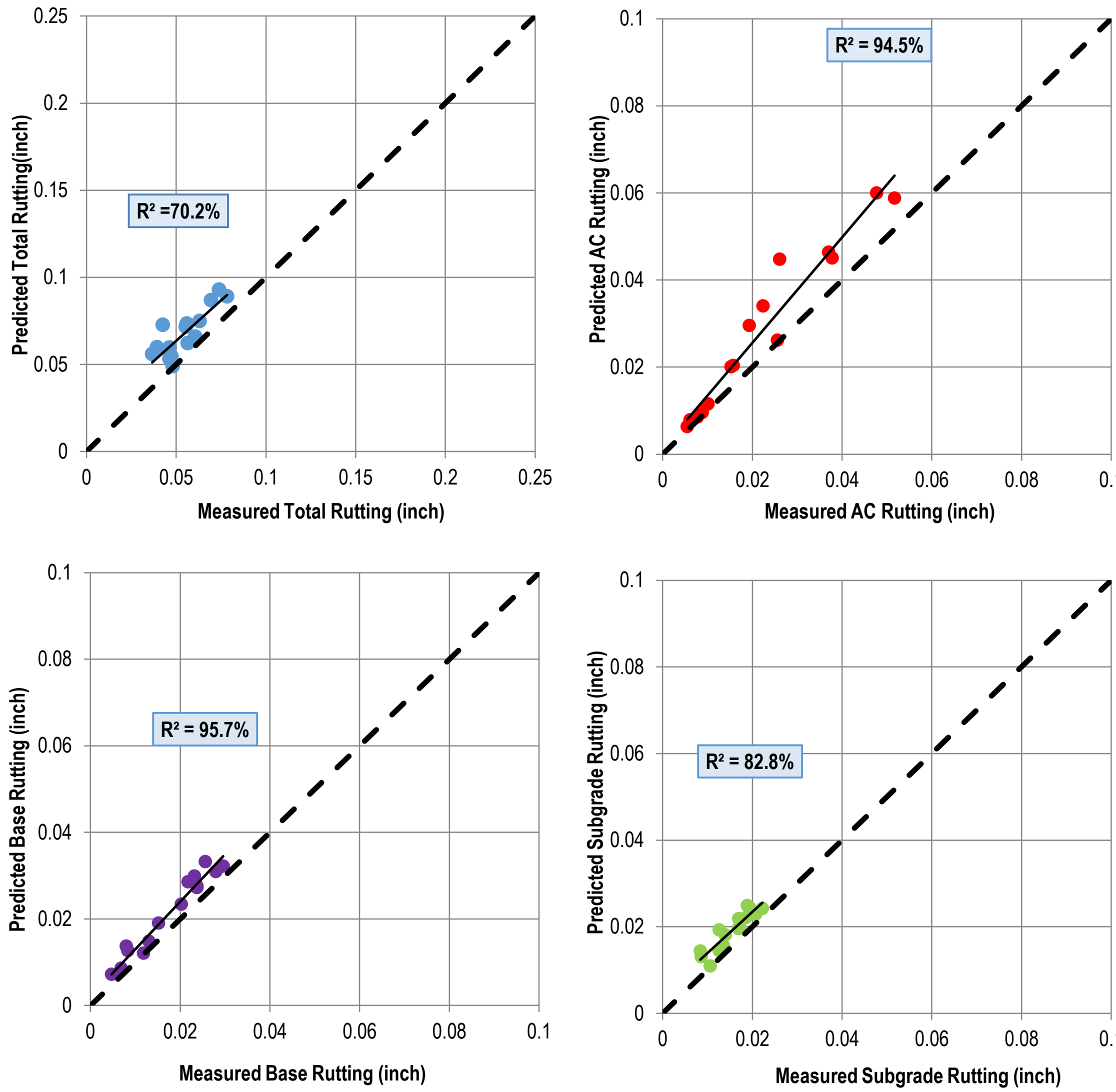

Figure 13.10-Rutting Verification Plots District III – New